Characterization of a novel DNA binding domain in the N-terminus of BRCA2 and evaluation of BRCA2 variants identified in breast cancer patients in the same region

Catharina Von Nicolai

NNT : 2016SACLS123

THESE DE DOCTORAT

DE

L'UNIVERSITE PARIS-SACLAY

PREPAREE A

UNIVERSITE PARIS SUD – FACULTE DE MEDECINE ET INSTITUT CURIE

ECOLE DOCTORALE N° 582

CANCEROLOGIE – BIOLOGIE, MEDECINE, SANTE (CBMS)

ASPECTES MOLECULAIRES ET CELLULAIRES DE LA BIOLOGIE

Par

Catharina von Nicolai

Characterization of a novel DNA binding domain in the N-terminus of BRCA2 and evaluation of BRCA2 variants identified in breast cancer patients in the same region

Thèse présentée et soutenue à Orsay, le 13 Juin 2016

Composition du Jury :

Saule, Simon	Professeur à l'Université Paris Sud	Président
Callebaut, Isabelle	Directrice de Recherche IMPMC Paris	Rapporteur
Modesti, Mauro	Directeur de Recherche CRCM Marseille	Rapporteur
Charbonnier, Jean-Baptiste	Chargée de recherche 1ère classe CEA Saclay	Examinateur
Zinn-Justin, Sophie	Chargée de recherche 1ère classe CEA Saclay	Examinatrice
Carreira, Aura	Chargée de recherche 1ère classe Institut Curie Orsay	Directrice de Thèse

NNT : 2016SACLS123

THESE DE DOCTORAT

DE

L'UNIVERSITE PARIS-SACLAY

PREPAREE A

UNIVERSITE PARIS SUD – FACULTE DE MEDECINE ET INSTITUT CURIE

ECOLE DOCTORALE N° 582

CANCEROLOGIE – BIOLOGIE, MEDECINE, SANTE (CBMS)

ASPECTES MOLECULAIRES ET CELLULAIRES DE LA BIOLOGIE

Par

Catharina von Nicolai

Characterization of a novel DNA binding domain in the N-terminus of BRCA2 and evaluation of BRCA2 variants identified in breast cancer patients in the same region

Thèse présentée et soutenue à Orsay, le 13 Juin 2016

Composition du Jury :

Saule, Simon	Professeur à l'Université Paris Sud	Président
Callebaut, Isabelle	Directrice de Recherche IMPMC Paris	Rapporteur
Modesti, Mauro	Directeur de Recherche CRCM Marseille	Rapporteur
Charbonnier, Jean-Baptiste	Chargée de recherche 1ère classe CEA Saclay	Examinateur
Zinn-Justin, Sophie	Chargée de recherche 1ère classe CEA Saclay	Examinatrice
Carreira, Aura	Chargée de recherche 1ère classe Institut Curie Orsay	Directrice de Thèse

INDEX

ACKNOWLEDGEMENTS

This work would not have been possible without the financial support I received from the Training Unit of Institut Curie for the International PhD Fellowship for the first three years of my thesis. Moreover, the Fondation pour la Recherche Médicale financed my 4th year of PhD.

I would like to thank the members of my Jury for having accepted to evaluate my work: Simon Saule, Sophie Zinn-Justin, Jean-Baptiste Charbonnier, Isabelle Callebaut and Mauro Modesti.

My special thanks go to Isabelle Callebaut and Mauro Modesti for reading and evaluating this manuscript.

Thanks to the members of my comité de these for the half-time evaluation: Mounira Amor-Guéret who also accepted to be my directrice de thèse during the first year of PhD. Gerald Peyroche from the École Doctorale Cancérologie, Marie Dutreix as my tutor, Isabelle Callebaut and Sophie Zinn-Just as external experts.

Special thanks to my directrice de these and supervisor Aura Carreira who accepted me as PhD student and guided me during the last 4 years. Thank you for teaching me how to work scientifically. Thanks to your relentless incentive and motivation I was able to finish this work and to overcome some lows. Hopefully it could contribute to the success of the lab as you expected.

I am thankful for joyful moments to all present and former lab members.

I would like to give special credit to Åsa Éhlen, my bench colleague and collaborator in several projects, who helped me a lot with experiments especially in the beginning of my thesis. I will miss our daily exchange, be it scientific or rather life-related. The same goes for Juan Martinez for replying with patience to all my questions and giving me a lot of advice. I hope you guys will continue to work with the same success without losing your motivation and passion for science.

Merci à notre bon âme du labo, Charlotte Martin, pour ton aide avec les clonages sans fin et autres petits travaux et pour que tu étais toujours disponible pour des petites discussions en français!

And of course thank you to all the other lab members I was lucky to meet during the last years: Tommy Holthausen, Céline Baldeyron, Stephanos Papaefstathiou, Virginie Boucherit and all the students we saw coming and leaving.

Some of the projects presented here would not have been possible without the help of our collaborators: Patricia Duchambon and Ahmed El Marjou from the recombinant protein platform at I. Curie for the help with the purification of the CTD and RAD51. Xiaodong Zhang and her team from Imperial College London for the EM of the N-

terminus and the ongoing crystallography studies of the CTD. Alexandra Martins from the Université Rouen for the splicing assays. Thanks to Fergus Couch and his team from the Mayo Clinic for the IP studies of the variants. We are also happy about the successful work on the intermediate variant risk paper and say thank you to all the collaborators from the ENIGMA network, especially the lab of Fergus Couch and Maaike Vreeswijk.
Thanks to Frederic Garzoni and Imre Berger from the EMBL Grenoble for inviting me to their lab and teaching me the Baculovirus Expression System.
I would also like to thank all the members of the Genotoxic stress and cancer unit (UMR3348). It has always been a nice working atmosphere and everyone was very helpful.

But of course all the success at work would not have been possible without the support I got from my friends and family, near and far.

I am grateful to my parents, for their tremendous support during all the years of studies.

I could not be luckier to call five persons my awesome siblings who motivate and inspire me. This specifically applies to my brother Constantin who shared scientific and life-related highs and lows with me. And my sister Christina who was always there being it with advice, a chat or a spontaneous trip to Paris with prosecco in her hands.

This thesis would probably not exist without the everlasting motivation, cheering up and help that I got from Christophe: Merci, I can't wait to cycle to the end of the world with you.

And thanks of course to all the people who read and appreciated this thesis.

"If you think you've reached the top of the world, there's always a hill left to climb"

Greg Graffin

CHAPTER 1 - INTRODUCTION

Our genome inherits all essential information to ensure the proper functioning and survival of the organism. Due to its chemical nature, the DNA interacts with many factors originating from inside and outside the cell, which often leads to the damaging of the DNA. In the introduction, I will outline the various existing kinds of DNA lesions and their origins. The highly specialized DNA damage response and the specialized pathways that are responsible for the repair of these damages are illustrated afterwards. I will then go further into detail about the repair of DNA damage by Homologous Recombination (HR). The focus of my PhD involves the function of the breast cancer susceptibility gene 2 (*BRCA2*) that not only plays a role in this particular pathway but also in other cellular processes like mitosis, cytokinesis and meiosis. Hence, I will then give a detailed overview of the various roles of BRCA2 to familiarize the reader with the current knowledge in the field. Even though there has been a lot of progress in the last 20 years of research on BRCA2, still many conundrums remain to be solved. Some of these open questions were central to this thesis and are outlined in the project description.

1. MAINTAINING GENOME INTEGRITY AFTER DNA DAMAGE

1.1 THE DNA DAMAGE RESPONSE

Chromosomal instability gives rise to most cancers. Aberrations in chromosome number and structures originate from unrepaired DNA damage throughout the cell cycle favoring tumor development. Our cells are constantly exposed to endogenous and exogenous DNA damage by a plethora of hazardous agents and processes. Each cell receives up to ten thousand lesions in the DNA per day [1]. Our cells have evolved multiple mechanisms to accurately respond to each kind of DNA insult with a particular repair pathway. Endogenous damage originates from oxidative stress, spontaneous base modifications, replication errors and oxygen radicals resulting from normal metabolic pathways. Exogenous sources include the UV component of radiation and sunlight, chemical and genotoxic compounds and intercalating agents that alter the DNA structure [2] (Figure 1). As a consequence of DNA damage, the cell cycle is transiently arrested and the DNA metabolism including transcription and replication processes is inhibited until the damage is repaired. Often the cell is forced to induce apoptosis as a result of non-repairable or excessive damage that entails accumulation of mutations and genome instability (Figure 1). To prevent these events, the cells count on highly organized surveillance mechanisms and fine-tuned repair pathways. Inherited disorders involving defects in factors of any of these pathways predispose to malignancy [2]. For example, Ataxia telangiectasia (A-T) is a rare neurodegenerative disease caused by a mutation in the gene coding for ATM kinase and results in hypersensitivity to radiation, as cells are not able to activate the DNA damage response [3].

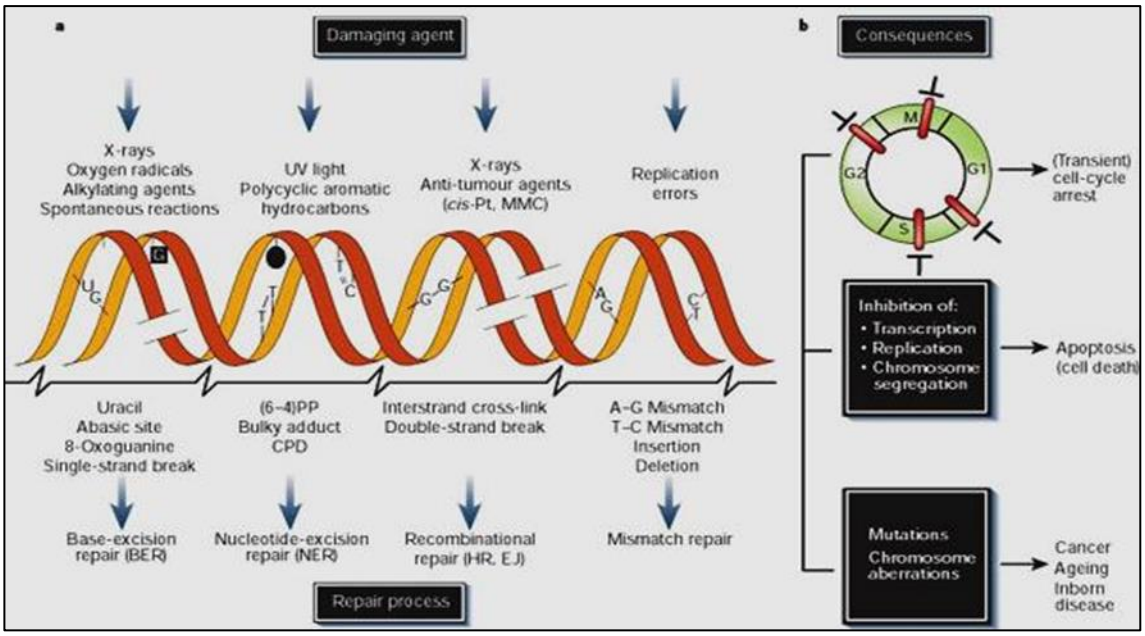

Figure 1: A) Common DNA damaging agents (top) and resulting lesions in the DNA (middle). Each kind of lesion is repaired by a specialized repair process (bottom). **B)** Consequences of DNA damage in the cell: Transient cell cycle arrest at checkpoint (top) and inhibition of DNA metabolism (middle). Permanent changes in the DNA like mutations or chromosome aberrations can lead to cancer, ageing and diseases (bottom). Adapted from Hoeijmakers, 2001[2].

1.2 SENSING AND SIGNALING DNA DAMAGE

The DNA damage response (DDR) is a signaling transduction cascade that is activated by the cell upon DNA damage for the initiation of, among others, DNA damage repair processes, cell cycle arrest or apoptosis (see Figure 2). The complex network involves a plethora of different protein players such as sensors, mediators, transducers and effectors [1]. After the DNA damage has occurred, the lesion is detected by sensor proteins that are specialized for each kind of damage: Small lesions in the DNA and replication stress result in the formation of stretches of ssDNA that subsequently recruit the ssDNA binding protein RPA. The persistence of RPA on the ssDNA recruits the sensor complex ATR-ATRIP for the stabilization of the structure, the arrest of the cell cycle and activation of the repair process [4]. DNA double strand breaks (DSBs) are recognized by the sensor complex Mre11-RAD50-Nbs1 (MRN) that subsequently processes the DNA ends 5'-3' by its nuclease activity and recruits other repair proteins [5]. Blunt ended DSBs are detected by the Ku protein, which recruits DNA-PK, a kinase that activates end-processing enzymes [1].

The information is transmitted from the sensor to the transducer that in turn, activates mediator proteins and downstream kinases [6]. Besides DNA-PK that senses DSBs through Ku and directly activates DNA repair, two main DNA damage response signaling pathways have been described: Ataxia Telangiectasia Mutated (ATM)-dependent and Ataxia Telangiectasia and RAD3-related (ATR)-dependent signaling [7]. Like DNA-PK, ATM and ATR are PI3K-like protein kinases that phosphorylate mostly serine and threonine residues. ATM signaling cascade is activated by DSBs while ATR responds to replication stress and other small DNA lesions [8,9]. ATM/ATR signaling

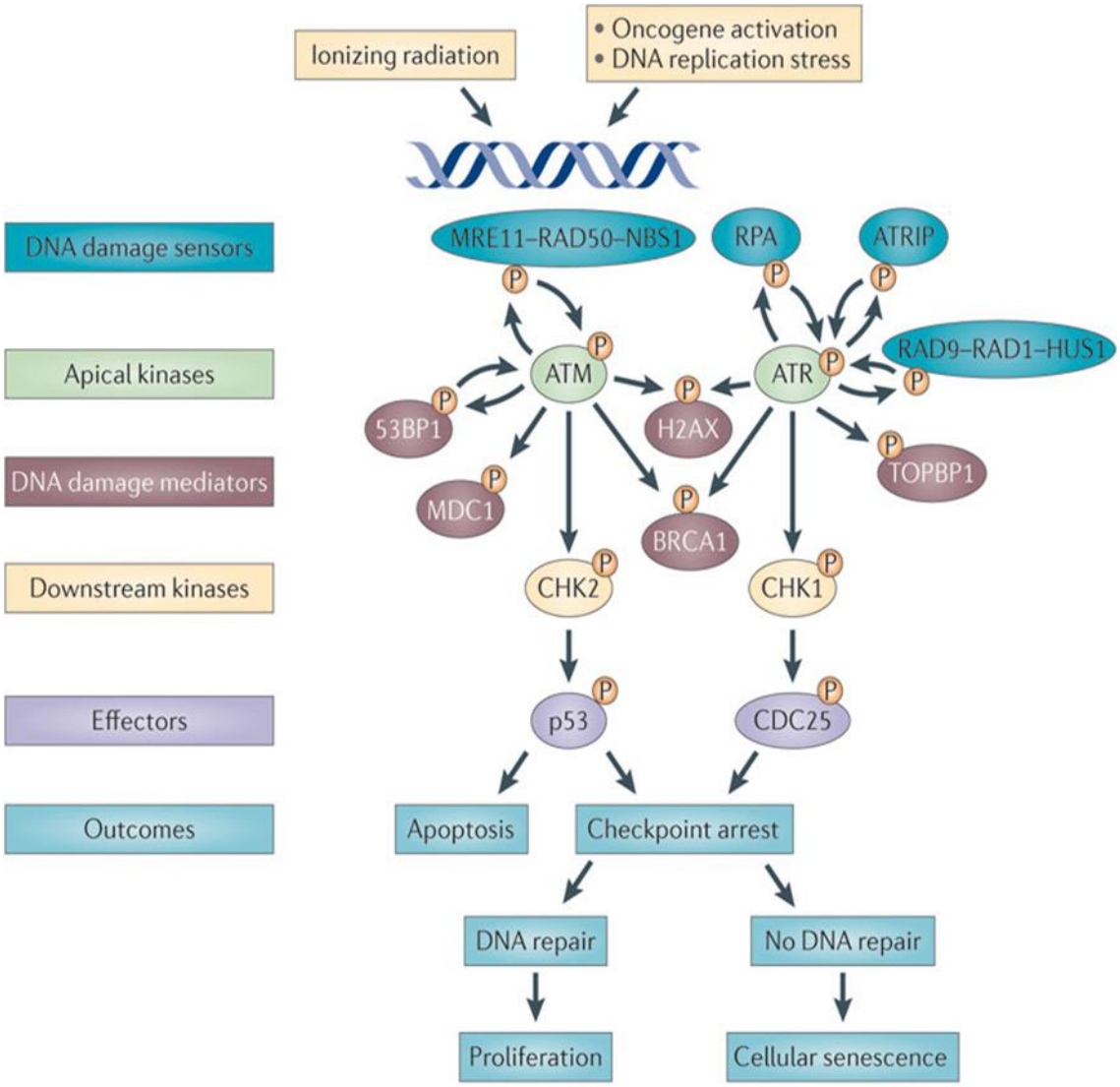

Figure 2: The DNA damage response is induced by damage sensors upon DNA damage or replication stress. Sensors activate the ATM/ATR kinases for the regulation of mediator proteins or downstream kinases that control effector proteins. Effectors are responsible for the control of processes such as cell cycle control, DNA repair or apoptosis. Adapted from Sulli *et al.,* 2012 [247].

activates the downstream kinases CHK1 and CHK2 that in turn induce the activity of

effectors like CDC25 (cell division cycle 25) or p53. The effectors are responsible for arresting the cell cycle at G1/S, intra-S and G2-M cell cycle checkpoints to ensure sufficient time to repair the DNA [1]. CDC25 is a phosphatase that removes inhibitory phosphate residues from target cyclin-dependent kinases (CDKs), controlling in this way the entry and progression through the cell cycle. p53 is a central player in the transcriptional regulation of the cell cycle, apoptosis and senescence in response to DNA damage [8]. At the same time, ATM and ATR activate mediator proteins for the DNA repair such as BRCA1 or 53BP1 via post-translational modifications. More than 700 proteins regulated by ATM and ATR have been identified [10].

Because the DNA is packaged into chromatin, chromatin-remodeling factors are important to give access to the sites of DNA damage. Phosphorylation of the variant histone γ-H2AX by ATM or ATR allows accumulation of the chromatin master regulator MDC1 at DNA damage sites acting as a platform for DNA repair proteins. The repair proteins recruited by MDC1 accumulate in discrete foci at DNA repair sites and are a sign of active repair [10,11] (Figure 2).

Taken together, a multitude of factors are controlled through the DNA damage response to further mediate DNA replication, repair, cell cycle or apoptosis. In the following sections I will illustrate the different DNA repair pathways that are activated by the signaling cascade.

1.3 DNA REPAIR PATHWAYS

Several specialized pathways exist for the repair of particular lesions. However, some of these lesions are repaired by a combination of pathways (Figure 3). In this section I will shortly present the different repair pathways described. Afterwards, I will go into further detail for the recombinational repair of DSBs (HR) and the repair of stalled replication forks as the protein of interest of my thesis, BRCA2, is directly involved in these pathways. Note that the protein names mentioned belong to the human/mammalian systems.

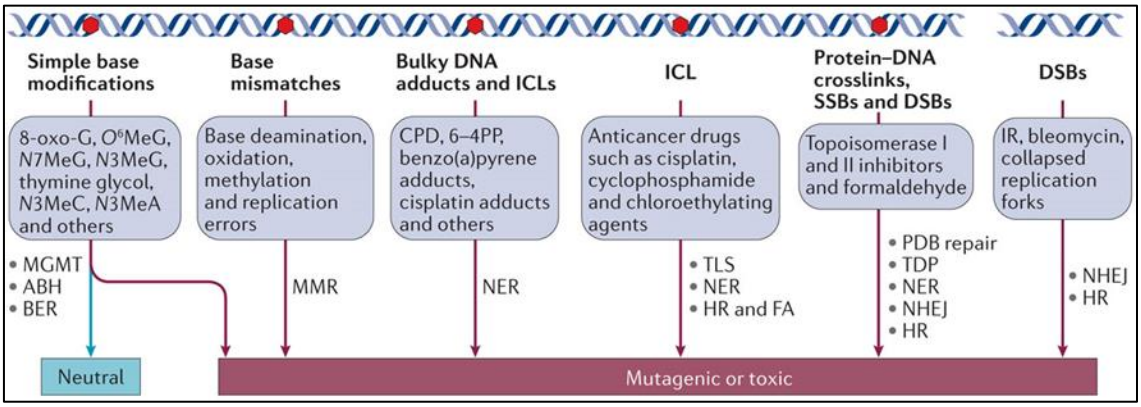

Figure 3: DNA damage repair mechanisms in response to various types of DNA lesions **(top)** originating from exogenous and endogenous sources (in blue boxes). Base modifications can be repaired by direct reversal by MGMT or ABH enzymes or by base excision repair (BER). Base modifications such as deamination or replication errors are corrected via the mismatch repair (MMR). Bulky DNA adducts can be removed by nucleotide excision repair (NER). For the elimination of inter-strand crosslinks (ICL), translesion synthesis (TLS), NER, fanconi anemia pathway (FA) and homologous recombination (HR) are used. Protein-DNA crosslinks are repaired by a combination of PDB repair, TDP enzyme, NER, NHEJ and HR. Double-strand breaks (DSBs) are removed via HR or NHEJ; single-strand breaks (SSBs) by a SSB or DSB repair pathway. Unrepaired DNA lesions are mutagenic or toxic for the cells. Adapted from Roos *et al.,* (2015)[248].

1.3.1 DIRECT REPAIR, BASE EXCISION REPAIR, NUCLEOTIDE EXCISION REPAIR AND MISMATCH REPAIR

Alkylating agents are a group of chemicals that are ubiquitously present in our environment. External alkylating agents can originate as nutritional byproducts, from tobacco smoke or pollutants. In the cells, they can arise from oxidative and biochemical reactions. Some cytotoxic agents are deployed as anti-cancer drugs since the beginning of therapy. Mono-or bifunctional alkylating agents react with the Nitrogen (N) or Oxygen (O) of DNA bases leading to simple or complex alkylated base lesions depending on the agent. Alkylating adducts in the DNA are usually N7-methyl guanine (7meG), N3-methyladenine (3meA) and O6-methylguanine (O6meG) that can give rise to mismatches during replication, depurination or replication arrest. Contingent on the kind of lesion, they can be repaired by several different repair processes [12] (Figure 3, left). By catalyzing the reversal of alkylated bases, simple modifications can be removed by **direct DNA repair (DDR)** with the help of O6-methylguanine DNA methyltransferase (MGMT) or members of the α-ketoglutarate-dependent dioxygenase family (ALKBH). Cancers with decreased *MGMT* expression are a suitable target for alkylating drugs [13]. If not repaired before replication starts, O6-methylguanine (O6meG) will be reversed by the **mismatch repair (MMR)** system after the first genome duplication or by nucleotide excision repair [12] (Figure 4D).

Base Excision Repair (BER) is the major pathway to remove deaminated, oxidized or alkylated bases and to repair single-strand breaks (SSBs) resulting from endogenous ROS or exogenous sources such as ionizing radiation or alkylating agents [14]. As indicated by its name, the damaged bases are excised and the gap is filled with the correct bases to avoid mismatching and incorporation of an incorrect base during replication[15]. Abasic sites like uracil and hypoxanthine are caused by spontaneous hydrolytic deamination. Reactive oxygen species (ROS) oxidize DNA bases like guanine, leading to 8-oxoguanine, prone to mismatch with adenine. Also, some N-alkylations of DNA bases require the repair by BER, as well as UV-light induced thymidine dimers that can be excised by BER glycosylase, although the preferred mechanism is NER[16].

The excision of the damaged base is performed by mono- or bi-functional DNA glycosylases, a class of enzymes that catalyze the cleavage of the glycosidic bond connecting the DNA base with the backbone, leaving an apurinic or apyrmidinic (AP) site. Each of these glycosylases recognize a small subset of corrupted bases that are cleaved off from the sugar-phosphate backbone [2]. When single strand breaks are repaired by BER, PARP1 binds to the broken site and recruits polynucleotide kinase

(PNK) to create 5'-phosphate/3'-hydroxyl termini for BER. The APEI endonuclease nicks the strand at the abasic site. In the dominant 'short patch' repair pathway, the 5' sugarless residue is removed by DNA polymerase β and the correct nucleotide is filled in, followed by XRCC1-DNA ligase3-sealing of the nick (Figure 4b). The 'long patch' pathway uses DNA Polδ/ε and PCNA to displace the 3' strand by 2-10 nucleotides, the old strand is then cut by FEN1 endonuclease and the nick is sealed by DNA ligase1[16,17].

Mice defective in any of the genes coding for DNA glycosylases have often no or minor defects. In contrast, the deletion of the genes coding for the enzymes downstream the glycosylases display severe phenotypes or are not viable [15].

While base excision repair is responsible for minor base damages, **Nucleotide Excision Repair (NER)** removes a wide variety of bulky DNA lesions that distort the DNA structure:

UV light causes photolesions such as cyclobutane–pyrimidine dimers (CPDs) and 6–4 pyrimidine photoproducts (6–4PPs). Chemicals developing from endogenous or exogenous sources cause bulky adducts, while interstrand cross-links are induced by platinum drugs. For the removal of these lesions, two mechanisms exist that differ in the way the damage is recognized: Global Genome NER (GG-NER) and Transcription-Coupled NER (TC-NER) [18] (Figure 4C).

During GG-NER, the entire genome including also transcriptionally inactive genes is screened for irregularities in the DNA structure. The XPC-hHR23B complex recognizes helix distortions. The XPE/UVDDB complex assists in the recognition of mild lesions such as cyclobutane pyrimidine dimers. Binding of Xeroderma Pigmentosum complementation group C (XPC) to the lesions recruits the multifunctional transcription factor TFIIH. Transcription-coupled NER commences when the RNA polymerase II encounters a DNA lesion during transcription. Many protein factors are involved in TC-NER, among these the CSA–CSB proteins ubiquitylate RNA Pol II to target it for degradation and render the DNA lesion accessible for repair [19,20]. After the damage recognition, the stalled transcription apparatus recruits TFIIH and both GG-NER and TC-NER are channeled into a common repair pathway. The DNA damage is cut out by XPG 3′ and XPF–ERCC1 5′ nucleases and stabilized by XPG, XPA and RPA, surveilled by the TFIIH complex. The final gap-filling step of the lesions is achieved by the replication factors PCNA, replication factor C (RFC), DNA Pol δ, DNA Pol ε or DNA Pol κ and ligated by LigaseI or XRCCI-LigaseIII [18,19] (Figure 4C).

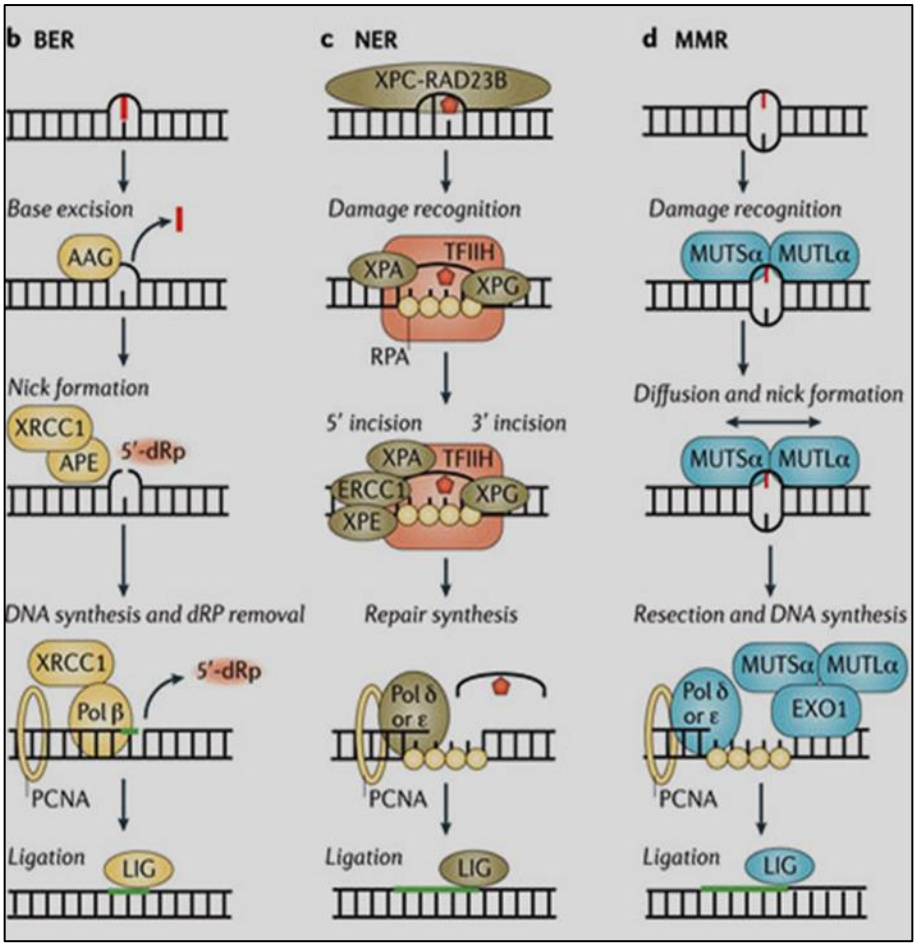

Figure 4: Mechanisms of BER, NER and MMR. **B)** A set of glycosylases (AAG) recognizes different kinds of damaged bases that are flipped out and cleaved off. Abasic sites are recognized by APE1 to nick the DNA. In short-patch BER, Polβ fills the nick and removes the 5‘ residue. DNA ligase3/XRCC1 complex seals the gap. **C)** In GG-NER, disrupted base pairs are detected by XPC-hHR23B complex, whereas TC-NER is activated when the RNA Pol II is stalled and replaced by CSB/CSA before recruitment of the TFIIH complex. The helicases of the complex unwind the DNA and XPF- ERCC1 cuts out the damaged piece so the replication machinery can fill the gap. **D)** In MMR, damage is recognized by MutS/MutL that nicks the DNA and recruits the EXO1 nuclease for strand resection. The ssDNA stretch is subsequently filled by polymerases and ligated. Adapted from Fu *et al*., 2012[12].

Many diseases are connected to defective NER; most of them predispose to an elevated cancer risk but also neurodegenerative disorders, highlighting the importance of this repair pathway.

Defective GG-NER repair forces the cell to use TLS, an error-prone pathway to over-replicate lesions (explained in replication stress chapter 1.3.2). The accumulation of mutations originating from TLS explains the high cancer incidence in Xeroderma Pigmentosum (XP) patients. They suffer from dry skin, abnormal pigmentation, photosensitivity and a 1000 fold risk to develop skin cancer induced by UV lesions. This is due to deficiencies in one or several XP genes coding for important NER factors. Cockayne-syndrome patients have a defective TC-NER and display a

moderate risk to develop skin cancer but show severe neurological disorders. In mouse models, defective NER has been connected with both cancer development and neurodegeneration, whereas in humans it was observed that mutations in GG-NER genes predispose to cancer and defective TC-NER to neurological disorders [18–20]. The **DNA mismatch repair** (MMR) is a mechanism to correct erroneous incorporated (mismatched) bases during replication and also mismatches arising from base alkylations such as O6meG that mispair with thymidine in replication [12]. During normal replication, polymerases are highly precise and possess a proofreading mechanism to excise wrongly incorporated bases. However, when the replication is blocked, translesion synthesis polymerases that are more prone to insert wrong bases over-replicate the lesions. In eukaryotes, the enzyme MutSα recognizes the mismatch in the discontinuous strand, which is then nicked by the MutLα endonuclease.

The EXO1 exonuclease removes the segment including the mismatch while the exposed ssDNA strand is stabilized by RPA. With the help of PCNA, DNA polymerase δ synthesizes the missing piece and DNA ligase I re-ligates the 5’ and 3’ ends (Figure 4d) [21–23]. Defects in the MMR system increase spontaneous mutations up to 1000 fold causing base substitutions and recombination between sequences that are not exact homologous. A defective mismatch repair often gives rise to hereditary nonpolyposis colon cancer (HNCC) as well as sporadic tumors in different tissues [24].

1.3.2 DNA DAMAGE-ASSOCIATED REPLICATION STRESS

The genome has to be duplicated accurately during replication to avoid genomic instability. The DNA is especially vulnerable during S phase because DNA lesions and other obstacles such as telomere ends, the transcription machinery or DNA secondary structures can interfere with the progression of the replisome leading to stalled replication forks. The resulting **replication stress** triggers the S-phase checkpoint to put the cell cycle on hold until the problem is solved.

The blockage of replication forks leads to the uncoupling of the strand synthesis and the continuous activity of the MCM helicase, leaving long stretches of ssDNA behind that are subsequently covered by RPA to protect them from degradation by nucleases. The ssDNA-RPA complex is the signal to activate ATR-ATRIP kinases that

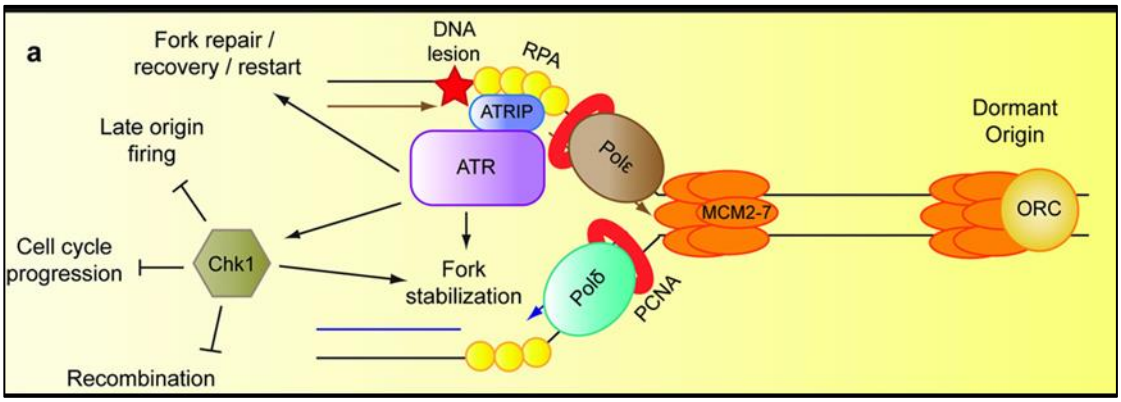

Figure 5: Events at stalled replication forks: When the replication machinery encounters a DNA lesion (red star), DNA synthesis can resume downstream, generating a ssDNA-RPA stretch that is recognized by ATR/ATRIP. ATR then initiates a signaling cascade primarily mediated by the effector kinase CHK1. The signaling promotes fork stabilization, repair and restart, while preventing progression through the cell cycle, late origin firing and recombination until the damage is removed and replication can resume. Adapted from Zeman & Cimprich, 2014[4].

phosphorylate downstream components for the stabilization of the fork, activation of fork repair and restart, the arrest of cell cycle progression but also the activation of dormant origins nearby [25,26] (Figure 5).

Replication stress due to unrepaired DSBs extant from G1 phase or one-sided DSBs introduced at DNA nicks or abasic sites activates ATM or ATR after resection by endonucleases [26,27]. If the lesion cannot be repaired and replication is not resumed, the replication fork is considered as collapsed, the stalled fork structure is probably degraded but the replisome remains chromatin-associated [28].

The recovery of the fork can occur via several pathways (Figure 6): When the damage resides at the leading strand, the lagging strand synthesis can continue and a Translesion synthesis (TLS) polymerase over-replicates the damage on the leading

strand, leaving it to be repaired at a later time point by the post replication repair (PRR) [29] (Figure 6, left).

TLS polymerases are recruited by the monoubiquitination of PCNA on Lys164 by Rad6Rad18 once the replication fork stalls. In contrast to the replication polymerases, TLS polymerases display low fidelity and low speed but can accommodate base adducts into their active site, allowing the replication to continue. The TLS polymerase bypasses the lesion after polymerase switching and either the same or a different polymerase extends the strand before the polymerase is once more swapped to a high-fidelity DNA polymerase to continue replication [26,30]. Loss of the TLS polymerase Pol η triggers the development of a type of Xeroderma Pigmentosum leading to cancer susceptibility [4].

Homologous recombination (HR) is required to repair one-sided DSBs originating from stalled replication forks or from ssDNA nicks or gaps (Fork incision, Figure 6, bottom). End resection of the ssDNA is followed by strand invasion into the homologous sister chromatid by RAD51 nucleoprotein filament, DNA pairing and resolution of a Holliday junction [25,31]. For an extensive description of the HR pathway and its factors involved, please refer to the homologous recombination section (1.4).

In addition, the high-fidelity polymerase might reprime replication downstream the lesion, leaving a “daughter strand” ssDNA gap. This gap can either be filled by TLS polymerases or also repaired by HR (template switching, daughter strand gap repair). This error-free bypass of the lesion occurs via template switch where the newly synthesized sister chromatid is used as a template [26,29,32] (Figure 6, bottom).

Which factors influence the choice between TLS and template switching as a mechanism for damage avoidance is not clear yet. While the repair by HR is more accurate and less error-prone, the formation of DSBs also endangers the DNA as it can give rise to dangerous lesions if misregulated. It was suggested that TLS is the preferred pathway during recombination as PCNA polyubiquitiylation has been less observed than monoubiquitylation[33].

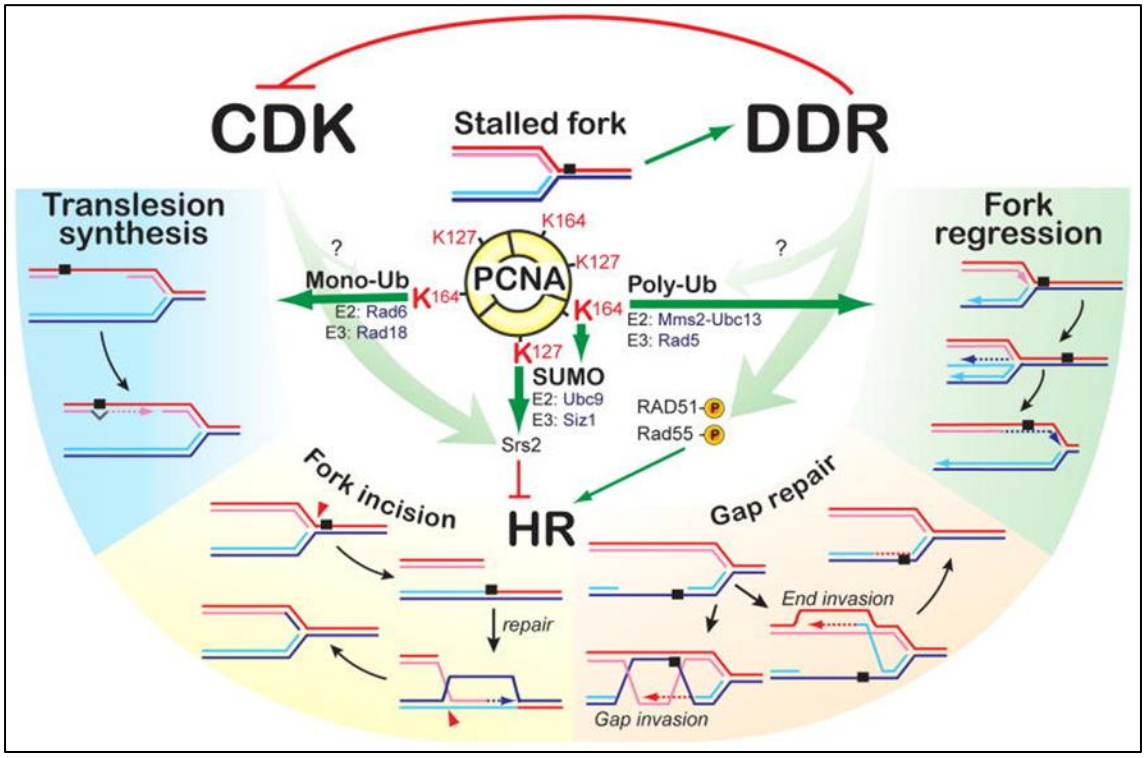

Figure 6: The DNA damage response (DDR) for the recovery of stalled replication forks and cell cycle arrest. The pathway choice is regulated by PCNA modifications. The stalling leads to downstream reinitiation of the polymerase, leaving a daughter strand gap that can be filled by translesion synthesis **(left)** or homologous recombination via template switching to avoid the damage (gap repair). Incision of the fork leads to a one-sided DSB that can be repaired by HR **(bottom).** The fork can also regress and the opposite strand is used as a template for replication until the lesion is repaired or bypassed by branch migration **(right)**. Adapted from Heyer *et al.,* 2010 [32].

Fork regression is induced by polyubiquitilation of PCNA Lys163 by the Rad5/Ubc13/Mms2 ubiquitin ligase complex leading to a rearrangement of the fork promoted by RecQ helicases [34] (Figure 6, right). The fork can be reversed to push back the damage into the duplex region making it accessible for DNA repair by unwinding the leading and lagging strand. The replication fork is regressed by using the newly synthesized daughter strand of the undamaged sister chromatid as DNA template. This so-called “chicken foot” structure is similar to that of a Holliday junction and can be cleaved by the endonuclease MUS81, resulting in a single-ended DSB that is repaired by HR. Alternatively, the reversed fork is restarted behind the lesion via branch migration by helicases like RAD54 [25,29].

Stalled replication forks are protected by RAD51 that forms a nucleoprotein filament at newly replicated forks that are stuck or reversed, preventing the newly synthesized ssDNA from degradation by the endonuclease MRE11. BRCA2 stabilizes this RAD51 nucleoprotein filament by interaction with its C-terminal RAD51 binding domain. Once the obstacle is removed, the replication machinery can progress to complete genome

duplication. The BRCA2-RAD51 interaction is then disrupted by CDK1/2 phosphorylation which allows entry into mitosis [35].

Although the exact mechanisms and pathway choices for the removal of replication stress have not been completely elucidated yet, it is evident that replication stress is a primary driver of genetic instability and early onset tumorigenesis, for example in colorectal cancer [36]. Unrepaired, non-fully replicated DNA leads to intertwined chromosomal segments (anaphase bridges) or chromosomal breaks that impair the proper segregation of the chromosomes in mitosis. Aberrant structures like lagging and acentric chromosomes or chromatid pieces get embedded in their own nuclear envelop which are transferred to daughter cells as extranuclear bodies (micronuclei), giving rise to genetic loss. To allow proper repair of chromosomal lesions these structures together with DNA repair proteins can be sequestered in 53BP1 inclusion bodies and transferred into G1 phase [25,37].

1.3.3 INTERSTRAND CROSS-LINK REPAIR

Interstrand cross-links (ICL) are caused by toxic agents used in cancer therapy such as cisplatin or mitomycin C but can also occur during metabolic reactions in the cell. They pose a toxic barrier for replication and transcription as they hinder the unwinding of the DNA by helicases [28]. ICL induce the linkage of bases of the opposite strands that are impossible to remove without specialized repair mechanisms. Unresolved interstrand cross-links lead to chromosome rearrangements, breakage and cell death [38]. Sensitivity to ICLs is also characteristic of the pediatric cancer predisposition syndrome called Fanconi anemia, which is marked by bone marrow failure, developmental defects, and a high incidence of cancer [39].

The pathway to repair ICLs depends on the mode of lesion recognition. In non-replicating cells, ICLs are repaired by NER. The lesion is first recognized by XPC-HR23B-centrin complex or when the transcription complex encounters the lesion. XPF-ERCC1 and XPG endonucleases cut on either side of the ICL (unhooking) and the resulting gap is filled by TLS polymerases. This initiates the second cycle of repair by NER, the excision of the flipped-out overhang by XPF-ERCC1 and gap filling by DNA polymerases and Ligase 3 [40]. The recombination-dependent ICL repair pathway (FA pathway) acts in S or G2 phase, when the lesion is recognized upon stalling of the replication fork. This complex repair pathway includes NER, HR and TLS. Many proteins participate in this process; shortly, FANCM recognizes the ICL and associates with the FA core complex (group I) constituted of seven of the FA proteins. Subsequently, FANC1 and FANCD2 (group II) are ubiquitylated to recruit other

recombination proteins required for the repair process: RAD51, RAD52, RAD54, BRCA1, as well as the FANCN (PALB2), FANCJ (BRIP1) and BRCA2 (FANCD1) (group III) for stabilization of the complex. At the same time, FANCD2 and FANCI factors bind endonucleases for the removal of the cross-link, TLS synthesis and repair of the lesion by HR [40,41].

1.3.4 DNA-PROTEIN CROSS-LINK REPAIR

The interaction between proteins and DNA is required for all forms of cellular processes. When these DNA-protein interactions are trapped by cross-linking of the protein with the DNA, they become highly toxic DNA adducts (DNA protein cross-links; DPCs) which need to be removed. Enzymatic DNA-protein cross-links arise when enzymes such as topoisomerase, glycosylase or polymerase transiently bind to the DNA and their release is inhibited by structural changes in the DNA or small molecules. Non-enzymatic DPCs can result from random protein-DNA interactions that are cross-linked by potent endogenous or exogenous agents such as formaldehyde, acetaldehyde or irradiation. These bulky DNA adducts inhibit the progression of transcriptional or replication machinery and if left unrepaired, cause sister chromatid exchange, micronuclei and gross chromosomal rearrangements [42]. Due to the high diversity of possible DPCs, several repair pathways are implicated in their repair. Tyrosyl-DNA phospho-diesterase 1 (TPD1) and tyrosyl-DNA phospho-diesterase 1 (TDP2) remove topoisomerase I and II adducts, respectively, by cleaving the tyrosine bond between the enzyme and the DNA [43]. MRE11 and CTB-interacting protein (CtIP) can remove DCPs at DSBs. Small DPCs can be repaired by the NER pathway. Stalling of the replisome can recruit the DPC protease that proteolyses the DPC and releases the stalled helicase but not the polymerase, leaving an ssDNA gap to be filled by TLS polymerases. In the absence of DCP protease, the fork stalls and is cleaved resulting in a single-ended DSB to be repaired by HR. Alternatively, the fork can converge with an incoming fork to unwind the DNA past the DPC or repair it by an ICL repair-like mechanism. When only the polymerase is stalled at the DPC, it is either removed by proteases and the ssDNA gap is filled by TLS or repaired by template switching as discussed for stalled replication fork repair above. Taken together, DPC proteases have been only recently shown to be a crucial measure for protection of the genome and are a potential target for cancer therapy [44].

1.3.6 DNA SINGLE-STRAND BREAK REPAIR

Single-strand breaks (SSB) occur frequently in the genome, most commonly through the oxidative attack of reactive oxygen species (ROS) on DNA bases or sugar residues, resulting in the loss of one nucleotide and damaged 5' or 3' termini [45]. SSB can also be produced during BER when abasic sites and oxidized or damaged bases are removed. It was also shown that abortive topoisomerase I functioning result in SSBs as well as ribonucleotides erroneously integrated into the DNA [46]. In S-phase, replication stress is induced when the fork stalls at SSBs, usually leading to the formation of one-ended DSBs that are repaired by HR. Even though SSBs can either arise from different sources, the enzymes responsible for the repair have similar mechanisms: Detection of the SSB, DNA end processing, gap filling and ligation [45].

When the sugar residue is damaged, SSBs are recognized by Poly-ADP ribose polymerase 1 (PARP-1), an enzyme that catalyzes the transfer of Poly (ADP-ribose) chains to itself and to other proteins activating the SSB repair pathway. Indirect SSBs that occur during BER do not require PARP1 for detection as they are directly channeled to DNA end processing when APE1/lyase remains bound to the abasic site. SSBs emerging in ribonucleotide excision repair or resulting from abortive topoisomerase I cleavage activity are assumed to also be recognized by PARP1.

The DNA end-processing complex to resect damaged 5' or 3' ends is either recruited by APE1 and Polβ or via PARP1 and XRCC1. It involves many repair enzymes including APE1, Polβ, PNKP, APTX, and TDP1. Once the damaged 3' or 5' end is restored, the gap can be filled by short-patch (one nucleotide) or long-patch (several nucleotides) repair. The polymerases that are implicated in gap filling are Polβ, δ and ε. In long-patch repair, FEN1 removes the 5' nucleotides. Ligase 1 and 3, stabilized by XRCCI and PCNA, respectively, are the gap filling enzymes to complete SSB repair [45–49]. Given that SSB are the most common DNA damage (up to 10.000 lesions per day/cell), it is not surprising that defects in SSB repair proteins such as XRCC1 and Polβ are connected to cancer. Ataxia-oculomotor apraxia 1 and Spinocerebellar ataxia with axonal neuropathy 1 are inherited neurological disorders with mutations in genes involved in the SSB repair pathway [46].

1.3.7 DNA DOUBLE-STRAND BREAK REPAIR

DNA double-strand breaks (DSBs) are among the most toxic and mutagenic lesions and if not repaired, lead to chromosome loss or fragmentation, gross chromosomal rearrangements and genetic instability. In addition, in higher organisms, the HR

pathway is also necessary in meiosis I.[50]. A DSB is considered as a breakage of the phosphor-sugar backbones of two DNA strands at the exact same position or in close proximity leading to the dissociation of the double helix [51].

The sources for the breakage of the DNA double-strand are diverse: exogenous sources like ionizing radiation (IR), radiomimetic drugs such as alkylating agents and crosslinking agents, or topoisomerase inhibitors used for cancer therapy.

Endogenous agents causing DSBs include metabolically created reactive oxygen species (ROS), stalled replication forks or when telomeres become critically shortened [52,53].

Besides the classical two-ended DSBs arising during the cell cycle by direct fracture of the DNA (Figure 7A), other forms of DSBs are produced during replication. When the replication fork stalls at unrepaired SSBs, they can be transformed into one-ended DSBs to be repaired by HR (Figure 7B). Likewise, daughter strand gaps can arise when the DNA synthesis is resumed after a lesion in the context of the replication fork (Figure 7C) [50]. To maintain genome stability, the DSBs have to be faithfully repaired for which the cells have evolved highly specialized mechanisms; the DNA repair pathway involved will depend on the phase of the cell cycle.

So far, four pathways for the repair of DSBs have been described: classical non-homologous end-joining (c-NHEJ), homologous recombination (HR), single-strand annealing (SSA) as well as a recently discovered pathway called mirochomology-mediated end joining (MMEJ) or alternative end-joining (a-NHEJ) [54].

As described in Chapter 1.2, after the recognition of a DSB, the DNA damage response is activated via the ATM/ATR signaling cascade by phosphorylation of downstream mediators and effector kinases to regulate cellular processes including

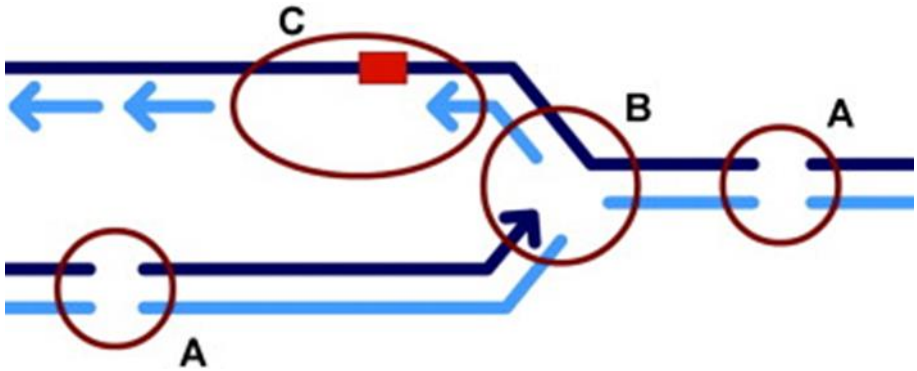

Figure 7: Origins of DNA substrates for the recombinational repair. **A)** Direct DSBs arise from fractures of the dsDNA**. B)** One-sided DSBs can be created when the replication machinery stalls at DNA lesions. **C)** A DNA lesion can be bypassed by the replication machinery and the daughter strand gap will be repaired by postreplicative recombinational repair. Adapted from Helleday *et al*. 2007[50].

DNA repair, cell cycle progression and apoptosis.

Classical **non-homologous end-joining (c-NHEJ)** can operate throughout the cell cycle as it does not require a homologous template or further DNA end resection for initation of the repair. DNA end resection is normally restricted to S/G2 phases and controlled by CDKs. During G1 and M phase, c-NHEJ is the primary pathway of choice [55,56].

The c-NHEJ process starts when a blunt DSB end is recognized by the Ku70/80 heterodimer (KU) that binds to the DNA termini and recruits the catalytic subunits of DNA-PK. Phosphorylation by DNA-PK assembles enzymes such as XLF-XRCC4 scaffold proteins for the stabilization of DNA ligase 4 to ligate the DSB ends. This results in a loss of nucleotides and can be mutagenic. If the 5'-3'-termini cannot be aligned directly, the endonuclease Artemis is recruited to process the ends and allow ligation [54,57] (Figure 8A). When Ku recognition of the DSB is inhibited in S/G2 phase, the DSB is first bound by the MRE11–RAD50–NBS1 complex (MRN complex), recruiting ATM to phosphorylate downstream targets. In contrast to NHEJ, the other DSB repair pathways rely on the resection of the 3' end as well as the assembly of the BRCA1-PALB2-BRCA2 complex. The ubiquitylation of PALB2 by G1 factors inhibits the complex assembly with BRCA1 while deubiquitilyation in S-phase allows the repair by HR [58].

Alternative end-joining (a-NHEJ) or **microhomology mediated end joining (MMEJ)** was thought to be a back-up pathway to repair DSBs when the canonical NHEJ pathway was not available. Since recently, a-NHEJ is known to be active in cells proficient of c-NHEJ which points to differential activation of these pathways depending on the cell cycle state [54].

Ku protein has a higher propensity for the association with DSBs than PARP-1 and thus determines the pathway choice between c-NHEJ and a-NHEJ. Moreover, in G2/S phase, the decision for HR or a-NHEJ depends on the resection state. Extensive resection by EXOI/BLM DNA2 complex favours HR whereas short resection by CtIP/MRE11 channels into the a-NHEJ pathway [59]. It is assumed that PARP1 is responsible for the detection of the DSB whose ends are subsequently bound by the MRN complex. MRE11 and CtIP are then required for the 5' and 3' resection, respectively.

In a-NHEJ, the DNA ends are joined together thanks to the presence of microhomologies. This pathway is highly mutagenic, leading to large deletions/insertions or chromosome translocations [54]. For the successful end-joining, microhomologies of 1 nt are already sufficient to anneal with the complementary strand. If the annealed product is stable, the overhangs are directly cut by endonucleases. Otherwise flanking single-stranded regions require fill-in synthesis which is probably achieved by the TLS polymerase theta (Pol θ). The resulting flap

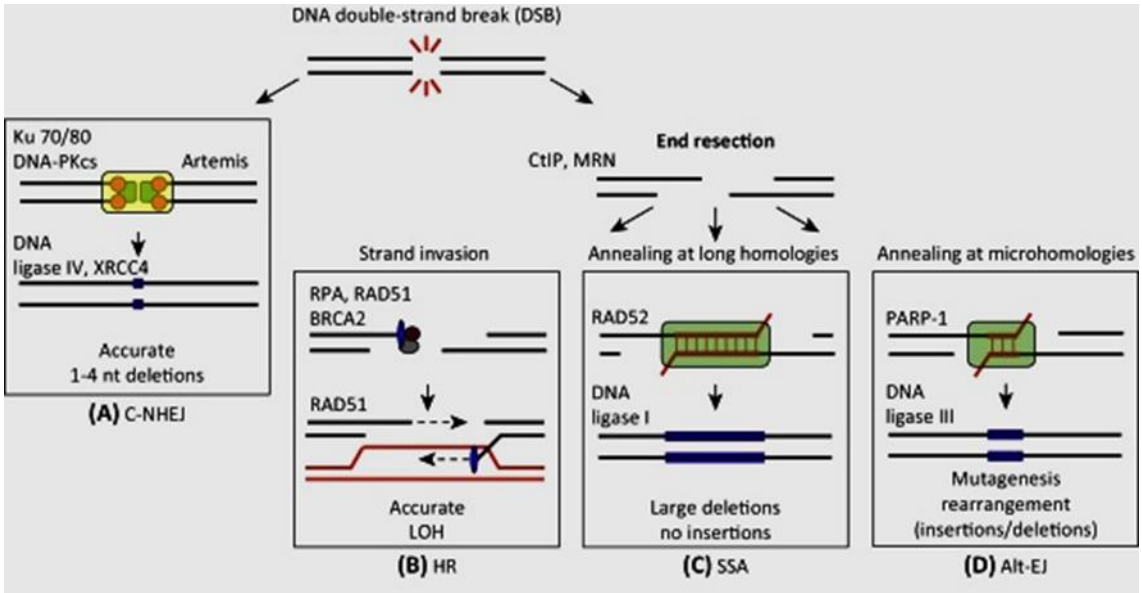

Figure 8: DSB repair pathways. End resection of the DSB occurs primary in G1/S phase and determines pathway choice. **A)** Blunt DSBs can be repaired via NHEJ in G2/M phase when no homologous template is present. 3' end resection of the DSB channels into HR, SSA or Alt-EJ. Here the pathway is chosen dependent on the resection state. **B)** Extensive resection initiates HR that blocks the SSA way **(C)**. Short resection induces the Alt-EJ pathway **(D)**. Adapted from Ceccaldi *et al*., 2016[55].

overhangs have to be removed by endonucleases and the ends are ligated using the XRCC1/Ligase III complex [54,55,57,59].

Extensive resection by helicases coupled to nucleases generates long stretches of ssDNA that can be annealed by **single-strand annealing (SSA)** [60] (Figure 8C). The DSB ends are resected until homologous regions on both sides of the breaks are exposed. RAD52 promotes the annealing of the complementary ssDNA/RPA complexes. The non-homologous overhangs are removed by XPF/ERCC1, leading to deletion of long stretches of DNA that can cause genomic instability like translocations or chromosome fusions [32,61,62]. SSA is a RAD51-independent pathway and is blocked by the proteins involved in HR when the two pathways compete for the resected DNA ends [63].

Homologous recombination (HR) is considered as one of the most reliable ways for DNA repair and executes also other biological roles. HR 1) is critical for DNA double-strand break repair arising from exogenous and endogenous sources 2) rescues stalled replication forks by repairing ssDNA breaks, gaps and one-sided DSBs. 3) provides telomere maintenance and 4) is essential for meiotic recombination by generating cross overs [64] (Figure 9). The notion that HR is important for the repair of DSBs comes from studies with *Rad51* deficient mice that exhibited embryonic lethality [65]. Here I will separately discuss the roles of HR in its different biological functions and go into further detail about the mechanisms of HR for DSB for which BRCA2 is needed.

1.4 REPAIR OF DNA DOUBLE-STRAND BREAKS BY HR

The defining step of homologous recombination is the invasion of the damaged strand into a homologous template, either the sister chromatid or homologous chromosome to prime DNA synthesis [66]. As mentioned in S/G2 phase, HR is the pathway of choice for the repair of DSBs over c-NHEJ. After recognition of the break, the ATM kinase activates a signal cascade that initiates DSB repair and regulates the cell cycle. The committing step into HR (pre-synapsis) is the resection of the DSB at the 5' end to produce 3' ssDNA overhangs by the MRN complex (MRE11/RAD50/NBS1) and CtIP. MRN recruits BLM helicase-DNA1 helicase/nuclease or EXO1 exonuclease-BLM complexes to extensively resect the DNA [67]. The ssDNA binding protein RPA binds to the exposed stretches of ssDNA, thus preventing secondary structures and unwanted

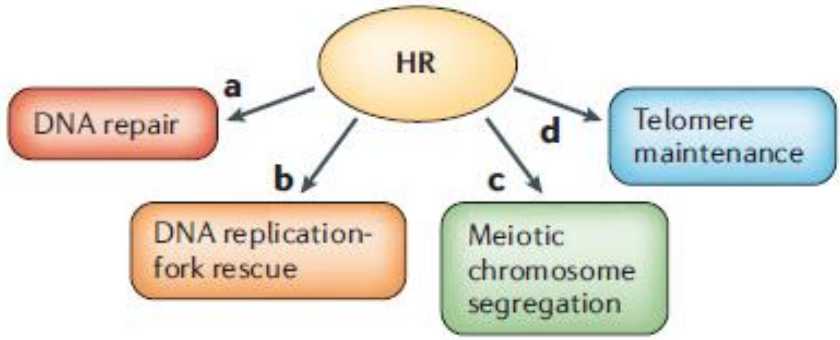

Figure 9: Homologous recombination is required in **A**) repair of DNA double-strand breaks during G2/S phase in mitotic cells when a template is available **B**) the rescue of stalled replication forks at DNA breaks **C**) meiotic recombination of programmed DSBs to ensure segregation of the chromosome homologues **D**) the maintenance of telomere ends to avoid telomere shortening. Adapted from Sung & Klein, 2006 [64].

resection. Subsequently, ATR phosphorylates its targets for activation of DNA repair such as BRCA1 or 53BP1 [66,67]. RPA-coated ssDNA poses a kinetic barrier that has to be overcome by the central recombinase RAD51 to access the DNA and start the HR process [61]. HR mediator proteins including BRCA2 and the RAD51 paralogs are needed to ensure RAD51 binding to and filament formation on the ssDNA. Cells deficient of the central mediator protein BRCA2 are highly sensitive to DNA damage, reflecting its importance in HR [68]. Shortly, BRCA2 binds RAD51 via its BRC repeats to facilitate binding and nucleation on the ssDNA [69–72]. For an extensive description of BRCA2 function, please refer to Chapter 1.7. In humans there exist five RAD51 paralogs with sequence similarity, but without recombination activities that form two complexes: RAD51B/RAD51C/RAD51D/XRCC2 and RAD51C/XRCC3. Their exact role in HR is not known but it is assumed that the complexes exist to stabilize the RAD51

filament formation in response to DNA damage. Mice deficient in one of the *RAD51* paralogs are also embryonically lethal. However, cells depleted of the paralogs are less sensitive to DNA damage than cells deficient of *BRCA2*. Hence, RAD51 paralogs together with BRCA2 stabilize the RAD51 filament formation by blocking RAD51 association with dsDNA and allowing it to nucleate on the ssDNA [61,73–75].

During synapsis, the second stage of HR, the RAD51 filament starts homology search and once it is found, invades the homologous template strand, either the sister chromatid or a homologous chromosome [76–78]. RAD51 associates with the motor protein RAD54 that functions to translocate RAD51 along the filament, remodel the chromatin and to open of the duplex DNA using its ATPase activity. Invasion of RAD51-ssDNA nucleoprotein filaments into the dsDNA results in the formation of a heteroduplex displacement loop (D-loop). In post-synapsis, DNA synthesis is primed from the 3'end of the invading strand and extended with PCNA by TLS DNA polymerases (Figure 10) [32,76–79]. The dissolution of the extended D-loop can be achieved by three different pathways: double Holliday Junction (dHJ) subpathway, synthesis-dependent strand annealing (SDSA) or break-induced replication (BIR) (Figure 10).

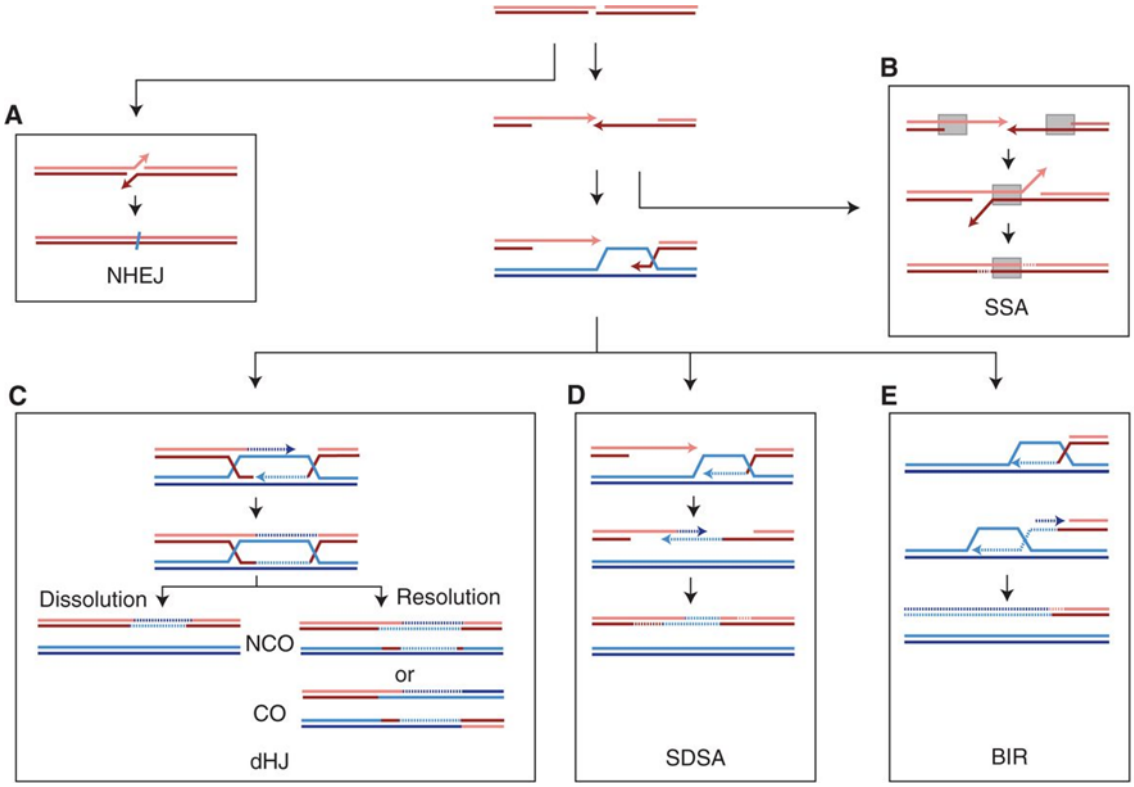

Figure 10: DNA double-strand break repair pathways. The DSBs are resected resulting in a 3' ssDNA overhang. **A)** NHEJ can ligate the blunt ends **B)** SSA anneals flanking homologous regions, resulting in a loss of DSB ends. Homologous recombination can occur via **C)** double-Holliday Junction pathway, where the invading strand captures then second end on the opposite site to stabilize the D-loop. It is then dissolved by helicases and topoisomerases resulting in non-crossovers (NCO) or resolved by endonucleases which can result in cross-overs (CO) or non-crossovers (NCO). **D)** In synthesis-dependent strand annealing (SDSA), the newly synthesized strand dissociates and is ligated. **E)** break-induced repair (BIR) is required for the repair of one-ended DSBs (e.g. in replication). A new replication fork is established at the D-loop for DNA synthesis. The new strand is then used as a template for lagging strand synthesis, resulting in loss-of-heterozygosity. Adapted from Metha & Haber, 2014 [81].

In the double Holliday Junction (dHJ) pathway, the invading strand of the D-loop captures with and connects the end of the non-invading strand to form a double Holliday Junction intermediate. This branched structure migrates in the direction of DNA synthesis for which the invaded sister chromatid is used as a template. After DNA synthesis, the dHJ can either be dissolved by BLM-helicase TOPOIIIα-RMI/2 topoisomerase complex resulting in a non-crossover structure. Resolution by the endonucleases GEN1, MUS81-EME1 or SLX1-SLX4 leaves a crossover leading to gene conversion that can facilitate genomic instability [32,50,80,81] (Figure 10C).

SDSA resolves the D-loop by the helicase BLM and the newly synthesized ssDNA strand anneals with the complementary ssDNA strand resulting in non-crossover with the homologous strand (Figure 10D). Non-crossovers avoid the hazard of genomic

rearrangements induced by dHJ or BIR, making SDSA the preferred subpathway [63,81,82].

When the second end is absent, one-ended DSBs resulting from stalled replication forks during replication or at telomeres are also repaired by a HR pathway, Break-Induced Replication (BIR). Here, the D-loop structure is resolved by nucleases and a replication fork is re-established that can migrate semi-conservatively, duplicating the missing arm and may ultimately result in loss-of-heterozygosity (LOH) [83–85] (Figure 10E).

The evolution of these highly specialized mechanisms can be explained by the catastrophic consequences for the stability of the genome when DSB break repair is defective. First, unrepaired DSBs are toxic lesions for the cell. Second, the accurate rejoining of the two ends of a DSB and the reinsertion of the one-ended strand in the replication process, respectively, are of upmost importance to avoid chromosome breaks, chromatid translocations, deletions, inversions or amplifications that ultimately provoke tumorigenesis [86]. In contrast, in meiosis, DSBs created by the endonuclease Spo11 activates genetic recombination between homologous chromosomes serve to generate genetic diversity which will be explained in detail in chapter 1.10[50].

1.5 TELOMERE MAINTENANCE

At telomeres ends, the reverse transcriptase telomerase adds TTAGGG repeats to compensate for the loss of genetic material due to the inability of the replication machinery to progress to the ends of the DNA on the lagging strand. These repeats tend to form G-quadruplexes, which block replication fork progression. The G-quadruplexes are unwound by the RecQ helicases WRN and BLM. Defects in these proteins are reflected by the cancer-prone disorders Werner's and Bloom's syndrome [87]. It is suggested that BRCA2 loads RAD51 to the telomeres for the formation of a T-loop (telomere loop) structure for protective telomere end capping [88]. In addition, BRCA2 protects the stalled replication fork at telomere ends from degradation by MRE11 in a way independent from DSB repair as it was shown before at replication forks outside the telomeres [35,89].

1.6 MEIOTIC RECOMBINATION

Meiosis is a specialized process in the germ line to produce haploid gametes. The homologous chromatids are duplicated by replication, followed by the exchange of genetic material during recombination. Two segregation phases, Meiosis I and Meiosis II separate homologous chromosomes and then the sister chromatids to obtain a haploid set of chromosomes in the gametes [90]. Recombination was initially studied in Meiosis I where it is responsible for the exchange of maternal and paternal homologous chromosomes to generate diversity by crossovers. In addition, HR is important for the physical connection of the homologues, termed chiasmata, which ensure the proper orientation at the meiotic spindle before segregation to the opposite poles [91]. Meiotic recombination is initiated by the induction of a DSB by the topoisomerase-like protein Spo11 (Figure 11). Then, Spo11 is removed and exonucleases (MRN, CtIP, EXOI) generate the 3' ssDNA tail that will serve as HR substrate [90]. The central recombination protein in meiosis is DMC1, but the recombination proceeds as described in the HR section [83,90,92–94]. *DMC1* mutants show almost complete absence of meiotic recombination which is also the case for *RAD51* mutants, suggesting that both recombinases are needed for meiotic recombination events in non-overlapping functions [91,95]. Although it was known that DMC1 interacts with BRCA2, the exact contribution of BRCA2 in meiotic recombination was unclear. During my PhD, I collaborated in a project to address this question (see Chapter 4). I will go into further detail about the current knowledge about the role of BRCA2 in meiotic recombination in Chapter 1.10.

After completion of recombination and exchange of genetic material, cells undergo two meiotic divisions. First, the two homologous chromosomes segregate from each other in Meiosis I. Subsequently, the sister chromatids are pulled to the opposite spindle poles during Meiosis II, resulting in four genetically non-identical haploid gametes [96].

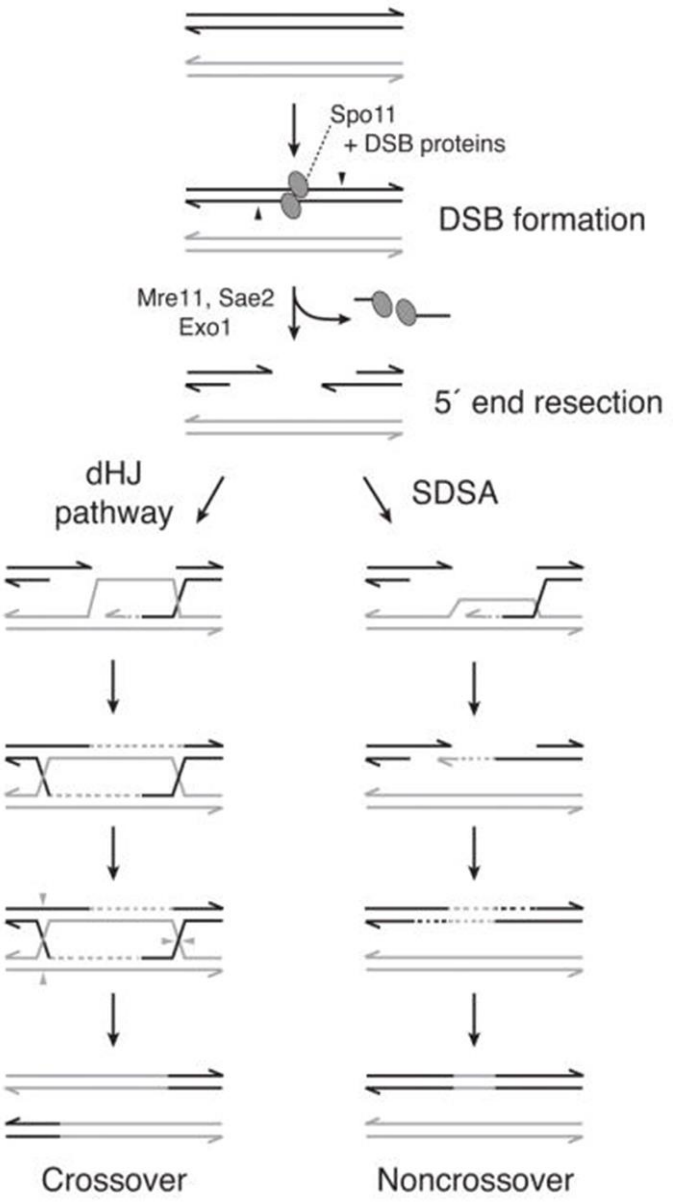

Figure 11: Mechanism of meiotic recombination. A DSB is created by Spo11. This allows resection of the 5' end by nucleases. The recombination protein DMC1 bind to the 3' ssDNA overhangs generated, perform strand invasion, homology search and strand exchange in the template strand to prime DNA synthesis. RAD51 is thought to play an accessory role in this context[95]. The outcome of strand exchange will depend on e the pathway, dHJ or SDSA. In the dHJ pathway, the invading strand captures the second end of the invaded strand to form a dHJ that is resolved leading to crossover products. In the SDSA pathway, the invading strand is displaced after DNA synthesis and anneals to the other end of the DSB, yielding a noncrossover. Adapted from Lam & Keeney, 2015[90].

1.7 BRCA2, A VERSATILE PROTEIN

BRCA2 (breast cancer 2) was discovered as a breast cancer susceptibility gene when individuals with heterozygous germline mutations in *BRCA2* were shown to have an elevated risk to develop breast, ovarian or pancreatic cancer. Mutations in *BRCA1* or *BRCA2* account for 15% of the genetic variants predisposing to breast cancer [97]. The first hints to BRCA2 function came from *Brca2* knock-out mice showing embryonic lethality as well as radiation and MMC hypersensitivity [68]. The analysis of chromosome spreads on these mice cells displayed a chromosomal abnormalities like chromatid breaks and translocations, implicating a defective DSB repair and involvement of BRCA2 in this pathway [98]. Shortly after, BRCA2 was found to interact with RAD51, linking the two proteins in the same pathway of DNA repair, Homologous Recombination (HR) [99].

As a caretaker of genomic maintenance, BRCA2 is involved in mechanisms to ensure faithful genome duplication during replication (S phase), the repair of DNA damage before entering mitosis (S/G2) as well as the proper segregation of the chromosomes and cytokinesis in M phase [100] (Figure 12). Moreover, BRCA2 is also involved in meiotic recombination and telomere maintenance (1.5; 1.6). In the following chapters, I

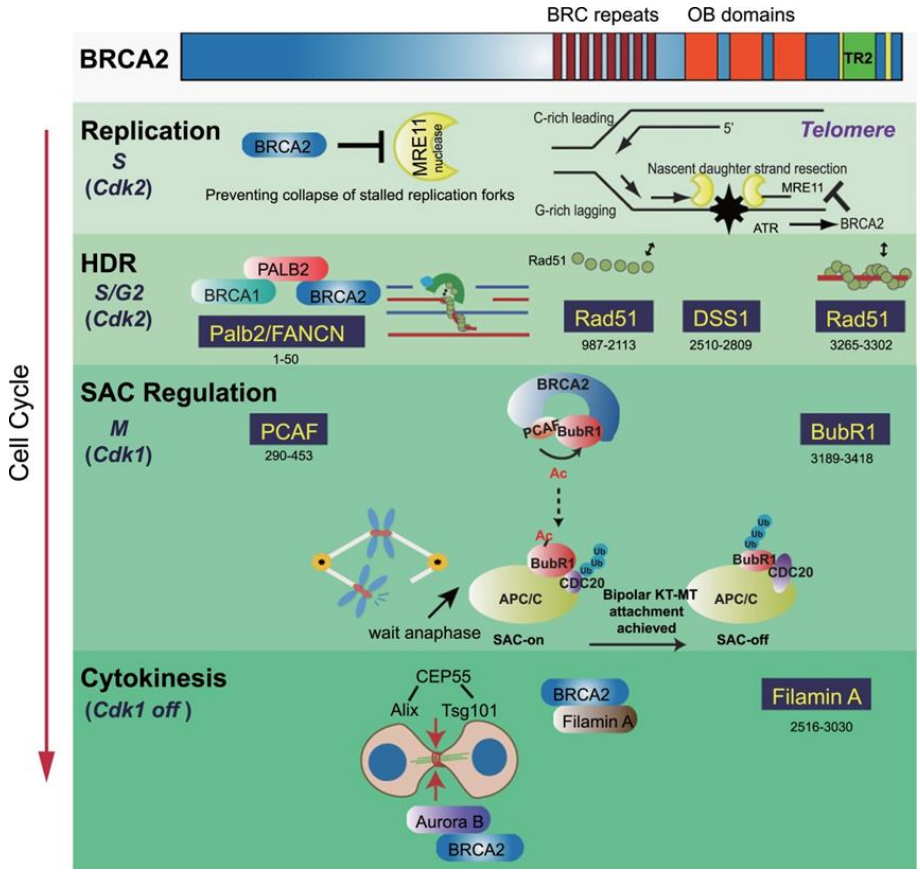

Figure 12: BRCA2 functions at various stages during cell cycle progression via via its numerous domains (numbers below correspond to the amino acid residues involved). Adapted from Lee, 2014 [100].

will explain how BRCA2 fulfills its versatile roles.

1.7.1 STRUCTURE, FUNCTIONAL DOMAINS, INTERACTION PARTNERS AND MODIFICATIONS OF BRCA2

The tumor suppressor protein BRCA2 is a large multi-domain protein consisting of 3,418 amino acids (390 kDa) that constitute 26 Exons of different sizes [101]. It has no sequence similarity to any other protein described and only little sequence conservation in evolution, making it difficult to predict the functions of the domains by *in silico* tools [102]. In addition, many regions of BRCA2 are predicted to be intrinsically disordered and do not show any folding patterns, this is especially the case for the N-terminal domain. The enormous difficulties to purify the full-length protein in sufficient quantities have hampered the investigation of BRCA2 by biochemical characterization for years. However, since the first successful purifications of BRCA2 in 2010 [70–72], it is

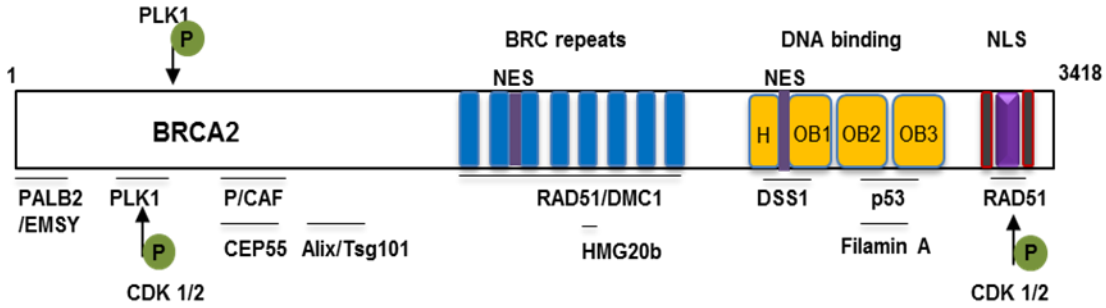

Figure 13: BRCA2 structure displaying its functional domains (in color) and its interaction partners (below) as well as posttranslational modifications (P). Details are described in the text.

possible to further study its individual domain functions and interaction partners in the context of the full-length protein. In my PhD project, I used the purification protocol developed in our lab to perform biochemical *in vitro* assays with full-length BRCA2 as well as with BRCA2 fragments. Indeed, as described in Chapter 1.14, the main project of my thesis aimed at identifying and characterizing new functional domains in the N-terminus of BRCA2.

Here, I will briefly discuss the current knowledge of BRCA2 functional domains and interaction partners. A more detailed description of the functions in the different pathways for the domains and interactions of BRCA2 described here can be found in the related chapters.

The N-terminus comprises the first 1000 amino acids of BRCA2 and there is very little information about its function (Figure 13). Applying BRCA2 aa 1-1000 to FoldIndex software [103] reveals that half of the N-terminus is predicted to be intrinsically disordered. The prediction of its function based on sequence or domain conservation is

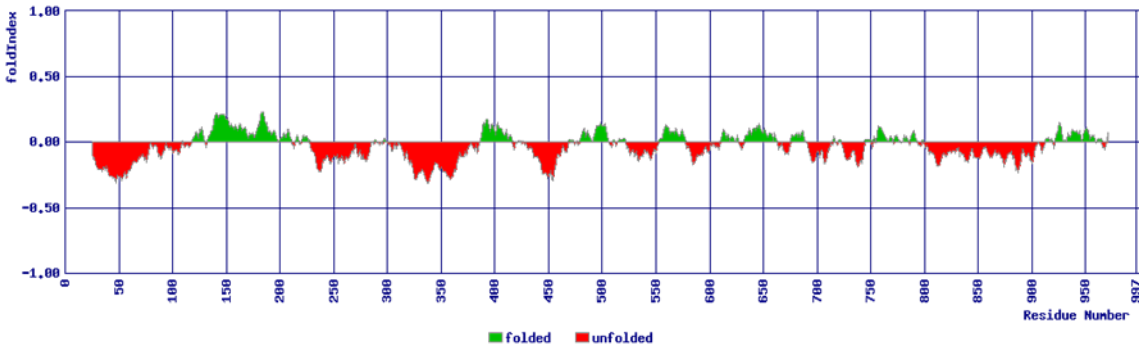

Figure 14: Probability of folding of BRCA2 amino acids 1-1000 as predicted by FoldIndex. BRCA2 is highly disordered (red) and bears only some folded regions (green). FoldIndex Webtool kindly provided by Prilusky *et al*., 2005[103].

hence much more challenging [104] (Figure 14). Most of the known functions of the N-terminal region come from studies with its interacting partners.

PALB2 (Partner and Localizer of BRCA2) (PALB2) was identified in immunoprecipitation studies and shown to form a complex with BRCA1 and BRCA2 required for their localization to the nucleus. This PALB/BRCA2/BRCA1 complex stabilizes BRCA2 to exerts its HR function [105,106]. The interaction site with BRCA2 was mapped to the first 40 amino acids of the N-terminus, where missense mutations have been found, pointing to the importance of PALB2/BRCA2 interaction in HR. Indeed, the depletion of *PALB2* leads to DNA damage hypersensitivity and PALB2 is also considered as a tumor suppressor protein as it has been found mutated in tumors [106,107]. In vitro, PALB2 cooperates with BRCA2 to promote homologous DNA pairing by RAD51 [108,109]. Cells expressing either BRCA2 truncated at the N-terminus or C-terminus show a milder phenotype in response to genotoxic agents than cells expressing BRCA2 lacking both termini, suggesting that the recruitment of BRCA2 to the chromatin by PALB2 may compensate for the absence of BRCA2 C-terminal domain [109]. However, the results in the work presented here show that the lack of the C-terminal DNA binding domain might be compensated by a novel DNA binding domain in the N-terminal region (Chapter 2).

The PALB2 interaction site at the extreme N-terminus is shared with the transcriptional repressor EMSY that suppresses BRCA2 transactivation activity located in exon 3 [110]. EMSY's amplification has been observed in sporadic breast cancer suggesting a link between *BRCA2* and these types of cancers[111].

Downstream the primary sequence lays the Polo-like kinase 1 (PLK1) interaction site at amino acid T77. PLK1 phosphorylates BRCA2 at residue S193 and this phosphorylation is important in mitosis [112,113]. Phosphorylated BRCA2 is recruited to the midbody where it interacts with Myosin IIC [114]. The binding of PLK1 to T77 is regulated by CDK1/2 kinases and subsequently brings RAD51 in complex together with BRCA2

to ensure repair of DNA damage before entering mitosis [115]. Residues 290-453 of BRCA2 specifically interact with the transcriptional co-activator P/CAF that exhibits histone-acetyltransferase activity [112,116]. BRCA2 acts as a scaffold for P/CAF and BUBR1, an important player for the Spindle Assembly Checkpoint (SAC) at the kinetochore. Acetylation of BUBR1 by P/CAF activates the SAC ensuring proper chromosome segregation once they are aligned [117]. The midbody proteins CEP55, Alix and Tsg101 were found to immunoprecipitate with a BRCA2 fragment of amino acids 271-836. These proteins interact at the midbody for the formation of the contractile ring facilitating abscission to complete cytokinesis. Depletion of any of these factors causes multinucleation. BRCA2 depletion leads to disruption of localization of Alix and Tsg101 to the midbody as well as the interaction of CEP55 with these proteins causing defects in cytokinesis [118].

The central region of the protein harbors the BRC repeats as well as one nuclear export signal (NES). The NES is responsible for the export of BRCA2 together with chromosomal region maintenance 1 protein (CRM1) from the nucleus to the cytoplasm to regulate centrosome duplication during mitosis. Depletion of the NES causes centrosome amplification [119].

The BRC repeats span the central region of the protein between amino acids 1009 and 2082. They constitute the principal RAD51 interaction site with BRCA2 and all possess a similar sequence motif of about 35 amino acids [101,120]. The sequence fingerprint of the amino acids that interact with RAD51 in the BRC repeats is highly conserved among BRCA2 orthologs, emphasizing their importance in HR [99,121,122]. BRCA2 association with RAD51 monomers via the BRC repeats promotes RAD51 binding to ssDNA over dsDNA for the promotion of unidirectional nucleoprotein filament formation of RAD51. The first four BRC repeats bind RAD51 with high affinity to facilitate its assembly on the ssDNA, whereas BRC 5-8 bind to the RAD51 nucleoprotein filament to stabilize its growth [70,123,124]. In Chapter 4 of my PhD I will present the work in which we describe that BRCA2 interacts with DMC1, the meiotic counterpart of RAD51, through the BRC repeats. HMG20b or BRAF35, a kinesin-like coiled-coil high mobility group protein, binds to amino acids 1628-2190 in the BRC repeats of BRCA2. This interaction seems to regulate HMG20b function in the completion of cell division [125,126].

The crystal structure of the mouse C-terminal DNA binding domain (CTD) shows that it consists of five adjacent domains: a helical domain, three oligonucleotide/oligosaccharide binding (OB) folds and a tower domain that protrudes from OB2 (Figure 15). The DNA binding domain exerts high ssDNA binding affinity but low affinity for dsDNA [127]. This domain can enhance the DNA strand exchange activity of RAD51 and this is further promoted in a fusion peptide with one BRC repeat [128]. The

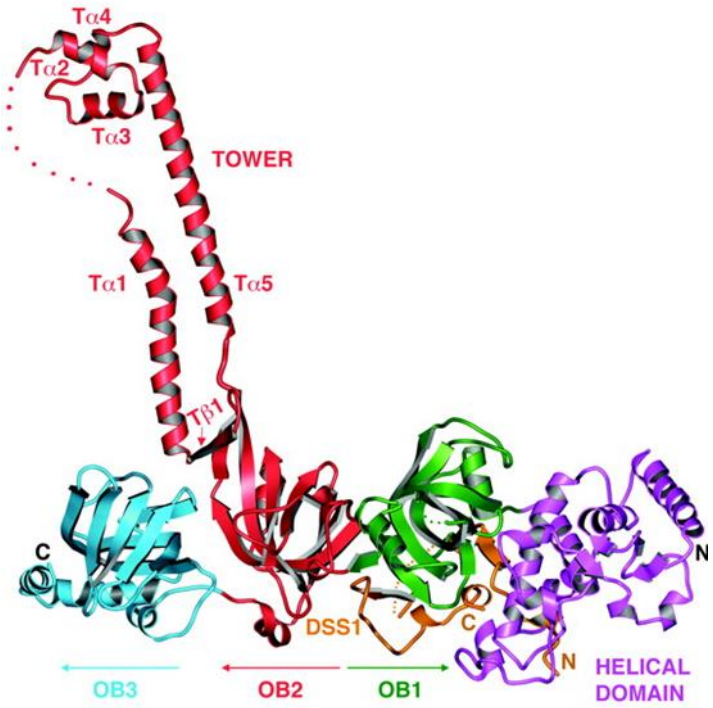

Figure 15: View of the mouse BRCA2 CTD DBD-DSS1 crystal structure. In magenta: Helical domain (H), in green, red and blue, OB1, OB2 and OB3. The tower domain in red originates from OB2. Orange: DSS1 is associated to BRCA2 between H and OB1. From Yang *et al.,* 2002 [127].

small 70 amino acids protein DSS1 (depleted in split hand split foot syndrome) binds to BRCA2 in the region between the helical domain and OB1 and confers stability to BRCA2 [129], an observation we also made during the purification of the CTD in this study (see chapter 2). Cells depleted for *DSS1* exhibit a HR-deficient phenotype in response to DNA damage implying an important function of DSS1 in HR [130]. Recently it was demonstrated that together with BRCA2, DSS1 targets RPA, decreases its affinity for ssDNA and facilitates RPA displacement by RAD51 [69]. A second NES is present in the C-terminus between the helical domain and OB fold 1. It is masked by binding of DSS1 to BRCA2, thus preventing the export of BRCA2/DSS1/RAD51 complex to the cytoplasm. A cancer associated BRCA2 variant (D2723H) in the CTD prohibits DSS1 binding and renders BRCA2 cytoplasmic [131].

The C-terminal domain also associates with the transactivation domain of the transcriptional regulator p53 which might be needed as a control mechanism for HR and apoptosis [132].

The midbody component Filamin A binds to OB2/OB3 and this association is required for the proper localization of BRCA2 to the midbody [118]. A second RAD51 binding site exists at the extreme C-terminus of BRCA2 [68]. Phosphorylation of this site at S3291 by CDK1/2 in G2/M phase disrupts BRCA2-RAD51 interaction, which is thought to be a

switch-off mechanism to control HR [133]. The RAD51 binding site at the C-terminus can also stabilize RAD51 filaments for the protection from degradation of the newly synthesized strand at stalled replication forks, but this function is independent of DSB repair [35]. Finally, BRCA2 localization to the nucleus is dependent on two Nuclear Localization Signals (NLS) that close to the C-terminal RAD51 binding site [134].
A detailed description of the functions and interactions of BRCA2 in the various pathways shortly touched here, are further detailed in the respective chapters.

1.8 BRCA2 ACTS AS MEDIATOR PROTEIN OF RAD51 RECOMBINASE IN HR

The first piece of evidence for BRCA2's role in HR came from the DNA damage sensitivity observed in *brca2* deficient mouse embryonic cells upon γ-radiation. Similar to *rad51* mutants, *brca2* deficiency is embryonic lethal [68]. RAD51 and BRCA2 were then found to physically interact in mice and human, suggesting a role for BRCA2 in DSB repair as an auxiliary protein for RAD51 function [127]. Indeed, the interaction of BRCA2 with RAD51 is important for RAD51 foci formation in response to irradiation and mutations in the BRC repeats found in cancer patients are sensitive to DNA damage [136–138]. In accordance with these findings, *BRCA2* deficient cells exhibit gross chromosomal rearrangements (GCR) as a result from defective DSB repair presumably because the breaks are repaired by error-prone pathways such as NHEJ or SSA that are not affected by loss of *BRCA2* [139,140]. First, BRCA2 is responsible for the localization of RAD51 to the nucleus. Overexpression of the BRC repeats blocks RAD51 assembly in a dominant-negative manner, suggesting that the BRC repeats sequester RAD51 monomers for the transport to the site of DNA damage [141]. The direct involvement of BRCA2 in HR was demonstrated when using a HDR-reporter assay as overexpression of BRCA2 in truncated CAPAN-1 cells and *Brca2*$^{Tr/Tr}$ MEFs rescued HR proficiency [142,143].
The HR mechanism involves the central strand exchange reaction by RAD51. The recombinase forms a nucleoprotein filament with the ssDNA in an ATP-dependent manner to search for homology in a homologous template. Once it is found, RAD51 filaments can invade the template and DNA synthesis is primed to repair the DSB. The role of recombination mediator proteins in pre-synapsis is to facilitate the loading of the recombinase on the ssDNA that is tightly bound by the ssDNA binding protein RPA posing a kinetic barrier for RAD51. The mediators also favor the binding to ssDNA rather than to dsDNA that is more abundant in the cell. Once the strand exchange protein is bound to the ssDNA, the mediator stabilizes the filament growth by inhibiting the ATPase activity of the recombinase [60,74,80,143,144]. The phenotype exhibited by

BRCA2 deficient cells as well as many *in vitro* and *in vivo* studies using fragments of the protein suggested that BRCA2 is the central mediator of RAD51 recombinase.

The required ssDNA binding function of BRCA2 was demonstrated in the crystal structure of mouse Brca2 C-terminus in a complex with Dss1 and DNA (Figure 15). Between OB2 and OB3, a tower domain comprising a three-helix bundle structure is consistent with the idea that CTD could associate with dsDNA, however, no dsDNA binding activity has been reported for this fragment. This complex is also able to promote strand exchange activity by Rad51 confirming Brca2 mediator function *in vitro* by facilitating RAD51 assembly on the ssDNA through interaction with the BRC repeats [127]. Insights into the mechanism by which the BRC repeats regulate RAD51 function in HR came from the crystallographic structure determination of the RAD51-BRC4 complex: BRC4 blocks the oligomerization interface of RAD51, thus allowing polymerization of RAD51 monomers. Specifically, the FxxA motif of the BRC repeats occupies a highly conserved interface of the catalytic domain of RAD51 [120]. A distant LFDE module present in all BRC repeats was also proposed to be important for RAD51 binding[146]. This region will become relevant in the context of the DMC1 work presented in Chapter 4.

The loading of RAD51 to the resected ssDNA would normally be hampered by RAD51's propensity to strongly bind to dsDNA. Several studies showed that the BRC repeats promote the RAD51 binding to ssDNA while blocking the association with dsDNA as a regulatory mechanism [83,123,147]. Important findings of how exactly the regulation of RAD51 by the BRC occurs were made by my PhD supervisor: Using purified BRC4, she found that by binding to RAD51 it reduces its ATP hydrolysis to keep it in an active state and prevent the ADP-RAD51-ssDNA complex from dissociation. This permits ATP-ADP exchange within the filament without dismantling it. BRC4 also prevents nucleation of RAD51 on the dsDNA and stimulate its strand exchange activity [123]. To assess the role of each of the BRC repeats in RAD51 filament formation, she investigated the roles of the individual BRC repeats. BRC1-4 bound with much higher affinity than BRC5-8 to free RAD51. Likewise, only BRC1-4 were able to reduce the rate of RAD51 ATP hydrolysis to stabilize the ssDNA-RAD51 nucleus. However, BRC5-8 showed higher affinity for RAD51-ssDNA complex suggesting that they are responsible for RAD51 filament stabilization at a later stage. Like BRC4 alone, BRC1-4 inhibited the association of RAD51 to dsDNA to promote unidirectional filament formation. The same repeats also stimulated strand exchange activity of RAD51 [124].

But yet how these functions in HR are achieved in the context of the full-length protein remained to be investigated. As said, in 2010 three groups succeeded in the

purification of full-length human BRCA2. Their studies revealed that BRCA2 preferentially binds to ssDNA or tailed substrates that represent a ssDNA/dsDNA junction resembling a 3' resected DSB. In contrast, only a weak affinity to dsDNA was observed. The RAD51 strand exchange activity promoted by BRCA2 in presence or absence of RPA was assessed in strand exchange reactions. BRCA2 could alleviate the inhibition of RAD51 binding posed by RPA bound to ssDNA probably by its high affinity to ssDNA. The RAD51 strand exchange activity was increased by BRCA2 even in the absence of RPA, confirming that BRCA2 facilitates RAD51 binding to ssDNA, probably by inhibiting dsDNA association. Quantification of BRCA2-RAD51 interaction revealed that approximately six RAD51 monomers can bind to one BRCA2 molecule [70–72]. As shown in the mouse crystal structure, the small acidic (70 aa) protein DSS1 binds to the CTD of BRCA2 (2472–2957 aa) and is important for BRCA2 stability [127,129] (Figure 15). In humans, DSS1 depletion causes defects in DSB repair as *BRCA2* mutant defective in DSS1 binding render BRCA2 and RAD51 cytoplasmic by exposing RAD51 NES, usually masked by BRCA2-RAD51 interaction [131]. Recently, DSS1 was shown to mimic the DNA reducing the affinity of RPA for ssDNA and thus allowing its displacement by RAD51 [69]. DSS1 is also a component of the proteasome, suggesting that DSS1 regulates DSB repair by proteolytic turnover of repair proteins [148].

The results summarized above contributed to the following model for the mediator protein role of BRCA2 in HR (Figure 16):

After the 3' end resection of the DSB, an ssDNA/dsDNA tail is coated by RPA. BRCA2 binds to the DNA junction, thereby replacing RPA and delivering RAD51 bound to BRC1-4 which facilitates its nucleation on the ssDNA. The same group of repeats enables RAD51 filament formation by inhibiting its ATP hydrolysis and avoiding its association with dsDNA. The further extension of the RAD51 filament is stabilized by BRC5-8. BRCA2 could then be released and RAD51 starts the invasion of the homologous template strand [124]. RAD51 binding to BRCA2 is regulated by CDK phosphorylation of the RAD51 binding site at the extreme C-terminus in a cell-cycle dependent manner. DNA damage induces dephosphorylation and stabilizes the RAD51 filaments in order to complete HR before entering mitosis [149,150].

Which BRCA2 domains are thus crucial for the repair of DSBs? Studies showed that fusion proteins comprising one or two BRC repeats and a DBD (CTD of BRCA2 or the DNA binding domain of RPA) was sufficient to restore HR activity [151–153]. In *U. maydis*, mutants expressing a truncated version of Brh2 that were missing the CTD/Dss1 region were resistant to DNA damage [154]. This was explained by the presence of a second DNA OB-fold like structure downstream the BRC with DNA binding activity.

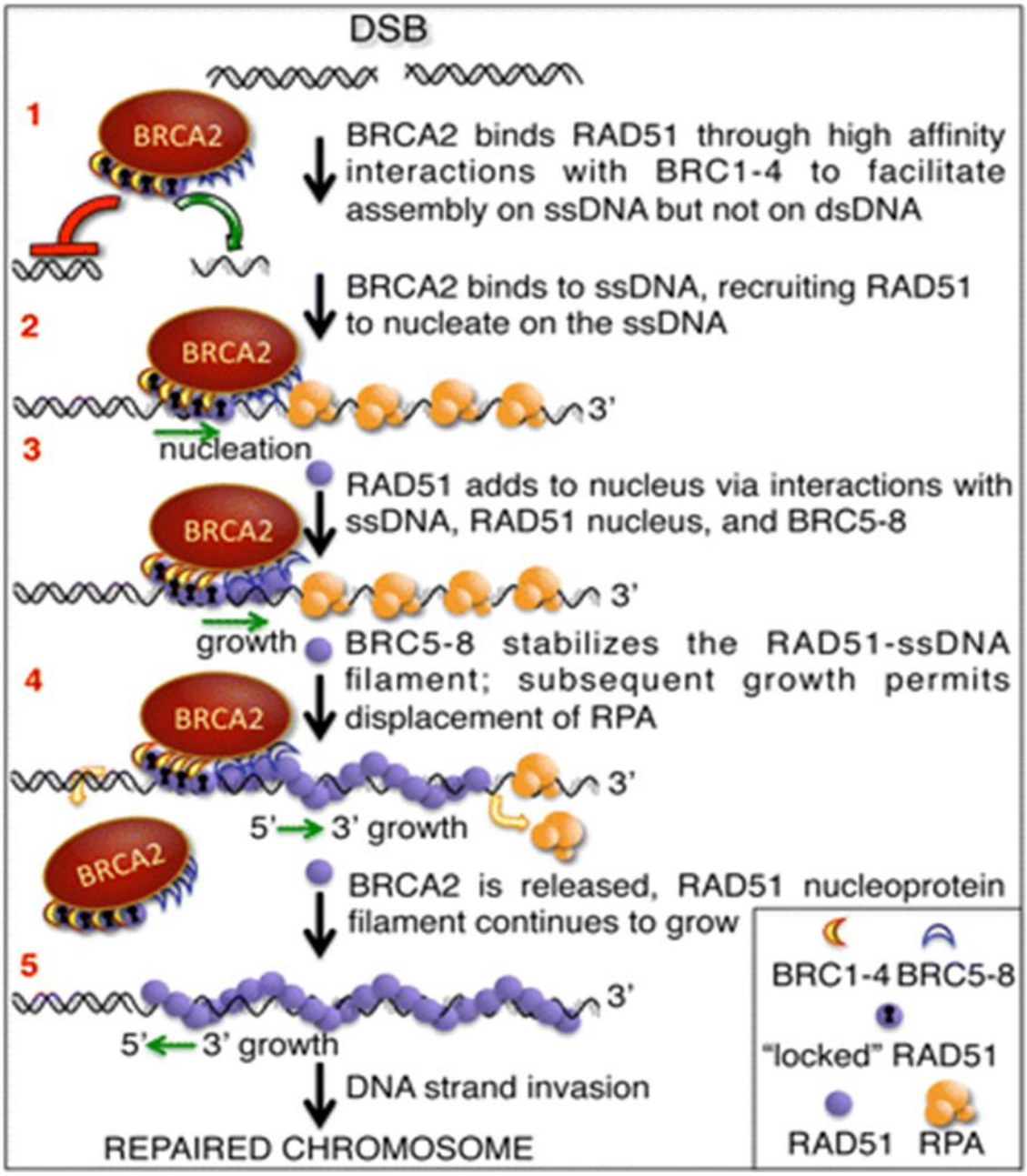

Figure 16: Model for the interaction between RAD51 and BRCA2 in presynapsis. Explanations can be found in the text. Adapted from Carreira & Kowalczykowski, 2011.

Surprisingly, this domain exhibited higher affinity for DNA than the CTD suggesting it to be the primary interaction site for DNA.

The same authors reported that the binding of the CTD to DNA is negatively regulated by Dss1, explaining the presence of two DNA binding sites. In their model the authors propose that the NTD unaffected by Dss1 makes the first contact with the DNA while the action of the CTD is inhibited by Dss1. Then, Dss1 is released due to an allosteric change and the CTD can tightly bind to the ssDNA, thereby stabilizing the exposed strand for Rad51 loading [155]. It should be noted that the observations were made in Brh2, a protein with a size of only one third of BRCA2, even though it possesses the

domains assumed to be necessary for the function in HR, namely one BRC repeat and the CTD. No sequence similarity was observed between Brh2 and BRCA2 N-terminal domains to ascribe a similar function or domain to BRCA2.

Nonetheless, a resembling situation to the one in Brh2 was found in the studies with small BRCA2 constructs: Peptides including a BRC repeat and the CTD are slightly proficient in HR but require DSS1 binding *in vivo.* However, the HR activity is reestablished to nearly wild type levels when expressing a fragment containing the N-terminal PALB2 binding site, two BRC repeats as well as the C-terminal RAD51 binding domain. The authors suggested that the ssDNA binding activity is achieved by PALB2 instead of BRCA2 [156]. If the PALB2 DNA binding is only needed when the canonical CTD is missing or if these functions are interdependent, was investigated in an *in vivo* study in DT40 chicken cells. It was observed before that when exposing DT40 cells expressing a truncated version of BRCA2 (*BRCA2*^{BRC3tr}*)* and C-terminal domain deficient cells (*BRCA2*$^{BRC\Delta CTD}$) to DNA damage, they have a significantly milder phenotype than *BRCA2*$^{-/-}$ cells. Likewise, when evaluating the phenotype of *BRCA2*$^{\Delta N}$, the expressing cells could survive the damage and showed a modest phenotype in stark contrast to cells depleted of the C-terminus and N-terminus (*BRCA2*$^{\Delta N+\Delta C}$). This genetic study also supported the hypothesis of the C- and N-terminus sharing a similar function which is, most probably, the interaction with the DNA. They also argued that the DNA binding activity of *BRCA2*^{BRC3tr} is dependent on PALB2 activity as the activity was not enhanced when overexpressing *BRCA2*^{BRC3tr} in *BRCA2*$^{-/-}$*/PALB2*$^{-/-}$ cells or when introducing mutations in the PALB2 binding site of BRCA2 [109].

In an earlier study researchers used human CAPAN-1 cells that lack a wild-type *BRCA2* allele but express a truncated version of the protein due to a deletion (6174delT) including the N-terminus and six BRC repeats to investigate the mechanism by which cells become resistant to PARP inhibitors. CAPAN-1 cells are usually highly sensitive to PARP inhibitors, displaying HR deficiency. The lab succeeded in deriving PARP inhibitor- and cisplatin-resistant CAPAN-1 clones (PIR) by continuous treatment and inferred the resistance to originate from a restored HR proficiency. When they looked at the expression profile of BRCA2 in the PIR clones, they observed new species of BRCA2 expressing the extreme C-terminal domain but not the CTD. Sequencing of the PIR clones confirmed these results and revealed a restoration of the ORF leading to the expression of a protein containing the N-terminus, five BRC repeats, the NLS and the C-terminal RAD51 binding domain. A DR-GFP-reporter assay showed that HR proficiency was reconstituted in these cells to nearly wild type levels [157]. This study not only emphasizes the risk of therapy resistance when applying

PARPi monotherapy to patients, but confirms that human BRCA2 devoid of the CTD can still fulfill its function in HR also in human cells in response to DNA damages.

Mechanistic insights in how the BRCA2-RAD51 interaction for the promotion of ssDNA binding is achieved came from recent three-dimensional EM constructions, visualizing the assumptions from the *in vitro* assays discussed above. These revealed the structure of the BRCA2-RAD51 complex that reconstitutes a BRCA2 dimer binding to two sets of RAD51 molecules consisting of four or five monomers each as it was described before [71]. As these sets are orientated in opposite directions, only one set could start nucleation imposed by the polarity of the DNA. Binding of BRCA2 to ssDNA was once more confirmed by EMSAs showing that longer patches of more than 66 nucleotides are needed for maximal binding. Although not with more affinity than for ssDNA, BRCA2 bound a gapped DNA substrate mimicking the 3' overhang at the resected end. EM reconstitution showed that the BRCA2 dimer can accommodate the gapped DNA close to the C-termini of the BRCA2 monomers where the DNA binding sites are located, indicating that these act together for ssDNA binding. The visualization of RAD51 recruitment by EM confirmed earlier results that RAD51 filaments are only formed in presence of BRCA2. As expected, BRCA2 bound to the end of the RAD51-ssDNA filament to allow the growth of the filament in the 3'-5' direction. Presence of BRCA2 also increased the number of RAD51 filaments (40-100 nm in length) and importantly, the nucleation events on the same ssDNA molecule, indicating that BRCA2 initiates the filament formation at several sites to allow 3'-5' growth in a gap-filling manner. However, RAD51 filament growth was not extended for which rather other mediator HR factors such as RAD54 or RAD51 paralogs are needed [158].

Thanks to the impressive amount of research we can now draw a clearer picture of how BRCA2 mediates RAD51 filament formation.

However, it is still questionable of how BRCA2 can load RAD51 to the site of DNA damage in absence of its CTD as it has been observed in the studies discussed above. Hence, there must be a different mechanism of BRCA2 action involving the N-terminus. PALB2 was proposed to overtake BRCA2 DNA binding function in the absence of its C-terminus. So far, this is the only known protein interaction that could explain a DNA binding mechanism. A secondary DNA binding site was revealed in the ortholog Brh2, but the N-termini of the two proteins do not resemble each other in sequence or structure. The DNA binding domain of Brh2 is constituted of an OB-fold like domain similar to RPA but this structure cannot be found in the N-terminus of BRCA2 [159] (CN own data). It is also notable that BRCA2 homologs from *C.elegans* and *D.melanogaster* do possess an N-terminal domain, one and three BRC repeats,

respectively, but no DNA binding domain similar to the CTD even though they both function in HR [101]. Further structural and functional investigation of this region of BRCA2 is needed for the proper understanding of how cells expressing a BRCA2 C-terminal truncation product can promote HR for which a DNA binding activity is vital.

In the main study of my PhD, we set out to investigate hitherto unknown functions of the N-terminal domain. We focused on the quest for a secondary DNA binding domain like it was revealed for Brh2 and to which all the studies using truncated versions or BRCA2 mutants missing the CTD point. Further explanation of our research plan will be given in the objectives (1.14). Here, I will continue in focusing on the functions of BRCA2 apart from its role in HR such as meiosis and mitosis.

1.9 BRCA2 AS A REGULATOR IN MITOSIS

Despite the remarkable progress achieved in elucidating the role of BRCA2 in HR, the multitude of chromosomal aberrations observed in *BRCA2* deficient cells could not only be ascribed to a defective DSB repair or unresolved replication stress. In particular, the numerical aberrations of chromosomes could also emerge from a defective mitosis. Several studies have provided evidence for a role of BRCA2 in mitosis. BRCA2 expression is regulated throughout the cell cycle; it peaks at the entry to S phase, stays upregulated in M phase, but is low in interphase and G1 phase [160]. Structural aberrations such as chromatid breaks as well as quadri- and triradial chromosomes are signs of defects in HR. This phenotype is also displayed in the cancer susceptibility syndrome Fanconi anemia. *BRCA2* codes for FANCD1 protein and its absence renders cells hypersensitive to crosslinking agents due to a defective ICL repair. In contrast, translocations, deletions or fusions between non-homologous chromosomes and aneuploidy rather result from incorrect chromosome segregation to the spindle poles [161].

Aberrant chromosomal segregation and aneuploidy can derive from centrosome amplification, a hallmark of various solid tumors including *BRCA2*-mutated associated tumors [25].

Centrosomes are the microtubule-organizing centers in the cell, consisting of two centrioles surrounded by a pericentriolar matrix that harbors a plethora of proteins. They duplicate once per cell cycle and migrate in opposite directions to form the poles of the mitotic spindle for the trustful segregation of the chromosomes. When the nuclear envelope breaks down in metaphase, the centrosomes form the mitotic spindles from where the microtubules can extend and capture the chromosomes [162,163].

Mouse cells expressing *Brca2* truncated in Exon 11 (BRC repeat region) exhibit defective centrosome duplication resulting in multinuclated cells that contain lagged chromosomes which leads to aneuploidy [139]. Aberrant centrosomes are also observed in *BRCA2* deficient VC8 hamster and FANC-D1 cells and are nowadays used as a measure for chromosome instability and BRCA2 activity for the evaluation of variants of unknown clinical significance [39,164,165]. Immunofluorescence studies in cycling HeLa cells with a BRCA2 antibody confirmed the assumption that BRCA2 localizes to the centrosomes. The localization is dependent on a centrosome localization signal (CLS) in the C-terminus of BRCA2, explaining also why cells expressing a truncated version of BRCA2 show centrosome amplification. When overexpressing the CLS motif and in turn suppressing BRCA2 association with the centrosomes, cells were multinucleated [163]. The localization of BRCA2 to the centrosome is also dependent on the Nuclear Export Signal (NES) interaction with CRM1 protein in Exon 11. Mutations inhibiting the proteins' nucleoplasmic shuttling give rise to centrosome amplification and multinucleation [119]. The removal of BRCA2 from centrosomes during mitosis is thought to be achieved by the membrane type-1 matric metalloprotease 1 (MT1-MMP) that cleaves BRCA2 in M phase at centrosomes and targets it for proteolysis [160]. Taken together, these findings suggest a role of BRCA2 in centrosome duplication but the exact mechanism by which BRCA2 regulates this process remains to be elucidated.

Faithful repair of DNA damage is vital for the cell before entering mitosis, which is surveilled by the G2/M checkpoint. The kinases AURORA A/BORA and PLK1 provoke a downstream cascade to activate cyclin B-CDK1 that promotes entry into mitosis [166]. First hints of BRCA2 having a role in G2/M checkpoint maintenance came from studies in which the overexpression of BRC4 in MCF-7 breast cancer cells not only impaired the interaction between RAD51 and BRCA2, but also led to a failure in radiation-induced G2/M checkpoint control [167]. The notion that the interaction of RAD51 with the C-terminal RAD51 binding domain of BRCA2 was important for the mitotic entry came from studies in DT40 chicken cells. Point mutations in the C-terminus of BRCA2 abolishing its phosphorylation and thus interaction with RAD51 lead to a faster fading of RAD51 foci and entry into mitosis even before repair was completed. CDK-phosphorylation of the C-terminus might thus be a control mechanism for the G2 checkpoint [149,150,168]. Moreover, BRCA2 and its interaction partner PALB2 were identified in a RNA interference screen for DNA repair proteins that regulate the G2 checkpoint induced by radiation. Depletion of BRCA2 and PALB2 individually and together abrogated the G2 checkpoint and unrepaired DNA damage persisted into mitosis. It was proposed that BRCA2/PALB2 controls the activity of the mitotic regulator PLK1/AURORA A/BORA activity to regulate the checkpoint [169].

Unequal segregation of duplicated chromosomes during anaphase can occur when the spindle assembly checkpoint (SAC) is defective. This phenotype has been described in *Brca2* deficient cells displaying micronuclei as a consequence of aneuploidy [170]. The spindle assembly checkpoint ensures the correct attachment of the chromosomes to the bipolar spindles before separation so that the two daughter cells receive the same number of chromosomes. If the chromosomes are not correctly attached, the SAC halts the progression into anaphase by inhibiting the APC/C E3 ligase responsible for the proteolysis of cyclin B.

BUBR1 is a component of the SAC and is involved in the regulation of the spindle-chromosome interaction by inhibiting APC/C upon its acetylation by P/CAF acetyltransferase [117,171]. BRCA2 was shown to interact with BubR1 and also associates with P/CAF via its N-terminus [172]. This interaction confers associated histone acetyl transferase activity to BRCA2 that serves as a platform for the acetylation of BubR1 by P/CAF at the kinetochore in prometaphase, important for the control of the SAC [117] (Figure 17E). P/CAF associates with BRCA2 in interphase to regulate BubR1 acetylation. P/CAF only binds to hypophosphorylated BRCA2, implicating that it dissociates in M phase upon BRCA2 hyperphosphorylation by PLK1 which is inhibited by DNA damage, halting mitotic entry [113,172].

Several studies suggested regulatory roles for BRCA2 by interacting with proteins important for midbody formation and abscission during cytokinesis[114,118,173]. The formation of the midbody starts in anaphase by generation of a contractile actin-myosin ring and furrow ingression at the spindle midzone. The ingression divides the cell into

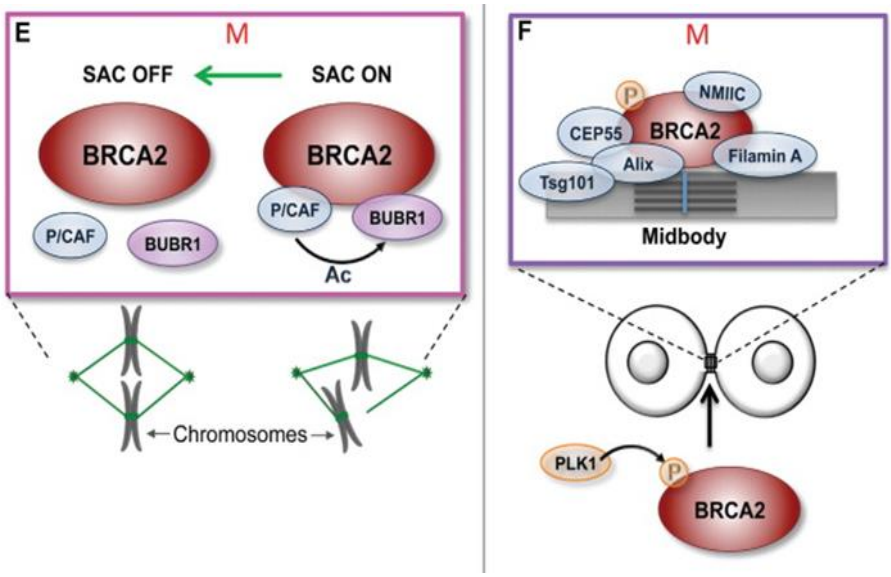

Figure 17: BRCA2 controls the SAC activity in M phase **(E)** and interacts with proteins for the formation of the midbody **(F).** Adapted from Martinez *et al.*, 2015[102].

two daughter cells but they remain connected via the midbody structure, an intercellular bridge composed of microtubule bundles [174]. For the final stage of cytokinesis, the separation of the two daughter cells is mediated by the Flemming body, a protein ring at the center of the midbody. Abscission is then achieved by the action of the endosomal sorting complex (ESCRT) that is responsible for the cleavage of the remaining intercellular bridge. The ESCRT complex components are recruited by CEP55 when it is associated with the microtubule binding protein MKLP1 at the midbody. The ESCRT machinery is needed for the bending of the membrane away from the cytoplasm and the cleavage of microtubules is subsequently accomplished by the AAA-ATPases Spastin and Vps4. CEP55 is the central organizer of the midbody as it recruits also Aurora B, MKLP2, PRC1, ECT2, Anillin and Syntaxin 2 for the completion of cytokinesis. CEP55 itself is regulated by the kinases CDK1 and PLK1 for the proper completion of cytokinesis [174–177].

The scaffold protein Filamin A, a component of the actinmyosin ring of the Flemming body, localizes with BRCA2 to the midbody upon its phosphorylation at S193 by PLK1 [114]. Some BRCA2 cancer-associated missense variants mutated in the Filamin A binding region disturb the interaction of the two proteins, indicating that the association with Filamin A is crucial for localization. At the Flemming body, BRCA2 interacts with Nonmuscle Myosin IIC (NM-IIC), an important regulator of the IIC ring formation. Depletion of *BRCA2* with siRNA impairs the localization of Myosin II to the actomyosin contractile ring at the cleavage furrow and leads to delayed or incomplete cytokinesis. Since many cells could eventually complete cytokinesis many, BRCA2 was suggested to serve as a regulatory factor at the midbody but is not essential for abscission [114,118,173,178] (Figure 18).

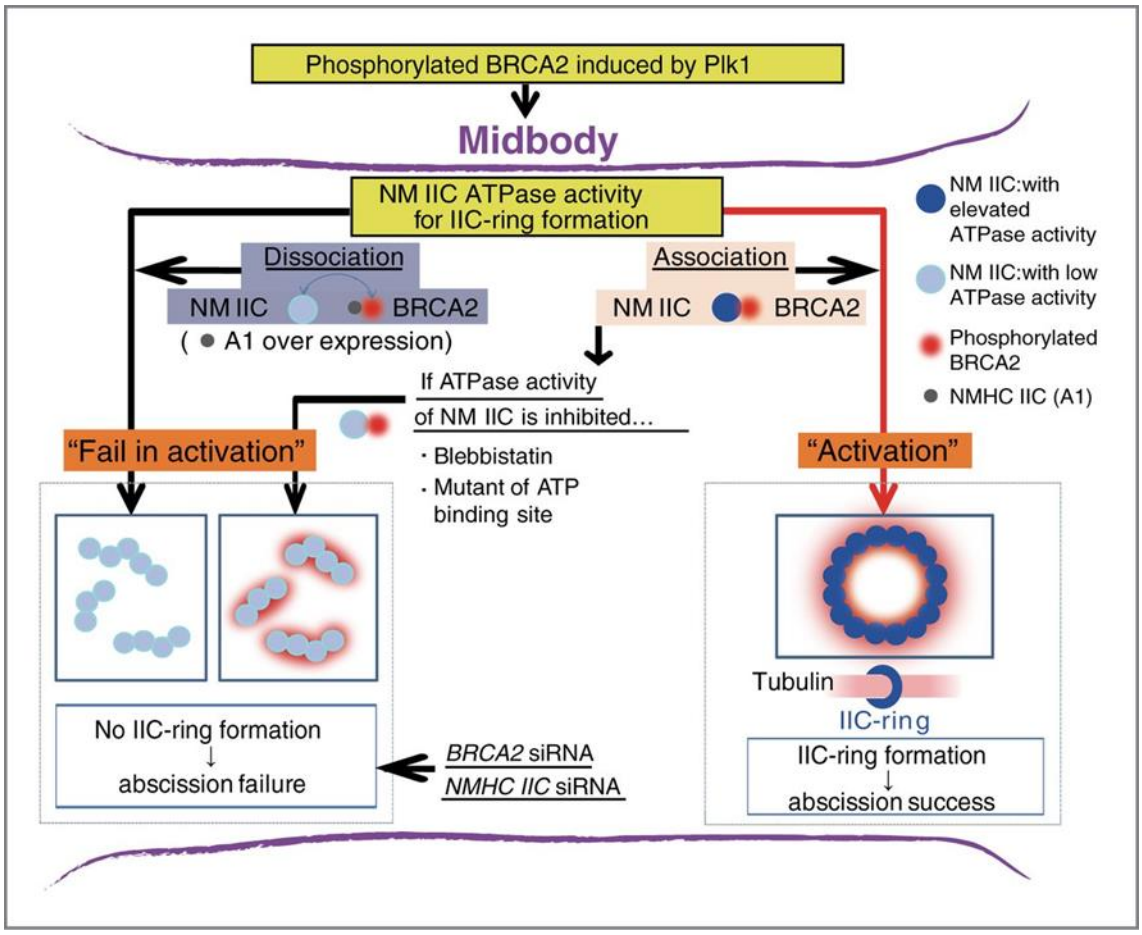

Figure 18: BRCA2 modulates midbody abscission. Once BRCA2 is phoshorylated by PLK1, it associates with NM IIC and activates the IIC-ring formation at the Flemming body and ensures proper abscission **(right).** Inhibition of this interaction leads to failure in ring formation and abscission **(left)**. Adapted from Takaoka *et al.,* 2014 [114].

Immunoprecipitation studies with BRCA2 revealed interactions with more midbody markers such as Aurora B kinase, PRC1, CEP55 and MLKP1. *Brca2*$^{-/-}$ cells displayed unresolved cytokinetic bridges and multinucleation. As shown before, absence of BRCA2 negatively influenced the localization of Myosin II as well as MKLP1, MKLP2, PRC1 and the ESCRT-associated components Alix, Tsg101 and Endobrevin to the midbody, whereas CEP55, Plk1, Aurora B, Eg5, CENP-E, Anillin, F-actin and Filamin A were not disturbed. BRCA2 formed complexes with CEP55, Alix and Tsg101 via different site at the N-terminus, and it was suggested that BRCA2 guides the formation of the complexes CEP55-Alix and Tsg101-CEP55 for the recruitment of the proteins to the midbody. In accordance with this, cancer-associated missense mutations in the N-terminus of BRCA2 disrupting the interactions with CEP55, Alix and Tsg101 increased the percentage of multinucleated cells and cytokinetic bridges.

Moreover, BRCA2 interacts with BRAF35 (BRCA2-associated factor 35 or High Mobility Group 20b HMG20b) BRCA2 as part of a large multidomain complex via BRC5. Overexpression of BRC5 inhibits the interaction of HMG20b and BRCA2

causing defects in cell division and binucleated cells, showing that the role of HMG20b in cytokinesis is dependent on an interaction with BRCA2, although the role of this interaction needs to be further investigated since the BRCA2/BRAF35 complex was also proposed to bind to condensed chromatin and injection of anti-BRCA2 or anti-BRAF35 caused a G2 delay [125126].

Although not without controversy [179], these studies identified BRCA2 as an important regulator of midbody components, supposedly to position important regulators of cytokinesis and components of the ESCRT complex at the correct site. Absence of BRCA2 from the midbody results in cytokinetic failure and can cause numerical chromosomal abnormalities, a hallmark of cancer development. Notably, this function is not related to its role in recombinational DNA repair [118].

In Chapter 3, I will describe the part of my PhD project dedicated to the characterization of BRCA2 VUS located in the N-terminus. Some of these VUS cause cytokinetic defects.

1.10 BRCA2 IN MEIOTIC RECOMBINATION

A role for BRCA2 in meiosis was suggested when it was found that mice with a defective *Brca2* gene show infertility due to incomplete recombination. Likewise, human spermatocytes lacking *BRCA2* do not progress beyond prophase I, probably because of defective DMC1/RAD51 foci formation [180,181]. Studies from *U. maydis* gave rise to a role of the BRCA2 ortholog Brh2 in meiotic recombination, where they found that *brh2* null mutants were not only defective in HR but also in meiosis when exposing them to radiation [182]. Investigations in the plant *A. thaliana* that encodes a shorter form of BRCA2 (AtBRCA2), showed interaction with the meiotic-specific recombinase AtDMC1 via the BRC repeats and the downregulation of AtBRCA2 highly disturbed meiotic recombination [181,183,184]**.** RAD51 and DMC1 are related recombinases with strand exchange activity that cooperate in meiotic recombination. The proteins resemble each other in structure (54% amino acid identity) and biochemical function namely the formation of a nucleoprotein filament, promotion of homology search in the duplex template and strand invasion by forming a D-loop structure to prime DNA synthesis [185,186]. While RAD51 is central in mitotic recombination, it plays only a supportive role for the meiotic-specific recombinase DMC1 during meiosis [93].

A direct interaction between DMC1 and BRCA2 was later shown in humans however the interaction site with BRCA2 was proposed to be distant to the BRC repeats unlike AtBRCA2 and was mapped down to a PhePP motif (2340–2472) that does not bind RAD51 [92]. Purified full-length BRCA2 also bound DMC1 in pull-down assays, but the

functional relevance of this interaction has not been studied [70,92,184]. Although the PhePP motif was described to be responsible for DMC1 binding *in vitro*, homozygous knockout mice expressing *Brca2* mutated in one of the conserved phenylalanine residues of the PhePP domain showed normal meiotic progression and Dmc1 foci formation [187]. Since *BRCA2*-deficient mutants exhibit meiotic recombination defects and BRCA2 was shown to interact with DMC1, it is conceivable that it assumes the same mediator function in meiosis as it was shown for RAD51 in mitosis. Nevertheless, RAD51 and DMC1 are regulated by different accessory proteins: DMC1 localization to the site of DNA damage and assembly in foci is accompanied by the Swi5–Sfr1 complex in yeast. RAD51 and DMC1 D-loop formation in meiosis is stabilized by HOP2/MND2 complex. In contrast to DMC1, RAD51-dependent D-loops are rapidly dissolved by RAD54 [91,186,188,189].

Even though the interaction between BRCA2 and DMC1 has been shown, it is unclear how exactly the two proteins collaborate in meiotic recombination and if there are other regions of BRCA2 that would bind DMC1 accounting for the lack of phenotype on PhePP domain mutation. In collaboration with Juan S. Martinez in the laboratory, we set out to address this question [190]. The objective of this project is described in Chapter 1.14 and the publication concerning this work can be found in Chapter 4.

1.11 BRCA2 AND ITS ROLE IN CANCER DEVELOPMENT

Germline mutations in *BRCA2* can give rise to hereditary breast, ovarian, prostate and also pancreatic cancer [191,192]. Although these types of cancers occur mostly spontaneously, mutations in *BRCA2* account for about 20% of all hereditary breast cancer cases [193]. Individuals with heterozygous mutations in *BRCA2* have an estimated risk of 45% to develop breast, and of 15% to develop ovarian cancer by the age of 70. The tumor development starts early and the cancer risk increases with age [194,195]. The existence of the cancer predisposing gene was proven by genomic linkage analysis of families at high risk to develop breast or ovarian cancer. *BRCA2* was found to be transcribed from chromosome 13q and was later on cloned for the first time in 1995 [192,196]. The hope to deduce the biological role of BRCA2 from its protein product was not fulfilled as BRCA2 showed no homology to any other protein described [197].

As explained in the previous chapters, several findings demonstrated the role of BRCA2 as a tumor suppressor protein by maintaining the chromosome stability both in structure and number in DNA repair and during the cell cycle. *Brca2* deficient embryo mouse models were not viable and very sensitive to γ-radiation, speaking for a role in DNA repair that was further supported by mouse models expressing truncated *Brca2*

that exhibited impediment of proliferation, problems in cell cycle progression, sensitivity to DNA damaging agents and increasing number of chromosomal aberrations such as chromatid breaks [68,98,198] (Figure 19). Human BRCA2 was later confirmed to be a nuclear protein of 390 kDa that serves as a central mediator during HR [140,142]. The exact mechanism by which BRCA2 mediates RAD51 activity at the site of DNA double strand breaks was only established in recent years [70–72], and is essentially described in Chapter 1.4 and 1.8. Absence of BRCA2 due to mutations forces the cell to repair the DSBs by other mechanism like non-homologous end joining or single strand annealing (NHEJ and SSA, further described in Chapter 1.2). These error-prone pathways can cause translocations and other chromosomal rearrangements. *BRCA2* deficient tumors

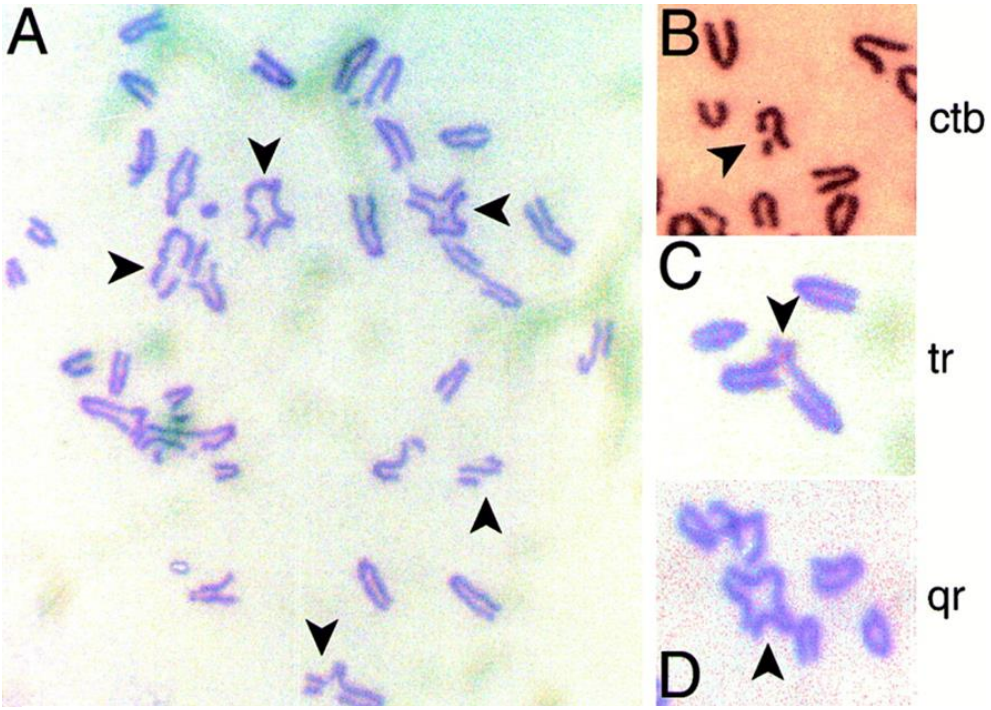

Figure 19: Metaphase spreads from *Brca2* truncated MEFs show **A)** Multiple structural aberrations such as **B)** chromatid breaks (ctb) **C)** triradial (tr) and **D)** quadriradial (qr) structures. From Patel *et al.*, 1998 [98].

show mutations such as short deletions at the break junctions. The mutations are likely to result from error-prone repair like NHEJ which can trigger the somatic mutations in the second allele of *BRCA2* leading to its complete inactivation.

This may subsequently promote the accumulation of mutations in other genes responsible for cell cycle control such as p53 which might lead to early-onset development of cancers [106,137,139,140,142,161,199,200].

The structural aberrations and gross chromosomal rearrangements observed when DNA repair is impaired can also result from defective rescue of stalled replication forks during S phase [201]. The polymerase complex halts when it encounters lesions, breaks, DNA adducts or DNA-bound proteins that impede its progression as extensively

described in Chapter 1.2. Because of its replication fork protective role (detailed in 1.3), absence of BRCA2 also increases replication stress during S phase, a hallmark of cancer [153].

In addition to the different kinds of cancers mentioned above, bi-allelic *BRCA2* mutations causes 3-5% of Fanconi Anaemia (FA) cases, a rare autosomal recessive disorder characterized by leukemia, bone marrow failure, congenital disorders, short stature and short life expectancy [39]. The numerous FA protein factors act in DNA interstrand cross-link repair (see 1.3) and patients are hypersensitive to cross-linking agents such as mitomycin C. BRCA2 was found to be identical to the FA factor D (FANCD1) and cooperates with FANCR (RAD51) in the last steps of the FA pathway to repair the toxic interstrand cross-link lesions that inhibit replication and transcription. FA cells show the same chromosomal structural aberrations as *BRCA2* deficient cells (Figure 19) [98,102,161].

BRCA2 biallelic mutation carriers show also changes in chromosome number, speaking for separation problems in cytokinesis [173]. Many studies have implicated roles for BRCA2 at late steps in cytokinesis as cells deficient in *BRCA2* accumulate display aberrant chromosome structures and polyploid nuclei that result from delayed or incomplete cytokinesis. This might be explained by the mis-localization or deregulation of important midbody components in absence of BRCA2 leading to impaired midbody and Flemming body formation which are needed for proper abscission of the two daughter cells[98,114,118,173].

The aneuploidy observed could also originate from defects in BRCA2 at other stages in the cell cycle such as chromosome segregation. The spindle assembly checkpoint (SAC) is responsible for the accurate attachment and segregation of the chromosomes to ensure the maintenance of correct chromosome number in each daughter cell. Anaphase onset is deregulated in some cancers with defective SAC leading to aneuploidy. Also, during metaphase to anaphase transition, centrosome amplification results in unequal segregation, a hallmark of many tumors [165,171,202,203].

Collectively, the research presented above illustrates how BRCA2 acts as a caretaker of genome integrity. The chromosome instability caused by defective BRCA2 is the driving force of carcinogenesis in *BRCA2*-associated tumors. Moreover, mounting evidence show that the increasing mutational rate observed in “gatekeeper” genes that control cell division and apoptosis is sufficient to predispose carriers to tumorigenesis. As an example, there is a higher frequency of p53 mutations in *BRCA2*-deficient cancers [153,161,199]. The continuous effort to understand the different functions of BRCA2 will help to elucidate further the mechanisms by which mutations in *BRCA2* drive tumorigenesis.

1.12 BRCA2 VARIANTS OF UNKNOWN CLINICAL SIGNIFICANCE AND THEIR CLASSIFICATION

Mono-allelic mutations in *BRCA2* increase the risk to develop breast, ovarian or pancreatic cancer as described in Chapter 1.11. Genetic screening for known deleterious mutations is offered to cancer patients and individuals with a family history of cancer. However, the prerequisite to predict the impact of a missense mutation in *BRCA2* remains that this mutation has already been described and characterized [204]. Mutations classified as deleterious can be the reason for the mislocalization of the protein, expression of a non-functional truncated protein version or interference with an important domain. Neutral mutations do not affect BRCA2 function and in turn do not confer an elevated risk to develop cancer. Many missense mutations identified are classified as "variant of unknown clinical significance" as their impact on the protein function is not known [205]. This poses problems in genetic counselling as persons carrying variants of unknown clinical significance (VUS) cannot be provided with appropriate clinical advice. In an early study with breast cancer patients, 13% of the women were diagnosed with a VUS, emphasizing the need for better classification and screening systems [206].

A multifactorial likelihood posterior probability model was developed in order to classify VUS. The model integrates the frequency of the mutation in carriers and controls, the co-occurrence with deleterious mutants, the co-segregation with disease in pedigrees, family history, the nature and position of the amino acid substitution, the degree of conservation of the amino acid among species, and the results of functional assays for which the VUS was already tested [207]. However, many of these VUS are rare and their pathogenicity cannot be predicted based on a likelihood model but needs to be evaluated by applying functional assay. The missense mutations are introduced in *BRCA2* and the capacity of the variants to fulfill BRCA2 functions is tested [208]. To improve the accuracy of classification, there are several international initiatives to collect clinical and functional data from VUS, not only for *BRCA2* but also *BRCA1* and other tumor suppressor genes. One of them is the Evidence-based Network for the Interpretation of Germline Mutant Alleles (ENIGMA) consortium of which our team is part. We meet twice a year to share data, methods and facilities for the classification of variants. Information is collected from different working groups who analyze clinical data, perform functional assays, analyze tumor histopathology and perform large-scale splicing studies on VUS. This information is then available through a dedicated database. My host laboratory has several ongoing collaborations from members of the functional working group in which I have participated. This work is presented in

chapters 3 and 5 of this thesis and will contribute to the classification of rare VUS whose impact cannot be assessed due to the lack of genetic evidence. The Breast Cancer Information Core (BIC) and the BRCAshare databases gather more than 2000 entries for BRCA2 VUS that have been found in clinical screening of cancer patients or family members at high risk to develop breast, ovarian or pancreatic cancer [209,210]. Unlike truncating mutations of which the influence on BRCA2 function can be clearly assessed, mutations, the impact of missense variants is not easily predictable as they result in a single amino-acid change. Genetic analyses (co-occurrence with pathogenic mutation in trans) combined with in silico predictions allow variants classification; however, the majority of BRCA2 variants (62%) remain unclassified. This represents a very important clinical drawback as it complicates cancer risk assessment. To cope with this problem, many groups develop and optimize functional assays [211,212].

Because of the complexity of BRCA2 protein in size and little homology with other proteins, the application of functional assays has been limited to the VUS that are located in known functional regions such as the CTD needed for HR, the PALB2 binding site or the BRC repeats and C-terminal RAD51 binding domain [165].

Indeed, many highly penetrant pathogenic missense mutation have been found in the CTD [212]. With the discovery of new interacting proteins in other less explored regions such as the N-terminus, there is now the possibility for the evaluation of other VUS. For example, the laboratory of Fergus Couch could localize the interacting region of BRCA2 with midbody proteins to the N-terminal domain and characterized VUS that disrupt this interaction result in defective abscission and multinucleated cells [118]. As part of my PhD (Chapter 2, 3, 5), I have contributed to the evaluation of VUS found in the N-terminal region, and used DNA binding assays or DNA strand exchange assays that could contribute to infer the impact of VUS in causality.

A very common assay that has been applied for the evaluation of BRCA2 VUS is the homology directed repair assay (HDR). In this test, a DSB is induced by SceI nuclease in a GFP-reporter construct that is expressed together with wild type or variant BRCA2 in *BRCA2* deficient cells. The DSB can only be repaired when wild type or variant BRCA2 are proficient in HR which can be assessed by the percentage of GFP positive cells [142,211,212]. Missense mutations can impair BRCA2 function at the centrosomes that leads to a phenotype showing multiple instead of two daughter centrioles. The centrosome amplification assay visualizes possible centrosome amplification when expressing BRCA2 variants in *Brca2* deficient cells (VC8) in situ immunofluorescence with centrosome markers[165].

BRCA2 deficient cells are hypersensitive to DNA damaging agents such as Mitomycin C and can be rescued by overexpression of BRCA2. VC8 *BRCA2*$^{-/-}$ cells

complemented with wild type or variant BRCA2 can be tested for DNA damage sensitivity by using clonogenic survival assay where cells proficient in the repair of DNA damage will form colonies [165,213].

The treatment of *BRCA2*$^{-/-}$ cells with PARP inhibitors leads to cell death as the cells are neither proficient in SSB nor HR [214,215]. In survival assays with PARP inhibitors, BRCA2 or variant complemented VC8 cells are treated with the inhibitor and cell viability is measured by using the MTT colorimetric assay.

The embryonic stem cell-based assay applies mouse ES cells with a defective *Brca2* allele and one functional allele than can be switched off and reconstituted by BAC clone carrying WT or mutant DNA of *BRCA2*. Evaluation of the impact of the mutation is based on its ability to rescue the lethality in biological assays (DNA damage sensitivity, HR, chromosome instability). One big advantage of this assay is the non-mutagenic background in ES cells [212].

One important feature of BRCA2 to exert its function is the localization to the nucleus, an important aspect to test as many variants are mis-localized due to mutations in the NLS, mis-folding of the protein or disrupted interaction with PALB2 that localizes BRCA2 [106,163,187]. Likewise, *in vivo* and *in vitro* biochemical assays to test the interaction of purified BRCA2 with its protein partners or its DNA binding capacity are a good measure for BRCA2 function. In the laboratory, we make use of the DNA binding assays (EMSAs) to test one of the most important functions of BRCA2 in HR, the association with DNA.

Another assay involves the assessment of aberrant splicing variants, which is a major cause for the expression of a non-functional protein product. The impact of aberrant splicing mutants on BRCA2 function is difficult to deduce especially because many of these variants lead to partial exon skipping. The use of functional assays is becoming more powerful in the absence of sufficient genetic evidence [212]. However, because of the plasticity of BRCA2 demonstrated in studies with BRCA2 fragments [108,109], the evaluation of the impact of one variant on a certain function, e.g. HR, may not imply increased cancer risk. The improvement of functional assays and the growing knowledge about BRCA2 function will further help characterize and classify VUS. This will facilitate genetic counseling and cancer risk assessment.

1.13 PREVENTION AND THERAPY MANAGEMENT OF *BRCA2* PATHOGENIC MUTATION CARRIERS

Women with a high risk of developing *BRCA2*-associated cancer either because they carry a known deleterious mutation or having a strong family background, are

medically accompanied to reduce the risk of developing cancer, morbidity and mortality. In general, the first measure is the regular screening to detect a tumor at an early stage. One can also reduce the risk to develop cancer by prophylactic surgery of one or both breast (risk-reducing mastectomy) or apply chemoprevention by using hormonal drugs such as Tamoxifen. Surgical approaches are currently the most successful, reducing the risk to develop a cancer by up to 90%, but unsurprisingly, many women refuse to take advantage of these methods [97]. Individuals who have developed *BRCA2*-associated breast or ovarian cancer are treated in the same way as patients with sporadic breast cancer. This therapeutic approach consists of surgery to remove the cancer, followed by chemotherapy and radiotherapy, the latter being still responsible for about 40% of the cured cases [216].

Importantly, *BRCA2*-associated tumors respond particularly well to chemotherapeutic treatment that induce DNA damage, such as cross-linking agents mitomycin C or cisplatin, because of the impaired HR in these tumors [216,217]. These observations led to the development of targeted therapies to specifically attack cancer cells without harming normal cell tissues by exploiting their impaired DNA damage response. The first DNA damage response inhibitors were topoisomerase inhibitors, which cause DNA breaks. Other inhibitors target checkpoint kinases (CDK, CHK), protein kinases (DNA PK, ATM, ATR), or telomerases [218,219]. The idea behind this strategy lies on the fact that when a DNA repair pathway is defective in a tumor, it becomes dependent on other pathways [1]. Thus, the absence of a gene important for one DDR pathway such as *BRCA2* in HR will be synthetically lethal with the inactivation of another protein working in an alternative repair pathway such as BER [220]. This concept was first successfully exploited in the case of PARP inhibitors [215]. PARP-1 detects gaps, breaks or base changes in ssDNA and activates the BER pathway that is comprised in the absence of PARP-1 [214]. As a consequence, the ssDNA breaks are converted into dsDNA breaks and repaired by HR. In *BRCA2*$^{-/-}$ cells, HR is inactive and as a consequence, lethal DSBs accumulate and ultimately lead to tumor cell death whereas normal cells can repair the DNA damage. Many different PARP inhibitors are currently in clinical trials, one of them has been approved for monotherapy recently after successful trials in the treatment of *BRCA1* and *BRCA2*-associated tumors [219]. Nevertheless, several studies showed resistance mechanisms of cancer cells to PARP inhibitors such as the restoration of *BRCA2* open reading frame and expression of a protein version functional in HR [157,221].

Over the last decade, the research for the development of specialized therapies for cancers with a "*BRCA*ness" imprint, that is mutations in genes involved in the HR pathway, has progressed a lot [200]. The detection of inherited mutations in this pathway

using next generation sequencing technologies together with improved functional assays will enable widespread genetic testing and personalized risk assessment for breast and ovarian cancer [222].

1.14 HYPOTHESES AND OBJECTIVES OF THIS WORK

Inactivating germ-line mutations in *BRCA2* predispose to breast and ovarian cancer. A wealth of evidence suggests that BRCA2 exerts its tumor suppressive function through its role in DNA repair by Homologous Recombination (HR). HR is the most reliable pathway to repair DNA double strand breaks. In this pathway, BRCA2 acts as a mediator protein by recruiting the recombinase RAD51 onto the DNA and promoting its HR function to repair the breaks. Thus, malfunction of BRCA2 can lead to genomic instability, a hallmark of tumor formation. BRCA2 deficiency also leads to centrosome amplification and failure in the late steps of cytokinesis, suggesting a function of BRCA2 in these processes that could account for the aneuploidy found in *BRCA2* associated cancers. To date, several functional domains of the 390 kDa BRCA2 protein have been described. However, the roles of other domains such as the N-terminus remain enigmatic. Thus, the functions, modifications and interaction partners of BRCA2 are under extensive scrutiny.

OBJECTIVE 1: INVESTIGATION AND CHARACTERIZATION OF A PUTATIVE DNA BINDING DOMAIN IN THE N-TERMINUS OF BRCA2

The first 40 amino acids of BRCA2 are well conserved and contain a PALB2 interacting domain, a protein that localizes BRCA2 to the chromatin. However, little is known about the remaining N-terminal region, which constitutes one third of the protein (~1000 aa) as described in Chapter 1.4. Interestingly, studies with PARP inhibitor resistant clones in human cells as well as with the BRCA2 ortholog in *U. maydis* (Brh2) showed that mutants lacking the C-terminal DNA binding domain (CTD) substantially restore recombination proficiency when challenged with DNA damage[157,159]. In the case of Brh2, the restoration of HR is likely to arise from a secondary DNA binding domain found downstream the BRC repeat. These indications prompted us to hypothesize that the HR proficiency and resistance to DNA damage observed in cells expressing a truncated version of BRCA2 missing the CTD may come from a second DNA binding domain outside the C-terminus. An in silico search for functional domains using the primary sequence of BRCA2 using SMART [223] performed in the laboratory revealed a putative zinc-finger like domain, frequently found in DNA binding proteins. Thus, the first objective of my PhD project was to investigate this putative DNA binding domain in

the N-terminus of human BRCA2. For this purpose, I used *in silico* tools to further validate the first findings and then planned to search for the DNA binding domain *in vitro.* With the identification and characterization of a secondary DNA binding site we would address the following questions: 1) Could it promote DNA strand exchange by RAD51 together with a BRC repeat *in vitro* as it was shown for other truncations of BRCA2 containing a DBD and a BRC repeat? 2) Could it rescue the sensitivity of *BRCA2* deficient cells to DNA damaging agents? 3) Would BRCA2 missense mutations (VUS) found in this domain impair these functions and hence infer their probability of causality? (Chapter 2).

OBJECTIVE 2: CHARACTERIZATION OF VUS LOCATED IN THE N-TERMINAL DNA BINDING DOMAIN OF BRCA2

To further characterize the functional relevance of the N-terminus and in particular the identified putative zinc-finger domain, we chose to study BRCA2 missense mutations present in families at high risk of breast cancer (found in BRCAshare and BIC database [209,210]) located in this region. The purpose of this strategy is two-sided: on the one hand, we could study the relevance of the new domain by looking at the impact of the variants in its function, and on the other hand, we could evaluate variants of unknown significance (VUS) which are by definition rare and difficult to assess its causality in breast cancer.

We selected several VUS located in the predicted zf-PARP like domain that based on their amino acid conservation and sequence alignments *in silico,* as well as the chemical nature of the amino acid change and their location in hydrophobic clusters, are more likely to be deleterious [207,224]. Indeed, all variant residues are highly conserved in mammalian species and predicted to have DNA binding activity by using BindN software[225]. In this work, I aimed to first introduce the selected missense mutations in the BRCA2 wild type protein, establish stable cell lines in *BRCA2* deficient cells and assess their subcellular localization. We wanted to evaluate their sensitivity to DNA damage such as MMC and PARP inhibitors, indirect measures for functional HR. As BRCA2 is implicated in cytokinesis (see section 1.9) *BRCA2* deficient cells exhibit chromosomal aberrations, centrosome amplification and abnormal cytokinesis [118,173]. To test a possible effect of the variants on cytokinesis I planned to use time-lapse microscopy, immunofluorescence with markers against centrosomal proteins, co-immunoprecipitation studies with midbody proteins, as well as their progression through the cell cycle.

One very interesting question we would like to address is whether possible abnormalities of VUS in mitosis and/or cytokinesis are related to the impaired DNA repair function or if these functions are independent from each other. Our ultimate goal was to better understand the function of NTD region of BRCA2 and at the same time, evaluate the impact of unique variants on the DNA binding activity of the protein (Chapter 3).

I also contributed to a side project in which we address whether intermediate functional phenotype corresponds to intermediate cancer risk. This was done in collaboration with members of the ENIGMA consortium and the Breast Cancer Association Consortium (BCAC). In the study, 20 BRCA1 and 33 BRCA2 missense variants were genotyped on ~40,000 breast cancer cases and 40,000 matched controls using the Collaborative Oncological Gene-Environment Study (iCOGS) custom genotyping array. Because the intermediate phenotype variants observed previously by a cell-based homologous recombination assay ([211]) are located in the C-terminal DNA binding domain, we tested whether the intermediate phenotype in HR is due to a decreased but not abolished DNA binding ability. We purified VUS proteins and used DNA binding assays to proof this hypothesis (Chapter 5).

OBJECTIVE 3: STUDY THE ROLE OF BRCA2 IN MEIOTIC RECOMBINATION

In somatic cells, BRCA2 catalyzes RAD51-mediated homologous recombination. The meiosis-specific DNA-strand exchange protein, DMC1, promotes DNA strand invasion generating what is termed a displacement-loop (D-loop) and DNA strand exchange between homologous molecules in a fashion similar to RAD51[226]. A direct physical interaction was established for purified full-length human BRCA2 and DMC1[70]. In plants this interaction was mapped to the BRC repeats whereas in humans, a conserved PhePP motif was suggested to be responsible for DMC1 binding[92] Substitution of the residues that disrupt the interaction with PhePP domain were found negligible for meiosis in mice, indicating that there could be another site of interaction for DMC1[187]. In addition, the sequence alignment of RAD51 paralogs including DMC1 indicate that the site of interaction of the BRC repeats to RAD51 is very well conserved in DMC1[101]. Therefore, we investigated whether the BRC repeats could also bind DMC1 and if so, the functional relevance of this interaction (Chapter 4).

RESULTS

BRCA2 is a multifunctional protein that acts in different pathways in the cell as outlined in the introduction. In our lab, we are interested in the functional characterization of domains and interaction partners of BRCA2 that have not been described yet. Moreover, we aim to characterize and evaluate variants of unknown clinical significance found in breast cancer patients located in these unexplored regions as explained in the project description (1.14).

The results of my PhD are presented in the following chapters. Since I worked on several related projects focusing on BRCA2 function, I dedicated each of them a separate chapter for easier understanding (2-5). The results that differ from the main topic of the thesis and have been already published or submitted for publication are presented in paper format.

A final conclusion about the thesis presented here can be found in the last section (6). All materials or methods not already listed in the methods sections are included in the appendix.

CHAPTER 2

2.1 FUNCTIONAL CHARACTERIZATION OF A PUTATIVE DNA BINDING DOMAIN IN THE N-TERMINUS OF BRCA2

As outlined in the project description (1.14) and in chapter 1.7, several lines of evidence led us to hypothesize that the HR proficiency and resistance to DNA damage observed in cells expressing a truncated version of BRCA2 missing the C-terminal DNA binding domain (CTD) come from a DNA binding activity exhibited by the N-terminus: First, the lab of Alan Ashworth described the phenotype of human pancreatic *BRCA2* deficient (CAPAN-1) clones with acquired resistance to PARP inhibitors. Some of these clones did not contain the CTD but could still form RAD51 foci and significantly increased the HR frequency to nearly wild type levels. Moreover, they also reduced the number of MMC-induced chromosomal aberrations compared to CAPAN-1 cells [157].

Second, mutants of the BRCA2 ortholog Brh2 (*U. maydis)* missing the canonical CTD were able to survive DNA damage. An OB-like DNA binding domain downstream the BRC repeat region termed N-terminal DNA binding domain (NTD) was found responsible for the rescue of this phenotype. The authors consider this domain as the primary interaction site with DNA. In their model, the NTD binds first the resected 3' tail DNA, leading to a conformational change in the CTD that releases Dss1 and subsequently associates with the ssDNA [155,159].

Third, experiments in DT40 chicken cells showed that overexpression of a *BRCA2* construct missing the CTD led to a milder phenotype than *BRCA2*$^{-/-}$ cells when exposed to different DNA damaging agents. The complemented cells also retained some HR activity, suggesting that the N-terminal part of BRCA2 is capable of restoring, at least partially, HR function in these cells [109]. Fourth, BRCA2 peptides containing the N-terminus, the BRC repeats and the extreme C-terminus but not the CTD, were efficient in restoring the HR proficiency in *Brca2* deficient VC8 cells [156]. Last, my host laboratory had started a search for new functional domains in BRCA2 by applying the amino acid sequence of the entire BRCA2 sequence to the web tool SMART (Simple Modular Architecture Research Tool). SMART is a web resource for the detection of protein domains using Hidden Markov Models (HMM) that are based on multiple sequence alignments with known protein domains[223]. This analysis revealed a putative zinc finger-PARP like (zf-PARP) domain located in the region between amino acids 265 and 349 of the N-terminus (Figure 1A), although the score of the E-value (2.4) was below the threshold.

Zinc finger domains were originally identified as DNA binding motifs, but are now known to bind RNA, proteins and lipids. Some of these zinc fingers modules coordinate a zinc ion to form the finger-like motif that contacts the target, however, most of them do not bind zinc and have evolved individually for their specialized function [227].

Thus, the goal of my PhD project was to search for a potential DNA binding domain in human BRCA2 that could explain the phenotypes observed.

Furthermore, we decided to select variants of unknown clinical significance located in this region that have been found in breast cancer patients to examine their impact on DNA binding, HR and cell cycle progression. This way, we would be able to 1) characterize and evaluate VUS to help infer causality and 2) find out if the putative DNA binding domain in the N-terminus plays an important role for BRCA2 function in homologous recombination. This work is presented in chapter 3.

2.2 RESULTS

The N-terminal region has no similarity to any other protein domain described and is intrinsically disordered, making it difficult to deduce a function of this region from sequence or secondary structure comparison (see also 1.7).

To identify possible DNA binding residues in the zf-PARP like domain, I used the web-based tool BindN that predicts possible DNA and RNA binding residues based on the biochemical properties of the amino acids [225]. I identified two clusters predicted to contain DNA binding residues. Using Clustal Omega multiple sequence alignment tool [228] I found that these clusters are conserved among several mammalian species suggesting that these residues might be important for BRCA2 function (Figure 1B).

The *in silico* analysis led us to investigate a possible DNA binding activity in this region. To ascertain this activity *in vitro*, we designed expression fragments of the N-terminus of BRCA2. First we used an expression construct of BRCA2 1-1000 amino acids

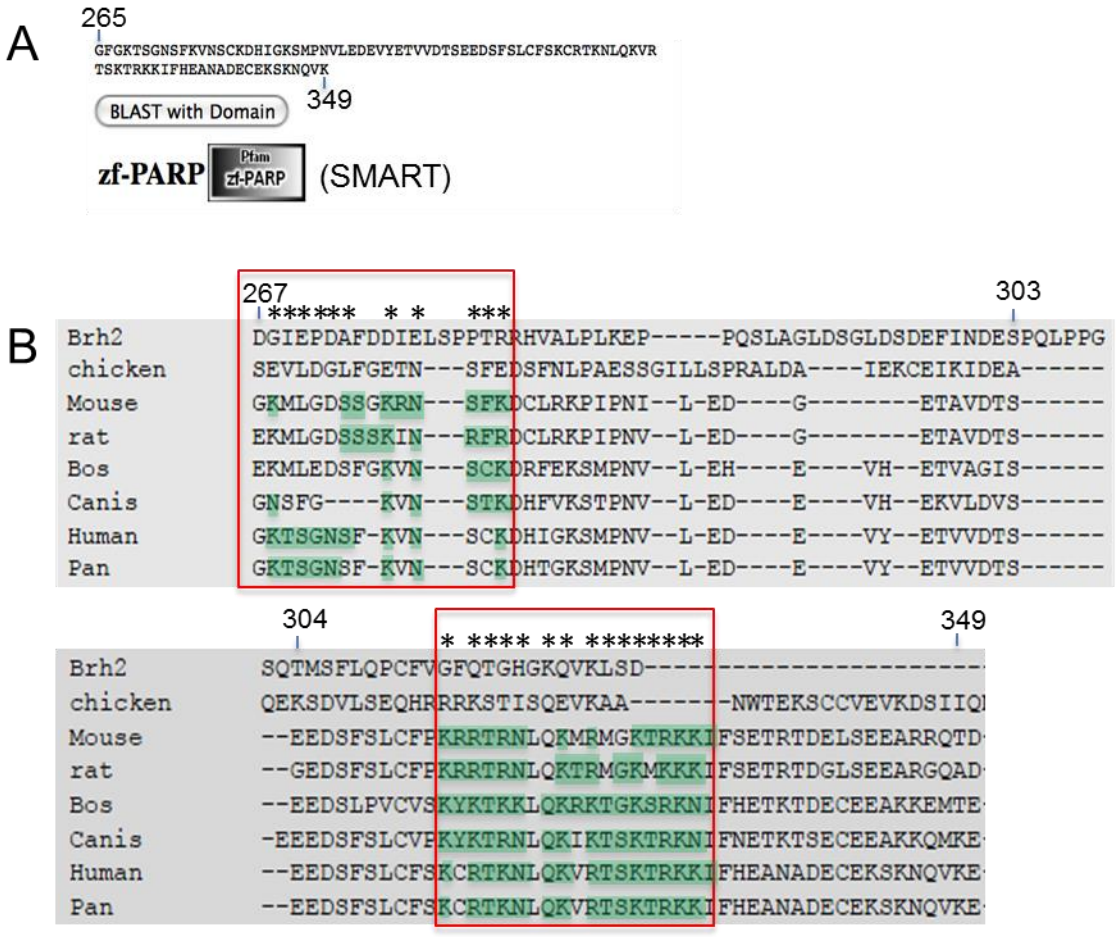

Figure 1A) SMART results showing a zinc-finger PARP like domain between amino acids 265 and 349 of the N-terminus of BRCA2. **B)** The region of the zf-PARP like domain contains residues predicted to bind DNA by the BindN prediction tool (highlighted in green). The same regions are also highly conserved in mammals as shown by the multiple sequence alignment using Clustal Omega. Conserved residues in two or more species are indicated by asterisks (*).

tagged with a 2x MBP tag and His-tag at the N-terminus that was cloned into a pFASTBac vector for the expression in insect cells. With the plasmid in hands, I went to the Eukaryotic Expression Facility at the EMBL Grenoble. Under the supervision of Frederic Garzoni, I learned how to use the MultiBac Expression System that was developed at the EMBL for the expression of recombinant eukaryotic proteins from Insect cells. This system has the advantage of expressing proteins in an eukaryotic host system that does not require additional safety measures and allows large-scale expression to obtain a high yield of protein. First, the gene of interested is transferred into the baculoviral genome by transposition and positive clones can be selected by blue-white screening. Adhesive Sf21 insect cells are then transfected with the baculovirus DNA and the successful infection of the cells can be observed under the microscope after 60 hours. The expression of the protein can be controlled by measuring the expression of YFP protein from the expression construct. This V_0 culture is then used for the amplification of the virus in a liquid culture until cells stop to proliferate and expression continues for about 3-4 days by diluting the cultures. Once the expression reaches a plateau observed in the YFP measurements, cells are harvested, lysed by sonication and the expression of the protein of interest is visualized by SDS PAGE and Western Blot.

We observed expression of the N-terminal fragment and could detect it in SDS PAGE after lysis. However, after several attempts to purify the protein, it was neither visible in SDS PAGE nor detectable by western blot. This probably implies that the protein was not correctly folded and thus precipitated during purification.

Hence, we decided to apply the purification protocol we successfully had used for the full-length BRCA2 protein before, although this meant that we would obtain much fewer quantities of the protein as expected.

For this purpose, we designed the following expression constructs of the N-terminus: $BRCA2_{LT3}$ (1-750 aa), $BRCA2_{LT2}$ (1-500 aa), $BRCA2_{T2}$ (250-500 aa), $BRCA2_{T1}$ (1-250 aa) with a 2x MBP tag and purified them from human HEK293 cells (Figure 2A). As shown in Figure 2B, 10x P150mm plates were transiently transfected with the respective expression construct and incubated for 30 hours. The cell lysate was incubated with amylose resin to let the 2x MBP tag bind to the beads and eluted with maltose. The eluate was further subjected to a weak ion exchange resin and step eluted in three fractions using a NaCl

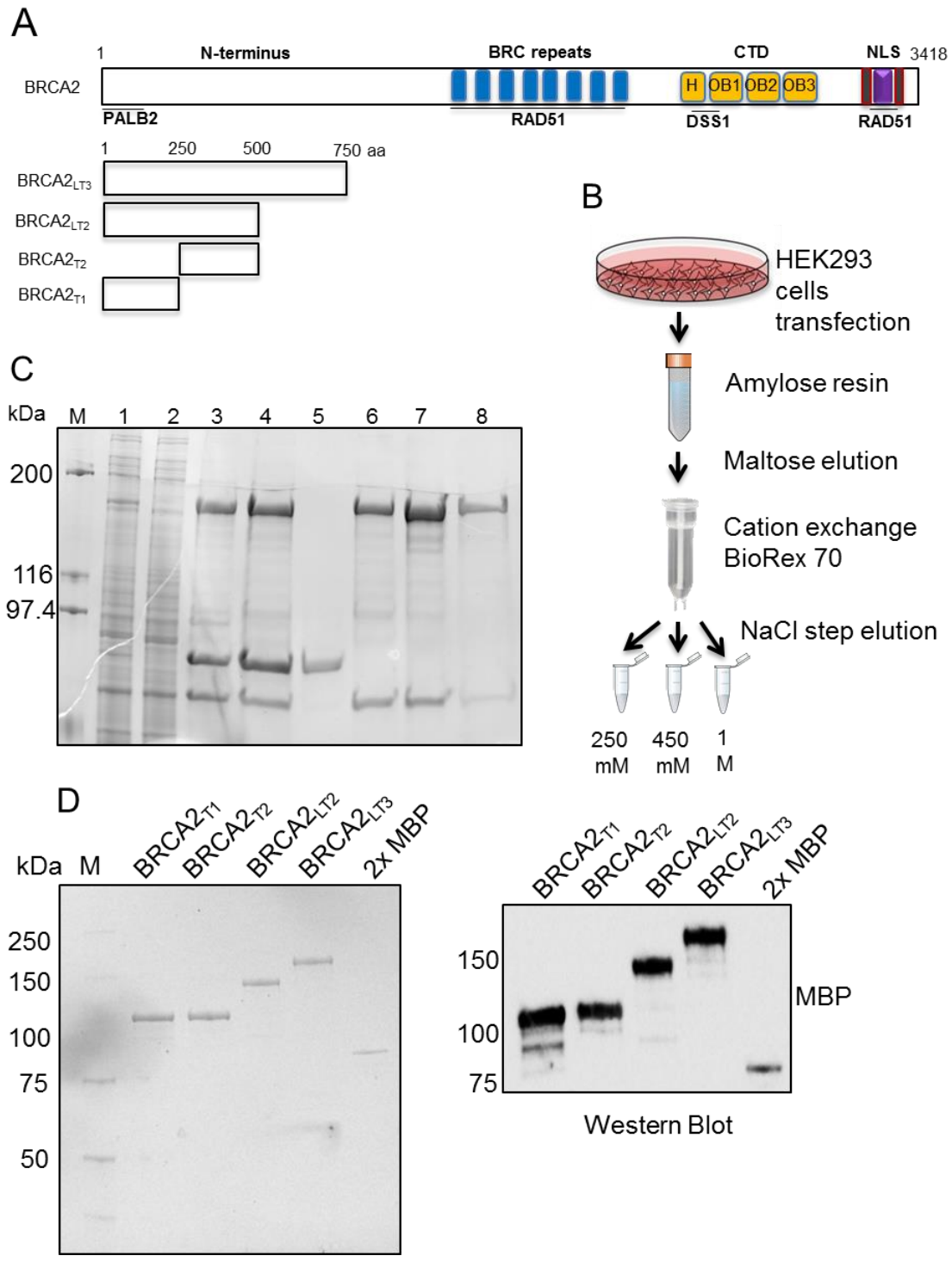

Figure 2: A) Structure of BRCA2 with functional domains and interacting partners. Below are shown the scheme of the size of N-terminal fragments used for purification. **B)** Purification protocol for fragments. **C)** 7.5% SDS gel (stain-free) with purification of $BRCA2_{LT3}$: M: molecular weight marker 1) Load 2) unbound 3)amylose beads 4) elution w. maltose 5) flow through 6) elution 250 mM NaCl 7) 450 mM NaCl 8) 1M NaCl. **D)** Purified NT fragments on 7.5% SDS gel (stain-free) 0.5 µg loaded (left) and western blot of the latter using an antibody for MBP tag (right).

gradient. The fractions of the purification steps were loaded on a SDS gel for visualization and we obtained protein with up to

95% purity in sufficient concentration for DNA binding tests (see Figure 2C for $BRCA2_{LT3}$ and Figure 2D left for all fragments). The authenticity of the protein

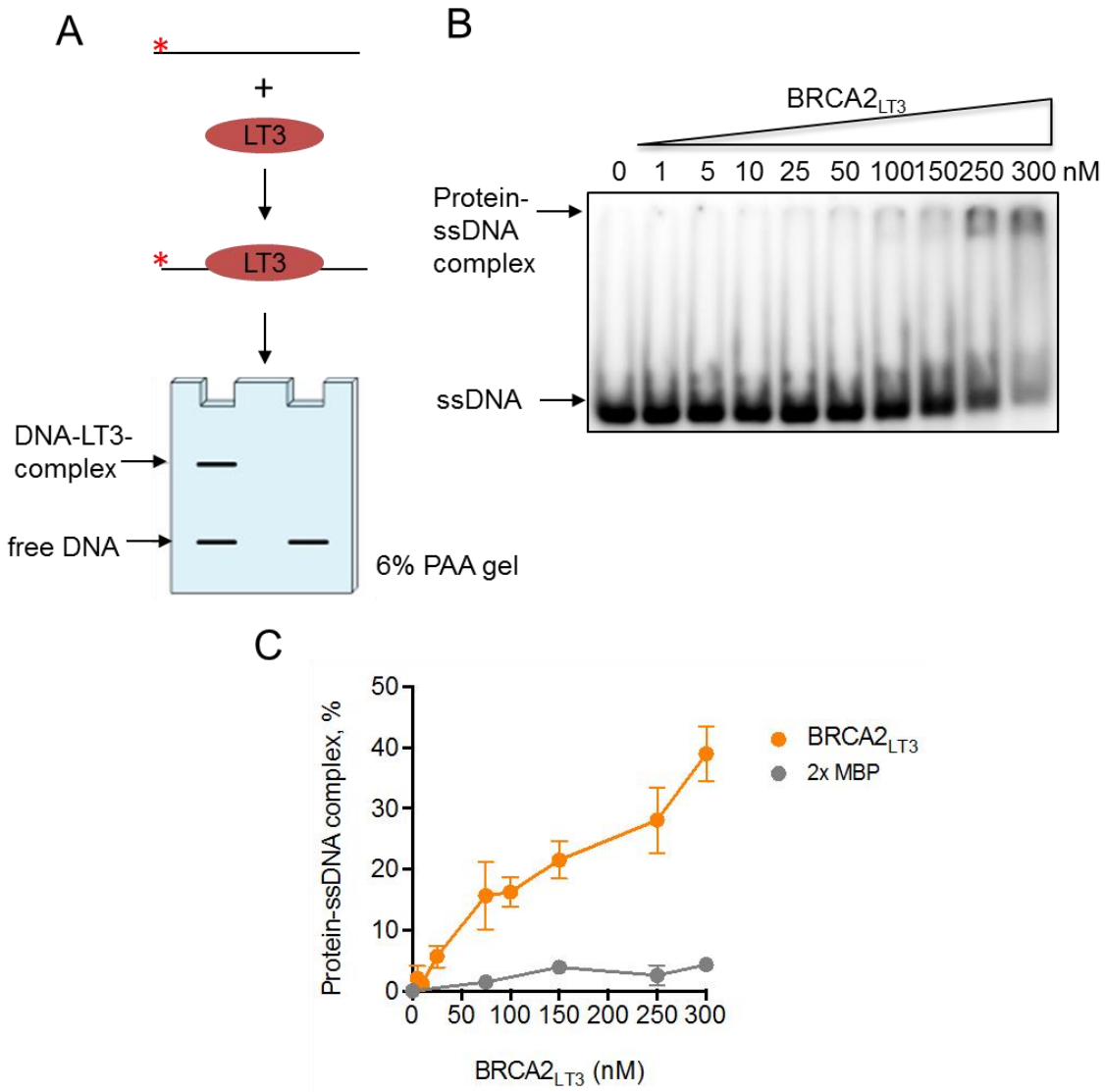

Figure 3: A) Scheme of the EMSA reaction: radiolabeled ssDNA is incubated with the protein of interest ($BRCA2_{LT3)}$ and reactions are loaded on 6% PAGEgel. ssDNA-protein complexes migrate slower on the gel than free DNA. **B)** Autoradiograph of EMSA with $BRCA2_{LT3}$ using increasing concentrations. **C)** Quantification of EMSA with $BRCA2_{LT3}$ and 2x MBP tag as negative control from three independent experiments using GraphPad Prism.

fragments was verified by western blot using an antibody against the MBP tag (Figure 2D right). We started our *in vitro* analysis by testing the largest fragment $BRCA2_{LT3}$ for its DNA binding capacity by using Electrophoretic mobility Shift Assays (EMSA). Here, a DNA substrate (dT_{40} homopolymer) is radioactively labeled with γ-^{32}P and incubated with the protein to allow binding. The samples are loaded on a 6% native

polyacrylamide (PAGE) gel to separate DNA-protein complexes from free DNA that migrate faster (Figure 3A). $BRCA2_{LT3}$ was indeed capable of forming complexes with the DNA that became more evident with increasing protein concentration and reached 40% of DNA-protein complexes (Figure 3B).

As a control, we performed the same assay using the MBP tag alone which did not associate with the DNA (4% complex formation), indicating that the DNA binding activity observed with $BRCA2_{LT3}$ is specific (Figure 3C). To map the DNA binding activity further, we used the same assay with the shorter N-terminal fragments (Figure 4A). While $BRCA2_{LT2}$ and $BRCA2_{T2}$ bound ssDNA to almost the same extent as $BRCA2_{LT3}$ (20-25%), $BRCA2_{T1}$, comprising the first 250 amino acids did not. Thus, the DNA binding domain lies

in the region of $BRCA2_{T2}$ between amino acids 250 and 500. This result coincided with the

DNA binding residues found in the *in silico* analysis of the N-terminus. By examining the partition of $BRCA2_{T2}$ compared to $BRCA2_{T1}$ between biotinylated ssDNA (dT_{80}) immobilized on streptavidin magnetic beads challenged with excess dT_{40} ssDNA as a

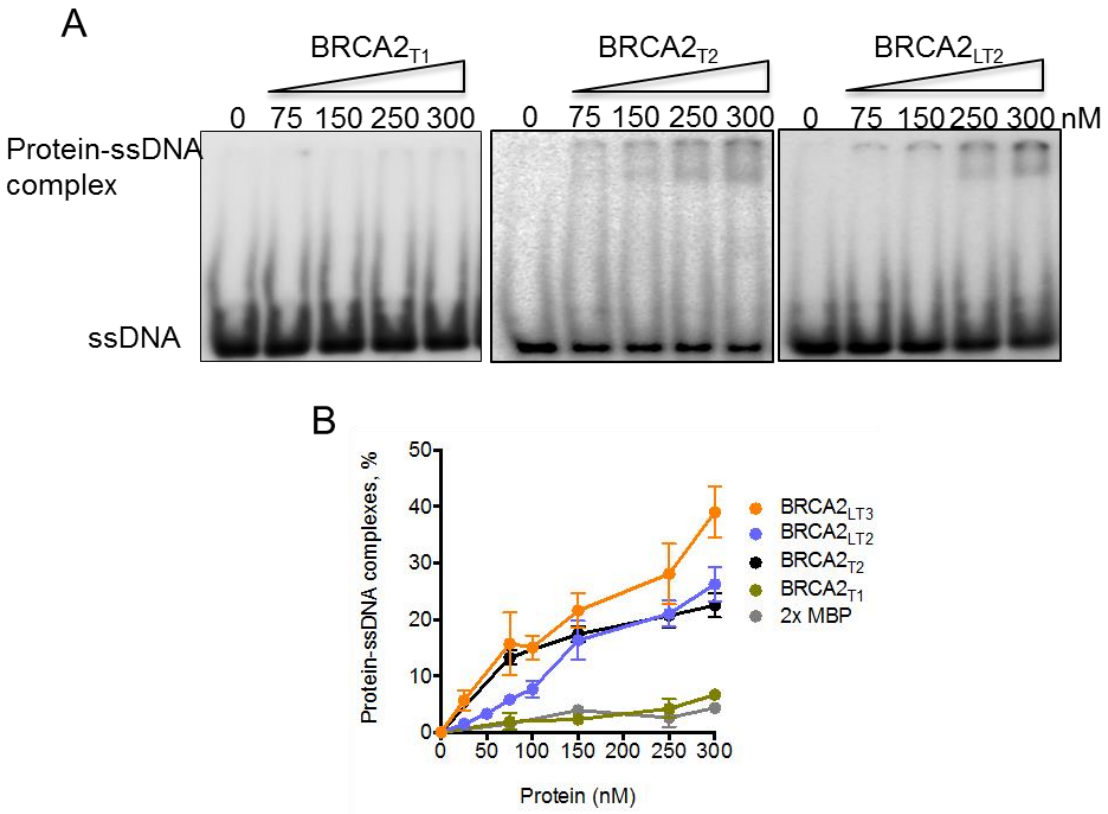

Figure 4: EMSA with N-terminal fragments and ssDNA **A)** Autoradiograph of reactions using $BRCA2_{T1,}$ $BRCA2_{T2,}$ $BRCA2_{LT2}$ with ssDNA in increasing concentrations and **B)** quantification of EMSAs with ssDNA and all fragments from three individual experiments.

control experiment, we could confirm our results; only $BRCA2_{T2}$ and not $BRCA2_{T1}$ was titrated out by adding excess dT_{40} indicating that $BRCA2_{T2}$ binds specifically to DNA (Figure 5).To verify the DNA binding activity of this region, the laboratory of Xiaodong Zhang used the longer fragment $BRCA2_{LT3}$ to visualize the direct interaction with DNA by electron microscopy. Our collaborators could observe the association of the N-terminal domain to a gapped DNA substrate mimicking a daughter strand gap generated after the replication fork encounters a DNA lesion. The BRCA2LT3-DNA complexes adopted V or Y-shaped structures, suggesting that the protein binds to the gap segment or to the ssDNA/dsDNA junction. Interestingly, PARP-like fingered enzymes have been described to bend the DNA upon binding to gap sites adopting a V shaped structure [229]. Using an antibody against the MBP-tag we confirmed that the density on the tip of the V or Y shaped particles corresponds to $BRCA2_{LT3.}$ Collectively, these results indicate that the N-terminal region of BRCA2 binds DNA and that the region of aa 250-500 of BRCA2 ($BRCA2_{T2}$) comprising the putative zf-PARP domain is sufficient for this activity.

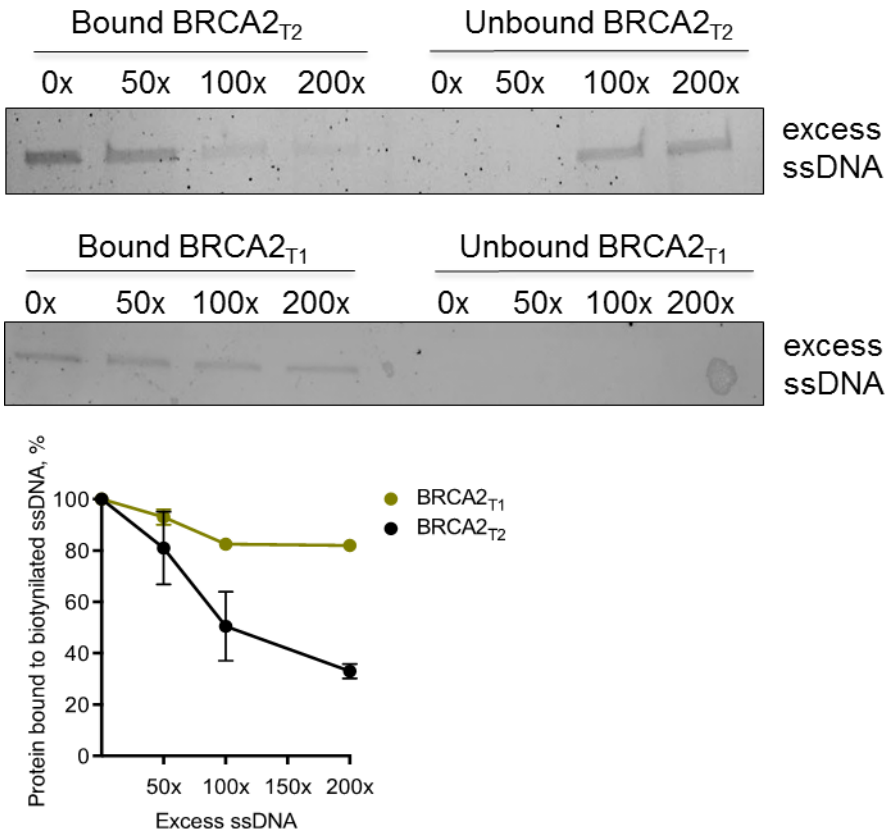

Figure 5: Pull down experiment with $BRCA2_{T2}$ or $BRCA2_{T1}$ using biotinylated ssDNA (dT_{80}) immobilized on streptavidin magnetic beads challenged with excess dT_{40} ssDNA (up) and quantification of 3 individual experiments using GraphPad Prism (bottom).

Zinc-finger PARP like motifs are DNA or protein-binding domains that have first been identified in Poly(ADP)ribose proteins (PARPs) but can be found in many enzymes. One or more zinc ions are coordinated via Cysteine and Histidine residues allows to adopt and stabilize a finger-like structure that contacts the DNA [230,231].

Because the DNA binding activity was assumed to originate from a zinc finger motif, we tested the NTD activity in presence of different cations to see if they intensified the DNA binding affinity.

We incubated $BRCA2_{T2}$ (1 µM) with ssDNA in presence or absence of different cations (Figure 6). Adding no metal or EDTA as a chelating agent to the reaction reduced the DNA binding activity of about 10% compared to the binding activity in our standard conditions with 1 mM Mg^{2+} & 2 mM Ca^{2+} (22-30%). Ca^{2+} (1 mM or 10 mM) stimulated

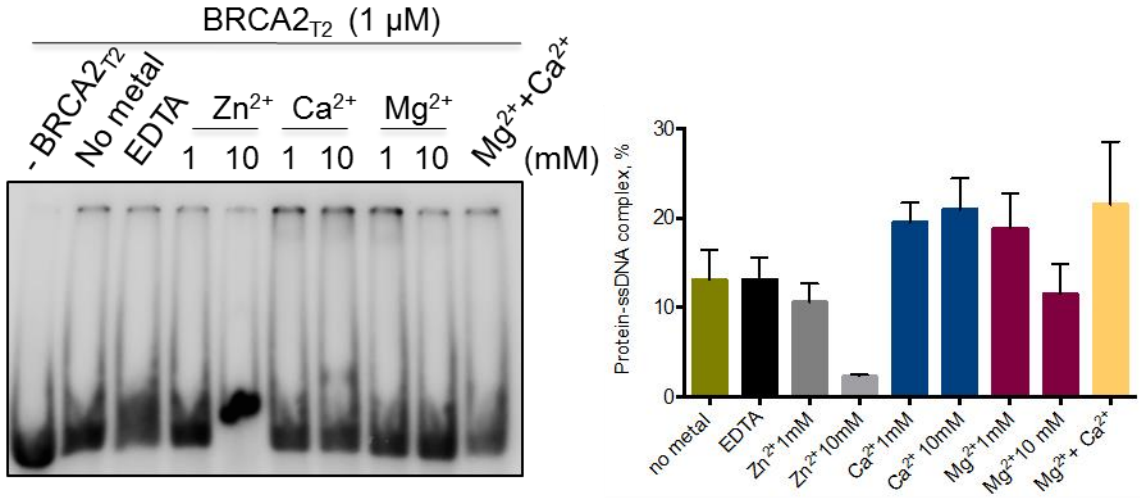

Figure 6: Left panel: EMSA with $BRCA2_{T2}$ (1 µM) and ssDNA (dT_{40}) in the presence or absence of no metal, EDTA (25 mM), Zn^{2+}, Mg^{2+}, Ca^{2+}, Mg^{2+}(1 mM) + Ca^{2+} (2mM) at the indicated concentrations. **Right panel:** Quantification of the EMSA (n=3).

the reaction (22%) but did not reach the highest level achievable, while Mg^{2*} at 1 mM stimulated the reaction to similar levels but was decreased 10 mM. Surprisingly, Zn^{2*} ions decreased the DNA binding activity by 2% at 10 mM. These results indicate that the DNA binding activity of the N-terminus of BRCA2 is not dependent on Zinc, however it is moderately enhanced by Ca^{2+} and Mg^{2+}.

Since BRCA2 contains a canonical DNA binding domain in the C-terminus, we next sought to investigate how the NTD differs from the CTD in terms of function and binding specificity. For this, we purified recombinant human CTD (aa 2474-3190, Figure 7A) from bacterial cells using a 6x His-tag for affinity chromatography and in fusion with SUMO protein to enhance the product yield.

The experimental set up for the expression and purification was achieved in collaboration with Patricia Duchambon and Ahmed El Marjou from the recombinant protein platform (I. Curie). The CTD was co-expressed with its protein partner DSS1 (see chapter 1.7) to confer stability and solubility to the protein as we observed massive degradation during purification attempts without it. DSS1 might be needed for proper folding of the CTD. This was also observed by Yang et al. (2002) who purified the mouse CTD in complex with DSS1 for crystallization studies [127]. *E. coli* cells were transformed with expression constructs for CTD and DSS1 and 7L of culture were induced for protein expression. The first purification step involved the incubation of the protein with Ni-NTA resin to which the His-tag binds. The protein was eluted with Imidazole and verified on a SDS gel (Figure 7B, left). After dialysis, the protein was subjected to a heparin column as this type of column is generally used for DNA binding proteins. The protein was eluted using a NaCl gradient (Figure 7B, right). The chromatogram showed several protein peaks when loading the fractions on a SDS gel but only the purest fractions (2-4) were pooled and dialysed against storage buffer and stored at -80C. DSS1 stayed bound to the CTD as verified by western blot using an antibody against the His-tag for the CTD and an antibody against DSS1 (Figure 7C).

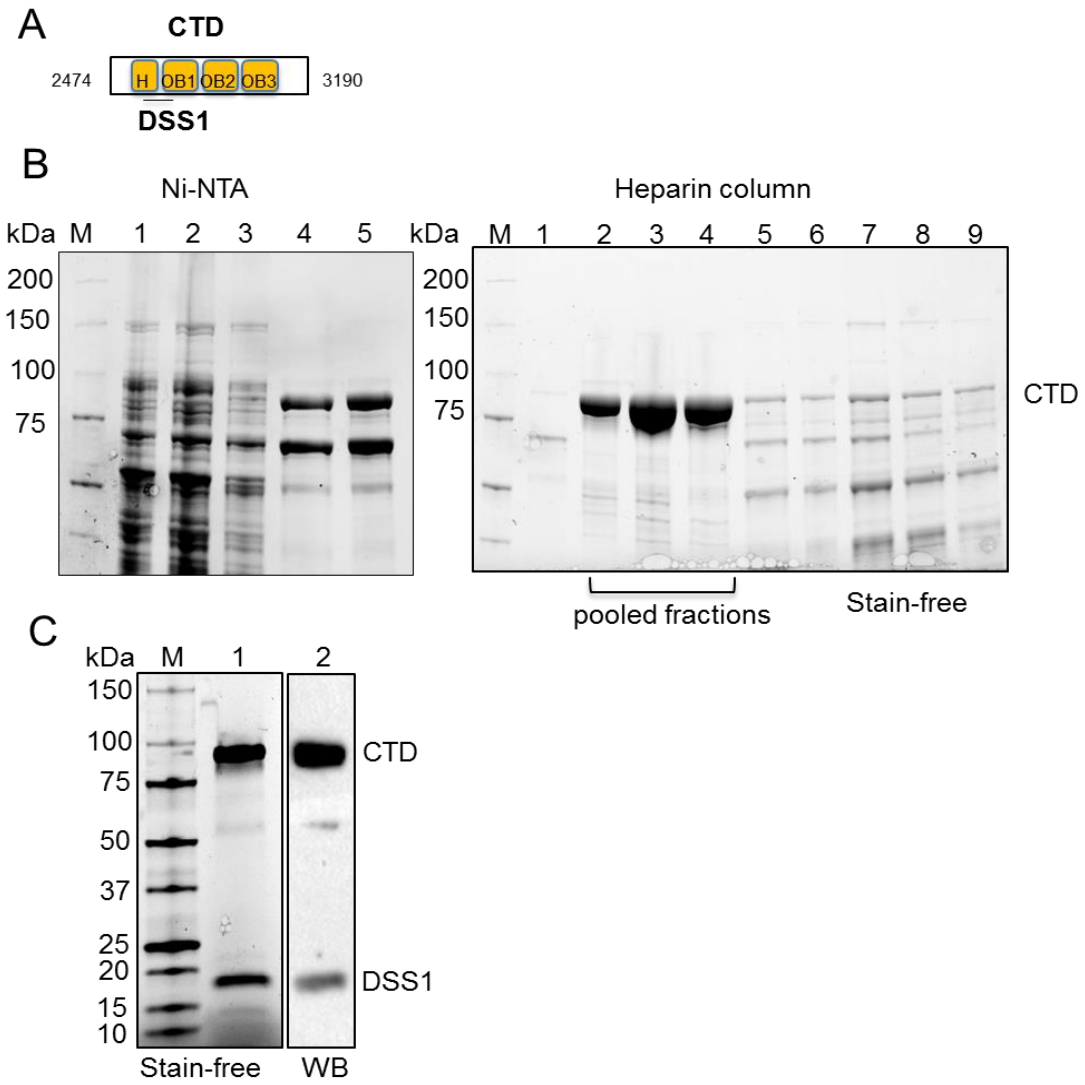

Figure 7: Purification of the C-terminal DNA binding domain of BRCA2. **A)** Scheme of the structure and size of the protein fragment purified. **B)** Left: SDS gel of first purification step with Ni NTA resin. Lane: 1) Sample loaded 2) unbound fraction 3) wash 4) elution with Imidazole 5) dialysed protein. Right: SDS gel of the second step of purification using a Heparin chromatography column: 1) unbound fraction, 2-9) fractions from elution with NaCl gradient indicating the fractions pooled for dialysis (2-4) **C)** 1) Purified protein (5 µg) loaded on a 4-15% SDS-PAGE gel. 2) Western blot with antibodies against His-tag for CTD and anti-DSS1 antibody.

We then used the CTD and NTD to compare their DNA binding activities and affinities to different DNA substrates mimicking recombination intermediates of DSBs and daughter strand gaps.

Using EMSAs as described above, we first tested the binding of both proteins to a

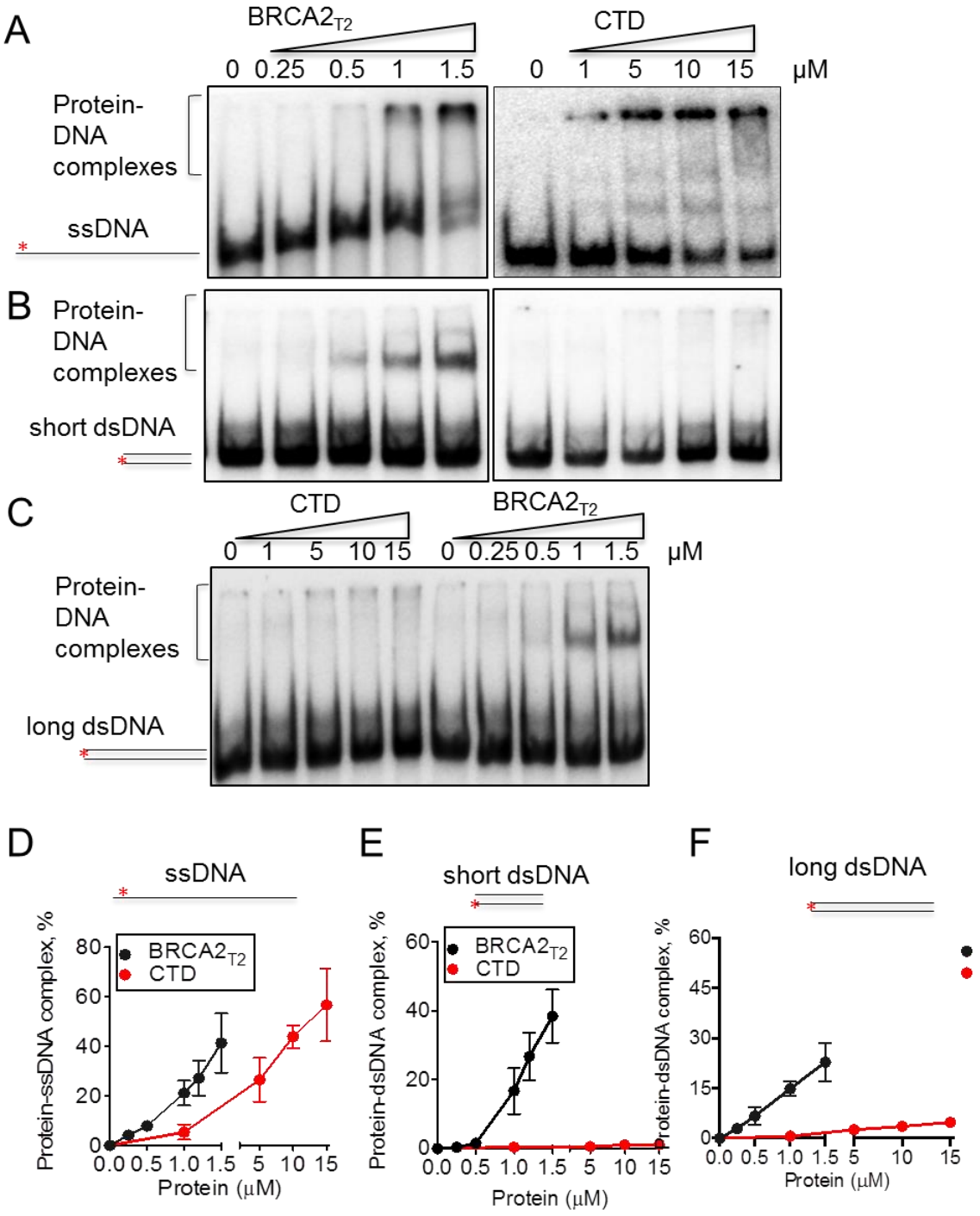

Figure 8: EMSA comparing the DNA binding activity of NTD and CTD. **A)** Binding of NTD and CTD to radiolabeled ssDNA (167mer) **B)** to short dsDNA substrate and **C)** to long dsDNA substrate. **D-F)** quantification of at least three experiments for all DNA substrates.

ssDNA substrate (167 nt polymer). It was shown before that the binding of the CTD to short substrates is very weak and increases from 60 nucleotides onwards [127,158]. Both proteins bound ssDNA but $BRCA2_{T2}$ formed a maximum of ~40% protein-ssDNA complexes at its highest attainable concentration (1.5 μM), whereas the concentration of CTD to reach that % of protein-ssDNA complex was 10 μM (Figure 8A and C). Thus, $BRCA2_{T2}$ shows either higher affinity or more stable complexes with ssDNA than CTD. Next we tested the binding of the two domains to substrates that mimic the ds/ssDNA junction at DSBs and daughter strand gaps. For this, we designed DNA substrates with 3' or 5' overhang as well as a DNA gap substrate and performed EMSAs. The CTD showed higher complex formation (~35%) with the 3'overhang DNA substrate however the $BRCA2_{T2}$ bound with higher affinity at low concentrations (Figure 9 A, C). A similar pattern was observed in EMSAs using a 5' overhang DNA substrate: Both proteins reached similar levels of complex formation of ~40% at the highest attainable concentration although CTD reached that yield at 6 times higher the concentration of the NTD (Figure 9 B, E). Last, $BRCA2_{T2}$ showed high affinity for the gapped DNA substrate reaching ~60% protein-DNA complex. In contrast, the CTD bound less tightly (~25%) even at concentrations 10 times higher than the ones used for the NTD (Figure 9 C, F). Taken together, our results from these DNA binding assays indicate that $BRCA2_{T2}$ comprising the NTD has an overall higher affinity for all DNA substrates tested, especially the substrates mimicking the ds/ssDNA junction or a daughter strand gap. Moreover and in contrast to the CTD, NTD binds dsDNA.

The crystal structure of the mouse CTD has been solved [127], however, because the mouse sequence shares only 68% homology with human BRCA2 and there are questions still unsolved regarding the DNA binding modes of this region, we also aimed to solve the structure of the CTD in complex with DNA by crystallization in collaboration with the group of Xiaodong Zhang (Imperial College London). Hence, we produced the CTD in a 7 liters bacterial culture in a fermenter and we were able to obtain the protein in sufficient purity and amount for the crystallography. This work is ongoing.

Some of the zinc finger proteins described do not coordinate a zinc ion for stabilization instead, they establish salt bridges for their association with DNA [232]. Since we did not observe a stimulation of DNA binding in the presence of Zn^{+2} we reasoned this could be the case of NTD. Even though cysteine residues do not form salt bridges, they could be

required for the shaping and stabilization of the zinc finger structure via disulfide bond formation. To find out the residues important for DNA binding, we mutated three of the cysteines present in the domain. We chose to mutate two cysteines that have been found substituted for serine in breast cancer patients (C315S, C341S) (BIC and BRCAshare databases[209,210]). The third one is an artificial alanine substitution of C279

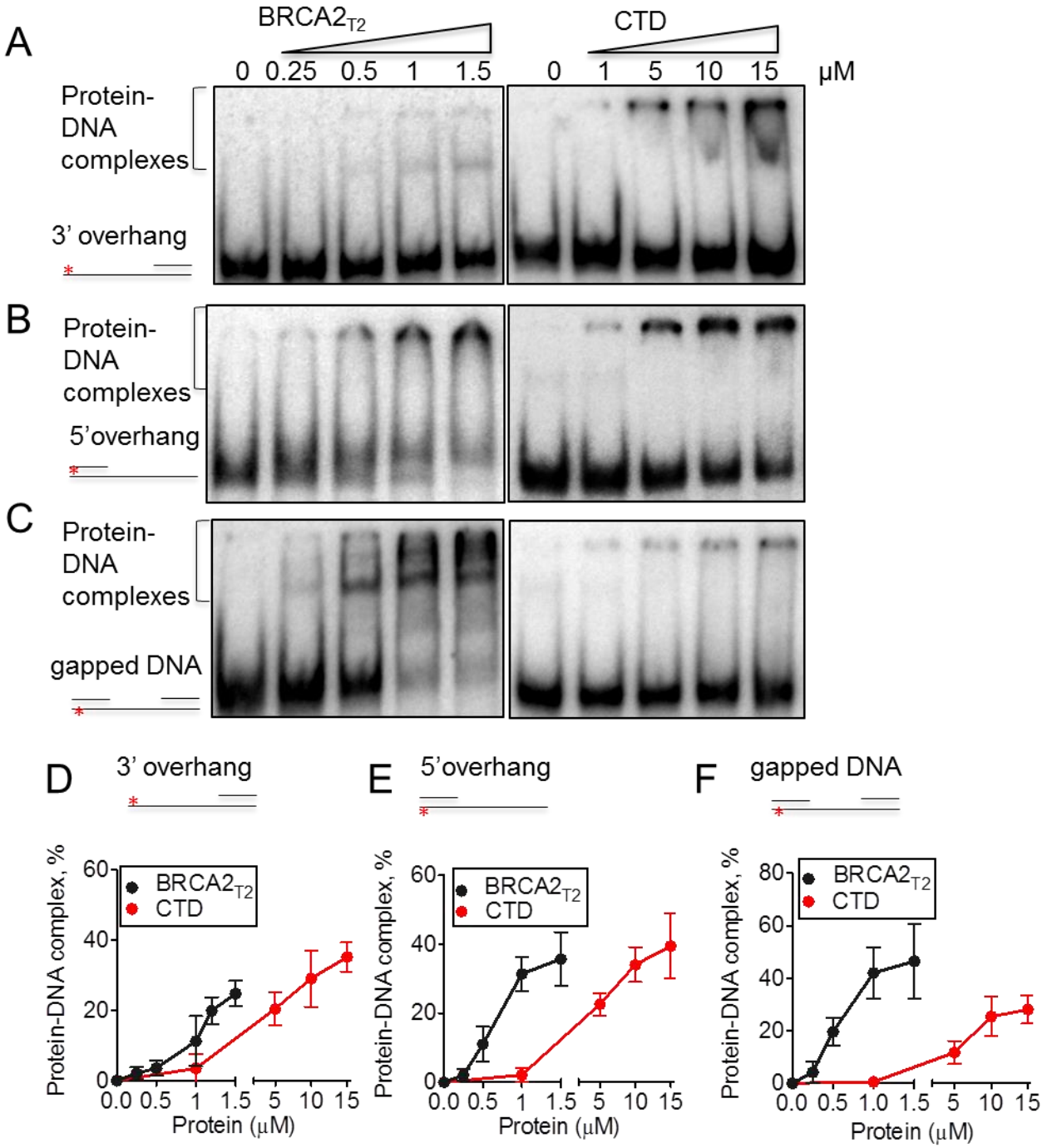

Figure 9: EMSA with different DNA substrates to compare NTD and CTD binding specificities. Autoradiographs of **A)** reaction with 3' overhang substrate **B)** 5' overhang substrate **C)** gapped DNA and **D-F)** quantification of A-C from at least three individual experiments.

(Figure 10 A). Single or combinations of double mutations were introduced in the $BRCA2_{T2}$ fragment by site-directed mutagenesis and purified to nearly homogeneity as described for the other fragments (Figure 10 B).

The fragments were then used for DNA binding assays as described before. First we tested the fragments containing the single missense mutations and compared their binding with the wild type fragment $BRCA2_{T2}$.

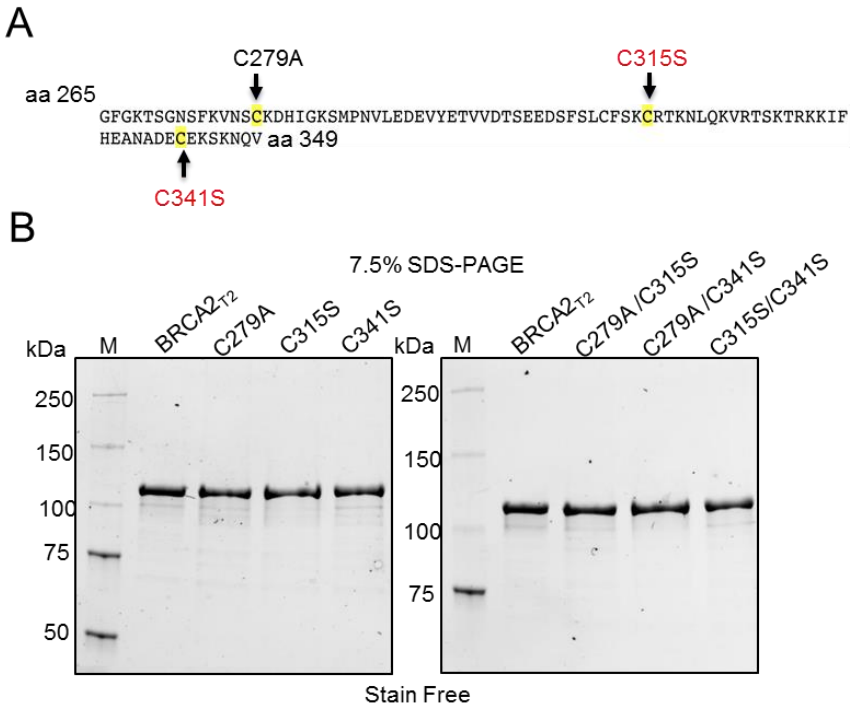

Figure 10: A) Amino-acid sequence comprised in the zf-PARP like domain showing the selected variants (red)/ mutations (black) mutated alone or in combination in $BRCA2_{T2}$ cDNA. **B)** Protein fragments expressed in HEK293s and purified using affinity chromatography and ion exchange as described for the other fragments. 1 µg of each protein loaded on a 7.5% SDS gel.

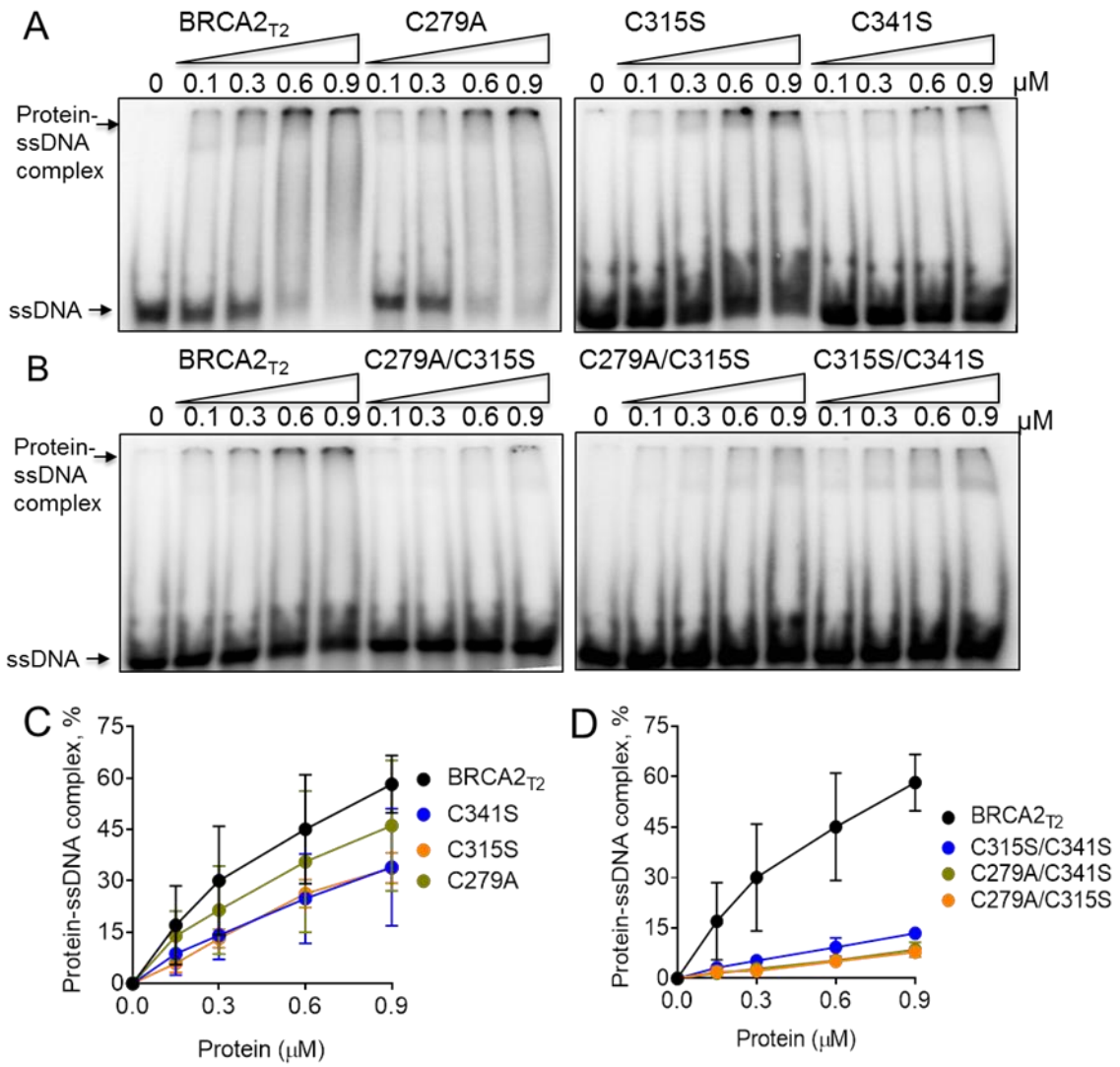

Figure 11: EMSA using $BRCA2_{T2}$ and variant fragments with dsDNA (40mer). Autoradiographs of A) Binding of $BRCA2_{T2}$ and single mutants to dsDNA B) Binding of $BRCA2_{T2}$ and double mutants to ssDNA in EMSAs. Quantification of C) (n=3) D) At least three individual experiments with $BRCA2_{T2}$ and double mutants.

As shown in Figure 11A and C, all fragments containing the single mutations were able to bind ssDNA, although the percentage of complex formation was slightly reduced for about 10-20% compared to $BRCA2_{T2}$. In contrast, the double mutants drastically decreased the ssDNA binding capacity to 5% at the highest attainable concentration in comparison to $BRCA2_{T2}$ that reached up to 60% ssDNA-protein complex formation (Figure 11B; D). This indicates that the cysteine residues tested are important for the ssDNA binding activity of the N-terminus, probably by conferring stability to the binding domain formed. Next, we evaluated the binding capacity of the single and double

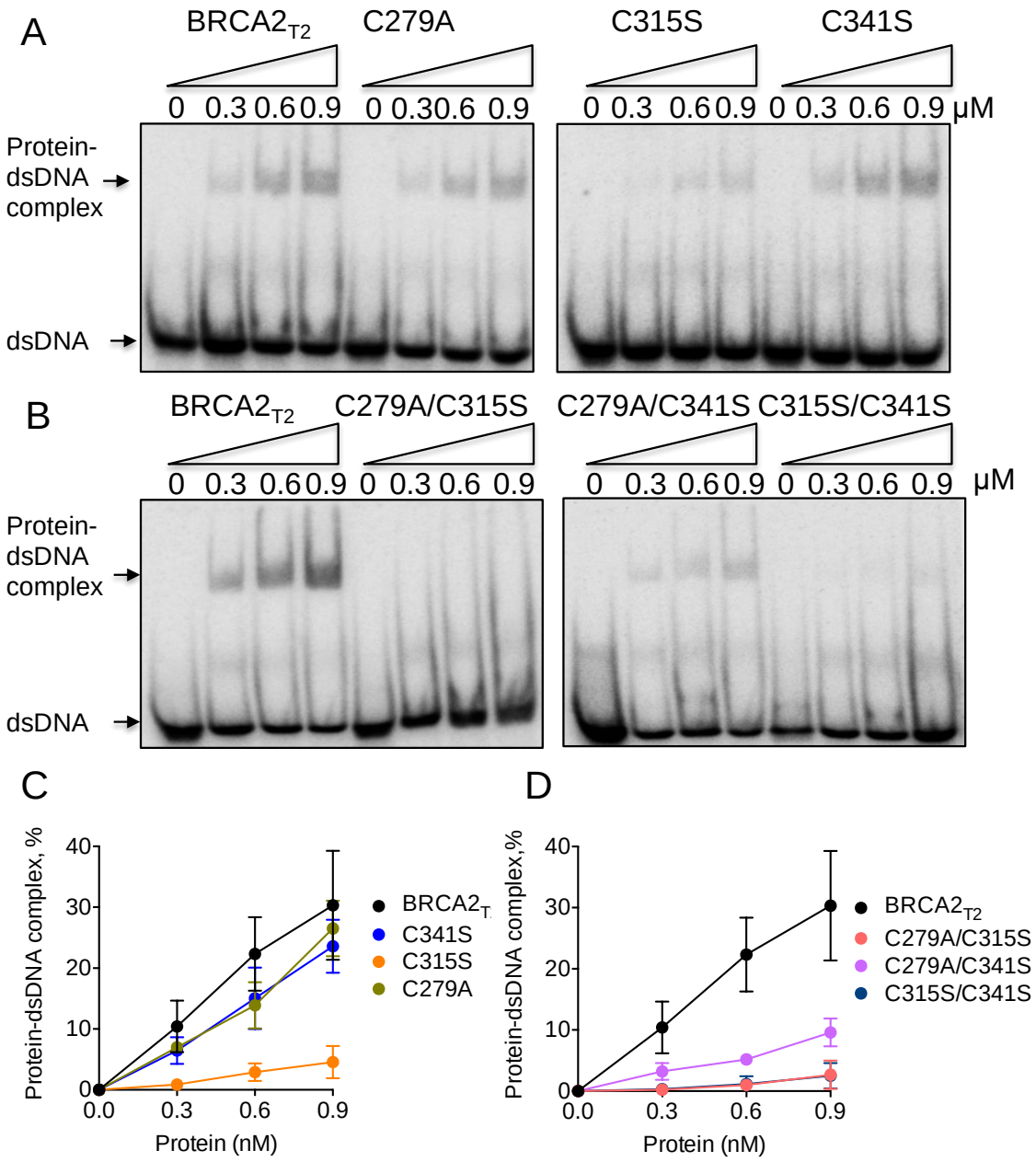

Figure 12: DNA binding assays (EMSAs) using $BRCA2_{T2}$ and variant fragments with dsDNA (40mer). Autoradiographs of **A)** Binding of $BRCA2_{T2}$ and single mutants to dsDNA. **B)** Binding of $BRCA2_{T2}$ and double mutants to dsDNA in EMSAs. Quantification of **C)** (n=3). **D)** at least three individual experiments with $BRCA2_{T2}$ and double mutants.

mutants to dsDNA. As shown before, unlike CTD, $BRCA2_{T2}$ readily binds dsDNA (Figure 8). The binding of the single mutants C279A and C341S was only slightly reduced in comparison to the wild type protein (30% dsDNA-protein complex formation). However, C315S almost abolished the binding activity (Figure 12A, C). In addition, the double mutants reduced the dsDNA binding activity even further, especially in the case of the double mutants containing C315S mutation (Figure 12 B, D). These results indicate that the C315 is particularly required for the association of the NTD to dsDNA, a function specific to this domain and probably of high importance

for the proper positioning of RAD51 on the DNA (see discussion 2.3). These results might also explain why C315S is frequently mutated in breast cancer patients although its clinical relevance is still unknown.

It has been shown that fusion peptides of one BRC repeat important for RAD51 binding and the CTD or RPA70 subunit are sufficient to enhance RAD51 recombination activity [151,152]. Thus, having shown the existence and functionality of a DNA binding site in the N-terminus, we wanted to know if a fusion peptide consisting of $BRCA2_{T2}$ and BRC4 would have the same effect. We first fused BRC4 at the C-terminus of $BRCA2_{T2}$ in the expression construct however the protein was not stable and rapidly degraded after purification. In a second attempt we cloned BRC4 between the N-terminal 2x MBP tag and $BRCA2_{T2}$. This expression construct was stable and we obtained a pure fusion peptide after the purification procedure as described for all other fragments (Figure 13A).

To test the recombination activity of RAD51 we used an in vitro short oligonucleotide DNA strand exchange assay as described before [70]; RAD51 is incubated with a 3' overhang substrate that mimics the 3' tail generated after DSB resection. After incubation, a radiolabeled dsDNA substrate is added that is complementary to the 3'tail and RAD51 will perform strand exchange between the two substrates. RAD51 strand exchange activity can be observed by loading the reactions on a native PAGE gel:

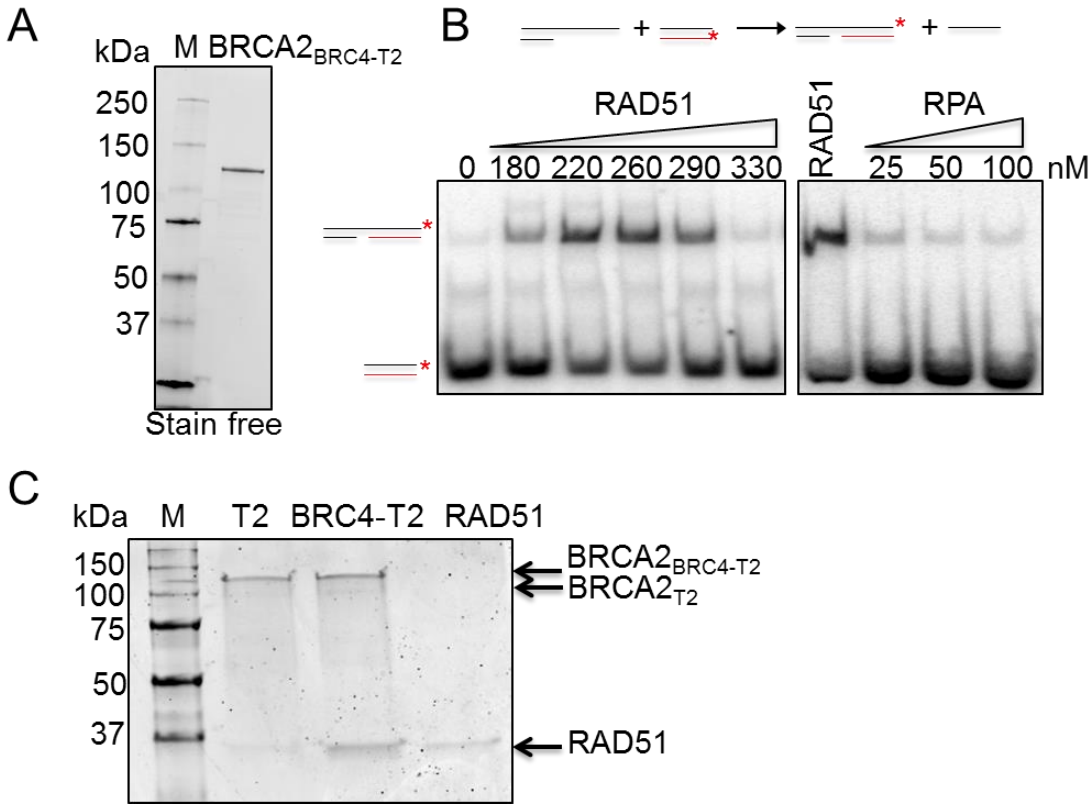

Figure 13: **A)** Purified $BRCA2_{BRC4-T2}$ (1ug on SDS gel). **B)** Top**.** Experimental set up for strand exchange assays: Scheme of the reaction. Autoradiograph of DNA strand exchange reaction using a 3' ssDNA overhang substrate at the indicated concentrations of RAD51 (left). DNA strand exchange reaction with increasing concentrations of RAD51 (left) or RPA (right). **C)** Pull-down experiment with $BRCA2_{T2,}$ $BRCA2_{BRC4-T2}$ with RAD51 and RAD51 alone loaded on a 7.5% SDS gel stained with SYPRO Orange.

The strand exchange product is larger and migrates slower than the free dsDNA (see Figure 13B). We first titrated RAD51 to find the optimal concentration for the reaction (Figure 13B left). The ssDNA overhang resulting from resection of the DSB is rapidly coated by the ssDNA binding protein RPA to avoid further resection and formation of secondary structures. However, RAD51 activity is inhibited by RPA as it binds ssDNA with higher affinity. The mediator activity of BRCA2 is based on two mechanisms: First,

it blocks RAD51 the unproductive assembly of RAD51 on dsDNA. Second, it alleviates RPA inhibition by facilitating its displacement by RAD51. To test a possible mediator activity of NTD we titrated RPA in the strand exchange reaction to find the optimal concentration for RAD51 inhibition (Figure 13B right).

We first tested the promotion of strand exchange activity of RAD51 in presence of $BRCA2_{BRC4\text{-}T2}$ and RPA. The 3' tail substrate was incubated with RPA before adding

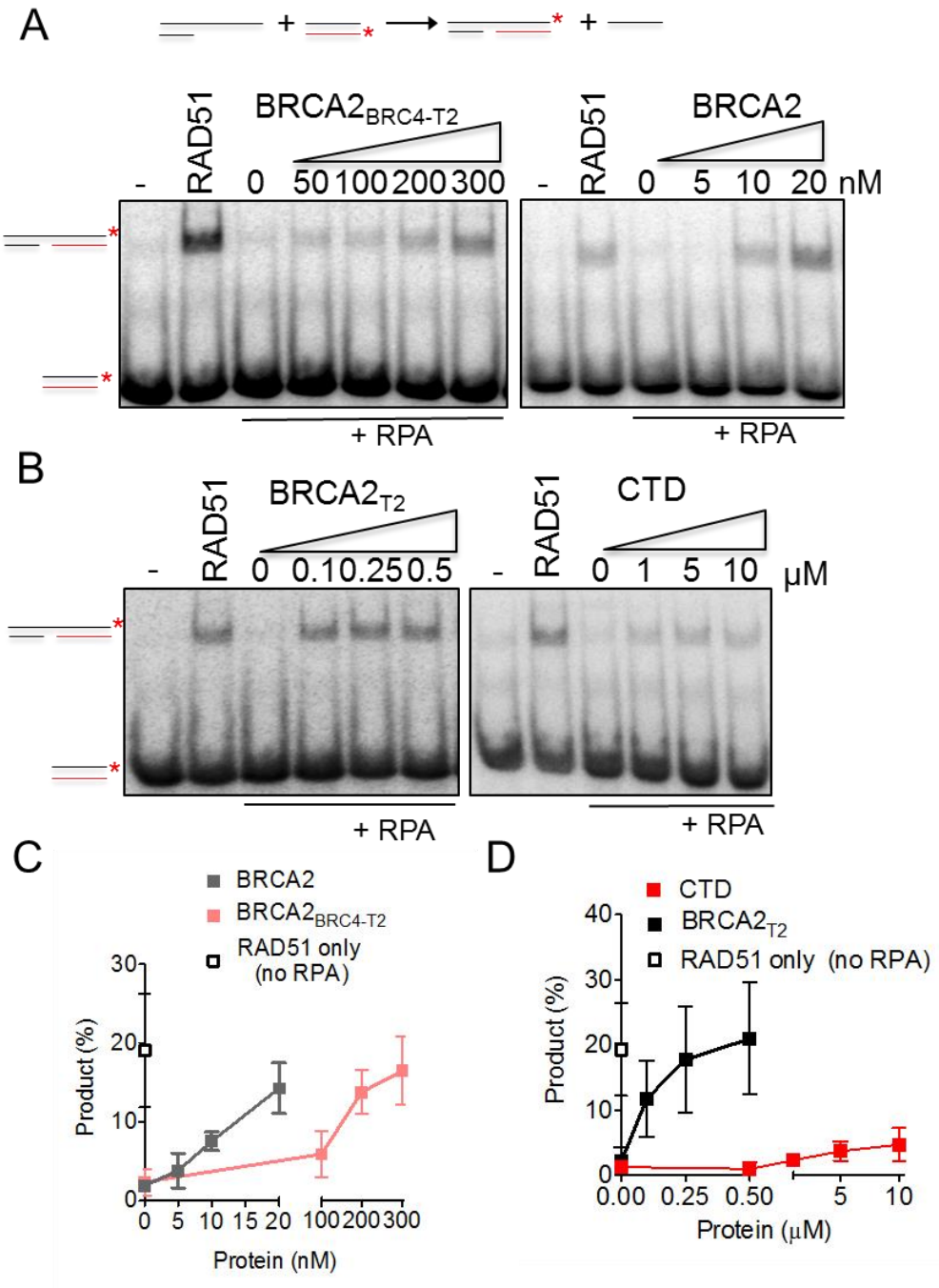

Figure 14: DNA strand exchange assays. **A)** Reaction scheme (up) and autoradiograph of the assay using $BRCA2_{BRC4\text{-}T2}$ or full length BRCA2 **B)** $BRCA2_{T2}$ or CTD in the indicated concentrations. Quantification of **C)** $BRCA2_{BRC4\text{-}T2}$ or full length BRCA2 and **D)** $BRCA2_{T2}$ or CTD (n=3)

RAD51 and $BRCA2_{BRC4\text{-}T2}$. After a short incubation, the radiolabeled dsDNA was added. As shown in Figure 14A (left gel), $BRCA2_{BRC4\text{-}T2}$ was able to alleviate the inhibitory effect of RPA (lane 3). The addition of increasing concentrations of $BRCA2_{BRC4\text{-}T2}$ almost restored the level of RAD51 strand exchange activity that RAD51 reaches in the absence of RPA (lane 2, Figure 14C). When comparing the stimulatory activity to that of the full length BRCA2, the stimulatory effect of the proteins was similar, although at a concentration of $BRCA2_{BRC4\text{-}T2}$ 10 times higher than that of BRCA2 (Figure 14A, right and 14C).

The CTD alone was shown before to have a stimulatory effect in strand exchange reactions [127]. We thus wanted to see if $BRCA2_{T2}$ is also capable to promote strand exchange activity without BRC4 by using strand exchange assays As $BRCA2_{T2}$ showed high affinity for dsDNA and ds/ssDNA junction substrates in DNA binding assays (Figure 8&9) we presumed that it could promote RAD51 binding to ssDNA over dsDNA in absence of a BRC repeat by outcompeting RPA.

Interestingly, $BRCA2_{T2}$ alone stimulated RAD51 activity to a similar extent as $BRCA2_{BRC4\text{-}T2}$ (Figure 14B; D). To make sure that this activity does not stem from an interaction between $BRCA2_{T2}$ and RAD51, we performed pull-down experiments comparing the binding of $BRCA2_{BRC4\text{-}T2}$ and $BRCA2_{T2}$ to RAD51 and showed that $BRCA2_{T2}$ doesn't bind RAD51 (Figure 12C). Hence, we could show that under our experimental conditions (saturating RAD51 concentration and short DNA substrate) $BRCA2_{T2}$ without BRC4 is sufficient to facilitate RAD51 recombination maybe by counteracting RPA binding to ssDNA. We next tested the proteins for the stimulation of strand exchange activity by RAD51 in absence of RPA. In contrast to $BRCA2_{T2}$, the fusion peptide with BRC4 stimulated the strand exchange reaction also in absence of RPA to the same extent as full length BRCA2 (Figure 15C, D).

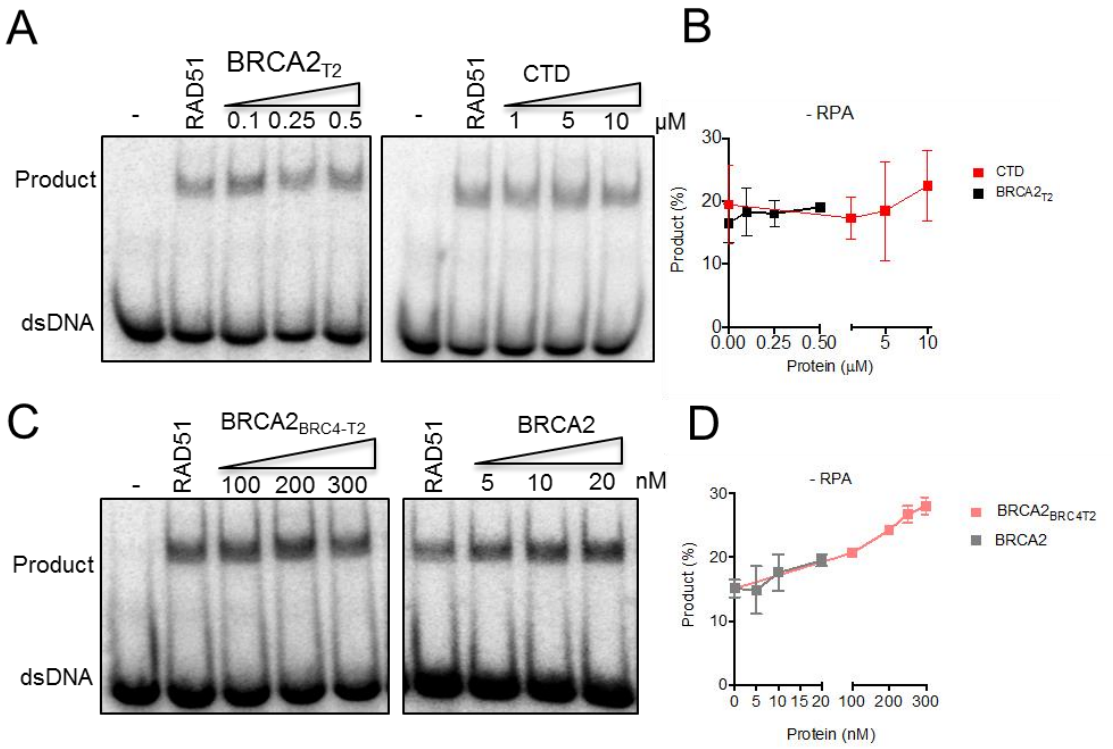

Figure 15: Effect of BRCA2 fragments on RAD51 DNA strand exchange activity in the absence of RPA. **A)** Autoradiogram showing the reaction with $BRCA2_{T2}$ and CTD alone **B)** quantification of A, (n=3). **C)** Autoradiogram showing the reaction with $BRCA2_{BRC4\text{-}T2}$ and full length BRCA2. **D)** Quantification of C, (n=3).

This activity probably stems from the ability of BRC4 to stabilize RAD51 filaments on the ssDNA by inhibiting its ATP hydrolysis. When we tested the CTD in strand exchange assays, we observed only little stimulation (4%) of the activity in presence of RPA as it was shown with the mouse CTD [127] (Figure 14B, D). Consistent with previous results[127], in the absence of RPA, the CTD had no effect on RAD51 DNA strand exchange activity, confirming that CTD-DSS1 complex removes RPA from the as it has been recently described [69] (Figure 15A, B). Also the concentration needed to achieve a small stimulatory effect was 10 times higher than for $BRCA2_{T2}$ similar to our observations in the DNA binding comparison (Figure 8 & 9).

Because we observed stronger enhancement of the strand exchange reaction by $BRCA2_{T2}$ compared to the CTD, we wondered if this activity could stem from the dsDNA binding activity of NTD. The single missense mutant C315S and the double mutants had shown a defective phenotype in dsDNA binding (Figure 12C; D). We thus tested the DNA strand exchange activity of $BRCA2_{T2}$ carrying C315S and C279C315S mutations when using the 3'tail substrate that has a ds/ssDNA duplex structure. Indeed, the C315S mutant and to a higher extent the C279AC315S mutant reduced RAD51 strand exchange activity suggesting that the dsDNA binding activity is important for the DNA strand exchange stimulatory effect observed with this type of substrate (Figure 16 A; B). To control that this effect stems from the inability of C315S to associate with ss/dsDNA and not from a folding defect due to the mutation, we conducted the same strand exchange assay using a ssDNA (167mer) substrate. Here,

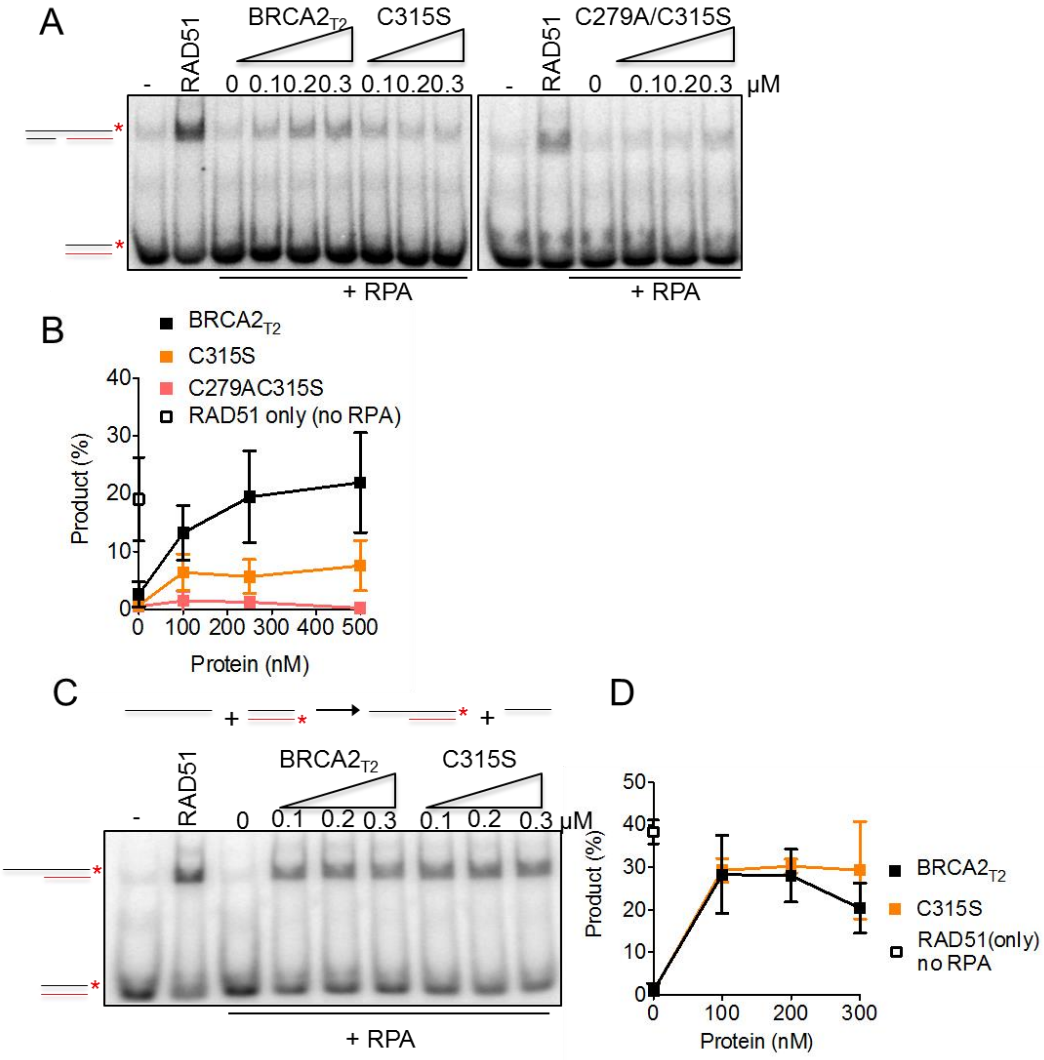

Figure 16: DNA strand exchange assays **A)** comparing $BRCA2_{T2}$ with C315S and C279AC315S double mutant, quantification in **B).** Strand exchange assay using ssDNA as a substrate **C)** comparing $BRCA2_{T2}$ with C315S **D)** quantification of C (n=3).

the C315S variants showed the same stimulatory activity on DNA strand exchange activity and product formation than wild type $BRCA2_{T2}$ (Figure 16 C; D).

2.3 DISCUSSION

In this work we demonstrate for the first time a DNA binding activity specific to the N-terminal domain of BRCA2. Our research was based on the assumption that the N-terminus must inherit a function similar to the CTD to rescue the HR proficiency in absence of the C-terminus as it was observed in several studies [108,109,151,156,157] (see 2.1).

PALB2 binds to the N-terminus of BRCA2 and can bind to DNA as well as promote HR by RAD51 *in vitro.* BRCA2 and PALB2 form a complex to localize to and cooperate at the DSB sites to promote D-loop formation [106,108,233]. It was suggested that in the absence of the CTD, BRCA2 is dependent on PALB2 interaction to restore HR [109].

However, the discovery of a second DNA binding domain in the BRCA2 ortholog Brh2 (*U. maydis*) [159] led us to investigate whether a similar function was present in human BRCA2.

This DNA binding domain is located next to the unique BRC motif in this organism. Brh2 mutants lacking the CTD can rescue the sensitivity to DNA damage and both DNA binding domains seem to collaborate in this function [155,159].

The unstructured nature of the N-terminal domain of BRCA2 makes difficult to foretell possible functions based on secondary structure prediction. However, it is known that the function of intrinsically disordered proteins (IDPs) depends mostly on their flexibility and ability for structural changes. Often, their active structure forms upon binding to an interacting protein or nucleic acid partner [234]. DNA-binding proteins often contain intrinsically disordered regions with which they contact the DNA [235]. Interestingly, unlike in the case of Brh2 NTD, the CTD of human BRCA2 or RPA70, where the DNA binding domain is an OB-fold like structure, the NTD revealed in this study is a zinc-finger PARP like domain.

The cysteine and histidine residues located in this zinc finger PARP domain in the N-terminus do not exactly follow any of the proposed patterns found in the motifs of zinc finger protein families, however, it could resemble or have evolved from the C_2HC-type (Zinc finger, C_2HC-type (IPR002515 – InterPro [227]) (Figure 17). In any case, using DNA binding assays with purified fragments of the N-terminus we could confirm the hypothetical DNA binding site and map it to $BRCA2_{T2}$ (250-500 aa), consistent with the *in silico* localization of the zinc finger PARP domain. Our results were supported by the identification of two clusters of putative DNA binding residues using BindN software [225] (Figure 2, 3). Importantly, $BRCA2_{T2}$ does not comprise the PALB2 binding site at the extreme N-terminus eliminating PALB2 as the possible mediator of the interaction with DNA. Indeed, we could not detect a DNA binding activity in the first 1-250 amino acids of BRCA2 ($BRCA2_{T1}$) (Figure 3) and this was further confirmed by examining the partition of $BRCA2_{T2}$ compared to $BRCA2_{T1}$ between biotinylated ssDNA (dT_{80})

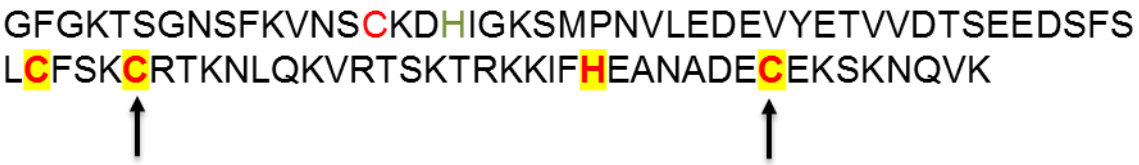

Figure 17: Amino acid sequence (249-349) of the N-terminus of BRCA2 predicted to contain a zinc-finger PARP like domain. Cysteine (C) and Histidine (H) residues are highlighted in red, the residues in yellow could constitute the C_2HC zinc-finger DNA binding motif. The residues C315S and C341S found in breast cancer patients are indicated with arrowheads.

immobilized on streptavidin magnetic beads challenged with excess dT_{40} ssDNA. In this experiment, only $BRCA2_{T2}$ and not $BRCA2_{T1}$ was titrated out by adding excess dT_{40} indicating that $BRCA2_{T2}$ binds specifically to DNA (Figure 5).

In addition, in negatively stained EM pictures, the N-terminal fragment bound to the gapped DNA and changed its conformation upon DNA binding into Y or V-shaped structures, a conformation that has been described for zinc finger motifs [232]. Being a zinc finger like motif, we examined whether NTD requires zinc ions to stabilize the binding of the finger to its target DNA [230]. However addition of Zinc ions did not stimulated but rather inhibited the reaction at the two concentrations tested. It's possible that this domain establishes salt bridges for its association with DNA as it is the case in other zinc finger proteins [227].

By purifying the CTD in complex with DSS1 we could confirm for the first time the observations made with mouse CTD[127] in the human homologue that the CTD is proficient in binding to several DNA substrates except dsDNA, even though it was suggested that the tower domain could be responsible for this function [127]. In contrast

to what was observed with the CTD and Brh2, the NTD bound efficiently long and short dsDNA substrates. In addition, it showed high affinity for gapped and 3'- or 5'-overhang DNA substrates, pointing towards a possible functional role of the NTD in binding to the ssDNA/dsDNA junction at resected DSBs or daughter strand gaps arising during replication (Figure 7-9). We examined the cysteine residues comprised in the zf-like domain. Although we could not find evidence of zinc coordination, these residues could be needed for shaping and stabilizing zinc finger folds via disulfide bonds. Interestingly, C315S showed a strong defect in dsDNA binding. The fact that this mutation is listed 19 times in the BRCA2 VUS databases BRCAshare and BIC [209,210] may indicate that this function is important for BRCA2. If the NTD can compensate for the absence of the CTD, it should do so by not only binding to DNA but also by mediating RAD51 localization to and unidirectional nucleation on the ssDNA. To test this, we performed DNA strand exchange assays by first incubating a 3'tail DNA substrate with RPA that binds with high affinity. RAD51 binding to the DNA and thus strand exchange activity is inhibited by RPA and can only be relieved when a mediator such as BRCA2 is present enabling association with DNA by displacing RPA [70]. Since at least one BRC repeat is

required for the binding to RAD51, we created a fusion construct consisting of BRC4 and $BRCA2_{T2}$ to test if the activity of $BRCA2_{BRC4\text{-}T2}$ was sufficient to promote strand exchange activity in comparison with full-length BRCA2 and the CTD (Figure 14 & 15). Surprisingly, not only $BRCA2_{BRC4\text{-}T2}$ but also $BRCA2_{T2}$ alone was capable of promoting RAD51 strand exchange activity in the presence of RPA. Because this stimulatory effect was only seen when RPA was incubated first with the DNA, this activity may come from the ability of $BRCA2_{T2}$ to bind dsDNA at the ssDNA/dsDNA junction, competing out RPA and facilitating RAD51 loading on the ssDNA. In line with this idea, we observed that the variant C315S, defective in dsDNA binding, could only promote strand the DNA strand exchange activity of RAD51 when using ssDNA but not when a 3'tail DNA was used as substrate. As previously described, the CTD had a small stimulatory effect on RAD51 DNA strand exchange activity and only in the presence of RPA [127]. As suggested for $BRCA2_{T2,}$ the CTD probably aids RAD51 assembly on ssDNA by replacing RPA but does not stabilize the filament. Our findings are in agreement with a recent publication where it was shown that DSS1 in complex with the CTD interacts with RPA reducing its affinity for ssDNA to allow its displacement [69]. We

verified that DSS1 was indeed present in our CTD preparation as it was co-expressed with it (Figure 7).

The important question originating from this study is why there are two DNA binding sites in BRCA2. Our study is compatible with two possibilities: 1) The NTD has an independent of CTD to allow the loading of RAD51 at specific DNA damage sites, especially those containing a duplex DNA. 2) The two DNA binding domains cooperate at the same DNA damage sites as it is the case in Brh2. In this scenario, when a ssDNA/dsDNA junction is generated upon resection of a DSB or at a daughter strand

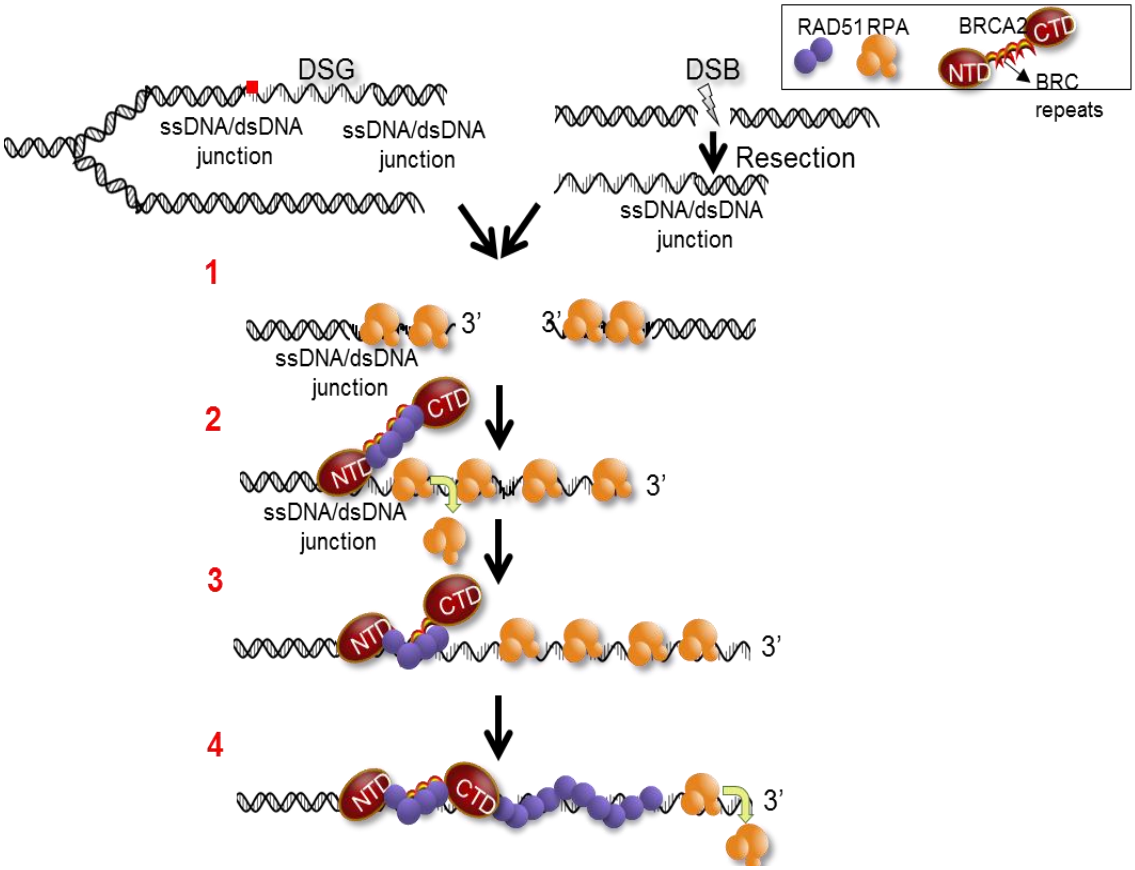

Figure 18: Model for interaction of the two DNA binding domains at daughter strand gaps (DSG) or double strand breaks (DSBs). Explanations can be found in the text.

gap occurring during replication, the ssDNA is subsequently covered by RPA rendering it inaccessible for RAD51 (1). BRCA2 binds RAD51 via interaction with the BRC repeats and delivers it at the ssDNA/dsDNA junction thanks to the NTD (2). This facilitates RAD51 nucleation on the ssDNA by the BRC repeats class I (BRC1-4) and the stabilization of the nascent RAD51 filaments by BRC repeats class II (BRC5-8) [124] (3). The CTD-DSS1 complex would bind next to the ssDNA facilitating RAD51 filament growth by displacing RPA (4). Whether the NTD is released after RAD51 loading remains to be elucidated (Figure 18). Our model suggests that in the context of the full

length protein, both DNA binding domains have independent functions but also work consecutively at the pre-synaptical stage to facilitate RAD51 filament formation and growth, a rate limiting step in recombination, enhancing the subsequent steps of the DNA strand exchange process. This could explain why full-length BRCA2 is only needed in substochiometric concentration to stimulate the DNA strand exchange activity of RAD51 whereas the isolated NTD and CTD stimulate the reaction only at stoichiometric concentration (observations from this study and [70]).

In addition, the compensating DNA binding function of NTD when CTD is not present explains why NTD or CTD can rescue the hypersensitivity to DNA damage in cells deficient in BRCA2. Whether the small construct of $BRCA2_{BRC4\text{-}T2}$ is capable of promoting HR *in vivo* as in the case of *U. maydis* Brh2 remains to be studied. In the human BRCA2, other domains such as the PALB2 interaction site or the extreme C-terminus important for RAD51 filament stabilization and cell cycle regulation might be required *in vivo*. Nevertheless, this study offers an explanation for the CTD being dispensable for HR function [157]. We also provide a functional approach to study VUS found in breast cancer patients located in the NTD region that might affect the DNA binding capacity of the protein. This could impair their HR function and predispose to the development of cancer. The possibility to characterize these variants will contribute to the classification of VUS in BRCA2 and help in genetic counseling.

2.4 OUTLOOK

In this study we found a novel DNA binding site in the N-terminus of BRCA2 that promotes RAD51-dependent homologous recombination. This works provides a possible explanation for the fact that cells lacking the canonical CTD can survive treatment with DNA damaging agents and restore HR. In the future, it will be of great interest to further investigate why two DNA binding sites co-exist in BRCA2. In our model (Figure 18), we propose that the NTD is the initial interaction domain at the ssDNA/dsDNA junction of resected DSBs or of daughter strand gaps to allow RAD51 nucleation on RPA covered ssDNA. The CTD-DSS1 complex is then needed for the active removal of RPA from the ssDNA to allow further RAD51 nucleation and/or filament extension. We propose that the ssDNA/dsDNA junction specificity is likely acquired by the dsDNA binding activity of the NTD. A bias towards this type of DNA intermediate is also observed in Brh2 and the functional homolog of BRCA2 in bacteria, RecFOR [236].

It remains to be investigated whether the NTD alone is able to restore HR in vivo or reduce the sensitivity to DNA damage in vivo. To examine this possibility in our lab we are currently establishing a system in HEK293 cells in which we can downregulate endogenous *BRCA2* and conditionally induce the expression of protein fragments or full-length variants of BRCA2. We will establish stable clones expressing fusion constructs of $BRCA2_{LT3\text{-}BRC4,}$ $BRCA2_{LT2\text{-}BRC4,}$ $BRCA2_{T2\text{-}BRC4}$ and $BRCA2_{T1\text{-}BRC4}$ and test them for their HR proficiency using a GFP-reporter homologous recombination assay. We will use these cell lines to monitor their ability for RAD51 foci formation and their sensitivity to DNA damage by clonogenic survival. Indeed, it is possible that the DNA binding activity and promotion of RAD51 recombination activity of the NTD we observe *in vitro*, is not sufficient for the survival of the cells after DNA damage because of the lack of the PALB2 binding site. PALB2 is required for the formation of the BRCA1-PALB2-BRCA2 complex and for the localization of the proteins to the DSB. Furthermore, PALB2 cooperates with BRCA2 to stabilize the D-loop structure. This is reflected in the HR defect of cells mutated in the PALB2 binding site [108,109]. If this is the case, we would expect that $BRCA2_{LT3\text{-}BRC4}$ and $BRCA2_{LT2\text{-}BRC4}$, will show better survival than $BRCA2_{T2\text{-}BRC4}$.

It would be interesting to know how the interplay of the two domains is achieved structurally. It was shown that BRCA2 forms a dimer and ssDNA binds across the two dimers via the CTD[158].

The human CTD-DSS1 complex purified, to our knowledge, for the first time in our work, and the crystalization study ongoing in collaboration with the group of Xiaodong Zhang will help us get further insights into the structural composition of the complex in association with DNA.

In Brh2, cells lacking the NTD or the CTD can repair UV-induced lesions, however, DNA lesions induced for example by HU treatment at replication forks require the interplay of both domains in the absence of the RecQ helicase Blm. In contrast to human NTD, the NTD in Brh2 forms a OB-like structure similar to the CTD and the two DNA binding domains show similar binding specificity for DNA substrates and the same affinity as the full length protein [237]. In human BRCA2 the full-length protein binds readily to DNA with much more affinity than NTD (~10 fold) and especially the CTD (~100 fold) alone. This is consistent with our working model in which both domains act consecutively to promote HR. How this mechanism is regulated to allow the two domains to exert their functions remains to be established.

During my PhD thesis, I also worked on the evaluation of variants of unknown clinical significance (VUS) found in breast cancer patients that are located in the NTD region (Exon 10). In this chapter, we already characterized the DNA binding features of single

and double mutants of conserved cysteine residues that are thought to be important for the protein's function. Simultaneously to the functional characterization of the NTD, we evaluated the phenotype of VUS of conserved residues located in the two DNA binding clusters predicted by *in silico* analysis in both HR and cell cycle regulation. Using the now established protocols for DNA binding and strand exchange assays *in vitro* and the cell-based assay for the characterization of VUS, we hope to obtain a more complete perception of the functions impaired in BRCA2 variants showing a deleterious phenotype in this region.

2.5 MANUSCRIPT FOR PUBLICATION

A novel DNA binding site in human BRCA2 promotes homologous recombination

Catharina von Nicolai[1,2], Åsa Ehlén[1,2], Taha Shahid[3], Yueru Sun[3], Charlotte Martin[1,2], Xiaodong Zhang[3] & Aura Carreira[1,2,#]

(submitted)

[1] Institut Curie, Centre de Recherche, Orsay, France [2]CNRS UMR3348, Genotoxic Stress and Cancer, Centre Universitaire, Orsay, France

[3] Department of Medicine, Imperial College London, SAF Building, London, SW7 2AZ

[#]To whom correspondence should be addressed:
Aura Carreira
Institut Curie - Research Center
UMR 3348 CNRS “Genotoxic Stress and Cancer”
Bâtiment 110, Centre Universitaire
91405 Orsay
France
Phone: +33 (0)1 69 86 30 82
Fax: +33 (0)1 69 86 94 29
E-mail: aura.carreira@curie.fr

BRCA2 tumour suppressor protein is well known for its role in DNA repair by homologous recombination (HR); assisting RAD51 recombinase loading at DNA

double strand breaks (DSB)[1-3]. This function is executed by the C-terminal DNA binding domain (CTD) which binds single-stranded (ss)DNA[4], and the BRC repeats, which bind RAD51 and modulate its assembly onto ssDNA[5,6], an important step in HR. However, intriguing results highlighting the apparently redundant function of distinct regions of the protein raise questions about the functional domains of BRCA2 and their interdependencies [7-10].

In this work, we identified a region in the N-terminus of BRCA2 comprising a putative zinc finger-PARP domain that exhibits DNA binding activity (NTD). In comparison to the CTD, the NTD has stronger affinity for all forms of DNA structures tested and, in contrast, also binds to double-stranded (ds)DNA. Importantly, the NTD can stimulate RAD51-dependent DNA strand exchange between RPA coated single-stranded (ss)DNA and homologous duplex DNA, which defines a mediator[11]. These results point to NTD as a novel functional domain with mediator activity in recombination. A missense variant of *BRCA2* detected in breast cancer patients located in the NTD exhibits defective dsDNA binding activity and impairs the recombination function of RAD51 on substrates containing a ds/ssDNA junction, but not on ssDNA, providing a molecular basis for the mediator function of the NTD at these sites.

We propose that the NTD provides BRCA2 with the specificity to load RAD51 onto dsDNA/ssDNA junctions while both CTD and NTD enable BRCA2 binding to ssDNA facilitating multiple nucleation events of RAD51 onto RPA-coated ssDNA. In addition, these findings shed light on the functional relevance of the N-terminus of BRCA2 and have implications for the evaluation of breast cancer variants identified in this region.

The DNA binding activity of BRCA2 is essential to load RAD51 at DNA breaks. This function is ensured by the DNA binding domain located at the C-terminus of the protein (CTD)[4]. Yet, cells resistant to DNA damage devoid of the entire CTD can still function in HR[7,10] suggesting that additional functional domains in BRCA2 could take over CTD's function. To test this hypothesis we used protein secondary structure prediction tools (see Extended Data Methods) and identified a zinc finger (zf)-PARP like domain containing residues predicted to bind DNA in the N-terminus of BRCA2 that are conserved in mammals

(Extended Data Fig.1). This analysis prompted us to test the functional relevance of this domain.

We expressed and purified from human cells several fragments of the N-terminus of BRCA2; $BRCA2_{T1}$ (aa 1-250), $BRCA2_{T2}$ (aa 250-500), $BRCA2_{LT2}$ (aa 1-500) and $BRCA2_{LT3}$ (aa 1-750) (Extended Data Fig.1c, d) and tested their DNA binding activity by Electrophoretic Mobility Shift Assay (EMSA). Incubation of a ssDNA homopolymer, dT_{40}, and increasing concentrations of $BRCA2_{T2}$, $BRCA2_{LT2}$ or $BRCA2_{LT3}$, but not $BRCA2_{T1}$, generated a slower mobility species corresponding to DNA-protein complexes. Their DNA binding activity reached 20- 40% of ssDNA-protein complex at 300 nM (Fig. 1a, b). These results suggest that the domains comprising $BRCA2_{T2}$ bind to ssDNA.

To further validate the DNA binding activity of this region, we used negatively stained electron microscopy (EM) with the larger N-terminal fragment, $BRCA2_{LT3}$. $BRCA2_{LT3}$ alone adopted a globular structure (Fig. 1c and Extended Data Fig. 2a). Incubation of $BRCA2_{LT3}$ with a gapped DNA substrate resulted in V or Y-shaped particles (Fig. 1d and Extended Data Fig. 2c) that were not observed in samples containing either protein or DNA substrate alone (Fig. 1d and Extended Data Fig. 2a, b) suggesting that this structure results from DNA-protein complex formation. We confirmed that the density on the tip of the V or Y shaped particles corresponds to $BRCA2_{LT3}$ with an antibody against the tag (Fig. 1e and Extended Data Fig. 2d). The V or Y-shaped particles suggest protein binding to the ssDNA (gap) segment or to the ssDNA/dsDNA junction. Interestingly, PARP-like fingered enzymes have been described to bend the DNA upon binding to gap sites adopting a V shaped structure[12].

Collectively, these results indicate that the N-terminal region of BRCA2 binds DNA and that the region of aa 250-500 of BRCA2 ($BRCA2_{T2}$) comprising the putative zf-PARP domain is sufficient for this activity.

To examine the possible function and specificity of the DNA binding domain identified in the N-terminal region (NTD), we compared the DNA binding affinity of $BRCA2_{T2}$ with that of the CTD (aa 2474-3190) (Fig. 2a) for different DNA substrates.

As described for the mouse CTD[4], human CTD bound to all DNA forms except dsDNA (Fig. 2b-f). Remarkably, at the attainable concentration (1.5 μM),

$BRCA2_{T2}$ showed higher yield of DNA-protein complexes than the CTD for all DNA substrates tested (Fig. 2b-f). In contrast to the CTD, $BRCA2_{T2}$ also bound to dsDNA resulting in a yield of protein-dsDNA complex of ~40 % at 1.5 μM, similar to that of ssDNA (Fig. 2c, Extended Data Fig. 3a, b). Moreover, $BRCA2_{T2}$ exhibited significantly higher yield of DNA-protein complexes when bound to gapped DNA compared to CTD, reaching a ~40-fold difference at 1 μM of protein concentration (Fig. 2f).

These results indicate that $BRCA2_{T2}$ exhibits an increased relative affinity or higher complex stability for all DNA substrates compared to CTD, especially those containing dsDNA or a dsDNA/ssDNA junction.

NTD comprises a putative zf-fold, which are usually stabilized by cysteine and histidine residues[13,14]. To find out the residues important for DNA binding, we mutated three of the cysteines present in the domain (Extended Data Fig.1) and tested their effect on DNA binding. We chose to mutate two cysteines that have been found substituted for serine in breast cancer patients (C315S, C341S) (Breast Cancer information Core and BRCAshare databases). The third one is an artificial alanine substitution of C279 (Fig. 3a). Single or double mutations were introduced in the $BRCA2_{T2}$ fragment and purified (Extended Data Fig. 4). The single mutations, C279A and C341S, only mildly affected the ssDNA binding activity of $BRCA2_{T2}$ (Fig. 3b, Extended Data Fig. 4b). Importantly, the three double mutations, C279A/C315S, C279/A341S and C315S/C341S, all reduced the yield of ssDNA-protein complex formation by ~7-fold (Fig. 3c, Extended Data Fig. 4c). We next tested the effect of the single or the double mutations on dsDNA binding. Interestingly, the single substitution C315S reduced the dsDNA binding by ~6.5 fold whereas the other single mutations did not or very mildly affected it (Fig. 3d, e). Accordingly, the double mutations containing the C315S substitution potentiated this effect (Fig. 3f, g). Moreover, C315S mutation mildly reduced the ability of $BRCA2_{T2}$ to bind a 3'overhang ssDNA by ~1.7 fold (Fig. 3h, i).

These results imply that the three cysteine residues tested are important for the interaction of NTD with DNA. Moreover, C315S, a missense mutation frequently observed in breast cancer, highly impairs the interaction of BRCA2 with dsDNA.

A fusion peptide containing a single BRC repeat of BRCA2 and the CTD or the large subunit of replication protein-A (RPA), which also binds to ssDNA, is able to enhance RAD51 recombination activity[15,16]. In the recombination process, replication RPA coats first the ssDNA to remove secondary structure, an interaction that is inhibitory for RAD51 assembly onto ssDNA due to the stronger affinity of RPA for ssDNA[17,18]. Mediator proteins like BRCA2 counteract the inhibitory effect of RPA. In view of the DNA binding activity exhibited by $BRCA2_{T2}$, we assessed whether a fusion of $BRCA2_{T2}$ and BRC4, $BRCA2_{BRC4\text{-}T2}$ (Extended Data Fig. 5a), could promote the DNA strand exchange activity of RAD51.

We used the optimal RAD51 and RPA concentrations (Extended Data Fig. 5b) in an *in vitro* short oligonucleotide DNA strand exchange assay[1]. RPA was incubated first with a 3'overhang ssDNA substrate (scheme in Fig. 4a), and as expected, RAD51 recombination activity was compromised (Fig. 4a, third lane). Importantly, $BRCA2_{BRC4\text{-}T2}$ was able to overcome the inhibition by RPA and stimulate the reaction by ~6-fold at 300 nM protein concentration (Fig. 4b). Strikingly, $BRCA2_{T2}$ alone also stimulated the reaction to a similar extent (Fig. 4d) though it does not interact directly with RAD51 (Extended Data Fig.5c).

These results suggest that at saturating concentration of RAD51 and with a short DNA sequence, the binding of $BRCA2_{T2}$ to DNA is sufficient to facilitate RAD51 recombination. One explanation is that $BRCA2_{T2}$ counteracts the competition of RPA for ssDNA allowing assembly of RAD51 onto the ssDNA (Fig. 4c, d). Consistent with this idea, $BRCA2_{T2}$ did not stimulate the DNA strand exchange reaction in the absence of RPA (Extended Data Fig.5d, e). In contrast, the fusion peptide $BRCA2_{BRC4\text{-}T2}$ showed a stimulatory effect of ~1.8 fold, comparable to that of full length BRCA2 although at 10 times higher the concentration (Extended Data Fig. 5f, g). Similar to mouse CTD[4], human CTD did not stimulate the DNA strand exchange reaction in the absence of RPA (Extended Data Fig.5d, e) but stimulated the RPA-containing reaction by ~3-fold at 10 μM (Fig. 4c, d).

In conclusion, $BRCA2_{BRC4\text{-}T2,}$ $BRCA2_{T2}$ and to a much lesser extent the CTD can all promote the RPA-dependent DNA strand exchange activity of RAD51.

Considering the binding of $BRCA2_{T2}$ to duplex DNA-containing structures, we reasoned that this activity might be required for the stimulation of DNA strand exchange when using dsDNA-containing substrates. We conducted a DNA strand exchange reaction using a 3' overhang ssDNA in the presence of the single mutant $BRCA2_{T2}$ C315S with reduced dsDNA binding activity. Indeed, $BRCA2_{T2}$ C315S decreased the stimulation of DNA strand exchange activity of RAD51 by ~3-fold compared to $BRCA2_{T2}$, an effect that was further potentiated by the double mutation C279A/C315S (Fig. 4e, f). To confirm that the defective stimulation of DNA strand exchange is due to the inability of $BRCA2_{T2}$ C315S to bind dsDNA and not to a faulty folding due to the mutation, we performed the same reaction using a ssDNA substrate. Indeed, C315S mutation stimulated the ssDNA-based strand exchange of RAD51 as much as $BRCA2_{T2}$ (Fig. 4g, h) or full length BRCA2 (Extended Data Fig. 6), suggesting that the single substitution C315S affects the stimulation of DNA strand exchange with the 3' ssDNA overhang substrate because of its defective dsDNA binding activity.

A bias towards ssDNA/dsDNA junctions has been described for the functional homologs of BRCA2, the bacterial RecFOR, and its orthologue in *U. maydis*, Brh2 but not for human BRCA2[1]. Although the helix-turn-helix motif present in CTD suggested dsDNA-binding[4], the interaction with this type of substrate has not been detected for CTD [4,19]. Our findings suggest that NTD specifically contributes the binding of BRCA2 to dsDNA allowing the association with dsDNA/ssDNA junctions.

Combining our results with previous findings [1-3,5,20,21] we propose a model whereby in the context of a ssDNA/dsDNA junction-containing lesion (Extended Data Fig. 7); NTD binds at the dsDNA/ssDNA junction first, facilitating the loading and stabilization of RAD51 nucleoprotein filament onto RPA-coated ssDNA by the BRC repeats[21]. CTD binds along the ssDNA and actively facilitates the displacement of RPA[22] allowing multiple nucleation events and RAD51 nucleoprotein filament extension. These activities enhance the subsequent steps of homologous recombination.

It is possible that both NTD and CTD are required for assembly of RAD51 onto ssDNA in the context of full length BRCA2. Alternatively, the two DNA binding

sites may act on different substrates depending on the DNA damage encountered. How the two DNA binding modules of BRCA2 are coordinated *in vivo* warrants further investigation.

Methods

Cloning, expression and purification of recombinant proteins

All BRCA2 N-terminal expression constructs containing the sequence coding for BRCA2 amino acids 1-250 ($BRCA2_{T1}$), 251-500 ($BRCA2_{T2}$), 1-500 ($BRCA2_{LT2}$) and 1-750 ($BRCA2_{LT3}$) were amplified by PCR from a 2xMBP-BRCA2 phCMV1 vector[1] and cloned by restriction digest with XhoI and NotI into a phCMV1 vector containing an N-terminal 2x MBP tag with two Nuclear Localization Signals (NLS) downstream the tag.

Point mutations were introduced using QuikChange II site-directed mutagenesis kit (Agilent) and verified by sequencing. $BRCA2_{BRC4\text{-}T2}$ fusion construct was generated by HIFI Gibson Assembly (NEB) in the phCMV1 2x MBP 2 NLS vector.

All the constructs mentioned above including the vector containing the MBP tag and the NLS used as control were amplified with NucleoBond Xtra Midi kit (Macherey Nagel) and used for transfection.

10 150 mm confluent plates of HEK293 cells were transiently transfected with TurboFect (Thermo Scientific) following the manufacturer specifications and harvested 30 h post-transfection. After lysis with 50 mM HEPES (pH 7.5), 250 mM NaCl, 5 mM EDTA, 1% NP40, 1 mM DTT, 1 mM PMSF and EDTA-free Protease Inhibitor Cocktail (Roche), the suspension was incubated for 3 h with amylose resin (NEB). 2x MBP tagged BRCA2 fragments were eluted with 10 mM maltose. The eluates were further purified with Bio-Rex 70 cation-exchange resin (Bio-Rad) by NaCl step elution (50 mM HEPES pH 7.5, 0.5 mM EDTA, 10% glycerol, 1 mM PMSF, 1 mM DTT, and 250 mM, 450 mM or 1 M NaCl).

The size and purity of the BRCA2 fragments were verified by loading the final fractions on a SDS-PAGE gel and detecting the MBP tag by Western Blot (mAB R29, Invitrogen).

The protein concentration of the nuclease-free fractions was determined using NanoOrange Protein Quantitation Kit (Thermo Fisher) and by density determination in SDS-PAGE gel using BSA as a standard.

The C-terminal DNA binding domain (aa 2474-3190) of human BRCA2 (CTD) was cloned into pET28 6His SUMO vector. pCDF DSS1 expression vector was generated by HIFI Gibson Assembly (NEB) from a pFASTBAC Dual-DSS1 vector (kind gift from R. B. Jensen). The CTD was co-expressed with DSS1 to ensure stability of the protein. *E.coli* BL21 DE3 pISO Dscb cells (kind gift of A. el Marjou) were transformed and grown at 37 °C in 7 litres of Terrific Broth and induced with 0.5% arabinose and 1mM IPTG overnight at OD (optical density) 2. Cells were collected in 20 mM Tris-HCl pH 8, 300 mM NaCl, 10% glycerol, 0.5 mM EDTA, 5 mM β-mercaptoethanol, 1x Protease Inhibitor Cocktail EDTA-free (Roche), 10 mM $MgCl_2$, 1x DNase, 0.5 mg/ml Lysozyme (Sigma Aldrich), and the suspension was lysed by disintegration at 1.7 kbar.

The His-tagged protein was incubated with Protino Ni-NTA agarose (Macherey Nagel) and eluted with 200 mM imidazole. After dialysis overnight against 20 mM Tris-HCl pH 8, 100 mM NaCl, 10% glycerol, 0.5 mM EDTA, 5 mM β-mercaptoethanol, the eluate was loaded onto a 5 ml HiTrap Heparin HP column (GE) and eluted using a continuous NaCl gradient (100-1M NaCl) in the same buffer.

The protein was visualized on a 7.5% SDS gel and the protein concentration was determined by Bradford assay.

To generate EGFP-MBP-BRCA2, one MBP-tag of a phCMV1 2x MBP-BRCA2 vector (kind gift from S.C. Kowalczykowski) was substituted by an EGFP tag amplified by PCR from a pEGFP-C1 vector (Invitrogen) and cloned by restriction digest with KpnI. EGFP-MBP-tagged BRCA2 was purified as described above for the BRCA2 fragments.

Human RAD51 was cloned into pCDF 6his SUMO vector. *E. coli* BL21 BRL were transformed and grown in 7 L of Terrific Broth at 37 °C in a fermenter. At OD =1, the temperature was decreased to 20 °C and protein expression was induced with 0.5 mM IPTG overnight at 700 RPM. Cells were harvested by

centrifugation at 6000 RPM for 10 min at 4°C and resuspended in 1xPBS, 350 mM NaCl, 20 mM imidazole, 10% glycerol, 0.5 mg/ml Lysozyme, 1x Protease Inhibitor Cocktail (Roche), 0.5 mM PMSF, 10 mM $MgCl_2$, DNase and extracted using a disintegrator at 1.8 kbar and collected by centrifugation at 20.000 RPM for 30 minutes. The His-tagged protein was incubated with Protino Ni-NTA agarose (Macherey Nagel) and washed with 20 mM Tris-HCl pH 8.0, 20 mM imidazole, 10% glycerol, 100 mM NaCl, 5 mM β-mercaptoethanol. The His-tag was cleaved by incubating the resin with 0.4 mg/ml SUMO Protease at 4 °C overnight. The supernatant from the Ni-NTA resin containing the cleaved RAD51 protein was then loaded onto a 5 ml HiTrap Heparin HP chromatography column (GE) in 20 mM Tris-HCl pH 8, 10% glycerol, 100 mM NaCl and 5 mM β-mercaptoethanol. RAD51 protein was eluted using a continuous NaCl gradient (100 mM-2M NaCl) in the same buffer. The eluate was dialysed against RAD51 storage buffer (20 mM Tris HCl pH 8, 50 mM KCl, 0.5 mM EDTA, 1 mM DTT, 10% glycerol, 0.5 mM PMSF) and visualized on a 7.5% SDS-PAGE gel stained with Coomassie Brilliant Blue. The protein concentration was determined by Bradford assay.

His-tagged RPA was a kind gift from M. Modesti (IGH, Marseille).

$BRCA2_{T2\text{-}BRC4,}$ fusion construct was generated by Gibson HIFI assembly (NEB) in the phCMV1-EGFP-MBP 2NLS BRC4 vector background (pAC138)**.**

After purification, all proteins and fragments were aliquoted, frozen in liquid nitrogen and stored at -80°C.

Electrophoretic Mobility Shift Assay (EMSA)

DNA substrates were purchased PAGE-purified from MWG Eurofins. The following oligonucleotides were used: oAC379: dT_{40} homopolymer. oAC423 (167mer):

5’CTGCTTTATCAAGATAATTTTTCGACTCATCAGAAATATCCGTTTCCTATA
TTTATTCCTATTATGTTTTATTCATTTACTTATTCTTTATGTTCATTTTTTATAT
CCTTTACTTTATTTTCTCTGTTTATTCATTTACTTATTTTGTATTATCCTTATC
TTATTTA-3’

oAC403 (42mer): 5'-CGGATATTTCTGATGAGTCGAAAAATTATCTTGATAAAGCAG-3'; oAC490 (42mer): 5'-TAAATAAGATAAGGATAATACAAAATAAGTAAATGAATAAAC-3'; oAC405 (40mer): 5'-TAA TAC AAA ATA AGT AAA TGA ATA AAC AGA GAA AAT AAA G-3'; oAC406 (40mer): 5'-CTT TAT TTT CTC TGT TTA TTC ATT TAC TTA TTT TGT ATTA-3'. The ssDNA substrates used in EMSA were oAC379 and oAC423 ^{32}P labelled at the 5' –end. To generate the dsDNA substrates, oAC405 was ^{32}P labelled at the 5'-end and annealed in a 1:1 molar ratio to oAC406. The 3' and 5' overhang substrates were produced by annealing ^{32}P labelled oAC490 (42mer -3') to oAC423 (167mer) or oAC403 (42mer -5') to oAC423 in a 1:1 molar ratio, respectively. oAC423, oAC403 and oAC490 were annealed in a 1:1:1 ratio to produce the gapped DNA substrate.

The long dsDNA substrate was a PCR product (134 bp) amplified from pAC138 by PCR using the oligonucleotides oAC596 and oAC597 and ^{32}P-labeled at the 5' end.

The proteins were incubated at the indicated concentrations with 0.2 µM nucleotides ^{32}P labelled DNA substrates for 1h at 37°C in EMSA reaction buffer (25 mM Tris Acetate pH 7.5, 1 mM DTT, 1 mM $MgCl_2$, 2 mM $CaCl_2$). The protein-DNA complexes were resolved on 6% native polyacrylamide gels in 1x TAE buffer (40 mM Tris Acetate, 0.5 mM EDTA) at 70V for 75 min. The gels were dried and analysed with a Typhoon PhosphorImager (Amersham Biosciences) using Image Quant software (GE Healthcare). In EMSAs in all figures except for Figure 3, the ratio of DNA-protein complexes was calculated as the percentage of bound DNA compared to the free DNA. In figure 3, the percentage of protein-DNA complexes was quantified as the free radiolabelled DNA remaining in a given lane relative to the protein-free lane. The protein-free lane defined the value of 0 % complex.

Electron Microscopy

$BRCA2_{LT3}$ (2xMBP-tagged fused to BRCA2 aa 1-750) was stored at a concentration of 0.25 µM in buffer comprising 50 mM Hepes pH 7.5, 250 mM NaCl, 0.5 mM EDTA, 10% glycerol, 1mM PMSF and 1 mM DTT. The sample was diluted five-fold to 50 nM for subsequent electron microscopy studies. The

complex with gapped DNA was prepared by mixing the diluted protein at 50 nM with 100 nM gapped DNA (final concentration). The 65 bp-70 nt-65 bp gapped DNA was based on the following sequence (5'–3'):

GAGTTTTATCGCTTCCATGACGCAGAAGTTAACACTTTCGGATATTTCTGAT
GAGTCGAAAAATTATCTTGATAAAGCAGGAATTACTACTGCTTGTTTACGAA
TTAAATCGAAGTGGACTGCTGGCGGAAAATGAGAAAATTCGACCTATCCTT
GCGCAGCTCGAGAAGCTCTTACTTTGCGACCTTTCGCCATCAACT.

The gapped DNA used in the control experiment had also been diluted to 100 nM (in the same buffer as the diluted protein). The antibody complex was prepared by incubating the protein-DNA complex with anti-MBP antibody (NEB) for 1-2 hours on ice at 50 nM and 100 nm final concentration, respectively.

2–3 µl of each sample was applied to either carbon-coated Quantifoil R2/2 (fragment, fragment + gDNA) or 300-mesh TAAB continuous carbon grids (gDNA, fragment + gDNA + anti-MBP), previously glow discharged for 30 s. After allowing adsorption for 1 min, the grids were washed twice with water and stained with 2% uranyl acetate solution. Excess stain was blotted and the grids air-dried at room temperature.

Images were collected with an FEI Tecnai T12 (120 kV) transmission electron microscope equipped with the TVIPS TemCam-F216 (2k x 2k) CMOS camera. A magnification of 52,000x (corresponding to 2.1 Å/pixel in the recorded images) was employed throughout. Defoci in the range of –2 to –2.5 µm were utilised in the case of protein complexes, and –4 µm for gapped DNA. An electron dose of ~ 40 e–/Å2 was used in all cases.

DNA strand exchange assay

For DNA strand exchange assays without RPA, proteins were incubated at the indicated concentrations with 4 nM molecules 3'tail DNA or ssDNA (oAC379 or oAC423) for 5 min at 37°C in 25 mM Tris Acetate pH 8.0, 1 mM DTT, 2 mM ATP, 1 mM $MgCl_2$, 2 mM $CaCl_2$, 0.1 mg/ml BSA before adding 4 nM molecules dsDNA (oAC405 and oAC406 1:1) and further incubation for 30 min at 37 °C. When RPA was added, the protein was incubated for 5 min with ssDNA or 3'tail DNA, then RAD51 alone or with BRCA2 was added and incubated for 5 min and the dsDNA was added last and further incubated for 30 min at 37 °C. The

reaction was stopped by incubation with 0.25% SDS and 0.5 mg/ml Proteinase K for 10 minutes. Samples were loaded on a 6% Polyacrylamide gel and migrated at 70V for 75 minutes. The gels were dried and analysed with a Typhoon PhosphorImager (Amersham Biosciences) using Image Quant software (GE Healthcare). The percentage of DNA strand exchange product was calculated as labelled product divided by total labelled input DNA in each lane.

Affinity pull-down with amylose beads

Prior to pull-down assays, amylose resin (NEB) was equilibrated with binding buffer: 50 mM HEPES (pH 7.5), 250 mM NaCl, 0.5 mM EDTA, and 1 mM DTT. Purified 2XMBP-BRCA2$_{BRC4\text{-}T2}$ or 2xMBP-BRCA2$_{T2}$ proteins (1.25 µg) were incubated with 1 µg purified RAD51 for 30 minutes at 37 °C and then batch bound to 30 µl of amylose resin for 1 h at 4 °C. The complexes were washed with binding buffer (50 mM HEPES (pH 7.5), 250 mM NaCl, 0.5 mM EDTA, and 1 mM DTT) containing 1% NP-40. Proteins were eluted with 30 µl 10 mM maltose in binding buffer, resuspended in 1x SDS sample buffer, heated at 54°C for 5 min and loaded onto a 4-15% gradient SDS-PAGE gel. The gels were stained with SYPRO Orange.

REFERENCES

1. Jensen, R. B., Carreira, A. & Kowalczykowski, S. C. Purified human BRCA2 stimulates RAD51-mediated recombination. *Nature* **467,** 678–683 (2010).
2. Liu, J., Doty, T., Gibson, B. & Heyer, W.-D. Human BRCA2 protein promotes RAD51 filament formation on RPA-covered single-stranded DNA. *Nat Struct Mol Biol* **17,** 1260–1262 (2010).
3. Thorslund, T. *et al.* The breast cancer tumor suppressor BRCA2 promotes the specific targeting of RAD51 to single-stranded DNA. *Nat Struct Mol Biol* **17,** 1263–1265 (2010).
4. Yang, H. *et al.* BRCA2 function in DNA binding and recombination from a BRCA2-DSS1-ssDNA structure. *Science* **297,** 1837–1848 (2002).
5. Carreira, A. *et al.* The BRC Repeats of BRCA2 Modulate the DNA-

Binding Selectivity of RAD51. *Cell* **136,** 1032–1043 (2009).

6. Pellegrini, L. *et al.* Insights into DNA recombination from the structure of a RAD51–BRCA2 complex. *Nature* **420,** 287–293 (2002).
7. Siaud, N. *et al.* Plasticity of BRCA2 Function in Homologous Recombination: Genetic Interactions of the PALB2 and DNA Binding Domains. *PLoS Genet* **7,** e1002409 (2011).
8. Zhou, Q., Kojic, M. & Holloman, W. K. DNA-binding Domain within the Brh2 N Terminus Is the Primary Interaction Site for Association with DNA. *J Biol Chem* **284,** 8265–8273 (2009).
9. Abo, Al, M. *et al.* Compensatory Functions and Interdependency of the DNA-Binding Domain of BRCA2 with the BRCA1-PALB2-BRCA2 Complex. *Cancer Res* **74,** 797–807 (2014).
10. Edwards, S. L. *et al.* Resistance to therapy caused by intragenic deletion in BRCA2. *Nature* **451,** 1111–1115 (2008).
11. Kowalczykowski, S. C. An Overview of the Molecular Mechanisms of Recombinational DNA Repair. *Cold Spring Harbor Perspectives in Biology* **7,** – (2015).
12. Petrucco, S. Sensing DNA damage by PARP-like fingers. *Nucleic Acids Research* **31,** 6689–6699 (2003).
13. Laity, J. H., Lee, B. M. & Wright, P. E. Zinc finger proteins: new insights into structural and functional diversity. *Current Opinion in Structural Biology* **11,** 39–46 (2001).
14. Iuchi, S. C2H2 Zinc Fingers As DNA Binding Domains. *Zinc Finger Proteins* (2005).
15. Saeki, H. *et al.* Suppression of the DNA repair defects of BRCA2-deficient cells with heterologous protein fusions. *Proc Natl Acad Sci USA* **103,** 8768–8773 (2006).
16. San Filippo, J. *et al.* Recombination mediator and Rad51 targeting activities of a human BRCA2 polypeptide. *J Biol Chem* **281,** 11649–11657 (2006).
17. Wold, M. S. Replication protein A: a heterotrimeric, single-stranded DNA-binding protein required for eukaryotic DNA metabolism. *Annu Rev Biochem* **66,** 61–92 (1997).
18. Sigurdsson, S. *et al.* Mediator function of the human Rad51B-Rad51C

complex in Rad51/RPA-catalyzed DNA strand exchange. *Genes Dev* **15,** 3308–3318 (2001).

19. Yang, H., Li, Q., Fan, J., Holloman, W. K. & Pavletich, N. P. The BRCA2 homologue Brh2 nucleates RAD51 filament formation at a dsDNA-ssDNA junction. *Nature* **433,** 653–657 (2005).
20. Shahid, T. *et al.* Structure and mechanism of action of the BRCA2 breast cancer tumor suppressor. *Nat Struct Mol Biol* 1–9 (2014). doi:10.1038/nsmb.2899
21. Carreira, A. & Kowalczykowski, S. C. Two classes of BRC repeats in BRCA2 promote RAD51 nucleoprotein filament function by distinct mechanisms. *Proc Natl Acad Sci USA* **108,** 10448–10453 (2011).
22. Zhao, W. *et al.* Promotion of BRCA2-Dependent Homologous Recombination by DSS1 via RPA Targeting and DNA Mimicry. *Molecular Cell* **59,** 176–187 (2015).

FIGURES

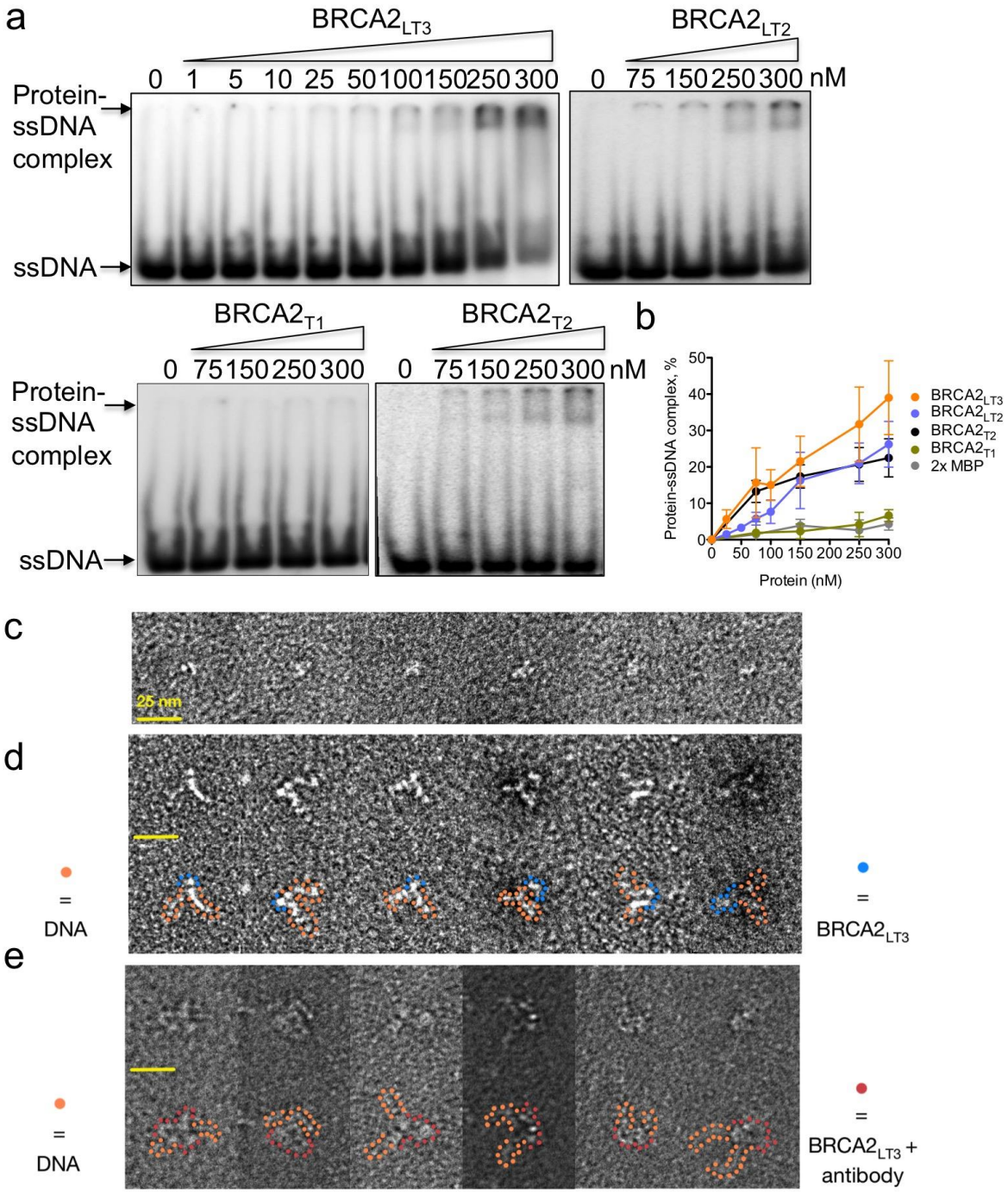

Figure 1: The N-terminus of BRCA2 binds DNA. a, EMSA showing $BRCA2_{LT3}$, $BRCA2_{LT2}$, $BRCA2_{T1}$ and $BRCA2_{T2}$ binding to ssDNA (dT_{40}). **b**, Quantification of **a**. Error bars, s.d. (n = 3). **c**, Electron microscopy (EM) visualization of selected particles of $BRCA2_{LT3}$ alone **d**, or in complex with gapped DNA (blue dots). The duplex DNA arms presumed to be flanking the

bound fragment are delineated (orange dots). **e**, EM visualization of selected particles of $BRCA2_{LT3}$ in complex with gapped DNA and incubated with an antibody against MBP. The additional mass due to the antibody is delineated (red dots); the DNA is delineated as before.

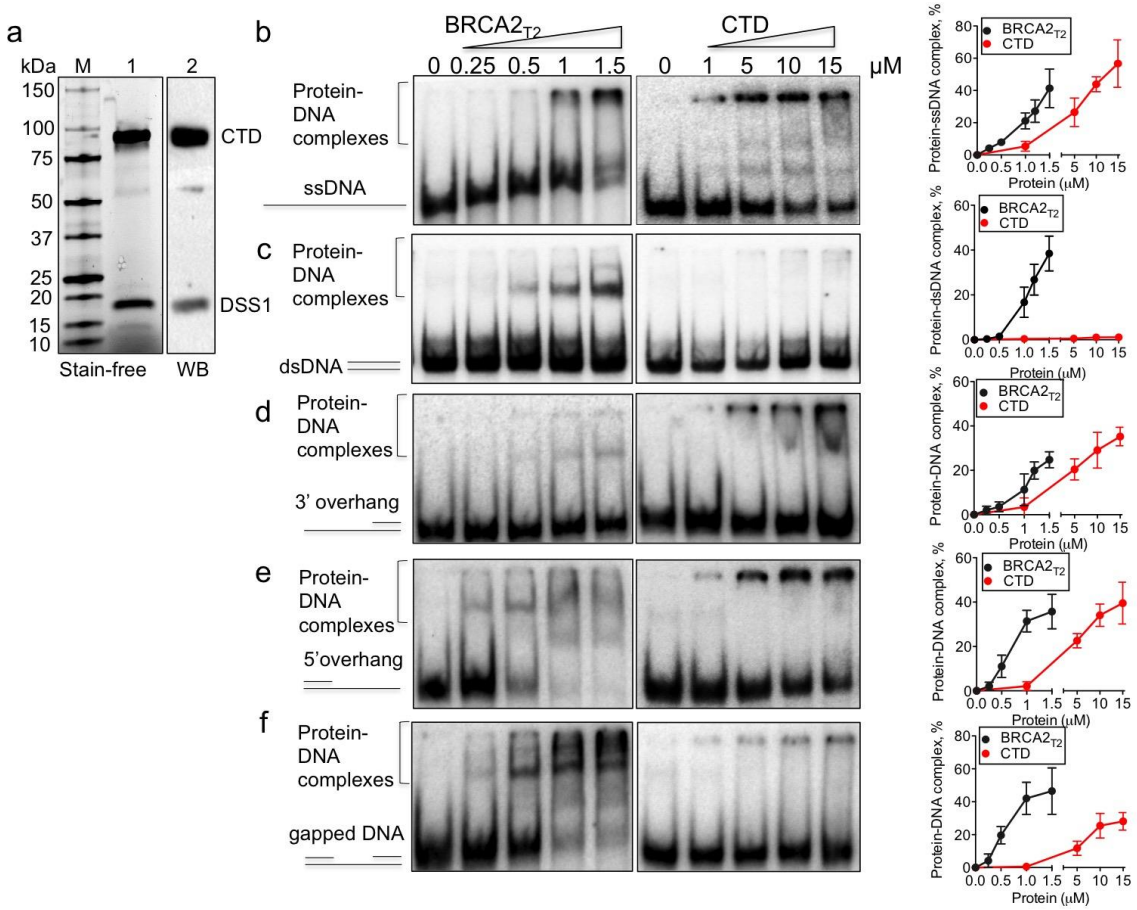

Figure 2: $BRCA2_{T2}$ binds to different DNA substrates and with stronger affinity than CTD. a, M. size markers. 1. SDS-PAGE showing purified CTD (5 µg) loaded in a 4-15% acrylamide gel**.** 2. Western blot of the gel shown in 2. with an antibody against the His tag of the CTD and an antibody specific to DSS1 protein co-purified with it. **b,** EMSA and quantification comparing the binding of $BRCA2_{T2}$ and CTD to ssDNA, **c**, dsDNA, **d**, 3' ssDNA overhang, **e**, 5' ssDNA overhang, **f**, gapped DNA. Error bars, s.d. (n = 3).

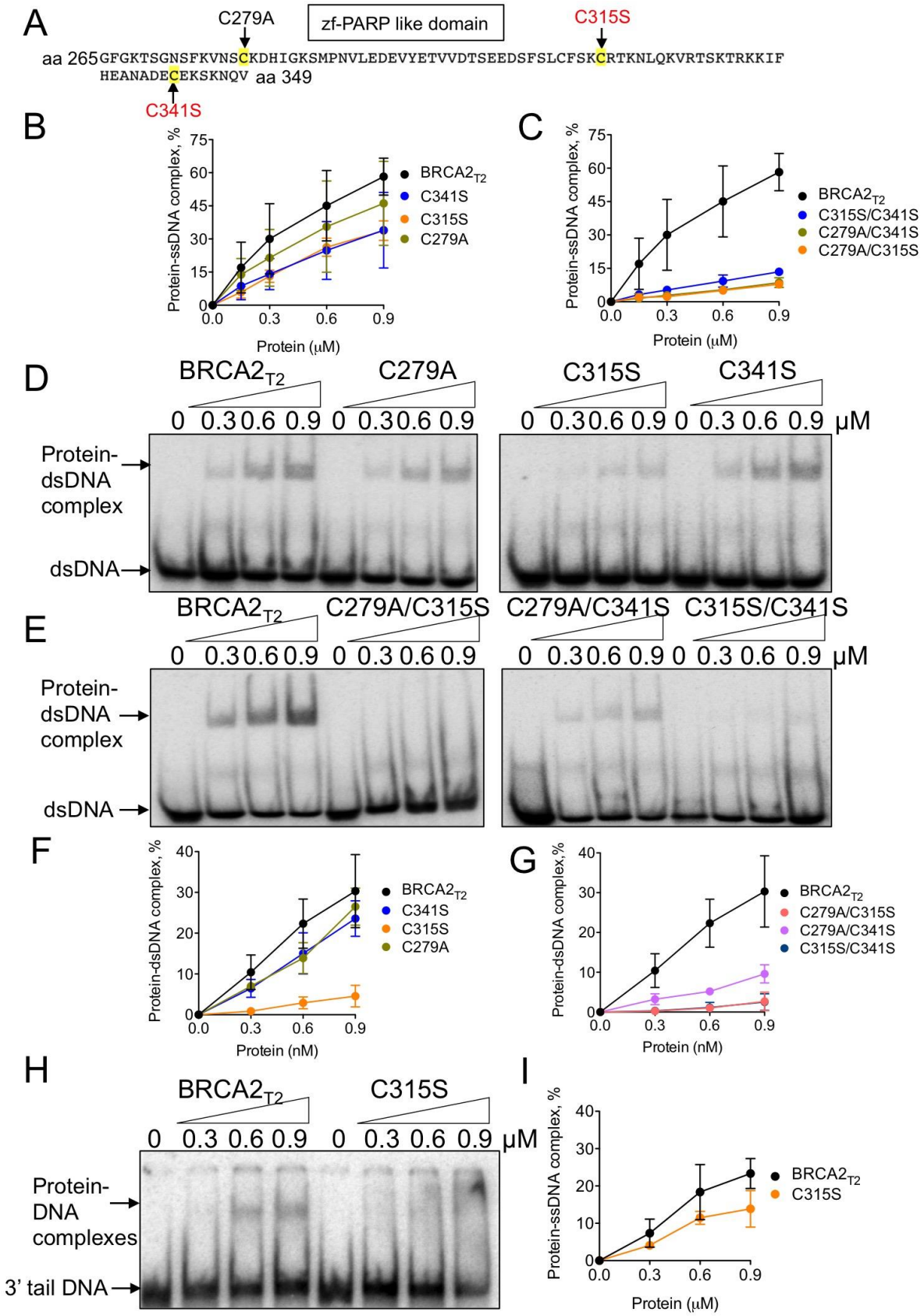

Figure 3: Cysteine residues located in the putative zf-PARP like domain

and mutated in breast cancer patients affect the DNA binding activity of $BRCA2_{T2}$. a, amino-acid sequence comprised in the putative zf-PARP like domain defined by SMART showing the mutated cysteine residues. The ones found in breast cancer patients are highlighted in red. **b**, Quantification of EMSA displayed in Extended Fig. 4b, c showing the binding of $BRCA2_{T2}$, the indicated single mutants **c**, and the double mutants to ssDNA. **d**, EMSA showing the binding of $BRCA2_{T2}$ and the indicated single mutants **e**, and the double mutants to dsDNA. **f**, Quantification of **d**. **g**, Quantification of **e. h**, EMSA showing the binding of $BRCA2_{T2}$ and BRCA2 C315S to 3' overhang ssDNA**. i,** Quantification of **h**. Error bars, s.d. (n = 3).

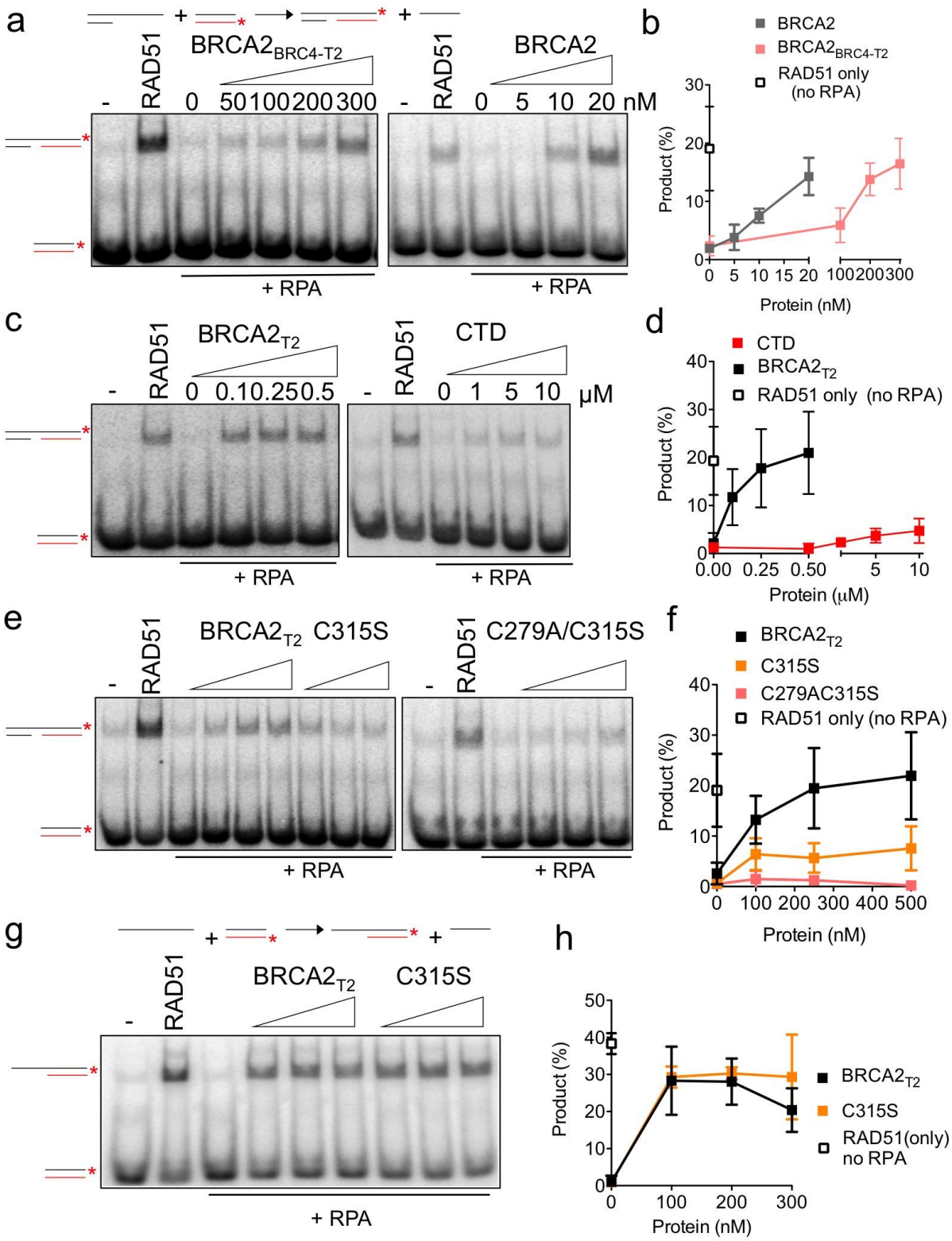

Figure 4: $BRCA2_{T2\text{-}BRC4}$ and $BRCA2_{T2}$ stimulate RAD51-promoted DNA strand exchange. a, DNA strand exchange reaction using a 3' overhang ssDNA substrate (scheme on top) in the presence or absence of RPA, RAD51, and increasing concentrations of $BRCA2_{BRC4\text{-}T2}$ or BRCA2. **b**, Quantification of

a. **c**, same reaction as in **a** with increasing concentrations of $BRCA2_{T2}$ or CTD. **d**, Quantification of **c**. **e**, same reaction as in **a** with increasing concentrations of $BRCA2_{T2}$ or $BRCA2_{T2}$ mutated in C315S, or C279A/C315S, as indicated. **f**, Quantification of **e**. **g**, same reaction as in **a** using a ssDNA substrate (scheme on top) with increasing concentrations of $BRCA2_{BRC4\text{-}T2}$ or $BRCA2_{T2}$ mutated in C315S, as indicated. **h**, Quantification of **g**. Error bars, s.d. (n = 3).

Extended Data

Extended Data Methods

Secondary structure prediction and alignment

Using SMART secondary structure prediction tool (http://smart.embl.de/) we identified a putative zinc finger-PARP-like domain between amino acids 265-349 of BRCA2 (Extended Data Figure 1a), a domain thought to assist on the recognition of DNA secondary structures[1]. The same query sequence was used in a web-based prediction tool for DNA binding residues, BindN[2], which predicted two clusters in this region highly enriched in residues with a strong propensity for DNA binding. A multiple sequence alignment using Clustal Omega[3] revealed that the DNA binding region is well conserved in mammals (Extended Data Fig.1b).

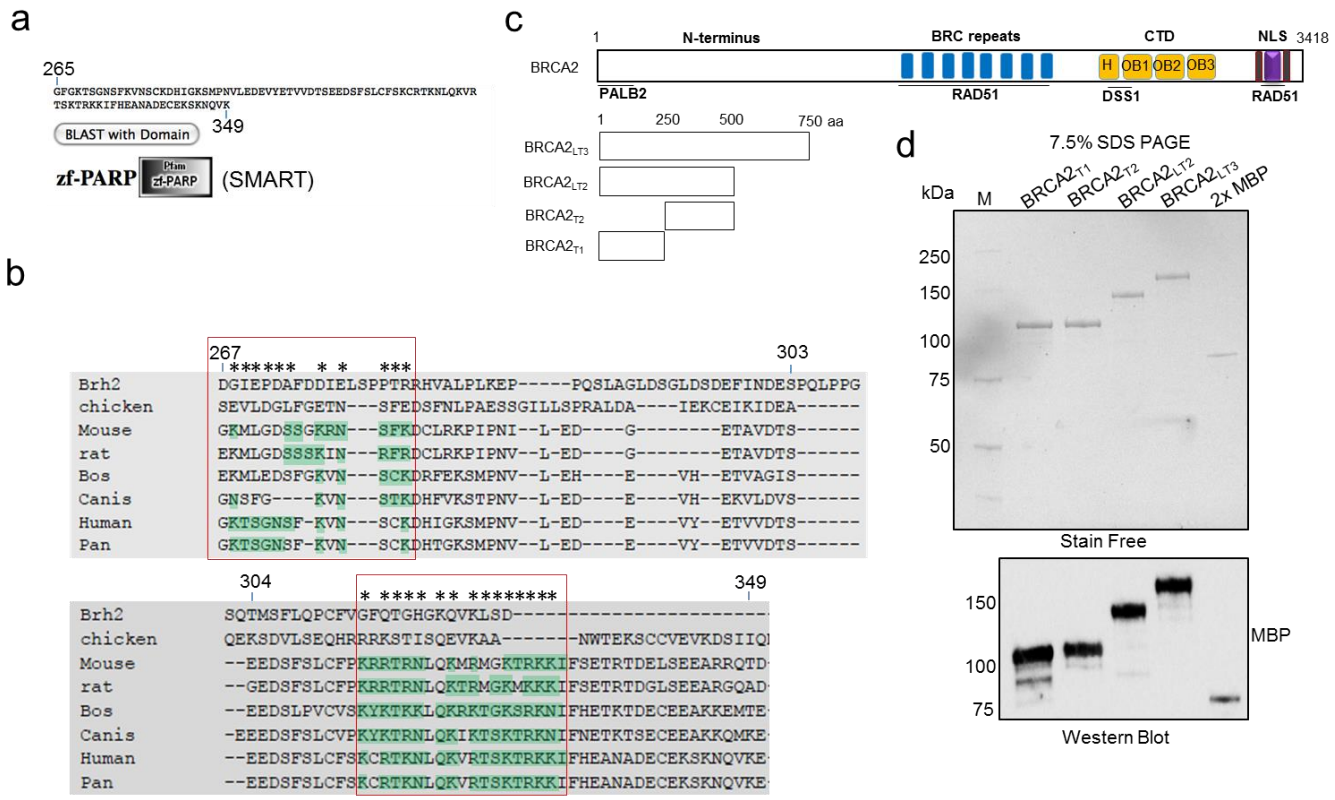

Green boxes: Residues predicted to bind DNA (BindN)
(*): Conserved residues in two or more species

Extended Data Figure 1: Bioinformatics analysis of the N-terminal DNA binding region in BRCA2 and purified fragments. a, SMART result showing the putative zf-PARP like domain in BRCA2**. b,** Multiple alignment using the query sequence indicated in **a** showing the probable DNA binding residues in the indicated species as defined by BindN online software (in green). The numbers corresponds to the human protein sequence. **c**, Schematic representation of BRCA2 and the fragments derived from the N-terminal region used in this work. **d**, Purified fragments of the N-terminal region of BRCA2 shown in a SDS-PAGE gel and detected by stain-free imaging (Bio-Rad) and by western blot revealed with an antibody against the MBP tag.

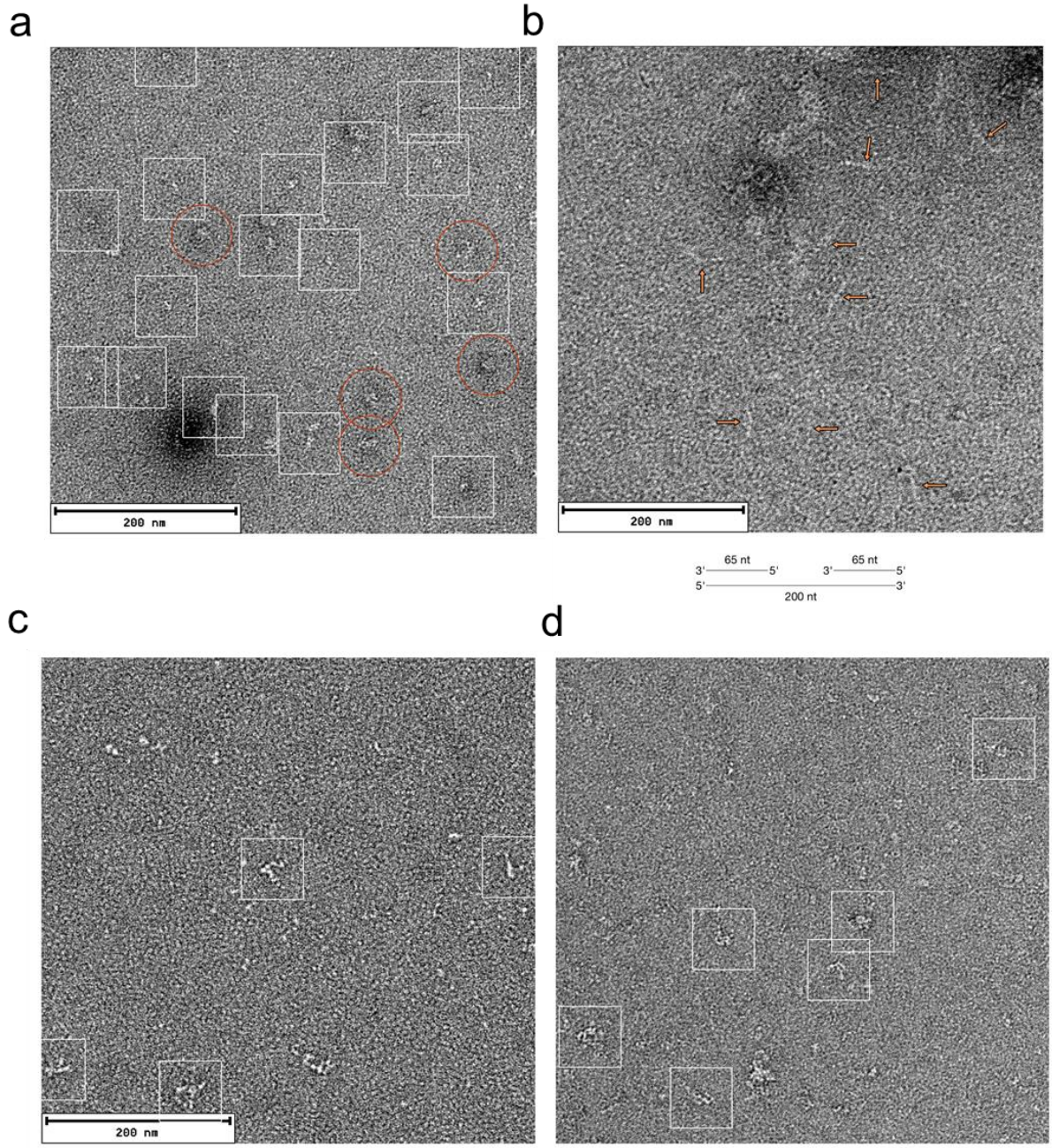

Extended Data Figure 2: Representative electron micrographs of $BRCA2_{LT3}$ bound to DNA

a, Electron microscopy visualization (orange arrows) of the gapped DNA used in Figure 1. **b**, DNA alone, **c**, $BRCA2_{LT3}$ in complex with DNA **d**, and that of the complex of $BRCA2_{LT3}$ with DNA with an antibody against MBP. White boxes indicate particles while brown circles in **a** indicate possible aggregates. Arrows in **b** indicate DNA.

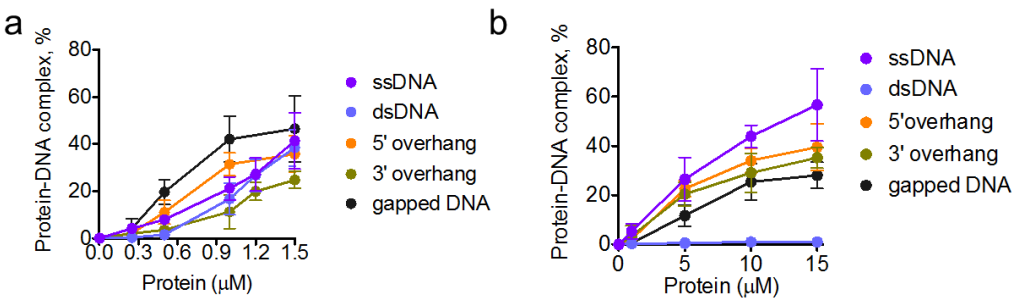

Extended Data Figure 3: $BRCA2_{T2}$ binds dsDNA and shows similar preference for dsDNA containing structures and ssDNA as opposed to the CTD. a, Comparison of the affinities of $BRCA_{T2}$ or **b**, CTD for binding to the different DNA substrates utilized in Figure 2. Error bars, s.d. (n = 3).

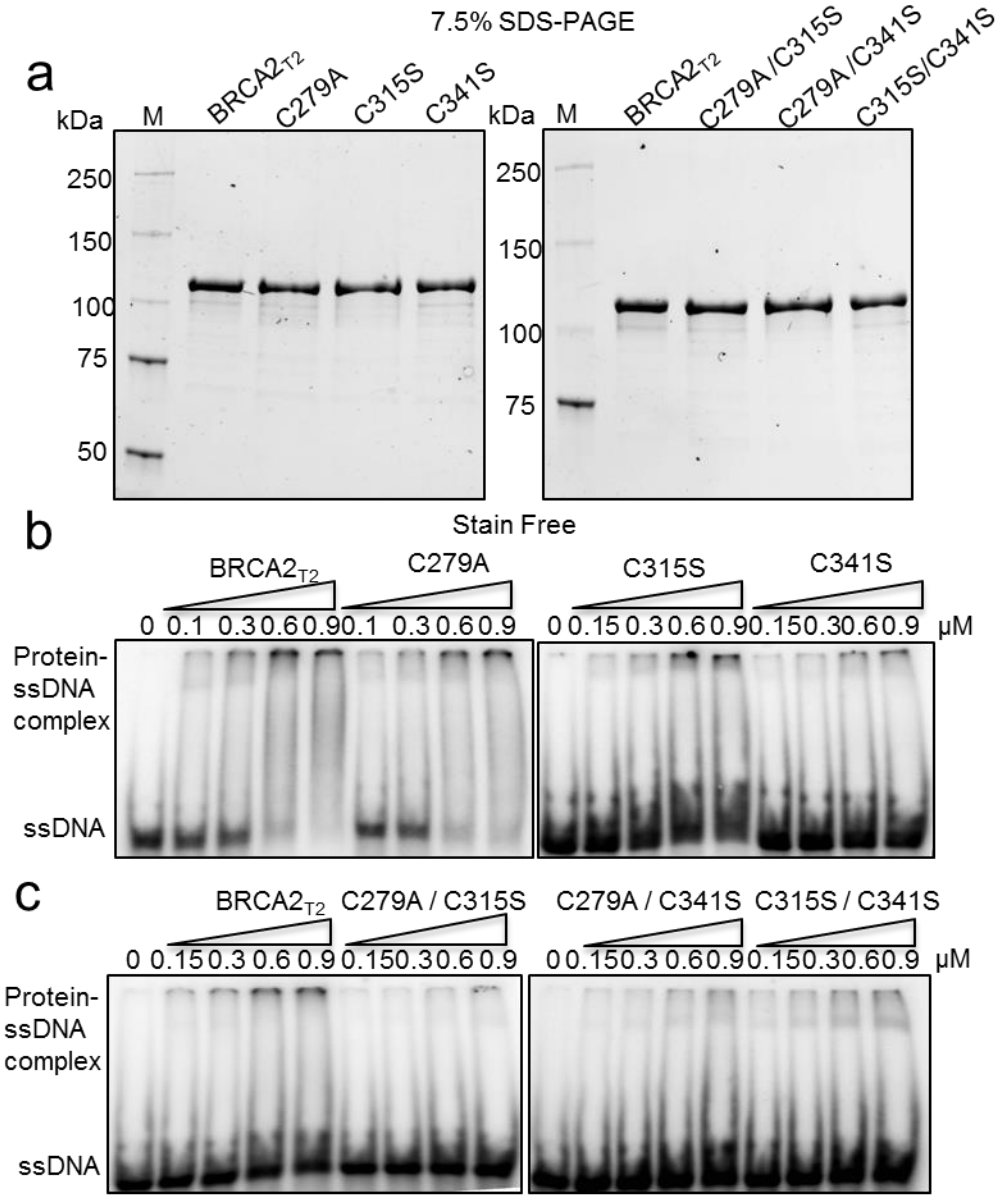

Extended Data Figure 4: ssDNA binding actvity of single or double cysteine mutated BRCA2$_{T2}$. **a**, 1 µg of each purified wild type or mutated BRCA2$_{T2}$ fragment as indicated is shown in an SDS-PAGE gel and detected by stain-free imaging. **b**, Autoradiogram of EMSA of BRCA2$_{T2}$ or the single mutants indicated binding to ssDNA and quantified in Figure 3b. **c**, same as **b** Autoradiography of EMSA of BRCA2$_{T2}$ or the indicated double mutants and quantified in Figure 3c.

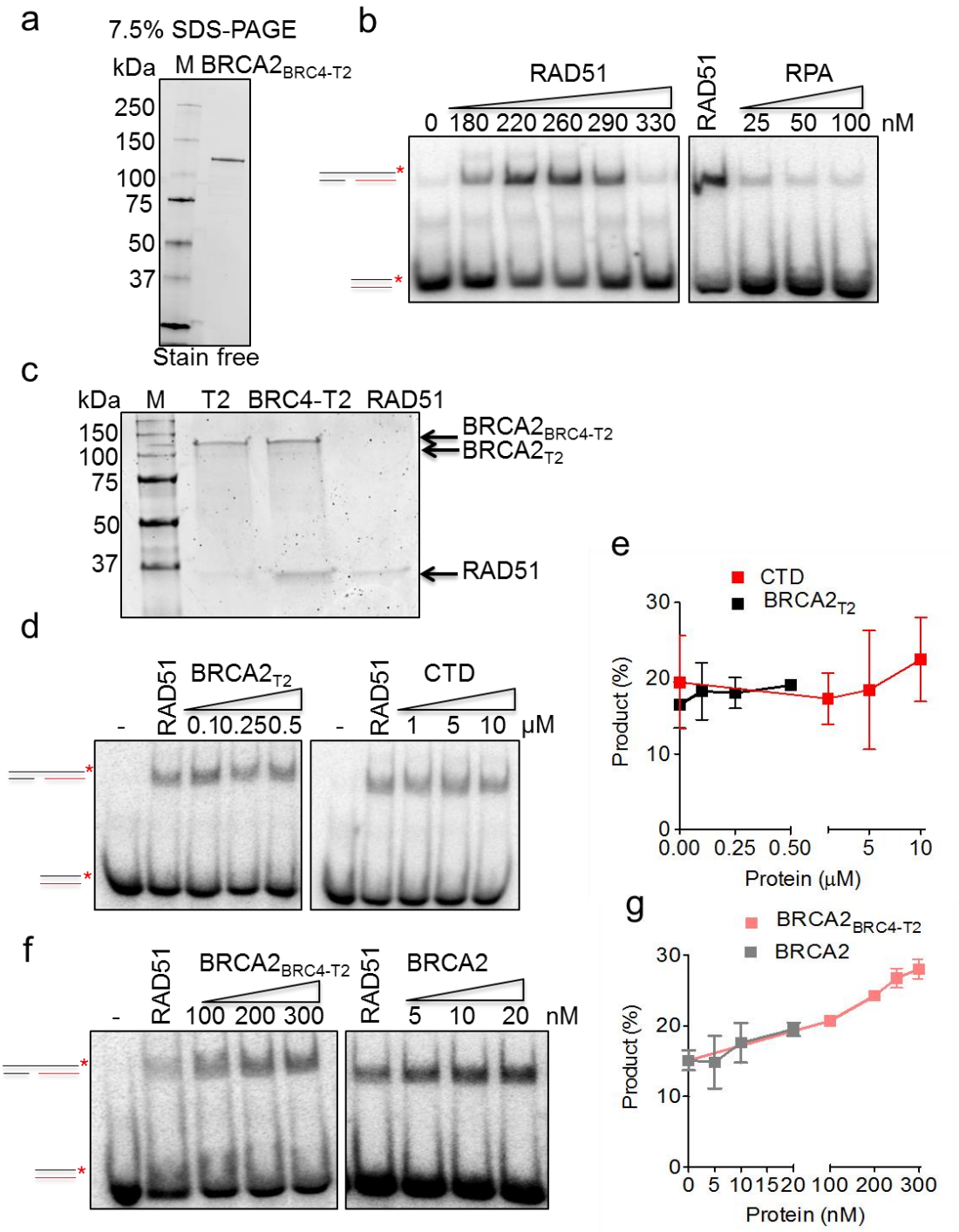

Extended Data Figure 5: $BRCA2_{BRC4-T2}$ but not $BRCA2_{T2}$ nor CTD can stimulate the DNA strand exchange activity of RAD51 in the absence of RPA. a, SDS PAGE gel showing purified $BRCA2_{BRC4-T2}$. **b**, Autoradiogram of DNA strand exchange reaction using a 3' ssDNA overhang substrate at the indicated increasing concentrations of RAD51 (left) or RPA (right). **c**, Pulldown of purified $BRCA2_{BRC4-T2}$ or $BRCA2_{T2}$ and RAD51. **d**, Autoradiogram of a DNA

strand exchange reaction in the presence of RAD51 alone or with increasing concentrations of $BRCA2_{T2}$ or CTD. **e**, Quantification of **d**. **f**, Autoradiogram of a DNA strand exchange reaction in the presence of RAD51 alone or with increasing concentrations of $BRCA2_{BRC4\text{-}T2}$ or BRCA2. **g**, Quantification of **f**. Error bars, s.d. (n = 3).

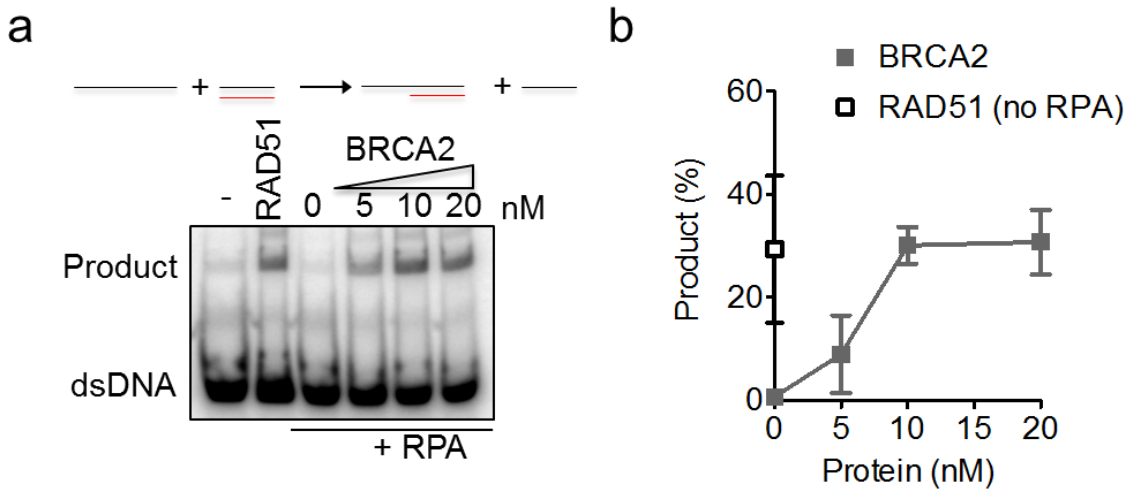

Extended Data Figure 6: BRCA2 stimulates the DNA strand exchange activity of RAD51 using a ssDNA substrate

a, Autoradiogram of a DNA strand exchange reaction in the presence of RAD51 alone, RPA and RAD51, or RPA, RAD51 and increasing concentrations of BRCA2 using a ssDNA substrate. **b**, Quantification of **a**. Error bars, s.d. (n = 3).

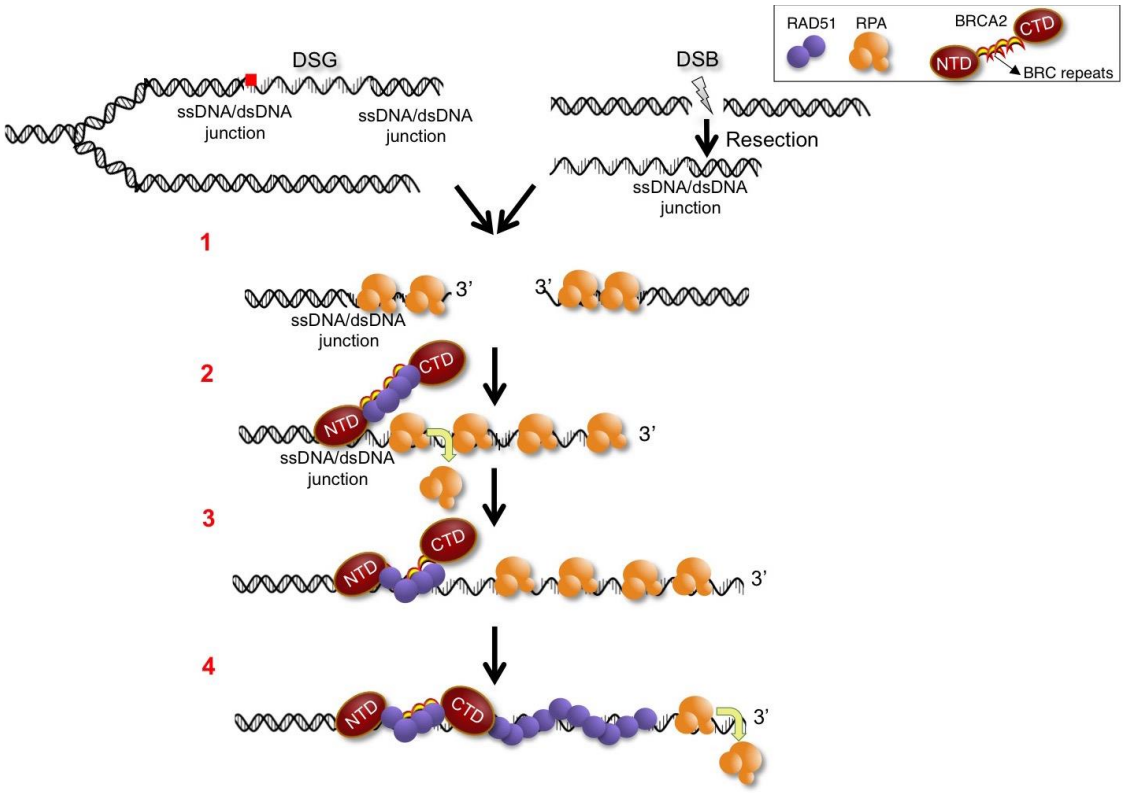

Extended Data Figure 7. Model for BRCA2 NTD and CTD coordination in the context of homologous recombination. (1) RPA binds the ssDNA generated upon resection of a DSB or the ssDNA flanking a DNA lesion during replication. (2) NTD binds at the dsDNA/ssDNA junction, facilitating the loading of RAD51 onto RPA-coated ssDNA by class I of the BRC repeats (BRC1-4)[4]. (3) Class II BRC repeats (5-8) stabilize the nascent RAD51 nucleoprotein filament [4]. (4) CTD binds along the ssDNA and actively facilitates the displacement of RPA[5,6] allowing multiple nucleation events and filament extension of RAD51. These activities enhance the subsequent steps of homologous recombination. These coordinated activities subsequent homology pairing and DNA strand exchange required for the template-driven repair in the context of both a DSB or in daughter strand gapped repair during replication.

REFERENCES

1. Petrucco, S. Sensing DNA damage by PARP-like fingers. *Nucleic Acids Research* **31,** 6689–6699 (2003).
2. Wang, L. & Brown, S. J. BindN: a web-based tool for efficient prediction of DNA and RNA binding sites in amino acid sequences. *Nucleic Acids Research* **34,** W243–8 (2006).
3. Sievers, F. *et al.* Fast, scalable generation of high-quality protein multiple sequence alignments using Clustal Omega. *Mol. Syst. Biol.* **7,** 539–539 (2011).
4. Carreira, A. & Kowalczykowski, S. C. Two classes of BRC repeats in BRCA2 promote RAD51 nucleoprotein filament function by distinct mechanisms. *Proc Natl Acad Sci USA* **108,** 10448–10453 (2011).
5. Zhao, W. *et al.* Promotion of BRCA2-Dependent Homologous Recombination by DSS1 via RPA Targeting and DNA Mimicry. *Molecular Cell* **59,** 176–187 (2015).
6. Jensen, R. B., Carreira, A. & Kowalczykowski, S. C. Purified human BRCA2 stimulates RAD51-mediated recombination. *Nature* **467,** 678–683 (2010).

2.5 METHODS

2.5.1 CLONING OF CONSTRUCTS USED FOR EXPRESSION, PURIFICATION AND CELL BASED ASSAYS

All BRCA2 N-terminal expression constructs containing the sequence coding for BRCA2 amino acids 1-250 (pAC097; $BRCA2_{T1}$), 251-500 (pAC098; $BRCA2_{T2}$), 1-500 (pAC101; $BRCA2_{LT2}$) and 1-750 (pAC102; $BRCA2_{LT3}$) were amplified by PCR from a 2xMBP-BRCA2 phCMV1 vector (Jensen et al., 2010) and cloned by restriction digest with XhoI and NotI into a phCMV1 vector containing an N-terminal 2x MBP tag with two Nuclear Localization Signals (NLS) downstream the tag.

Point mutations in $BRCA2_{T2}$ to produce 2xMBP 2 NLS $BRCA2_{T2C279A}$, 2xMBP 2 NLS $BRCA2_{T2C315S}$, 2xMBP 2 NLS $BRCA2_{T2C341S}$ and 2xMBP 2NLS $BRCA2_{T2C315SC315s}$, 2xMBP 2 NLS $BRCA2_{T2C315SC341s,}$ 2xMBP 2 NLS $BRCA2_{T2C315SC315s}$ were introduced using QuikChange II site-directed mutagenesis kit (Agilent) and verified by sequencing.

$BRCA2_{BRC4\text{-}T2}$ fusion construct was generated by HIFI Gibson Assembly (NEB). A PCR (see below for reaction setup) to create overlapping ends with NotI 2NLS BRC4 and BRC4 T2 was made from the pAC138 plasmid. A PCR reaction using pAC098 as a template to create T2 sequence overlapping with end of BRC4 and stop-XhoI was done. The BRC4, T2 and phCMV1 2x MBP 2 NLS vector cut with NotI and XhoI were then used for Gibson Assembly reaction. The correct assembly was verified by restriction digest and sequencing.

To generate eGFP-MBP-BRCA2, one MBP-tag of a phCMV1 2x MBP-BRCA2 vector (kind gift from S.C. Kowalczykowski) was substituted by an EGFP tag amplified by PCR from a pEGFP-C1 vector (Invitrogen) and cloned by restriction digest with KpnI.

Point mutations to create BRCA2 with missense mutation were created with QuikChange XL site-directed mutagenesis kit (Agilent) and verified by sequencing.

All constructs mentioned above including the vector 2xMBP-NLS used as control were amplified with NucleoBond Xtra Midi kit (Macherey Nagel) and used for expression and purification.

The C-terminal DNA binding domain (aa 2474-3190) of human BRCA2 (CTD) was cloned into pET28 6His SUMO vector.

pCDF DSS1 expression vector was generated by HIFI Gibson Assembly (NEB) from a pFASTBAC Dual-DSS1 vector (kind gift from R. B. Jensen).

All the constructs mentioned above were amplified with QIAprep Spin Maxiprep kit (Qiagen) and used for expression and/or purification.

2.5.2 PURIFICATION OF RECOMBINANT PROTEINS

2x MBP-tagged proteins proteins were purified using the following protocol:
20x150mm confluent plates of HEK293 cells were transiently transfected with 20 µg DNA and 40 µl TurboFect (Thermo Scientific) following the manufacturer's specifications and harvested 30 hours post-transfection. After lysis with 50 mM HEPES (pH 7.5), 250 mM NaCl, 5 mM EDTA, 1% Igepal CA-360, 1 mM DTT, 1 mM PMSF and 1x EDTA-free Protease Inhibitor Cocktail (Roche) for 20 minutes in rotation, the suspension was incubated for 3 hours with amylose resin (NEB), pre-equilibrated in lysis buffer. 2x MBP tagged proteins were eluted with 50 mM HEPES (pH 7.5), 250 mM NaCl, 0.5 mM EDTA, 1 mM DTT, 1x EDTA-free Protease Inhibitor Cocktail (Roche) and 10 mM Maltose. The eluates were diluted to 100 mM NaCl and further purified with Bio-Rex 70 cation-exchange resin (Bio-Rad), pre-equillibrated in 50 mM HEPES (pH 7.5), 100 mM NaCl, 0.5 mM EDTA, 1 mM DTT, 1x EDTA-free Protease Inhibitor Cocktail (Roche). After 1 hour of incubation with the resin on a rotating wheel, the proteins were eluted by NaCl step elution (50 mM HEPES pH 7.5, 0.5 mM EDTA, 10% glycerol, 1 mM PMSF, 1 mM DTT, 250 mM, 450 mM or 1 M NaCl) using a disposable column.
The size and purity of the BRCA2 fragments or BRCA2 full-length WT and variant proteins were verified by loading the final fractions on a SDS-PAGE gel and detecting the MBP tag by Western Blot (MBP Antibody, Invitrogen). All fractions were tested for nucleases by performing EMSAs with radiolabeled dT_{40} oligonucleotide incubated with the proteins (see EMSA below).
The protein concentration of the nuclease-free fractions was determined using NanoOrange Protein Quantitation Kit (Thermo Fisher) and by density determination in SDS-PAGE gel using BSA as a standard.
The CTD was co-expressed with DSS1 to ensure stability of the protein. *E. coli* BL21 DE3 pISO Dscb cells (kind gift of A. el Marjou) were transformed and grown at 37°C in 7 liters of culture medium and induced with 0.5% arabinose and 1mM IPTG overnight at OD 2. Cells were collected in 20 mM TrisHCl pH 8, 300 mM NaCl, 10% Glycerol, 0.5 mM EDTA, 5 mM β-Mercaptoethanol, 1x Protease Inhibitor Cocktail EDTA-free (Roche), 10 mM $MgCl_2$, 1x DNase (Roche), Lysozyme (Sigma-Aldrich) and the suspension was lysed by disintegration at 1.7 kbar (Constant System (CellD)). The lysate was centrifuged at 25.000 rpm for 30 minutes at 4°C. The His-tagged protein was incubated with Protino® Ni-NTA agarose (Macherey Nagel) pre-equlibrated with 300 mM NaCl, 20 mM TrisHCl pH 8.0, 5 mM β-Mercaptoethanol, 0.5 mM EDTA, 10% glycerol and 10 mM Imidazole at 4 C for 1 hour. The resin was extensively washed in 300 mM NaCl, 20 mM TrisHCl pH 8.0, 5 mM β-Mercaptoethanol, 0.5 mM EDTA, 10% glycerol and 20 mM Imidazole and centrifuged at 500 xg for 5 minutes each time. The

protein was eluted in 300 mM NaCl, 20 mM Tris pH 8.0, 5 mM β-Mercaptoethanol, 0.5 mM EDTA, 10% glycerol and 200 mM Imidazole. Dialysis followed overnight against 20 mM TrisHCl pH 8, 100 mM NaCl, 10% Gycerol, 0.5 mM EDTA, 5 mM β-Mercaptoethanol. The eluate was further subjected to a 5 ml HiTrap Heparin HP column (GE) in an Aktaprime chromatograph. The column was pre-quilibrated in 20 mM TrisHCl pH 8.0, 100 mM NaCl, 5 mM β-Mercaptoethanol, 0.5 mM EDTA, 10% glycerol prior to loading of the protein. After the protein had bound to the column, it was washed with the same buffer and then eluted using a continuous NaCl gradient (20 mM TrisHCl pH 8, 1 M NaCl, 10% Gycerol, 0.5 mM EDTA, 5 mM β-Mercaptoethanol). All fractions showing to contain protein on the chromatograph were visualized on a 7.5% SDS-gel and the fractions with the protein of interested were pooled and dialysed against 20 mM TrisHCl pH 8, 150 mM NaCl, 10% Gycerol, 0.5 mM EDTA, 5 mM β-Mercaptoethanol. The protein was heated in 1x SDS buffer for 5 min at 54°C visualized on a 7.5% SDS gel and the protein concentration was determined by Bio-Rad protein assay.

Human RAD51 was cloned into pCDF 6his SUMO vector*. E. Coli* BL21 BRL were transformed and grown in 7 L of terrific broth at 37°C in a fermenter.

At OD =1, the temperature was decreased to 20°C and protein expression was induced with 0.5 mM IPTG overnight at 700 RPM. Cells were harvested at 6000 RPM for 10 minutes at 4°C and resuspended in 1x PBS, 350 mM NaCl, 20 mM Imidazole, 10% Glycerol, Lysozyme 0.5 mg/ml (Sigma-Aldrich), 1x Protease Inhibitor Cocktail (Roche), 1 mM PMSF, 10 mM $MgCl_2$, 1x DNase (Roche) and extracted using a disintegrator at 1.8kbar, followed by centrifugation at 20.000 RPM for 30 minutes.

The His-tagged protein was incubated with Protino® Ni-NTA agarose (Macherey Nagel) and washed with TrisHCl 20 mM pH 8.0, 20 mM Imidazole, 10% Glycerol, 100 mM NaCl, 5 mM β-mercaptoethanol.

The protein was cleaved from the His-tag by incubating the resin with 0.41 mg/ml SUMO protease (Thermo Scientific) at 4°C overnight. The supernatant containing the cleaved protein was then subjected to a 5 ml HiTrap Heparin HP chromatography column (GE Healthcare) equilibrated in TrisHcl 20 mM pH 8, 10% Glycerol, 100 mM NaCl, 5 mM β-mercaptoethanol.

RAD51 protein was then eluted using a continuous NaCl gradient (20 mM TrisHCl pH 8, 2 M NaCl, 10% Glycerol, 5 mM β-mercaptoethanol). The eluate was dialysed against RAD51 storage buffer (20 mM TrisHCl pH 8, 50 mM KCl, 0.5 mM EDTA, 1 mM DTT, 10% Glycerol, 0.5 mM PMSF) and visualized on a 7.5% SDS-PAGE gel stained with Coomassie Brilliant Blue (Bio-Rad) or SYPRO Orange (Thermo Scientific). The protein concentration was determined using Bio-Rad protein assay.

His-tagged RPA was a kind gift from M. Modesti (IGH, Marseille).

2.5.3 SDS PAGE AND WESTERN BLOT ANALYSIS

All proteins

Samples were heated in 1x SDS sample buffer for 5 min at 54°C, loaded on a stain-free 7.5% SDS gel (Bio-Rad) with 6x SDS sample buffer and migrated at 130 volts for 90 minutes in running buffer (1x Tris-Glycine, 0.1% SDS). The gel was visualized using a ChemiDoc camera (Bio-Rad).

For transfer, a nitrocellulose membrane (VWR) was pre-equlibrated in $_{dd}H_2O$ and in transfer buffer (1x Tris-Glycine, 0.025% SDS, 10% methanol). The proteins were transferred for 2 hours at 0.35 ampere in a cold box. The membrane was blocked in 5% milk in 1x TBS-T at room temperature for 30 minutes and then incubated with the respective antibody in 5% milk in 1x TBS-T, shaking overnight at 4°C. After extensive washes in TBS-T, the membrane was incubated for 1 hour with the respective secondary HRP-antibody at room temperature on a shaker. After more washes, the membrane was developed using ECL prime western blotting detection reagent (VWR) and visualized using a ChemiDoc camera.

DSS1 Western Blot

Due to its small size, DSS1 is difficult to detect on WB and risks to be lost during transfer.

Protein samples were heated in 1x SDS loading buffer at 54°C for 5 minutes and migrated on a 4-15% stain-free SDS Page Gel (Bio-Rad) for 45 minutes at 100 volt in 1x SDS running buffer. A PVDF membrane (Dutscher) was activated in methanol for 5 minutes and equilibrated in 25 mM KH_2HPO_4 buffer (pH 7.0). The same buffer was used for transferring the proteins on the membrane for 1 hour at 0.35 ampere in a cold box. The membrane was then fixed for 45 minutes shaking in 0.25% v/v glutaraldehyde (Sigma). After washing with 1x TBS-T, the membrane was blocked 5% milk in 1x TBS-T at room temperature for 30 minutes and then incubated with the respective antibody in 5% milk in 1x TBS-T, shaking overnight at 4°C. After extensive washes in TBS-T, the membrane was incubated for 1 hour with the respective secondary HRP-antibody at room temperature on a shaker. After more washes, the membrane was developed using ECL prime western blotting detection reagent (VWR) and visualized using a ChemiDoc camera.

2.5.4 MOLECULAR CLONING

All oligos used were purchased from MWG Eurofins and are listed in table in the primer list in the materials.

PCR reactions in the study were performed using *Taq* DNA Polymerase (NEB) according to the manufactures manual and 1 ng of plasmid template.

The reaction set up was the following:

Component	**Final reaction**
10x Thermo Pol Buffer	1x
dNTPs	200 µM
Primer 1	0.2 µM
Primer 2	0.2 µM
Template DNA	1 ng
Taq DNA polymerase	1.25 Units
$_{dd}H_2O$	To 50 ul

Cycling conditions

Step	**Temperature**	**Time**
Denaturation	95°C	30 seconds
30 cycles	95°C 53°C 68°C	30 seconds 30 seconds 2 minutes
Extension	68°C	5 minutes

For **restriction digests,** enzymes were purchased from NEB and used according to the manufacturer's manual. **Ligation** reactions were performed using T4 DNA Ligase (NEB) in 10 µl of total volume according to the manufacturer's manual at 16°C overnight in a thermal cycler. The insert:vector ratio was calculated with Ligation Calculator (http://www.insilico.uni-duesseldorf.de/Lig_Input.html).

For small scale **plasmid isolation**, QIAprep Spin Miniprep kit (QIAGEN) was used.

For the purification of PCR products and purification of DNA products from agarose gels, Wizard SV Gel and PCR clean-up system (Promega) was used.

For electrophoretic separation of DNA samples, 6x DNA loading dye was added to DNA samples and samples were loaded on a 1% agarose (w/v) gels in 1x Tris Acetate EDTA (TAE) buffer gel and visualized using an UV transilluminator (Vilber).

Site-directed mutagenesis

For site-directed mutagenesis in small constructs, QuikChange II site-directed mutagenesis kit (Agilent Technologies) was used. Mutagenesis primers were designed using the QuikChange Primer Design program and purchased from MWG Eurofins.

Standard reaction for mutagenesis:

Component	**Final reaction**
10x reaction buffer	1x
dNTP mix	1 µl
Primer 1	125 ng
Primer 2	125 ng
Template DNA	45 ng
PfuUltra HF DNA polymerase	2.5 units/µl
$_{dd}H_2O$	To 50 µl

Cycling conditions

Segment	**Cycles**	**Temperature**	**Time**
1	1	95°C	30 seconds
2	16	95°C	30 seconds
		55°C	1 minute
		68°C	1 minute/kb
3	1	68C	5 minutes

PCR reactions were cooled down and incubated with 1 µl DPNI for 2 hours at 37°C, spun down for 1 minute in a table-top centrifuge and 1 µl of reaction was transformed into 45 µl DH5 alpha electro-competent cells by electroporation. Cells were plated on LB plates containing the appropriate antibiotic and colonies were picked the next day for overnight cultures. Cultures were used for plasmid isolation that was sent for sequence verification to MWG Eurofins.

For site-directed mutagenesis in large constructs, QuikChange II XL site-directed mutagenesis kit was used (Agilent). Mutagenesis primers were designed using the QuikChange Primer Design program and purchased from MWG Eurofins.

Standard reaction for mutagenesis:

Component	Final reaction
10x reaction buffer	1x
dNTP mix	1 µl
Primer 1	125 ng
Primer 2	125 ng
Template DNA	45 ng
Quik Solution	3 µl
PfuUltra HF DNA polymerase	2.5 units/µl
$_{dd}H_2O$	To 50 µl

Cycling conditions

Segment	Cycles	Temperature	Time
1	1	95°C	1 minute
2	18	95°C	50 seconds
		60°C	50 seconds
		68°C	1 minute/kb
3	1	68C	8 minutes

PCR reactions were cooled down and incubated with 1 µl DPNI for 2 hours at 37°C, spun down for 1 minute in a table-top centrifuge and 1 µl of reaction was transformed into 45 µl XL gold ultra-competent according to the manual. Cells were plated on LB plates containing the appropriate antibiotic and colonies were picked the next day for overnight cultures. Cultures were used for plasmid isolation that was sent for sequence verification to MWG Eurofins.

Ethanol Precipitation of DNA

$_{dd}$H2O was added to a total volume of 100 µl to the ligation or PCR product that was mixed with one tenth of volium of Sodium Acetate buffer pH 5.2 (3M). Three volumes of cold 100% ethanol was mixed to the solution and kept at -20°C for 2 hours. Sample was centrifuged for 15 minutes at 12.000 xg at 4°C. After the supernatant was removed without touching the pellet, 900 µl of cold 70% ethanol was added and centrifuged for 10 minutes at 4°C at 12.000 xg. The supernatant was carefully aspirated and the pellet dried on at room temperature or in a heating block at 37°C. The pellet was resuspended in the desired volume of TE buffer.

RT PCR

For extraction of RNA, cells were grown on a 60 mm culture dish and RNA was extracted using TRIzol Reagent (ambion RNA – life technologies) according to the manual. The yield of the extraction was determined using NanoDrop.

For the RT-PCR reaction, TITANIUM One-Step RT-PCR kit was used according to the manual using 0.5-1 µg of RNA sample and primers for the N-terminus (oAC14 and oAC033) as well as C-terminus (oAC041 and oAC188) for BRCA2 were used to ensure the presence of the whole cDNA in the stable clones. The PCR reactions were loaded on a 1% agarose gel and visualized using an UV transilluminator (Vilber).

2.5.6 ELECTROPHORETIC MOBILITY SHIFT ASSAY (EMSA)

DNA substrates were purchased PAGE-purified from MWG Eurofins. Sequences can be found in the oligo list in the materials.

The following oligonucleotides were used:

oAC379: dT_{40} homopolymer. oAC423 (167mer), oAC403 (42mer), oAC490 (42mer), oAC405 (40mer), oAC406 (40mer)

All DNA substrates were ^{32}P radiolabeled at the 5’ –end using T4 Polynucleotide Kinase (NEB) and column purified with illustra MicroSpin G-25 columns (GE) The DNA concentration was calculated after column purification.

ssDNA substrates used in EMSA assays were oAC379 and oAC423. To generate the dsDNA substrates, oAC405 was annealed in a 1:1 molar ratio to oAC406. The 3’ and 5’ overhang substrates were produced by annealing oAC490 (42mer -3’) to oAC423 (167mer) or oAC403 (42mer -5’) to oAC423 in a 1:1 molar ratio, respectively. oAC423, oAC403 and oAC490 were annealed in a 1:1:1 ratio to produce the gapped DNA substrate.

The long dsDNA substrate was a PCR product (134 bp) amplified from pAC138 by PCR using the oligonucleotides oAC596 and oAC597, purified and ^{32}P-labeled at the 5' end.

For the reaction, the proteins were incubated at the indicated concentrations with 0.2 µM nucleotides ^{32}P radiolabeled DNA substrates for 1 hour at 37°C in EMSA reaction buffer (25 mM Tris Acetate pH 7.5, 1 mM DTT, 1 mM $MgCl_2$, 2 mM $CaCl_2$). The protein-DNA complexes were mixed with 6x DNA loading dye and resolved on 6% native polyacrylamide gels in 1x TAE buffer (40 mM Tris Acetate, 0.5 mM EDTA) at 70 volts for 75 minutes. The gels were dried and analyzed with a Typhoon PhosphorImager (Amersham Biosciences) using Image Quant software (GE Healthcare). The ratio of DNA-protein complexes was calculated as the percentage of bound DNA compared to the free DNA. The protein-free lane defined the value of 0 % complex. Statistical analysis and graphs were made with GraphPad Prism (version Mac 6.0e). Error bars represent the standard deviation derived from at least three independent experiments.

2.5.7 BIOTINYLATED DNA PULL-DOWN ASSAY

A dT_{80} oligonucleotide with a 3'-end biotin modification was purchased from MWG Eurofins. The oligonucleotide was incubated with Magnetic streptavidin beads (MyOne Dynabeads®, Thermo Scientific) pre-equilibrated in binding buffer (25 mM Tris Acetate pH 7.5, 1 mM $MgCl_2$, 2 mM $CaCl_2$, 1 mM DTT) for 2 hours at room temperature. After washing the beads extensively in washing buffer (25 mM Tris Acetate pH 7.5, 1 mM $MgCl_2$ 2 mM $CaCl_2$, 1 mM DTT, 1 M NaCl, 0.3% Igepal-NP40), $BRCA2_{T2}$ or $BRCA2_{T1}$ were incubated with pre-equilibrated beads-DNA (4.2 µM nucleotides) at 37°C for 30 minutes on a rotating wheel. The samples were extensively washed in washing buffer before resuspension in 1x SDS loading buffer, boiled at 95°C and loaded on a 7.5% stain-free SDS gel (Bio-Rad). For competition assays, oAC379 (dT_{40} homopolymer) added to the protein sample at the indicated excess concentrations over the radiolabeled dT_{80} and the reaction was performed as described above.

2.5.8 DNA STRAND EXCHANGE ASSAY

DNA substrates were purchased PAGE-purified from MWG Eurofins. Sequences can be found in the oligo list in the appendix.

For DNA strand exchange assays without RPA, proteins were incubated at the indicated concentrations with 4 nM molecules 3' overhang DNA (oAC490 annealed to oAC423) or ssDNA (oAC423, see above for substrates) for 5 minutes at 37°C in 25 mM Tris Acetate pH 8.0, 1 mM DTT, 2 mM ATP, 1 mM $MgCl_2$, 2 mM $CaCl_2$, 0.1 mg/ml BSA before adding 4 nM molecules dsDNA (oAC405 and oAC406 in 1:1 ratio, not

labeled) and further incubation for 30 minutes at 37°C. When RPA was added, the protein was incubated for 5 minutes with ssDNA or 3'overhang DNA, before adding other proteins. The reaction was stopped by adding 0.25 % SDS and 0.5 mg/ml Proteinase K for 10 minutes. Samples were loaded on a 6% Polyacrylamide gel, migrated at 70 volts for 75 minutes. The gels were dried and analyzed with a Typhoon PhosphorImager (Amersham Biosciences) using Image Quant software (GE Healthcare). For quantification, the ratio of DNA strand exchange products was calculated as the percentage of product compared to the free ssDNA whereas the value for product formation of RAD51 and RPA only reaction (usually lane 3) was subtracted from all values as "no product" value. Statistical analysis and graphs were made with GraphPad Prism (version Mac 6.0e). Error bars represent the standard deviation derived from at least three independent experiments.

2.5.9 AFFINITY PULL-DOWN WITH AMYLOSE BEADS

Prior to pull-down assays, amylose resin (NEB) was equilibrated with binding buffer: 50 mM HEPES (pH 7.5), 250 mM NaCl, 0.5 mM EDTA, and 1 mM DTT. Purified 2XMBP 2NLS $BRCA2_{BRC4T2}$ or 2xMBP 2NLS $BRCA2_{T2}$ protein (1.25 µg) was incubated with 1 µg purified RAD51 for 30 minutes at 37 °C and then batch bound to 30 µL of amylose resin for one hour at 4 °C. The complexes were washed with binding buffer 50 mM HEPES (pH 7.5), 250 mM NaCl, 0.5 mM EDTA, and 1 mM DTT containing 1% Igepal CA-630. Proteins were eluted with 30 µL 10 mM maltose in binding buffer, the supernatant was taken off and 1x SDS sample buffer was added. Samples were heated at 54°C for five minutes and loaded onto a 4-15% gradient SDS-polyacrylamide gel (Bio-Rad TGX Stain-Free gel).

CHAPTER 3

3.1 CHARACTERIZATION OF VARIANTS OF UNKNOWN CLINICAL SIGNIFICANCE IN THE N-TERMINAL DNA BINDING DOMAIN OF BRCA2

Germ-line mutations in *BRCA2* gene give rise to hereditary breast, ovarian or pancreatic cancer. Variants of unknown clinical significance remain a major concern in genetic counselling of individuals at high risk to develop cancer. Many missense mutations do not directly affect the protein's localization or folding, thus their predisposition for tumorigenesis is uncertain. Because missense mutations in *BRCA2* associated with cancer risk can impair BRCA2 protein function, we set out to evaluate the phenotype of *BRCA2* variants located in or around the N-terminal DNA binding domain (NTD) we identified in Chapter 2. Moreover, we were interested if the selected variants could also influence the role of BRCA2 in mitosis as it has been described for other N-terminal variants located in the same region [118].

3.2 RESULTS

3.2.1 SELECTION OF VUS IN EXON 10 COMPRISING THE NTD OF BRCA2

Using the BRCAshare and Breast Cancer Information Core database[209,210], we selected a set of variants of unknown clinical significance in the NTD of BRCA2 that 1) lie in or around the region where the NTD is located (see chapter 2) and 2) have a comparatively high Grantham score that predicts the probability of being deleterious based on the amino acid conservation and the chemical nature of the substitution [207,238]. We expect the functional characterization of these variants to help us to assess their likelihood to predispose to cancer and in addition, evaluate if the NTD is essential for BRCA2 function. We chose the VUS G267E,S273L and N277K as well as an artificial mutation (K268R) as their Grantham score is high and they are all located in the two DNA binding clusters identified by BindN (see chapter 2) [225]. Moreover, the amino acids substituted in the selected VUS are highly conserved among mammalian species, as demonstrated by the multiple sequence alignment performed with Clustal Omega [228] (Figure 1). We also aim to phenotypically characterize the VUS C315S and C341S as well as the artificial mutation C279A that are relevant for DNA binding as described in Chapter 2.

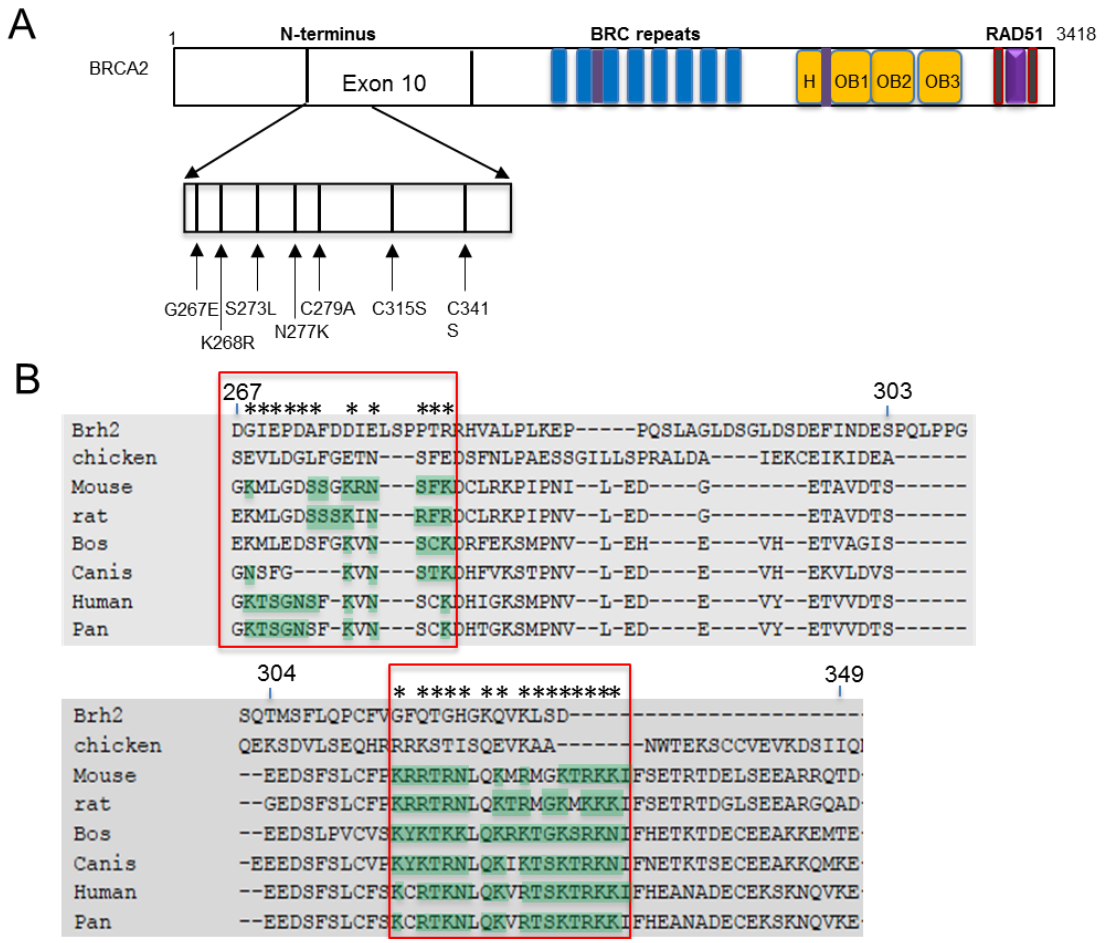

Figure 1 A) Selected variants in the NTD of BRCA2. Magnification of the region from which VUS where selected (shown in arrowheads, amino acid changes are indicated). **B)** Sequence alignment of BRCA2 residues 267-349 containing the missense mutations with other organisms using Clustal Omega. Asteriks (*) represent the conservation of residues in two or more organisms. Residues highlighted in green are predicted to bind DNA (BindN).

The **G267E** missense mutation has nine entries in BRCAshare and six in the BIC database (Table 1). The **K268R** mutation is an artificial mutation that was chosen because it could affect DNA binding and lies in a putative Walker A motif, a domain involved in ATP binding and hydrolysis [239]. **S273L** is recorded once in both databases. BRCA2 is implicated in midbody ring formation and in the recruitment of the endosomal-sorting complex required for transport (ESCRT) proteins necessary to complete cytokinesis [118,240]. Some of these interactions map to the NTD region. In particular, N277K has been reported to abrogate the interaction of BRCA2 with the midbody components CEP55, Alix and Tsg101 [118]. the overexpression of the variant N277K exhibited elevated levels of multinucleation and cytokinetic bridges [118]. We

included N277K in our analysis as it has been listed 12 times in the BIC database and ten times in BRCAshare, making it an interesting candidate for further characterization in response to DNA damage, which has not been tested in the literature.

VUS designation	BIC	BRCAshare	Grantham score
G267E	6	9	98
K268R (artificial)	N.A.	N.A.	N.A.
S273L	1	1	145
N277K	12	10	94
C279A (artificial)	N.A.	N.A.	N.A.
C315S	15	4	112
C341S	2	2	205

Table 1: Selected variants of unknown clinical significance showing the number of entries in BIC and BRCAshare databases as well as their Grantham score.

3.2.2 GENERATION OF STABLE CELL LINES IN *BRCA2*$^{-/-}$ CELLS

For characterization of the missense variants *in vivo*, we introduced the point mutations by site directed mutagenesis into a BRCA2 wild type construct, coding for cDNA of human *BRCA2* and a GFP-MBP tag at the N-terminus for visualization and purification of the protein. *BRCA2*$^{-/-}$ chinese hamster cell lines (VC8) [164] were transfected with the mutant constructs and put under Geneticin (G418) selection to create clones that stably express the wild type and mutant BRCA2 protein with G418 resistance. Surviving clones were verified by fluorescence activated cell sorting (FACS) for expression of the GFP-tag and further tested by RT-PCR with primers against the N-terminus as well as the C-terminus of *BRCA2* to verify the presence of the whole transcript (Figure 2 A, B).

A missense mutation may cause splicing defects leading to a deleterious phenotype, which could be confounded by the effect of the amino acid change or may lead to a compound effect. Thus, it is important to verify if the variants lead to splicing aberrations. *Ex vivo* splicing minigene assays can help to reveal splicing errors due to a point mutation [241]. Our collaborator A. Martins (Rouen Univ.) tested two of the

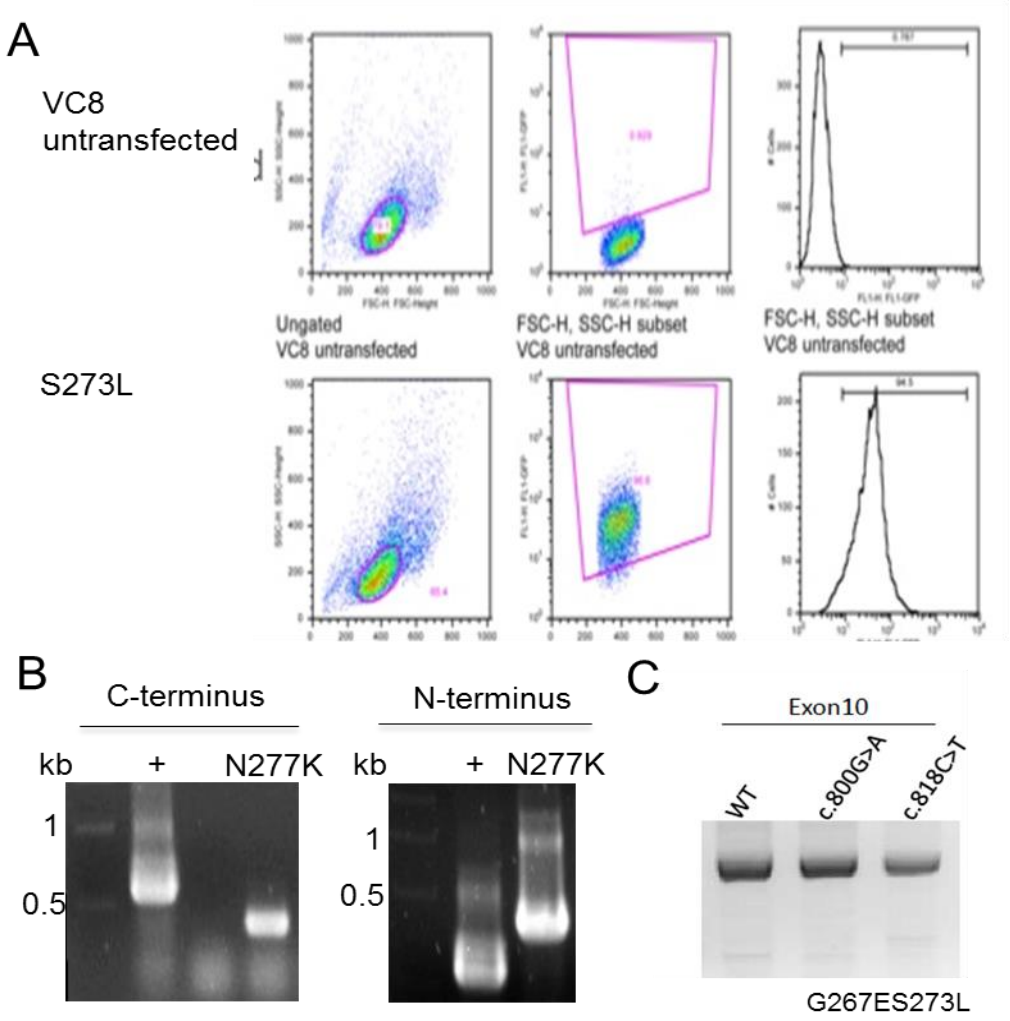

Figure 2: Generation of stable cell lines in VC8 hamster cells: **A)** Example of FACS analysis of stably transfected VC8 (S273L) and untransfected cells to test clones for the expression of GFP-MBP BRCA2 (or variant) construct. **B)** RT-PCR using mRNA extracted from clones positive for GFP expression. **C)** Evaluation of exon skipping using minigene assay (Collaboration with Omar Soukarieh & Alexandra Martins (Inserm U1079, Rouen).

mutations, G267E and S273L, using the minigene assay, however, she did not find a defect in splicing as reflected in the mRNA pattern (Figure 2C). K268R was not tested as it is not listed as VUS and N277K was shown before as fully expressed in cells and at the same levels as the wild type, discarding a splicing defect [118].

3.2.3 LOCALIZATION TO THE CHROMATIN

Many missense mutations in *BRCA2* cause the inability of the protein to translocate to the nucleus. These mutations either lead to the expression of truncated versions or deregulate nuclear localization signals (NLS) as well as nuclear export signals (NES) [131,134].

Because the mislocalization of the protein *per se* entails the inability of BRCA2 to fulfill its function, this analysis excludes further characterization of the variant if positive. Due to the difficulties in the detection of BRCA2 expression in VC8 stable cell lines, we used overexpression in human HEK293 cells to assess their nuclear localization. We first tested the presence of the variant S273L in the cytoplasm and nucleus in response to DNA damaging agent MMC, as BRCA2 is known to accumulate at the sites of DNA damage. However, we could not detect a difference in the pool of proteins after DNA damage, probably due to the overexpression. In an attempt to do so, we further fractionated chromatin from the nuclear soluble fraction. Under our experimental

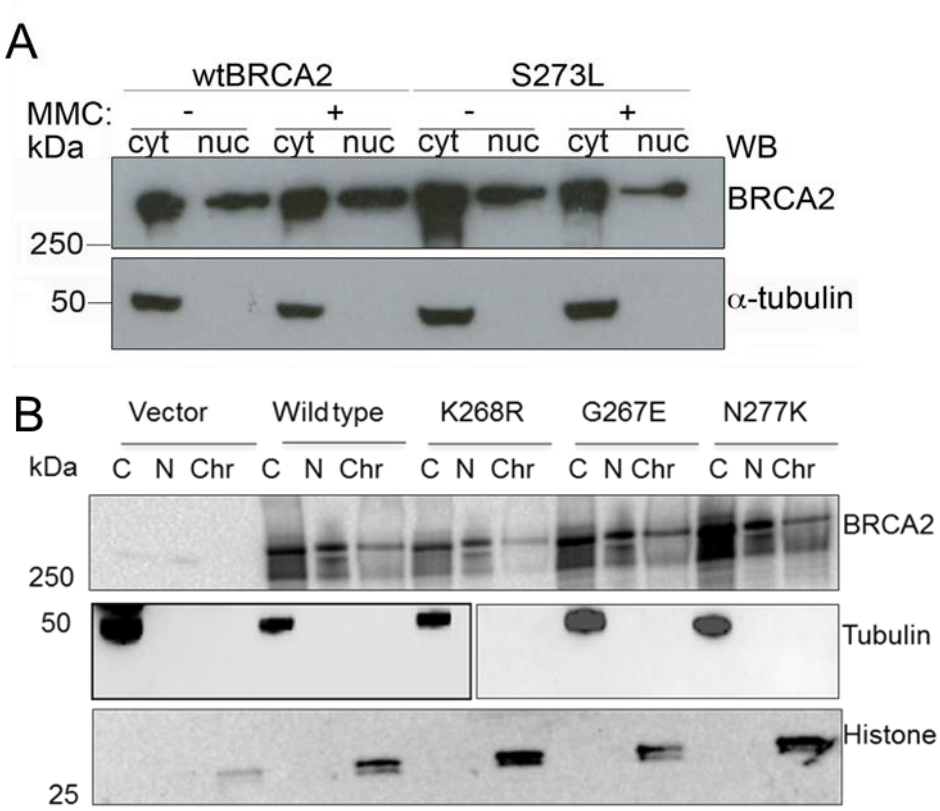

Figure 3: BRCA2 localization to the chromatin. **A)** Overexpression of wild type or variant protein in HEK293s in the absence (-) or presence (+) of MMC. Presence of the proteins in the cytoplasmic or nuclear fraction detected by western blot with markers for BRCA2 and cytoplasmic and chromatin fraction markers (Tubulin, Histone). **B)** Fractionation experiments of HEK293 cells expressing wild type BRCA2 or variant proteins. Detection of the proteins in cytoplasmic (C), nuclear (N) or chromatin (CHR) fraction by western blot.

conditions, most BRCA2 was found in the nuclear soluble fraction and the cytoplasm. All four variants could localize to the nuclear soluble and chromatin fractions as the wild type (Figure 3) excluding the mislocalization and allowing us to continue with the functional characterization.

3.2.4 RESPONSE TO DNA DAMAGE - SURVIVAL ASSAYS WITH MMC AND PARP INHIBITORS

BRCA2 exerts a mediator function during homologous recombination. Absence of BRCA2 causes chromosomal aberrations because of a defective repair of DSBs and renders cells sensitive to DNA damaging agents [140,142,191]. Indeed, *BRCA2*$^{-/-}$ cells are hypersensitive to DNA damage such as genotoxic agents, irradiation, UV light, MMS or MMC [39,98]. Overexpression of the wild type protein in *BRCA2* deficient cells rescues this phenotype and can be used as a functional tool to assess the effect of missense mutations [164,165].

We used the VC8 stable clones expressing GFP-MBP-tagged wild type or mutated BRCA2, and the GFP-MBP vector alone as a control to test the sensitivity of the variants to the cross-linking agent MMC using clonogenic survival assays.

Although we already tested the stable expression of the variant proteins by FACS and RT-PCR we wanted to see the protein expression by Western Blot analysis. We used the total cell lysate and visualized the proteins by Western Blot against BRCA2 (OP95). Surprisingly, we could only detect the expression of wild type BRCA2 and G267E but

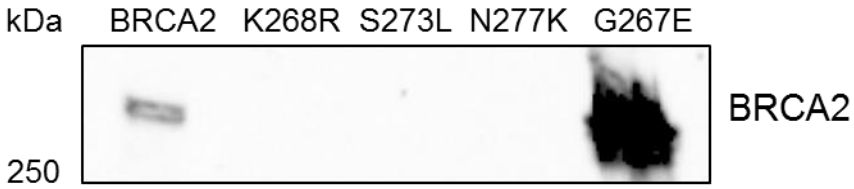

Figure 4: Expression test of stable clones. Equal amounts of total cell lysate were loaded on a 7.5% SDS PAGE and proteins were detected by Western Blot using an antibody against BRCA2 (OP95).

not of the three other proteins (K268R, S273L and N277K).

However, in other studies using VC8 complementation, the expression could only be detected by IP studies [70,165]. We will thus do the same tests using our VC8 stable cell lines and in addition set up a new human system where the cDNA of the variants is integrated into the genome (see 3.4).

Thus, we resumed to perform the clonogenic survival assays with the VC8 stable cell lines. Cells were treated with 0.1–0.5 µM MMC for 1 hour and then seeded in different densities in 6-well plates to allow colony formation during eight to ten days. Cellular sensitivity to MMC caused by the inability to repair DNA damage is reflected by fewer or no colony formation as the cells die from toxic DNA lesions. As expected, ectopically expressed wild type BRCA2 led to the survival of VC8 cells in response to DNA damage, compared to the vector and VC8 cells alone (Figure 5A, C). Cell expressing the G267E variant were able to complement the cells. In contrast, K268R and S273L mutants could not rescue the phenotype and showed similar sensitivity to MMC as the negative control (vector or VC8 cells, Figure 5A, C). Thus the K268R and S273L variants seem to have a defect in DSB repair. Figure 4C shows the colony formation of 1000 VC8 cells expressing wild type BRCA2, the empty vector or the variants treated with 0.5 µM MMC. Clearly, the ability of colony formation for wild type BRCA2 and G267E cells is normal, whereas vector control, K268R and S273L cells show almost no colony survival. In the case of N277K variant, a MTT assay was used in which cells are treated with the same MMC concentrations but the relative survival is measured based

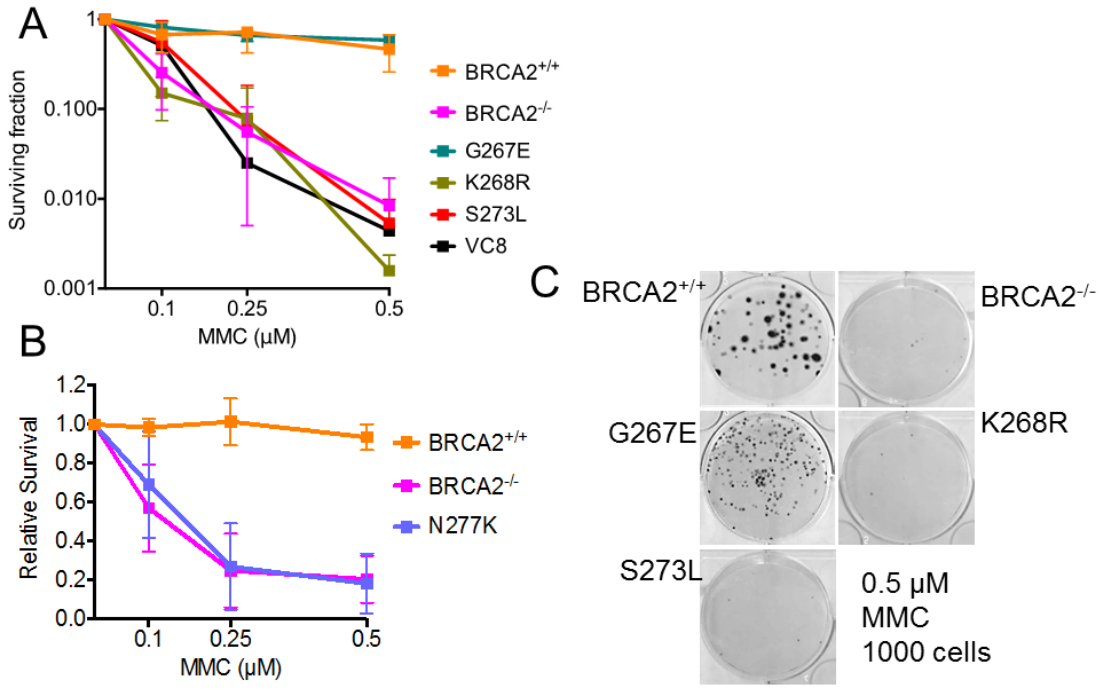

Figure 5: Response to DNA damage: **A)** Clonogenic survival assay with stable cell lines expressing wild type BRCA2, vector alone ($BRCA2^{-/-}$) or variant proteins, treated with different concentration of MMC (n=3). **B)** MTT assay of stable cell lines of wild type BRCA2, vector alone ($BRCA2^{-/-}$) or N277K after treatment with MMC (n=3). **C)** Colony formation after survival assay upon treatment with 0.5 µM MMC. 1000 cells were seeded for each cell line.

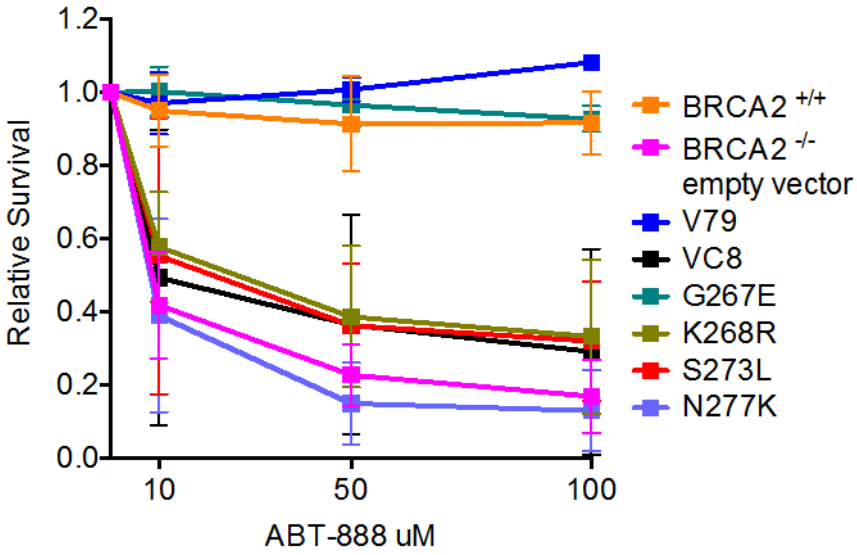

Figure 6: Relative survival of VC8 stable cell lines expressing wild type BRCA2, empty vector (BRCA2$^{-/-}$ 2xMBP) or VUS proteins (as indicated), in response to different concentrations of the PARP inhibitor ABT-888, n=3.

on the metabolic activity of the cells 72h after the treatment in a 96-well plate format. As shown in Figure 5B, wild type BRCA2 complemented the cells after exposure to DNA damage. The N277K mutant cells were sensitive to MMC and showed a decreased survival rate.

BRCA2 deficient cells are not only sensitive to cross-linking agents such as MMC [164] but also to Poly (ADP-ribose) polymerase (PARP) inhibitors that inhibit the enzyme PARP1, important for BER. In the absence of PARP, unrepaired damage can lead to the collapse of replication forks that may be converted into DSB [215], thus, the resistance to PARP inhibitors can be used as an indirect measure of HR. This principle has been exploited as a therapeutic tool for the treatment of *BRCA2*-deficient tumors as they depend on PARP1 to repair these DSBs [214].

We tested the survival of *BRCA2*$^{+/+}$ V79 cells (VC8 parental cell line) as a positive control, vector only and variant-complemented VC8 cells in their response to ABT-888, a PARP inhibitor in phase II clinical trial for the treatment of various cancers (https://clinicaltrials.gov/ct2/home). We monitored the cell survival after treatment with ABT-888 in different doses using a MTT assay as described above.

As expected, cells complemented with wild type BRCA2 and V79 cells survived the treatment (Figure 6). In agreement with the results obtained from the clonogenic survival assay, cells carrying G267E mutation were resistant to PARP inhibitor treatment. In contrast, cells complemented with the variants K268R, S273L and N277K could not survive the treatment.

Taken together, our results identify two VUS (S273L and N277K) and one artificial mutation (K268R), as being sensitive to the cross linking agent MMC as well as to the PARP inhibitor ABT-888, speaking for a defect of these variant proteins for the repair of DSBs via HR. The missense mutations seem to affect residues important for BRCA2 function in HR. In addition, we show that the G267E VUS is capable of repairing DSBs induced by MMC and is not affected by PARP inhibition. When we tried to see the expression of the proteins from total cell lysates, we could only detect wild type BRCA2 and G267E sufficiently expressed by western blot analysis (Figure 4). This poses a major concern for the results obtained in the survival assays as we now cannot totally exclude that the phenotypes observed for K268R, S273L and N277K originate from a possible loss of the cDNA and thus, the cells do not express the variants anymore.

3.2.5 BRCA2 VUS G267E EXHIBITS A COLONY GROWTH DEFECT

When we examined the shape and number of the colonies in the absence of treatment in the survival assay one of the variants that did not show sensitivity to DNA damage exhibited a small colony phenotype in comparison to wild type BRCA2 complemented cells The colonies of G267E were not only smaller but exceeded the colony number by two fold compared to the wild type (Figure 7). BRCA2 has been shown to have multiple roles in mitosis and cells expressing mutant forms of BRCA2 show cytokinetic abnormalities resulting in alterations of chromosome number and structure [173]. In particular, these cells progress slower in mitosis and display defects in the completion of cytokinesis. This is probably due to the role of BRCA2 as a scaffold to allow the localization of components of the central spindle to the midbody (see 1.9). Thus, one

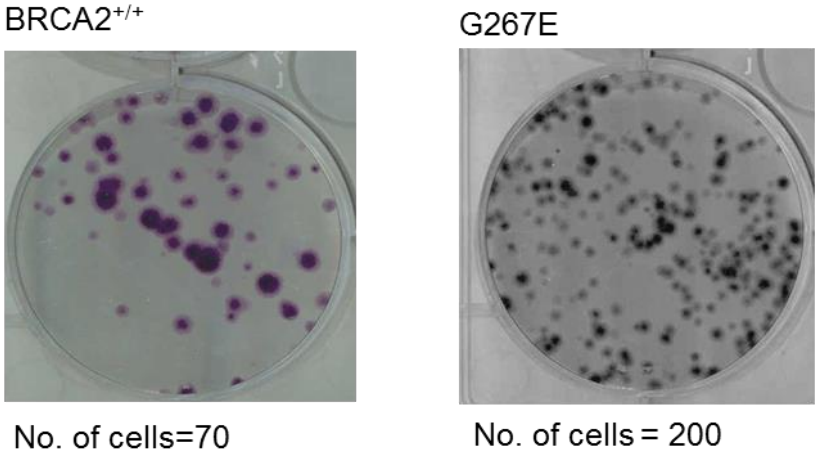

Figure 7: Colony formation in the absence of DNA damage in clonogenic survival assay of cells complemented with wild type BRCA2 (left) or with the mutant G267E. 1000 cells seeded. (n=3).

possibility to explain G267E phenotype could be that it affects this function. This is the case of N277K, a mutation known to disrupt the interaction between BRCA2 and CEP55, leading to an increase of multinucleated cells and unresolved cytokinetic bridges due to incomplete abscission [118].

3.2.6 BRCA2 G267E VARIANT SHOWS ABNORMAL CYTOKINESIS

Because G267E didn't show a defect in survival after DNA damage, but led to a small colony phenotype that could be indicative of a failure in cell duplication we set out a time –lapse microscopy experiment to follow cells through mitosis in living cells.

We synchronized the VC8 stable cells via G1/S phase arrest using double thymidine block and released the cells after 48h to monitor their progression through the cell

cycle. Cells were recorded during 16 hours and pictures were taken every 5 minutes from 4 different positions in each well. Time-lapse pictures were analyzed by evaluating the time needed for individual cells to complete cytokinesis from the beginning of mitosis. Normal progression was based on V79 parental cell line (*BRCA2*$^{+/+}$).

Analysis of representative images of the time-lapse microscopy showed that after entering mitosis (≥ 10 minutes), wild type BRCA2 cells divided after 45 minutes and cytokinesis was eventually completed in about 60-70 minutes (Figure 8A, left panel), which is considered as a normal timeframe for mitotic progression [173]. In contrast, BRCA2 deficient cells complemented with the vector only entered mitosis but started to divide at a later time point (≥ 55 minutes) and were not able to separate even after ~200 minutes. Interestingly, some of the daughter cells failed to separate completely (Figure 8A, right panel). Hence, in our experimental conditions, *BRCA2* deficient cells display a defect in cytokinesis as described before [165] Importantly, when we performed the same time-lapse microscopy analysis with variant G267E we observed a similar pattern as for the *BRCA2*$^{-/-}$ cells (Figure 8A lower left panel).The cells entered mitosis normally (≥ 15 minutes) and started to separate into two daughter cells (45 minutes). However, daughter cells stayed connected until ~300 minutes after entering mitosis, when they completed abscission as illustrated for G267E in Figure 8A (lower panel, in 200 and 300 minutes pictures).In addition, similar to the vector alone-transfected cells, 60% of the cells expressing G267E took longer than 100 minutes to complete cytokinesis (Figure 8B).

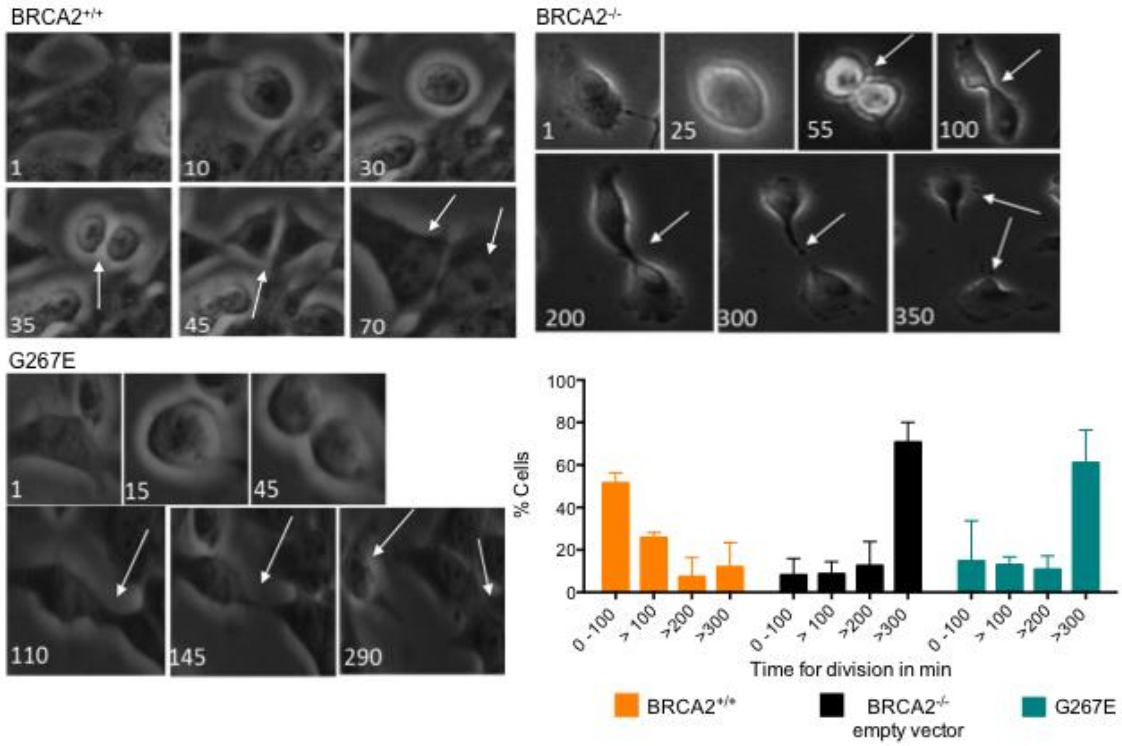

Figure 8: Time-lapse microscopy of stable cell lines after double thymidine block and release in G1/S phase during 16h. **A)** Representative images of cells undergoing mitosis are shown for wild type BRCA2, empty vector (BRCA2$^{-/-}$) and G267E. Arrowheads indicate the separation of daughter cells during cytokinesis and individual cells after completion of abscission. **B)** Quantification of time-lapse experiments shown in A). Percentage of cells that needed a certain time for division (0-100 minutes, 100-200, 200-300, > 300 minutes or failed to divide) were analyzed.

3.2.7 BRCA2 VARIANT G267E LEADS TO MULTINUCLEATED CELLS

Incomplete cytokinesis leads to the formation of bi-and multinucleated cells which ultimately favors aneuploidy and multiple spindle poles, hallmarks of many tumors [242]. Thus, we next evaluated the effect of G267E on cell division by performing in situ immunofluorescence using an antibody against the microtubule-associated protein alpha-tubulin as a marker of cell division. As shown in Figure 9 (panels on the left and quantification on the right), wild type BRCA2 complemented cells and V79 (*BRCA2*$^{+/+}$ control cells) showed almost no multinucleation. In contrast, expression of either the vector

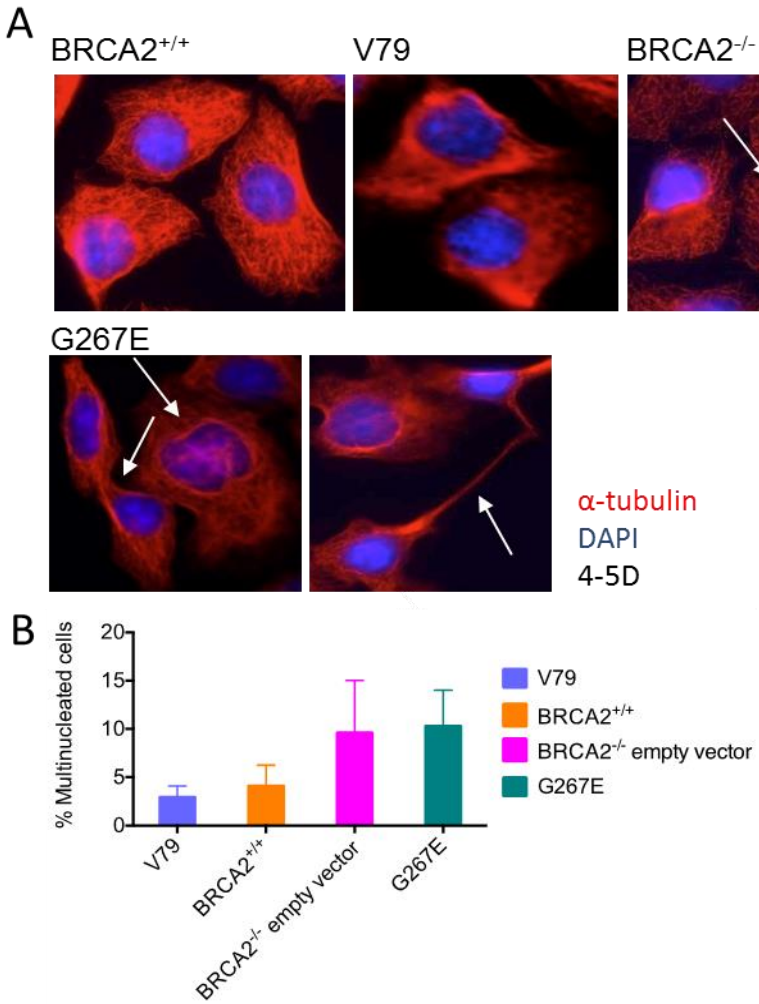

Figure 9: In situ immunofluorescence (IF) microscopy images of the stable cells lines showing bi-and multinucleated cells. **A)** Representative images for each cell line, arrows indicate binucleated cells and unresolved cytokinetic bridges. **B)** Quantification of bi-or multinucleated cells from 3 individual experiments. Nuclei are stained with DAPI (blue) and microtubules are stained with an antibody against alpha-tubulin (red). Images were taken using a 4-5D microscope.

or the G267E variant in VC8 resulted in up to seven fold increase of multinucleated cells. In addition, G267E stables often stayed connected via microtubule bridges (G267E, Figure 9 right panel). This phenotype may result from the failure in cytokinesis that was observed in the time-lapse experiments (Figure 8A lower panel and 8B). Together, these results show that G267E variant leads to cytokinetic defects as observed for *BRCA2*$^{-/-}$ cells and other BRCA2 variants [118] resulting in multinucleated cells.

3.2.8 G267E DOES NOT AFFECT CENTROSOME DUPLICATION

Centrosomes are the microtubule organization centers in the cell and are important for proper segregation of the chromosomes in mitosis. Centrosome amplification might be a consequence of incomplete cytokinesis leading to chromosome instability and aneuploidy. BRCA2 deficient cells show centrosome amplification and multinuclei, both hallmarks of several tumors [203]. BRCA2 localizes to the centrosomes via its centrosome-localization signal (aa 2884–2903) and may have a role in their duplication by interacting with centrosomal proteins such as CEP55 [163]. We evaluated the effect of the variant G267E on centrosome duplication by IF using an antibody against the centrosome-associated protein Centrin-2. Unlike *BRCA2* deficient cells, VC8, cells carrying G267E variant did not exhibit centrosome amplification (Figure 10) indicating that the multinucleation phenotype does not originate from defective centrosome duplication.

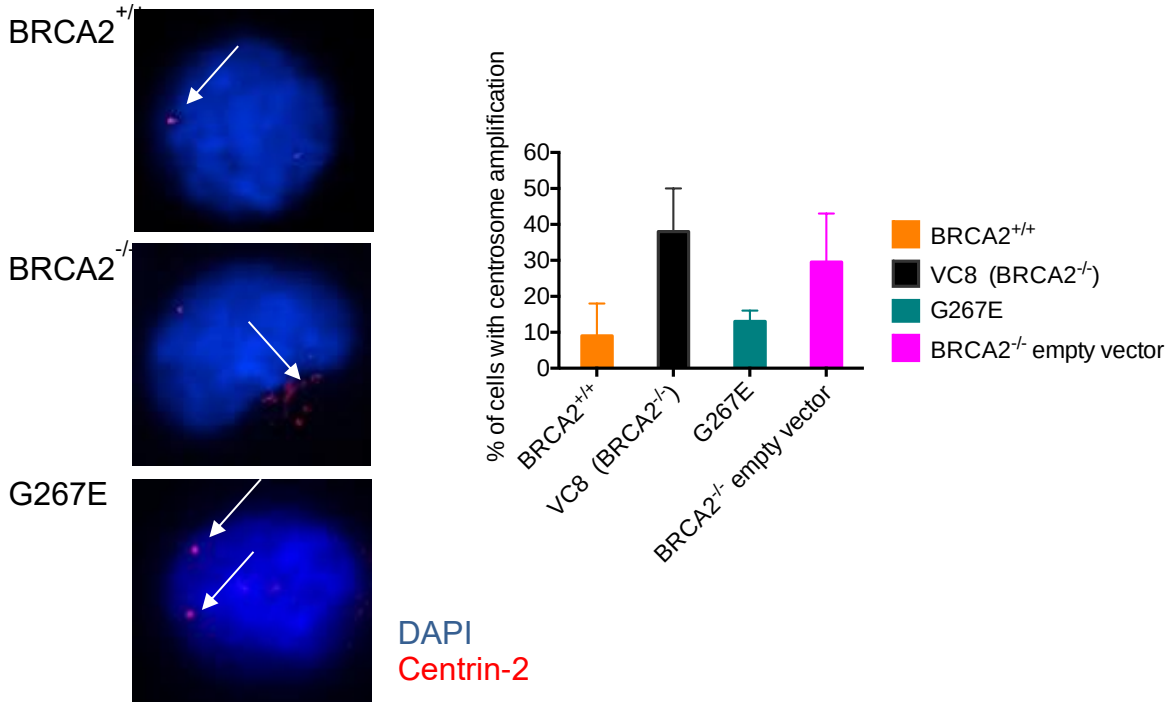

Figure 10: In situ immunofluorescence microscopy images showing centrosomes using an antibody against centrin-2 (red), DAPI staining is used for DNA **A)** Representative images of cell lines tested. **B)** Quantification of three independent experiments showing the percentage of cells with centrosome amplification (>2 centrosomes).

3.2.9 G267E DOES NOT AFFECT THE INTERACTION WITH MIDBODY PROTEINS

Cytokinetic failure and multinucleated cells may also arise from defects in midbody formation. Filamin A recruits BRCA2 to the midbody, where it interacts with CEP55, needed for formation of the midbody ring and the localization of the ESCRT complex components required for cell separation. In particular, BRCA2 regulates the complex formation of CEP55-Alix and CEP55-Tsg101 at the midbody [118,176] (see Figure 11A).

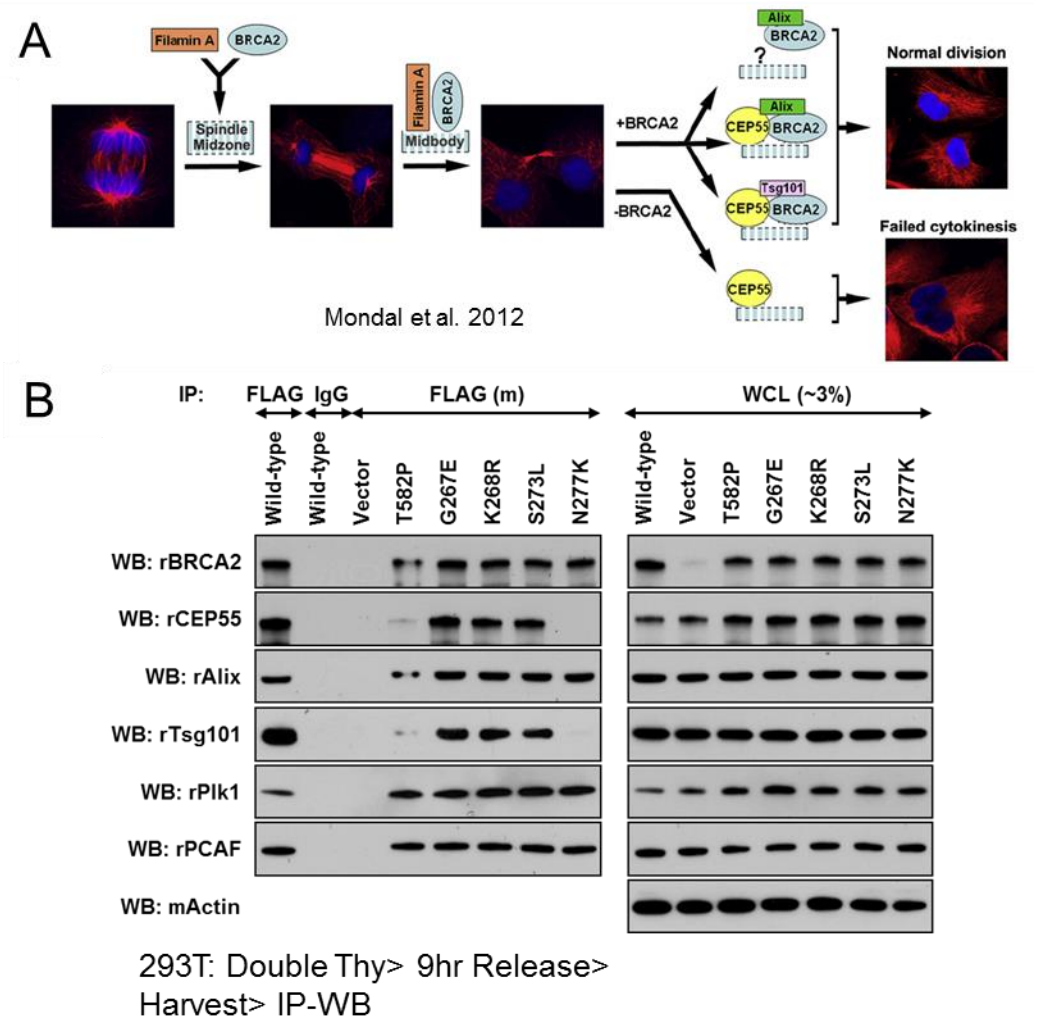

Figure 11: BRCA2 is involved in midbody formation. **A)** Model of BRCA2 interaction with several midbody proteins (Mondal et al. 2012). BRCA2 localizes with Filamin A from the spindle midzone to the midbody where it interacts with midbody components CEP55, Alix and Tsg101. Absence of BRCA2 causes failure in cytokinesis and multinucleated cells. **B)** Effect of BRCA2 missense variants on interaction with proteins involved in midbody formation and in mitotis. Analysis of anti-FLAG IPs with FLAG-BRCA2 WT or variant proteins overexpressed in HEK293T cells after double thymidine block and 9h release (Collaboration w. F. Couch, Mayo clinic).

The group of F. Couch had shown previously that N277K variant favors multinucleated cells and unresolved cytokinetic bridges due to the disruption of the interaction with CEP55 and Tsg-101. So, we established collaboration with F. Couch group to test G267E, K268R and S273L for the interaction with the midbody components. In addition, the variants were tested for the ability to interact with PLK1 that phosphorylates BRCA2 in order to localize to the midbody [114] as well as the acetyltransferase P/CAF for which BRCA2 acts as a scaffold to acetylate BubR1 at the spindle assembly checkpoint [117] (see 1.9). Surprisingly, inspite of the cytokinetic phenotype, and in contrast to N277K, G267E did not disrupt any of the interactions with midbody proteins; neither did K268R and S273L (Figure 11B).

Thus, cells carrying G267E variant are proficient in the survival after DNA damage, and the small colony phenotype observed probably stems from the defective cytokinesis, however, it remains unclear what is the mechanism underling the cytokinetic failure observed. Because of their localization in the NTD of BRCA2, we are currently testing the DNA binding ability of the mutants G267E, K268R, S273L and N277K.

3.3 CONCLUSIONS

We applied several functional assays to study variants of unknown clinical significance located in a novel N-terminal DNA binding domain we identified. The selection of the variants was based on their high probability to have a deleterious phenotype. In Table 1, I have summarized the results from the functional assays for each variant. More assays have to be applied to further study their phenotype.

The **G267E** variant has a Grantham Score of 98 and is listed in total 12 times as VUS (BRCAshare; BIC). Cells complemented with this variant are not sensitive to DNA damage (Figure 4 & 5) excluding an HR defect. They show faster growth than wild type BRCA2 cells (Figure 7), but the colonies are small and 60% of them show a delayed completion of cytokinesis (Figure 8). This phenotype correlates with an increased level of multinucleated cells (Figure 9). Both phenomenons speak for a defect in the late steps of cytokinesis. However, this defect is not due to a disrupted interaction with important midbody components or centrosome amplification (Figure 11).

The other variants tested showed deleterious phenotypes in our assays. Since we could not detect their expression as for wild type BRCA2 and G267E (Figure 4), we cannot conclude that this comes from an impaired function conferred by the variant or absence of expression. So far we can only be certain that all variants showed a normal localization to the nucleus and interaction with midbody proteins in HEK293 cells.

The **K268R** is an artificial mutation not listed in any database for BRCA2 VUS. In survival assay with MMC and after treatment with PARP inhibitors, the cells have a DNA damage-sensitive phenotype. They also exhibit a cytokinetic defect in the time-lapse analysis but we have not analyzed their status of multinucleation and centrosome amplification yet. However, the variant protein was able to interact with the midbody components. We will need to further test if the HR defect we see might be in connection with the growth defect.

The same phenotype we observed for the **S273L** VUS, listed two times in the databases [209,210]. Hence, the same functional analysis will be applied for this variant as for K268R.

We selected the **N277K** mutant as it has been already tested in functional assays, revealing a defective phenotype in midbody formation and cytokinesis [118]. We were interested in its behavior in functional assays for HR. The MMC and PARP inhibitor treatments revealed a defect DSB repair. We are now interested if there could be a

Variant	**MMC/ PARPi sensitive**	**Cyto-kinetic defect**	**Multi-nucleation**	**Centrosome amplification**	**Interaction with midbody proteins**	**DNA binding proficient**
G267E	No	yes	yes	no	Yes	TBT
K268R	Yes	yes	TBT	TBT	Yes	TBT
S273L	Yes	yes	TBT	TBT	Yes	TBT
N277K	Yes	yes	TBT	TBT	Yes	TBT

Table 2: Summary of the results from functional assays obtained in this study for each variant tested (TBT – to be tested).

connection between the defects in HR and mitosis as the BRCA2 protein is also involved at different cell cycle checkpoints [117,169,172].

In addition to these variants, we are currently characterizing the variants located in the NTD described in chapter 2, C279A, C315S and C341S by clonogenic survival and homologous recombination proficiency

3.4 DISCUSSION AND OUTLOOK FOR THE CHARACTERIZATION OF VUS

For the cancer risk assessment of individuals carrying VUS, it is of major importance to evaluate their influence on BRCA2 function [207,213]. Goldgar et al. (2004) developed a multifactorial likelihood-ratio model that predicts the causality of a VUS based on a combination of co-segregation, family history of individuals carrying the mutation, co-occurrence of VUS and deleterious variants in cis, and multiple sequence alignment of

Figure 12: Scheme of TREX Flag eGFP BRCA2 shR construct stably integrated in the genome of HEK293 cells using the FLPin system at the FRT site. Upon Doxycyclin induction of the Tetracyclin Response Element (TRE) promoter, EGFP-BRCA2 or variant proteins are expressed while downregulation of endogenous BRCA2 with siRNA to which construct is resistant. Courtesy of Å. Éhlen.

the protein regarding the amino acid conservation and the biochemical nature of the substitution [207]. However, this model is only applicable for frequent VUS with enough family data available [243]. Hence, functional assays that focus on the effect of the amino acid changes on the function of the protein are still needed to classify VUS. In the work presented here, we assessed the impact on the function of several missense variants located in the NTD of BRCA2 that remain unclassified.

Due to the difficulties to detect the expression of some variant proteins in VC8 cells (Figure 6), we are currently setting up a system where the cDNA of the variant is integrated into the genome.

The cDNA of EGFP-BRCA2 or VUS proteins are integrated at the FRT site in the genome of HEK293 cells by using the FLP-IN (Invitrogen) system. The expression of endogenous BRCA2 can be downregulated by siRNA and expression of the siRNA-

resistant protein of interested is induced using Doxycyclin that binds to the Tetracycline responsive element (TRE) (see Figure 12).

In these cells we will assess the cellular localization, survival assays with DNA damaging agents, time-lapse and immunofluorescence microscopy as described above to confirm the cytokinetic defects observed with G267E and to test the phenotype of the variants for which the expression was not detected in VC8.

To further assess the impact of the variants on BRCA2 function we will use a cell-based recombination assay employing site-specific endonucleases in a modified protocol from the one described [244]: Briefly, cells are transfected with a pZDonor AAVS1-EGFP plasmid as well as zinc-finger nucleases (TALENs) AAVS1R and AAVS1L. The nucleases create a DSB at a native AAVS1 locus. The promoter-less mCherry gene in the donor plasmid is located between sequences homologous to those flanking the AAVS1 site. DSB-promoted gene targeting results in GFP expression from a PPP1R12C native promoter when the donor plasmid is repaired at the AAVS1 site by HR (see Figure 13). Using this system, we will evaluate the impact of the variants on the HR function of BRCA2.

In addition, because these variants are located in the DNA binding site in the N-terminus we will use the DNA binding and DNA strand exchange assays described in Chapter 2 to evaluate their impact on DNA binding and promotion of RAD51 recombination activity in vitro. A defect of the mutants in DNA binding, could explain the DNA damage hypersensitivity observed in some of these variants. However, as the DNA binding activity could be accomplished by the CTD in cells, a reduced DNA

Figure 13: from Yata et al. 2012: Schematic representation depicting DSB-induced gene targeting. Cells are transfected with zinc-finger nucleases (TALENs) AAVS1R and AAVS1L that cut at the AAVS1 ZFN site creating DSB. The pZDonor AAVS1-EGFP plasmid is integrated in the AAVS1 site by HR repair and promoterless GFP can be expressed from the PPP1R12C native promoter.

binding activity of the NTD might not affect the survival.

It has been suggested that unsegregated chromosomes due to unrepaired DNA damage can persist after anaphase and provoke unresolved chromatin bridges and ultra-fine bridges that result in delayed or failed abscission and cytokinesis [174]. However, these structures were not observed in BRCA2 mutant cells affecting cytokinesis arguing that the role of BRCA2 in cytokinesis is independent of its function in DNA repair[118]. Our data with mutant G267E is consistent with this idea as the survival after DNA damage was not affected by this mutation whereas it showed a clear defect in cytokinesis..

To obtain a more complete picture of variants in the NTD, we will apply the cell-based assays for testing HR and cytokinetic defects in the variants chosen during our biochemical study of the NTD (C279A, C315S, C341S). Moreover, there are several VUS candidates listed with many entries in the BRCA2 databases that would be also interesting to test.

The advantage of combining cell-based assays to test DNA damage repair and cytokinetic defects with *in vitro* DNA binding assays is clearly the capability to explain the phenotype observed and understand the impaired mechanistic behind.

3.5 METHODS

3.5.1 CLONING OF CONSTRUCTS USED FOR EXPRESSION, PURIFICATION AND CELL BASED ASSAYS: SEE 2.4

3.5.2 PURIFICATION OF RECOMBINANT PROTEINS: SEE 2.4

3.5.3 SDS PAGE AND WESTERN BLOT ANALYSIS: SEE 2.4

3.5.4 MOLECULAR CLONING: SEE 2.4

3.5.5 GENERATION OF STABLE CELL LINES

VC8 *brca2*$^{-/-}$ deficient hamster cells lines were cultured in HAM's F10 media with 10% FCS and grown to 70% confluency in a P100 mm plate. Cells were transfected with 10 µg DNA of the respective phCMV1-GFP MBP plasmid containing the WT, variant or vector only cDNA using Turbofect transfection reagent (Invitrogen) according to the manual. 48 hours later 1 µg ml^{-1} Geniticin (G418) was added to the cells to select only the transfected cells expressing the G418 resistance markers.

Cells were cultured until individual clones had formed that were transferred to 96-well plates and cultured until the stable cell lines grew in P100 mm plates and were ready for testing the expression of the proteins. First, the expression of the GFP tag was tested in FACS analysis: Cells were harvested from P60 mm plates and washed twice in 1x PBS. As a negative control, non-transfected VC8 cells were used. Several clones of each cell line created were tested in a FACScalibur using the FL-1: 530/30 (FITC, Alexa488, GFP, YFP) laser measuring the GFP content. The clones with GFP expression over the threshold were selected and used for RT-PCR analysis. Cells were harvested from a confluent P60 mm plate and mRNA was extracted with Trizol as described above. mRNA was transcribed into cDNA using RT-PCR protocol (see above) and positive clones containing both N-terminus and C-terminus of the protein of interested were selected and kept for further *in vivo* assays.

3.5.6 CLONOGENIC SURVIVAL ASSAY WITH MMC

For clonogenic survival assays with transiently transfected cells, VC8 *brca2* deficient variant hamster cells were cultivated in HAM's F10 media (Invitrogen) plus 10 % FBS (Invitrogen). The cells were transiently transfected using TurboFect (Thermo Scientific) at 70 % confluency with 10 µg of DNA. 30 hours post-transfection, cells were transferred to HAM's F10 media (Invitrogen) plus 10 % FBS (Invitrogen) containing 1 µg ml^{-1} G418 for 3 days. The protein expression was verified by incubating 3-5 mg of total cell lysate (determined by Bio-Rad protein assay) with amylose beads (NEB) overnight at 4°C with rotation. The beads were extensively washed in Lysis Buffer H (50 mM HEPES (pH 7.5), 250 mM NaCl, 5 mM EDTA, 1% Igepal CA-360, 1 mM DTT, 1 mM PMSF and EDTA-free Protease Inhibitor Cocktail (Roche) and resuspended in 1x SDS sample buffer, boiled and loaded on a 7.5% stain-free SDS PAGE gel. The gel was transferred on a nitrocellulose membrane (VWR) and detected by Western Blot using anti-MBP antibody (mAB R29, Invitrogen). In survival assays with stable cell lines, cells were used directly for the assay.

For the survival assay, 0.8 $x10^6$ cells were seeded in 6 cm dishes and the next day were treated with Mitomycin C (Sigma-Aldrich) at the following concentrations: 0.1 µM, 0.25 µM or 0.5 µM or 1 µM for 1 hour in the dark in media without serum. The cells were then counted, serially diluted and plated out in triplicate into 6-well plates. Cells were re-fed with media containing penicillin/ streptomycin (Sigma-Aldrich= to prevent any contamination during eight to ten days of cell growth. After eight days, the colonies were stained with crystal violet solution (Bio-Rad) for 1 hour, washed and dried overnight. The colonies were counted on each plate using ImageJ software and the surviving fraction was determined for each drug treatment. Statistical analysis and graphs were done with GraphPad Prism (version Mac 6.0e). Error bars represent the standard deviation derived from at least three independent experiments.

For survival **MTT assays** in 96-well format, stable cell lines were seeded in 96-well plate and treated the next day with 0 µM, 0.1 µM, 0.25 µM and 0.5 µM MMC for 1 hour. The media was removed and cells recovered for 72 hours until 0.5 mg/ml MTT in 1x PBS was added and incubated for 4 hours. The media was then removed and DMSO was added to the wells, incubated for 5 minutes at room temperature and the absorbance was measured in a plate reader at 570 nM.

3.5.7 TREATMENT WITH PARP INHIBITORS

Stable VC8 cell lines were tested for their survival in response to PARP inhibitor Veliparib (ABT-888) purchased from Selleck Chemicals that inhibits PARP-1 and PARP-2. Cells were seeded in 96-well plates. The next day, cells were treated with 0 µM, 10 µM, 50 µM or 100 µM ABT-888 for 24 hours in selection medium. On day three, the inhibitor was removed and cells could recover for 72 hours. 0.5 mg/ml MTT solution was added to the wells and incubated for 4 hours at 37C before replacing the media by DMSO. After 5 minutes of incubation at room temperature, the absorbance was measured in a plate reader at 570 nm.

3.5.8 IMMUNOFLUORESCENCE MICROSCOPY WITH VC8 STABLE CELL LINES

The day before VC8 stable cells ($0.8x10^5$ to $1x10^5$) were seeded in 24-well plates on coverslips for attachment on the glass. The next day, the media was removed and coverslips were washed with 1x PBS and then washed in CSK buffer for pre-extraction (10 mM PIPES pH 7.0, 100 mM NaCl, 300 mM Sucrose, 3 mM $MgCl_2$, 1x Protease Inhibitor cocktail (EDTA-free, Roche). Cells were incubated for 5 minutes at room temperature in CSK buffer (100 mM NaCl, 300 mM Sucrose, 3 mM $MgCl_2$, 10 mM PIPES (pH 6.8) plus 0.5% Triton X-100 and washed again in CSK buffer and 1x PBS. Cells were then fixed with 3% paraformaldehyde in 1x PBS for 20 minutes at room temperature. After washing, cells were permeabilized with 1x PBS + 0.5% Triton X-100 on ice for 10 minutes and washed. Blocking was done in 5% BSA in PBS for 1 hour at room temperature. The primary antibody (1:500 Centrin-2 antibody for centrosome amplification assay; 1:500 alpha-tubulin antibody for visualization of bi-and multinucleated cells) was added in 5% BSA and incubated overnight. After washing in 1x PBS, secondary antibodies, coupled to fluorophores (Alexa555 anti-mouse for tubulin and Alexa555 anti-rabbit for Centrin-2 at 1:750) were incubated for 1 hour at room termperature in the dark. ddH_2O was added to the well and after drying, the coverslip was mounted on mounting media (ProLong® Gold antifade reagent with DAPI). Immunofluorescence microscopy was performed in a 3D deconvolution microscope (Leica).

3.5.9 TIME LAPSE MICROSCOPY

For time-lapse experiments, stable cell lines were seeded on 12-well plates in duplicates in the morning and treated with Thymidine (2 mM) for 16h. After two washes, fresh media was added and cells grew for 8h, before adding thymidine for a second time (2 mM) to block cells in S phase. After 16h, the media was removed and

cells were washed two times before adding normal media and let them grow for 6 more hours. Time-lapse microscopy was performed during 17h and pictures of four different positions were taken every 5 minutes of each well (two wells per clone) using a 4-5D video microscope (Nikon). The data was analyzed using Image J and GraphPad Prism for quantification.

3.5.10 FRACTIONATION EXPERIMENTS

HEK293 cells were grown to 70% confluency and transfected with 10 µg of the respective GFP-MBP plasmid DNA using TurboFect transfection reagent (Invitrogen). After 30 hours of expression, cells were harvested in 1x PBS (500 xg, 5 minutes at 4°C).

For fractionation experiments with HEK293 cells plus MMC treatment, transfected cells were incubated with 1 µM MMC (Sigma-Aldrich) for 1 hour at 37°C and then collected in 1x PBS (500 xg 5 minutes at 4°C).

Cells were resuspended in BAD-T buffer (50 µl buffer per 1^6 cells): 10 mM HEPES pH 7.5, 10 mM KCl, 10% glycerol, 1.5 mM $MgCl_2$, 0.34 M Saccarose, 0.1% Triton X-100 and incubated for 20 minutes on ice. After centrifugation at 1300 xg for 5 minutes at 4°C, the supernatant was taken off and stored on ice (cytoplasmic fraction). The nuclear pellet was washed with 2 ml BAD buffer (10 mM Hepes pH 7.5, 10 mM KCl, 10% glycerol, 1.5 mM $MgCl_2$, 0.34 M Sucrose) and spun down at 1300 xg for 5 minutes at 4°C. The nuclear pellet was resuspended in Lysis Buffer H (50 mM Hepes pH 7.5, 250 mM NaCl, 5 mM EDTA, 1% Igepal-NP40, 1 mM DTT, 1mM PMSF and 1x Protease Inhibitor Cocktail (EDTA-free, Roche) and lysed for 20 minutes on a rotating wheel at 4°C. After centrifugation at 10.000 xg for 20 minutes at 4°C, the supernatant was collected (nuclear fraction). The remaining pellet was resuspended in 500 µl no-salt buffer (3 mM EDTA, 0.2 mM EGTA, 1 mM DTT, 0.1 mM PMSF, 1x Protease Inhibitor Cocktail (EDTA-free, Roche)) and incubated on ice for 30 minutes with occasional vortexing. Suspension was spun down at 1780 xg at 4°C and the pellet was washed with no-salt buffer, centrifuged again and the pellet was then resuspended in 1x SDS loading buffer, heated for 3 minutes at 95°C and sonicated for 15 seconds (6 microns peak to peak) before loading on a gel. The protein content of cytoplasmic and nuclear fractions was determined by Bio-Rad protein assay for equal loading. Cytoplasmic, nuclear and chromatin fractions equally in protein concentrations were loaded on a 4-15% SDS gel and ran at 130 volts for 1hour 30 minutes in 1x SDS running buffer. The gel was then transferred to a nitrocellulose membrane as described for Western Blotting. Proteins were visualized with the appropriate antibody, histone H3 antibody

was used as a control for correct fractionation of the chromatin fraction, tubulin to test for the cytoplasmic fraction.

CHAPTER 4

4.1 STUDY OF THE INTERACTION BETWEEN BRCA2 AND THE MEIOTIC RECOMBINASE DMC1

DMC1 is the meiotic counterpart of RAD51 as it forms nucleoprotein filaments for homology search and strand invasion (D-loop formation) in meiosis I in a similar fashion. As described in Chapter 1.10, the physical interaction between DMC1 and BRCA2 has been demonstrated before however, the functional significance of this interaction remained unclear. In humans, a motif conserved in mammalian species was reported to be responsible for the binding [70,101,181,183,184] . However, in mice a mutation predicted to disrupt the conserved motif had no impact on meiotic recombination [187]. Because of the structural conservation of RAD51 and DMC1, especially at the interface where the BRC repeats bind to RAD51, [120,146] we set out to investigate if the BRC repeats can interact with DMC1 and if so, whether or not BRCA2 acts as a mediator on meiotic recombination, analogous to its function in mitotic recombination.

First, we examined the binding affinities of DMC1 to the BRC repeats of BRCA2 using purified protein and peptides, respectively. Almost all BRC repeats bound DMC1 although the affinities where, in some cases, much lower than for RAD51. The BRC repeat interact with RAD51 via 2 modules (4.2 Figure 1A) [146]. Surprisingly, a BRC4 repeat mutated in module I, necessary for the interaction with RAD51, could still bind DMC1 even at higher affinity than BRC4, indicating that the BRC repeats bind DMC1 via a different motif than RAD51 (4.2, Figure 1 B, C).

To find out the functional relevance of this interaction we next determined whether the BRC repeats could stimulate DMC1 recombination function. Juan Martinez (postdoc in the lab) performed a joint-molecule assay, and found that the individual BRC repeats promote joint molecule (D-loop) formation by DMC1 (4.2, Figure 2).

In RAD51, two classes of BRC repeats, class I (BRC 1-4) and class II (BRC5-8), promote RAD51 filament formation and DNA strand exchange. On the one hand, class I limits RAD51 ATPase activity to stabilize the ssDNA-RAD51 filament and blocks dsDNA binding for the promotion of strand exchange activity. On the other, class II further supports the filament growth by facilitating binding and stabilizing already formed RAD51 filaments on ssDNA [124]. Thus, to find out the mechanism behind the stimulation of D-loop formation observed we tested the ssDNA binding of DMC1 in the presence of each BRC repeats. All BRC repeats promoted the ssDNA binding except BRC4 that, inhibited D-loop formation, In addition, none of the BRC repeats except BRC4 inhibited assembly on dsDNA (4.2, Figure 5), discarding this as a mechanism for

the stimulation of D-loop formation. These results suggest that the stimulatory action on DMC1-ssDNA complex stabilization is the basis for the enhanced joint molecule formation observed. The BRC repeats only marginally affected the ssDNA-dependent ATP activity of DMC1 (4.2, Figure 4 & S3) distinguishing the mechanism of stimulation from that of RAD51.

To confirm these results with the full-length protein we purified BRCA2 as described in chapter 2 and analyzed the effect on the ATPase, joint molecule formation and DNA strand exchange. BRCA2 did not affect the ssDNA dependent ATPase of DMC1 confirming the results with the BRC repeats and in contrast to the effect on RAD51 [70] . Juan Martinez performed the joint molecule assay with DMC1 and increasing concentrations of BRCA2 and found that, indeed, BRCA2 stimulates DMC1 D-loop formation. In addition, in collaboration with the group of Steve Kowalczykowski, we showed that BRCA2 was also able to alleviate the kinetic barrier posed by RPA on the ssDNA and allowed DMC1 DNA strand exchange in vitro, a feature that defines a mediator of recombination (4.2, Figure 6&7).

We thus identified BRCA2 as a mediator of meiotic recombination. The detailed experimental setup, results and discussion can be found in the published version of this work in the following section.

PNAS

BRCA2 regulates DMC1-mediated recombination through the BRC repeats

Juan S. Martinez[a,b,1], Catharina von Nicolai[a,b,1], Taeho Kim[c], Åsa Ehlén[a,b], Alexander V. Mazin[d], Stephen C. Kowalczykowski[c,2], and Aura Carreira[a,b,2]

[a]Genotoxic Stress and Cancer Unit, Institut Curie, Research Center, Orsay 91405, France; [b]CNRS UMR3348, Centre Universitaire, Orsay 91405, France; [c]Departments of Microbiology and Molecular Genetics and of Molecular and Cellular Biology, University of California, Davis, CA 95616-8665; and [d]Department of Biochemistry and Molecular Biology, Drexel University College of Medicine, Philadelphia, PA 19102-1192

Contributed by Stephen C. Kowalczykowski, February 2, 2016 (sent for review October 5, 2014; reviewed by Douglas K. Bishop and William K. Holloman)

In somatic cells, BRCA2 is needed for RAD51-mediated homologous recombination. The meiosis-specific DNA strand exchange protein, DMC1, promotes the formation of DNA strand invasion products (joint molecules) between homologous molecules in a fashion similar to RAD51. BRCA2 interacts directly with both human RAD51 and DMC1; in the case of RAD51, this interaction results in stimulation of RAD51-promoted DNA strand exchange. However, for DMC1, little is known regarding the basis and functional consequences of its interaction with BRCA2. Here we report that human DMC1 interacts directly with each of the BRC repeats of BRCA2, albeit most tightly with repeats 1–3 and 6–8. However, BRC1–3 bind with higher affinity to RAD51 than to DMC1, whereas BRC6–8 bind with higher affinity to DMC1, providing potential spatial organization to nascent filament formation. With the exception of BRC4, each BRC repeat stimulates joint molecule formation by DMC1. The basis for this stimulation is an enhancement of DMC1–ssDNA complex formation by the stimulatory BRC repeats. Lastly, we demonstrate that full-length BRCA2 protein stimulates DMC1-mediated DNA strand exchange between RPA–ssDNA complexes and duplex DNA, thus identifying BRCA2 as a mediator of DMC1 recombination function. Collectively, our results suggest unique and specialized functions for the BRC motifs of BRCA2 in promoting homologous recombination in meiotic and mitotic cells.

BRCA2 | DMC1 | RAD51 | mediator | meiosis

The breast cancer susceptibility protein 2, BRCA2, regulates RAD51-mediated homologous recombination (HR) (1–3). Both RAD51, a DNA strand exchange protein, and its meiotic counterpart, DMC1 (disrupted meiotic cDNA 1 or DNA meiotic recombinase 1), promote HR through the formation of a nucleoprotein filament on ssDNA (4). This filament finds and invades a homologous template, resulting in a DNA strand invasion product called a joint molecule or a displacement-loop (D-loop). The joint molecule provides a primer template for the new DNA synthesis required to repair the DNA double strand break (DSB).

The first evidence implicating BRCA2 in meiosis came from studies in *Ustilago maydis*, where strains lacking the BRCA2 ortholog, Brh2, resulted in absence of meiotic products (5). Shortly thereafter, mouse BRCA2 was inferred to coordinate the activities of RAD51 and DMC1 (6). The first direct interaction between BRCA2 and DMC1 was observed in plants (7) and later in humans (8). In the plant, *Arabidopsis thaliana*, the interaction between Brca2 and Dmc1 was mapped to the BRC repeats (9), a highly conserved motif comprising a sequence of ∼35 amino acids that is present at least once in all BRCA2-like proteins (10). In humans, BRCA2 contains eight BRC repeats that bind with different affinities to RAD51, and they segregate into two functional classes (11). Within a BRC repeat, two motifs that bind RAD51 have been identified: one comprising the consensus sequence FxxA that mimics the oligomerization interface (12) and contacts the catalytic domain of RAD51; the other binding module comprises the alpha-helical region of the BRC repeat, contains the consensus sequence LFDE, and binds to RAD51 through a different hydrophobic pocket (13).

Importantly, loss of Brca2 in plants causes chromosomal aberrations during meiosis (14). In humans, GST-pull down assays using peptide fragments of BRCA2 mapped a unique DMC1 interacting site to residues 2386–2411 (8). However, in mouse, mutation of a key residue (Phe-2406) within this site, which had been shown to disrupt the interaction of BRCA2 with DMC1 by peptide array analysis, had no effect in meiosis (15), suggesting that another site or sites in BRCA2 provide the functions needed during meiosis in this organism (6). A direct physical interaction was indeed established for purified full-length human BRCA2 and DMC1 (2), but the functional relevance of this interaction was not elaborated.

We have previously shown that the BRC repeats of BRCA2 modulate the DNA binding selectivity of RAD51 to stimulate the assembly on ssDNA by inhibiting its ATP hydrolysis and preventing its association with dsDNA (2, 11, 16); as a result, BRCA2 catalyzes the recombination activity of RAD51 (17).

A comprehensive analysis of aligned sequences of RAD51 orthologs and human RAD51 paralogues suggested that most eukaryotic RAD51 proteins, including DMC1, could interact with the BRC repeats, at least in principle (10). Here we investigate whether and how BRCA2 modulates DMC1-mediated recombination.

Results

The BRC Repeats of BRCA2 Bind DMC1. DMC1 forms a helical structure on ssDNA similar to that of RAD51 (18). A superposition

Significance

The function of BRCA2 (breast cancer susceptibility protein 2) in mitotic homologous recombination is well established; this role for BRCA2 includes promotion of RAD51 recombination function by regulating its assembly on DNA. However, loss of BRCA2 also leads to aberrant meiosis. Even though interaction of BRCA2 and the meiotic counterpart of RAD51, DMC1 (DNA meiotic recombinase 1), was reported, the specific role of BRCA2 in meiotic recombination is unknown. We demonstrate that the BRC repeats interact with DMC1 to stimulate both association with ssDNA and homologous DNA pairing. Furthermore, we demonstrate strong stimulation by BRCA2 of DNA strand exchange promoted by DMC1, even using ssDNA complexed with RPA (replication protein-A). These findings define BRCA2 as a mediator of meiotic recombination.

Author contributions: A.V.M., S.C.K., and A.C. designed research; J.S.M., C.v.N., T.K., Å.E., and A.C. performed research; J.S.M., C.v.N., Å.E., A.V.M., and A.C. contributed new reagents/analytic tools; J.S.M., C.v.N., T.K., Å.E., A.V.M., S.C.K., and A.C. analyzed data; and A.V.M., S.C.K., and A.C. wrote the paper.

Reviewers: D.K.B., University of Chicago; and W.K.H., Cornell University Weill Medical College.

The authors declare no conflict of interest.

Freely available online through the PNAS open access option.

[1]J.S.M. and C.v.N. contributed equally to this work.

[2]To whom correspondence may be addressed. Email: sckowalczykowski@ucdavis.edu or aura.carreira@curie.fr.

This article contains supporting information online at www.pnas.org/lookup/suppl/doi:10.1073/pnas.1601691113/-/DCSupplemental.

BIOCHEMISTRY

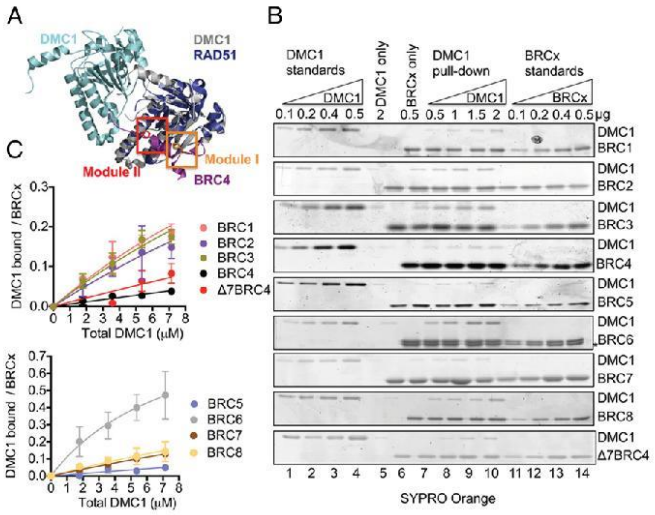

Fig. 1. The BRC repeats bind to DMC1 in vitro. (*A*) Structural conservation of DMC1 and RAD51. Superposition of DMC1 (1V5W) onto RAD51-BRC4 interface (1N0W) showing the structural conservation of DMC1 and RAD51 at the subunit interface which is shown in the complex with the BRC4 repeat (purple). The conserved Phe of the FxxA motif (module I) and Phe of LFDE motif (module II) are highlighted in orange and red, respectively (sticks). (*B*) SDS/PAGE gel showing a pull down experiment with each GST-tagged BRC peptide or BRC4 mutant (Δ7BRC4) (0.4 µM) and increasing concentrations (0.3, 0.6, 1, 1.3 µM) of DMC1. The asterisk denotes contaminating GST. (*C*) The data from *B* was fitted to a single-site binding curve. Error bars represent the SD for three or more independent experiments.

of DMC1 on the RAD51–BRC4 structure reveals that the critical residues involved in RAD51 oligomerization and in BRC-binding are also conserved in DMC1 (Fig. 1*A*).

To test whether the BRC repeats bind DMC1, we used purified His-tagged DMC1 (hereafter referred to as DMC1) and GST-tagged BRC1, -2, -3, -4, -5, -6, -7, and -8. In addition, we examined a BRC4 mutant, Δ7BRC4, which lacks seven conserved amino acid residues (1524-FHTASGK-1530) that are necessary to bind RAD51 (16) (Fig. 1*A*, module I). Each GST-BRC fusion was immobilized on glutathione beads (Fig. 1*B*, lane 6) and was tested individually for interaction with DMC1 (Fig. 1*B*, lanes 7–10). Using known concentrations of purified DMC1 (Fig. 1*B*, lanes 1–4) and each GST–BRC fusion (Fig. 1*B*, lanes 11–14) as a calibration standard, the binding of increasing concentrations of DMC1 to a fixed concentration of BRC peptide was quantified to generate binding curves (Fig. 1*C*). The control lane with DMC1 alone was subtracted as background for the calculations (Fig. 1*B*, lane 5). All of the BRC repeats and Δ7BRC4 showed binding to DMC1 to different extents. The strongest affinity for DMC1 was manifest by BRC6 (apparent K_d = 8 ± 0.8 µM; Table S1), with significant affinities also manifest by BRC1, -2, -3, -7, and -8.

Unexpectedly, DMC1 displayed one of the lowest affinities for BRC4 (apparent K_d estimated to be ~172 ± 14 µM) (Fig. 1*C* and Table S1), whereas our previous studies with RAD51 revealed this interaction to be one of the strongest for RAD51. Moreover, the mutant Δ7BRC4, which is unable to bind RAD51 (16), showed a slightly higher (approximately twofold) affinity for DMC1 relative to BRC4 (Table S1 and Fig. 1*C*). These results suggest that the interaction with DMC1 involves a C-terminal motif of the BRC repeats (Fig. 1*A*, module II) different from the one essential for binding to RAD51 and its oligomerization (Fig. 1*A*, module I).

Most BRC Repeats Stimulate DMC1-Mediated Joint Molecule Formation. To test the relevance of the BRC–DMC1 interaction with respect to the recombination activity of DMC1, we analyzed the effect of each BRC repeat on DMC1-mediated joint molecule formation in vitro. We used a saturating concentration of DMC1 (75 nM) relative to the ssDNA (225 nM nt) (19) and a molar excess of DMC1–ssDNA filaments (ssDNA at 2.5 nM molecule) over plasmid scDNA (0.8 nM molecule). Except for BRC4, the other BRC repeats increased joint molecule formation by DMC1 to some extent, up to as much as ~threefold (Fig. 2 *A* and *B*). The stimulation generally began to plateau at between 1 and 2.5 µM, depending on the BRC repeat (Fig. 2*B* and Fig. S1 *A* and *B*). BRC1, -2, -3, -6, and -8 showed the highest stimulation, whereas BRC4 inhibited the reaction, as did BRC6 at higher concentrations; the inhibition by BRC6 is more evident at higher BRC6 concentrations (Fig. S1 *A* and *B*). Compared with BRC4, the Δ7BRC4 mutant stimulated joint molecule formation approximately threefold, showing that the deleted FHTASGK sequence of module I is responsible for the inhibition (Fig. 2 *A* and *B*).

The Same BRC Repeats That Stimulate DMC1-Mediated Joint Molecule Formation Also Stimulate Association of DMC1 with ssDNA. To obtain mechanistic insight into the stimulatory effect exerted by the BRC repeats in joint molecule formation, we tested whether the repeats could stabilize DMC1–ssDNA complexes, as it is the case for RAD51 (11, 16). An electrophoretic mobility shift assay (EMSA) was used with the same ssDNA oligonucleotide used in

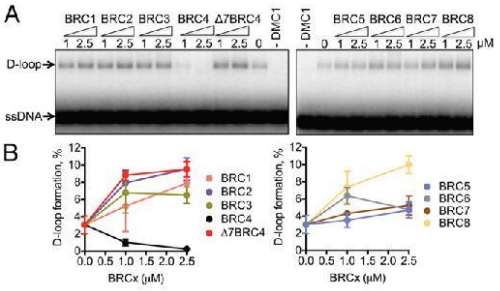

Fig. 2. The BRC repeats enhance joint molecule formation by DMC1. (*A*) DMC1 (75 nM) and the indicated concentrations of each BRC peptide, Δ7BRC4, were preincubated with a 5′-end ^{32}P-labeled 90-mer ssDNA [oAC203, 0.2 µM nt; (2.4 nM, molecule)] for 10 min at 37 °C and the supercoiled DNA (scDNA), (pUC19, 0.8 nM, molecule) was added last to start the reaction. The mix was incubated at 37 °C for 30 min and the products were resolved on a 1% agarose gel. (*B*) Quantification of joint molecule formation from *A*. Error bars, s.d. (n = 3).

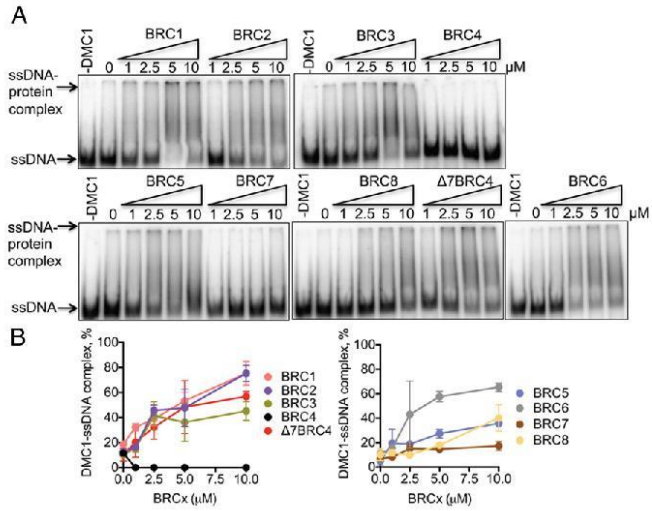

Fig. 3. BRC1, -2, -3, -5, -6, -8, and Δ7BRC4 enhance DMC1 assembly on ssDNA. (*A*) DMC1 (25 nM) was incubated with the individual BRC repeats for 15 min at 37 °C before addition of 5′-end ^{32}P-labeled ssDNA (oAC203, 0.2 μM nt) and further incubation for 1 h. The complexes were analyzed by PAGE and visualized by autoradiography. (*B*) Quantification of the EMSA from *A*. Error bars, s.d. ($n = 3$).

the D-loop reactions and the same assay conditions to determine whether the BRC repeats could stimulate DMC1 assembly on ssDNA. DMC1 (25 nM) was incubated with each of the individual BRC repeats, followed by addition of ssDNA. We note, as previously reported (11, 16), that none of the BRC repeats alone bind DNA (Fig. S2). We found that BRC1, -2, -3, -5, -6, -8, and Δ7BRC4 stimulated formation of a slower migrating species by up to sixfold, suggesting enhancement or stabilization of the DMC1–ssDNA complex by these repeats. BRC7 showed a marginal effect, but BRC4 clearly inhibited ssDNA binding by DMC1 (Fig. 3), providing an explanation for its inhibition of joint molecule formation seen in Fig. 2. The stimulation of ssDNA binding correlated exactly with stimulation of joint molecule formation, suggesting that enhancement of DMC1–ssDNA complexes formation is at least one basis for joint molecule stimulation. To verify that the BRC repeats also stimulated joint molecule formation at the lower DMC1 concentration used in the EMSA experiments, D-loop assays were conducted at 25 nM DMC1; at this concentration, the yields were low, but consistent behavior was detected (Fig. S1 *C* and *D*).

Most BRC Repeats Do Not Affect DNA-Dependent ATP Hydrolysis by DMC1. We previously showed that the BRC repeats segregate in two groups, based on the mechanism by which they stabilize RAD51–ssDNA complexes: BRC1–4 acts by decreasing the ssDNA-dependent ATPase activity of RAD51, a behavior that is also manifest by full-length BRCA2 (2, 11, 16). Consequently, we tested the effect of the BRC repeats on the ATPase activity of DMC1. None of the BRC repeats possess ATPase activity (Fig. S3). The ssDNA-dependent ATPase activity of DMC1 was examined in the presence of increasing concentrations of the BRC peptides using the conditions of the joint molecule formation assays. BRC4 reduced ssDNA-dependent ATP hydrolysis by DMC1, consistent with its reduction of ssDNA binding by DMC1. BRC6 and Δ7BRC4 stimulated the reaction up to 1.8-fold (Fig. 4 *A* and *B*); however, neither BRC1, -2, -3, -5, -7, nor -8 (Fig. 4 *A* and *B*) detectably altered the ATPase activity of DMC1.

Most of the BRC Repeats Do Not Alter Association of DMC1 with dsDNA. Because BRC1–4 and BRCA2 limit nucleation of RAD51 onto dsDNA, favoring its binding to ssDNA (2, 11, 16), we tested the effect of the BRC repeats on the formation of dsDNA–DMC1 complexes using EMSA as above. In the presence of ATP, Mg^{+2} and Ca^{+2}, ~75% of a short duplex DNA, dT_{40}•dA_{40}, was bound by 0.6 μM DMC1 (Fig. 5). BRC4 reduced the DMC1-dsDNA complexes by sevenfold, in a concentration dependent manner (Fig. 5 *A* and *B*). Under the same conditions, none of the other BRC peptides or the Δ7BRC4 mutant significantly affected DMC1–dsDNA complex formation. The increased binding of DMC1 to dsDNA (Fig. 5*B*) compared with ssDNA (Fig. 3*B*) is due to the higher protein concentration (600 nM) used in the dsDNA binding experiments relative to the ssDNA binding experiments (25 nM DMC1). To detect a possible stimulation of dsDNA binding by the BRC repeats, we decreased DMC1 concentration to 300 nM, at which only ~5% of dsDNA was bound by DMC1 (Fig. 5*C* and Fig. S4), whereupon only BRC5 and BRC6 modestly stimulated binding of DMC1 (Fig. 5C).

Purified Full-Length BRCA2 Stimulates DMC1-Mediated Joint Molecule Formation. Next, to determine whether our observed stimulation of DMC1-mediated joint molecule formation by the BRC repeats is

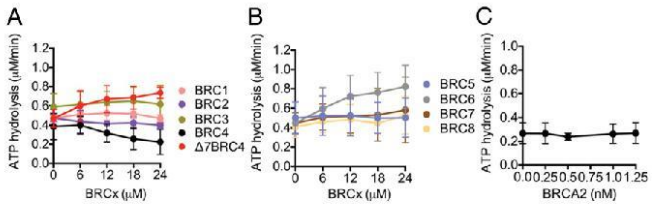

Fig. 4. Only BRC4 and BRC6, but not BRCA2, marginally alter the ssDNA-dependent ATPase activity of DMC1. DMC1 (3 μM) was incubated with increasing concentrations of GST-BRC peptide or BRCA2, as indicated, before addition of 90-mer ssDNA [oAC203, 9 μM (nt)] and was further incubated for 1 h in the presence of 1 mM $MgCl_2$ and 2 mM ATP. (*A* and *B*) Quantification of ATP hydrolysis by DMC1 as a function of BRC peptide. (*C*) Quantification of ATP hydrolysis by DMC1 as a function of BRCA2 concentration. (Error bars, SD; $n > 3$.)

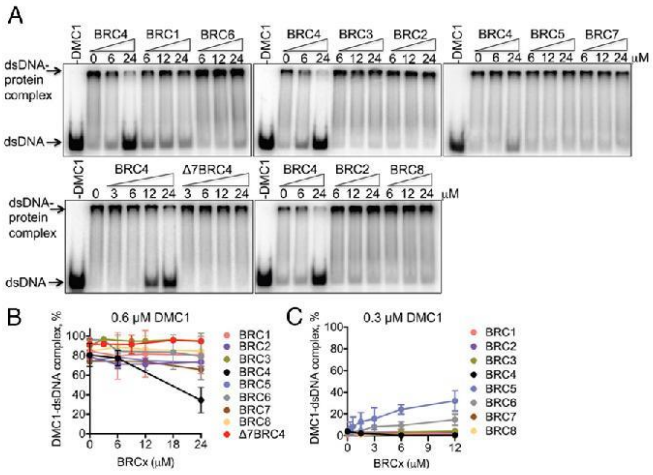

Fig. 5. Only BRC4 reduces DMC1 assembly on dsDNA. (*A*) dsDNA binding assay (EMSA) where DMC1 (0.6 μM) was mixed with each BRC repeat before addition of 5′-end ^{32}P-labeled dsDNA [dT_{40}•dA_{40}, 3 μM (bp)] and further incubated for 1 h. The complexes were analyzed by PAGE and visualized by autoradiography. (*B*) Quantification of *A*. (*C*) Quantification of EMSA as in *A* but with 0.3 μM DMC1. (Error bars, SD; $n > 3$.)

also manifest by full-length BRCA2 protein; we purified a GFP-MBP-tagged BRCA2 (Fig. S5*A*) using a protocol that was modified slightly from the one we described previously for 2xMBP-tagged BRCA2 (12) (hereafter referred to as BRCA2). We tested the effect of BRCA2 on DMC1-mediated joint molecule formation at the same conditions that we had used with the BRC repeats, i.e., a saturating concentration of DMC1 (75 nM) relative to the ssDNA (225 nM nt) and a molar excess of DMC1–ssDNA filaments (ssDNA at 2.5 nM molecule) over plasmid scDNA (0.8 nM molecule). BRCA2 stimulated joint molecule formation by up to 2.8-fold at the maximum attainable concentration of (10 nM), whereas BRCA2 alone did not promote joint molecule formation (Fig. 6). The effect of BRCA2 on ATP hydrolysis by DMC1 was also examined (Fig. 4C); in contrast to what had been observed with RAD51 (2), but in agreement with our observations on the BRC repeats (Fig. 4 *A* and *B*), BRCA2 did not alter the ATPase activity of DMC1.

BRCA2 Stimulates the DNA Strand Exchange by DMC1, Overcoming the Inhibition Posed by RPA. Both in meiosis and mitosis, after resection of a DSB, RPA binds rapidly to the newly generated ssDNA (4). Subsequently, displacement of the RPA by RAD51 is slow, unless catalyzed by a mediator protein (20). This particular ability to counteract the inhibitory effect of RPA to permit formation of a nucleoprotein filament defines a mediator protein, which, in the case of RAD51, is BRCA2 (2, 3). Consequently, we next tested whether BRCA2 could stimulate DNA strand exchange by DMC1, using ssDNA that was saturated with RPA (Fig. 7*A*). For this experiment, a more concentrated preparation of BRCA2 was needed; hence, the previously published 2XMBP-BRCA2 was used (2). RPA was preincubated with the ssDNA before addition of DMC1 or RAD51 and BRCA2, and then complementary dsDNA was added to initiate DNA strand exchange. As expected, RPA inhibited the RAD51-mediated DNA strand exchange (Fig. 7*B*, compare lanes 2 and 3, and Fig. 7*C*); BRCA2 overcame this inhibition and stimulated RAD51 by ~6.5-fold (Fig. 7*B*, lanes 4–6 and Fig. 7*C*). RPA also inhibited DMC1-dependent DNA strand exchange (Fig. 7*B*, compare lanes 8 and 9, and Fig. 7*C*). BRCA2 overcame this inhibition, stimulating DNA strand exchange in a BRCA2 concentration-dependent manner to a nearly comparable yield of product (Fig. 7*B*, lanes 10–12, and Fig. 7*C*). These results demonstrate that BRCA2 is a mediator protein for DMC1-promoted recombination.

Discussion

RAD51 and DMC1 share similar structure (Fig. 1*A*) and biochemical function (4, 18). Because BRCA2 has been implicated in meiosis in multiple organisms through direct protein-protein interaction (5, 7–9), we set out to investigate the functional relevance of BRCA2–DMC1 binding and whether or not the BRC repeats, interaction sites for RAD51, bind DMC1. Our results show that all BRC repeats bind DMC1 to some extent (Fig. 1), although with affinities that in some cases are 10-fold weaker than for RAD51 (Table S1), in agreement with a previous report (8).

To investigate whether the interaction observed with the BRC repeats had functional significance, we tested both the BRC repeats and full-length BRCA2 on joint molecule formation mediated by DMC1. Remarkably, all BRC peptides except BRC4 stimulated DMC1-mediated joint molecule formation to a different extent, up to threefold (Fig. 2). In agreement with these results, BRCA2 stimulated DMC1-mediated joint molecule formation by up to 2.8-fold (Fig. 6). Interestingly, although the magnitude of joint molecule stimulation achieved by using BRCA2 was similar to that of the BRC repeats, the concentration of BRCA2 required for this

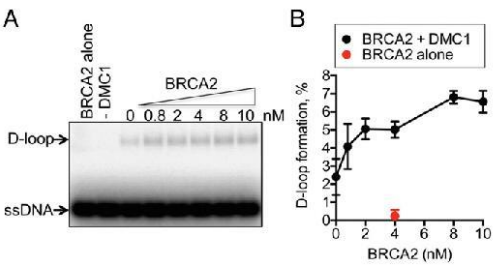

Fig. 6. Purified BRCA2 stimulates DMC1-dependent DNA pairing. (*A*) BRCA2 alone (0.5 nM), DMC1 (75 nM) alone, or DMC1 plus the indicated concentrations of GFP-MBP-BRCA2 were preincubated with the 5′-end ^{32}P-labeled 90-mer ssDNA (oAC203, 0.2 μM nt; 2.4 nM molecule) for 10 min at 37 °C, (left to right, respectively); scDNA (pUC19, 0.8 nM molecule) was added last to start the reaction. The mix was incubated at 37 °C for 30 min and the products resolved on 1% agarose gel. (*B*) Quantification of D-loop formation from *A*. (Error bars, SD; $n = 3$.)

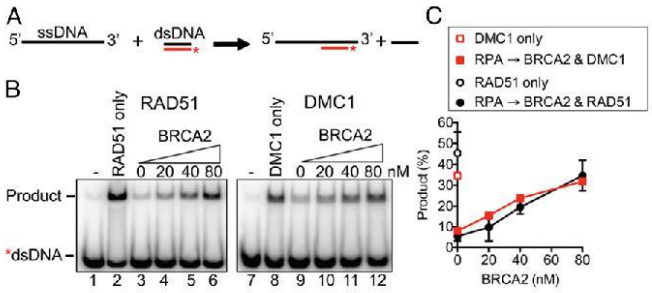

Fig. 7. BRCA2 stimulates DMC1-promoted DNA strand exchange. (*A*) Scheme of the DNA strand exchange reaction. (*B*) Gel showing a DNA strand exchange reaction where RPA (25 nM) was first incubated with an ssDNA substrate (167-mer, 4 nM molecule) for 5 min at 37 °C. Then, RAD51 or DMC1 (0.22 μM) and increasing concentrations of 2xMBP-BRCA2 (20–80 nM) were added and incubated for 5 min at 37 °C. A 5′-end ^{32}P-labeled 40 bp duplex DNA (4 nM molecule) complementary to the ssDNA was added last, and the reaction was further incubated for 30 min at 37 °C. (*C*) Quantification of the DNA strand exchange product formation shown in *B*. (Error bars, range; $n = 2$.)

stimulation was 250-fold lower, suggesting cooperation between the DMC1-interacting sites (BRC repeats) and the ssDNA binding domain of BRCA2; a similar stimulatory differential was seen for RAD51 (2, 11). Most importantly, we also established that BRCA2 stimulated DNA strand exchange by DMC1 involving RPA–ssDNA complexes, qualifying BRCA2 as a bona fide mediator of meiotic recombination (Fig. 7 *B* and *C*).

We previously reported that the BRC repeats of BRCA2 can be categorized in two classes (11): class I (BRC1, -2, -3, -4) stimulates assembly of RAD51 onto ssDNA by limiting its ATPase activity, reduces dsDNA-RAD51 complex formation, and stimulates DNA strand exchange; class II (BRC5, -6, -7, -8) stimulates assembly of RAD51-ssDNA filaments to a greater extent than class I without altering the ATPase activity but does not affect the dsDNA binding or the DNA strand exchange activity of RAD51. In the case of DMC1, we discovered that all of the BRC repeats that stimulated joint molecule formation also stimulated DMC1–ssDNA assembly (Fig. 4). Whereas BRC4, which decreased the yield of joint molecules, inhibited DMC1–ssDNA complex formation, implying that stabilization of DMC1–ssDNA filaments is the mechanism underlying stimulation of joint molecule formation. As with class II BRC repeats in the case of RAD51, here we observe that most of the BRC repeats stimulate the ssDNA binding activity of DMC1 without altering its ATPase activity (Fig. 4) but, in contrast to RAD51, this effect correlates with enhancement of joint molecule formation by DMC1, suggesting a different mechanism of action. For RAD51, BRC1–4 impeded filament formation on dsDNA, but for DMC1, only BRC4 decreased complex formation on dsDNA (Fig. 5*B*). However, disruption of DMC1 binding to dsDNA by BRC4 does not represent a stimulatory component of joint molecule formation, because BRC4 reduces joint molecule formation. Therefore, we propose that the major mechanism by which the BRC repeats, and by inference BRCA2, stimulate DMC1 recombination activity is likely a stabilization of the DMC1–ssDNA complex.

One unexpected result from this study is that BRC6 shows the strongest affinity for DMC1 (unlike for RAD51) and that the Δ7BRC4 mutant, which is unable to bind RAD51 (11), exhibits increased affinity for DMC1 relative to BRC4, and readily stabilizes the DMC1–ssDNA complex and stimulates joint molecule formation. This result indicates that the RAD51 oligomerization interface (Fig. 1*A*, module I), which is mimicked by BRC4 to bind RAD51 (12, 13), is dispensable for interaction with DMC1. Furthermore, it is possible that the conserved C-terminal LFDE motif (Fig. 1*A*, module II) of the BRC repeats could be the main site of interaction for DMC1. If so, it is tempting to speculate that in the context of meiosis, BRCA2 could accommodate binding of both DMC1 and RAD51.

The combined facts that a mutation disrupting a previously described site of interaction with DMC1, which mapped outside of the BRC repeat region of BRCA2, does not have a meiotic phenotype in mice (15) and the results reported here lead us to propose that the BRC repeats are directly involved in regulating the homologous recombination function of DMC1.

Work in *Saccharomyces cerevisiae* and *Arabidopsis* has established that Rad51 is needed for Dmc1 filament formation, and one model posits that Rad51 serves to initiate a Dmc1 filament (4, 21, 22). In our previous work, we showed that BRC1–4 bind with high affinity to free RAD51, enhancing ssDNA assembly and limiting its nucleation on dsDNA, resulting in a stimulation of DNA strand exchange. In contrast, BRC5–8 were shown to not bind free RAD51 but rather to stabilize preexisting filaments on ssDNA without altering the ATPase activity or dsDNA assembly of RAD51 and with no effect on DNA strand exchange (11). Our combined findings establish that free RAD51 binds to BRC1–5 with a 10- to 100-fold higher affinity than DMC1, but that free DMC1 binds to BRC6–8 with an uninhibited affinity because free RAD51 has no measurable affinity for these three BRC repeats. If arranged in a linear fashion in the BRCA2 structure, this arrangement of repeats thereby provides a bipartite sequence for ordering RAD51 and DMC1 monomers within the organization of a nascent filament. Putting together our previous results and this work in the context of DMC1, we therefore propose a model (Fig. 8) in which BRCA2 would bind free RAD51 through BRC1–5, and free DMC1 through BRC6–8 (Fig. 8*A*). Consequently, through its interaction with BRC repeats 1–5 and stabilized by the local inhibition of ATP hydrolysis, a nascent RAD51 homofilament would constitute a nucleus on ssDNA for a

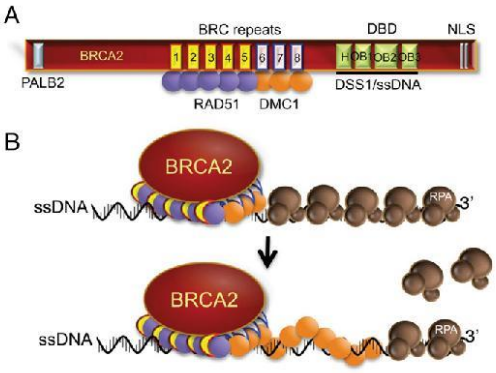

Fig. 8. Proposed model for BRCA2 function in meiotic recombination. (*A*) Schematic of BRCA2 primary structure showing the BRC repeats that would preferentially bind to free RAD51 (BRC1–5) or to free DMC1 (BRC6–8). (*B*) Hypothetical scheme showing BRCA2 binding ssDNA, displacing RPA, and delivering a stable nucleus of RAD51 and DMC1 to the ssDNA. The DMC1 nucleus enables growth of the nascent DMC1 filament away from the BRCA2 heteronucleus and concomitant displacement of RPA.

BIOCHEMISTRY

DMC1 homofilament assembly; up to three monomers of DMC1 would bind to BRCA2 adjacent to the RAD51 filament. BRCA2 would then deliver this nascent heterofilament to ssDNA, displacing RPA in the process of binding and enhancing DMC1 assembly on ssDNA. In principle, the DMC1 filament could grow from the DMC1 side of the heterofilament to form a DMC1 homofilament of sufficient length to promote DNA strand invasion and joint molecule formation (Fig. 8*B*).

Although it remains to be established how the multitude of accessory factors, mediators, and recombination proteins coordinate their activities to promote meiosis, our work identifies BRCA2 as a mediator for DMC1 recombination activity, implicates the BRC motifs in this function, and points to distinct motifs and mechanisms for the BRC repeats in mediating mitotic and meiotic recombination.

Materials and Methods

Protein Expression and Purification. The GST-tagged BRC repeats, the Δ7BRC4 mutant, RAD51, RPA, and 2xMBP-BRCA2 were purified as described (2, 11, 16). The GST-tag was purified as the GST-tagged BRC repeats. Human DMC1 was purified as detailed in *SI Materials and Methods* and manifested the expected biochemical activity (Fig. S6).

Clonogenic Survival Assay. The generation of stable clones with GFP-MBP-BRCA2 construct or the vector containing GFP-MBP tag in *brca2*-deficient hamster cells (VC8) and the clonogenic survival was done as described for 2xMBP-BRCA2 (2).

GST Pull Down Assay. The pull down assays were performed as described for RAD51 (11). Details can be found in *SI Materials and Methods*.

Joint Molecule (D-Loop) Assay. DMC1 protein (75 nM) was mixed with 5′-end ^{32}P-labeled oligonucleotide oAC203 (90-mer oligonucleotide complementary to pUC19), at a saturating concentration of 2.5 nM molecule (225 nM nt) (3:1 ssDNA:DMC1 ratio) or at 25 nM DMC1 and 2.4 nM molecule (200 nM nt) ssDNA (8:1 ssDNA:DMC1) in buffer B [25 mM Tris acetate (pH 7.5), 1 mM $MgCl_2$, 2 mM $CaCl_2$, 0.1 mg/mL BSA, 2 mM ATP, and 1 mM DTT], in the absence or presence of each BRC peptide (0.25–2.5 μM) or BRCA2 (0.8–10 nM), and the mixture was incubated for 10 min at 37 °C. Joint molecule formation was initiated by addition of supercoiled pUC19 dsDNA (scDNA) prepared by detergent lysis at 0.8 nM molecules (when using 75 nM DMC1) or 0.26 nM molecules (when using 25 nM DMC1) and further incubated for 30 min at 37 °C. All reactions were terminated by Proteinase K (Roche) treatment, followed by incubation for 10 min at 37 °C. The samples were analyzed by electrophoresis on a 1% agarose gel in 1× TAE run at 120 V for 1.5 h. Joint molecule yield is expressed as a percentage of the total label concentration and multiplied by 3 to get the yield with respect to the limiting scDNA.

DNA Strand Exchange Assay. The reactions and the generation of substrates were carried out essentially as described (2). Details can be found in *SI Materials and Methods*.

ATP Hydrolysis Assay. The experiments were carried out as described (11), except for the DNA substrate used. Details are found in *SI Materials and Methods*.

EMSA. The procedure was essentially as described (11). Details are found in *SI Materials and Methods*.

Analysis. In all graphs, error bars represent the SD derived from at least three independent experiments and, in some cases, error bars are smaller than the symbol; all analyses were conducted by using GraphPad Prism (version Mac 6.0e).

The structure superposition of DMC1 (1V5W) onto RAD51–BRC4 interface (1N0W) in Fig. 1*A* was generated using by PyMol Molecular Graphics version 1.3.

ACKNOWLEDGMENTS. This work was supported by the ATIP-AVENIR CNRS/INSERM Young Investigator grant, EC-CIG grant, and by Fondation pour la Recherche Médicale (FRM) Grant AJE201101 (to A.C.). J.S.M. was supported by a postdoctoral Fellowship from Fondation de France. C.N. was supported by a PhD Fellowship from Institut Curie and an FRM Fellowship for the 4th year of PhD; Å.E. was supported by Swedish Society for Medical Research. This work was also supported by NIH Grants CA100839 and P30CA056036 and a Basser Innovation Award to A.V.M., and by NIH Grant GM62653 and DOD Grant W81XWH-13-1-0322 (to S.C.K.).

1. Prakash R, Zhang Y, Feng W, Jasin M (2015) Homologous recombination and human health: The roles of BRCA1, BRCA2, and associated proteins. *Cold Spring Harb Perspect Biol* 7(4):a016600.
2. Jensen RB, Carreira A, Kowalczykowski SC (2010) Purified human BRCA2 stimulates RAD51-mediated recombination. *Nature* 467(7316):678–683.
3. Liu J, Doty T, Gibson B, Heyer WD (2010) Human BRCA2 protein promotes RAD51 filament formation on RPA-covered single-stranded DNA. *Nat Struct Mol Biol* 17(10):1260–1262.
4. Brown MS, Bishop DK (2015) DNA strand exchange and RecA homologs in meiosis. *Cold Spring Harb Perspect Biol* 7(1):a016659.
5. Kojic M, Kostrub CF, Buchman AR, Holloman WK (2002) BRCA2 homolog required for proficiency in DNA repair, recombination, and genome stability in Ustilago maydis. *Mol Cell* 10(3):683–691.
6. Sharan SK, et al. (2004) BRCA2 deficiency in mice leads to meiotic impairment and infertility. *Development* 131(1):131–142.
7. Siaud N, et al. (2004) Brca2 is involved in meiosis in Arabidopsis thaliana as suggested by its interaction with Dmc1. *EMBO J* 23(6):1392–1401.
8. Thorslund T, Esashi F, West SC (2007) Interactions between human BRCA2 protein and the meiosis-specific recombinase DMC1. *EMBO J* 26(12):2915–2922.
9. Dray E, Siaud N, Dubois E, Doutriaux MP (2006) Interaction between Arabidopsis Brca2 and its partners Rad51, Dmc1, and Dss1. *Plant Physiol* 140(3):1059–1069.
10. Lo T, Pellegrini L, Venkitaraman AR, Blundell TL (2003) Sequence fingerprints in BRCA2 and RAD51: Implications for DNA repair and cancer. *DNA Repair (Amst)* 2(9):1015–1028.
11. Carreira A, Kowalczykowski SC (2011) Two classes of BRC repeats in BRCA2 promote RAD51 nucleoprotein filament function by distinct mechanisms. *Proc Natl Acad Sci USA* 108(26):10448–10453.
12. Pellegrini L, et al. (2002) Insights into DNA recombination from the structure of a RAD51-BRCA2 complex. *Nature* 420(6913):287–293.
13. Rajendra E, Venkitaraman AR (2010) Two modules in the BRC repeats of BRCA2 mediate structural and functional interactions with the RAD51 recombinase. *Nucleic Acids Res* 38(1):82–96.
14. Seeliger K, Dukowic-Schulze S, Wurz-Wildersinn R, Pacher M, Puchta H (2012) BRCA2 is a mediator of RAD51- and DMC1-facilitated homologous recombination in Arabidopsis thaliana. *New Phytol* 193(2):364–375.
15. Biswas K, et al. (2012) Functional evaluation of BRCA2 variants mapping to the PALB2-binding and C-terminal DNA-binding domains using a mouse ES cell-based assay. *Hum Mol Genet* 21(18):3993–4006.
16. Carreira A, et al. (2009) The BRC repeats of BRCA2 modulate the DNA-binding selectivity of RAD51. *Cell* 136(6):1032–1043.
17. Carreira A, Kowalczykowski SC (2009) BRCA2: Shining light on the regulation of DNA-binding selectivity by RAD51. *Cell Cycle* 8(21):3445–3447.
18. Sheridan SD, et al. (2008) A comparative analysis of Dmc1 and Rad51 nucleoprotein filaments. *Nucleic Acids Res* 36(12):4057–4066.
19. Li Z, Golub EI, Gupta R, Radding CM (1997) Recombination activities of HsDmc1 protein, the meiotic human homolog of RecA protein. *Proc Natl Acad Sci USA* 94(21):11221–11226.
20. Kowalczykowski SC (2015) An Overview of the Molecular Mechanisms of Recombinational DNA Repair. *Cold Spring Harb Perspect Biol* 7(11):7.
21. Cloud V, Chan YL, Grubb J, Budke B, Bishop DK (2012) Rad51 is an accessory factor for Dmc1-mediated joint molecule formation during meiosis. *Science* 337(6099):1222–1225.
22. Da Ines O, et al. (2013) Meiotic recombination in Arabidopsis is catalysed by DMC1, with RAD51 playing a supporting role. *PLoS Genet* 9(9):e1003787.
23. Bugreev DV, et al. (2011) The resistance of DMC1 D-loops to dissociation may account for the DMC1 requirement in meiosis. *Nat Struct Mol Biol* 18(1):56–60.
24. Bugreev DV, Golub EI, Stasiak AZ, Stasiak A, Mazin AV (2005) Activation of human meiosis-specific recombinase Dmc1 by Ca^{2+}. *J Biol Chem* 280(29):26886–26895.

Supporting Information

Martinez et al. 10.1073/pnas.1601691113

SI Materials and Methods

Protein Expression and Purification.

DMC1 purification. 6xHis–DMC1 was produced in *E. coli* strain BLR (DE3) (Novagen) from 1 L of bacterial culture and subjected to ammonium sulfate precipitation. The ammonium sulfate pellet was resuspended in lysis buffer followed by affinity chromatography on a 1-mL HisTrap HP column (GE Healthcare). The protein was eluted with a 50–500 mM imidazole gradient in the presence of 500 mM KCl. The purest fractions were diluted 2.5-fold and applied to a 5-mL HiTrap Heparin HP column (GE Healthcare) and eluted with a 0.2–1.2 M KCl gradient. The fractions containing DMC1 were diluted to 100 mM KCl and loaded on a 1 mL Mono Q column. The purified protein was then dialyzed against a buffer containing: 50 mM Tris•HCl, pH 7.5, 50% glycerol, 350 mM KCl, 1 mM DTT, and stored at −80 °C.

Because low concentrations of DMC1 (25 nM and 75 nM) were used to facilitate experiment with BRCA2, we verified the activity of our DMC1 protein preparation by examining joint molecule formation at more standard literature conditions; i.e., in the presence Ca^{+2} alone, instead of Ca^{+2} and Mg^{+2} as used in this work. A DMC1 titration in the absence of Mg^{+2} showed, as expected, that joint formation was a maximum at 3 nt of ssDNA per DMC1 monomer, producing a yield of ∼28% (23); this yield was reduced in the presence of excess protein or excess ssDNA (Fig. S6). In the presence of Ca^{+2} and Mg^{+2}, the maximum yield was also reached at ∼3 nt of ssDNA per DMC1 monomer, but the inhibition at excess protein was less apparent (Fig. S6*B*). This phenomenon may be explained by the fact that, in the presence of Mg^{+2}, the turnover of DMC1 is faster due to a higher ATPase rate (24) and, therefore, the DMC1–ssDNA complex would be less stable, minimizing the inhibitory effect of excess protein. These results confirm that both the yield of joint molecule formation and the optimal ratio of protein to ssDNA are in agreement with the literature (23).

GFP-MBP-tagged BRCA2 purification and characterization. *Brca2*-deficient hamster cells that were stably transfected with the GFP-MBP-BRCA2 construct showed the same survival to mitomycin C as the *brca2*$^{+/+}$ parental cell line (V79), confirming the functionality of the GFP-MBP-BRCA2 construct (Fig. S5*B*).

GFP-MBP-BRCA2 was purified essentially as described (2), with a few modifications. Briefly, 10–20 15-cm plates of HEK293 cells were transiently transfected using TurboFect (ThermoFisher Scientific) following the manufacturer specifications and harvested 30 h posttransfection. Cell extracts were bound to Amylose resin (NEB), and the protein was eluted with 10 mM maltose. The eluate was then further purified by ion exchange using BioRex 70 resin (BIO-RAD) and step eluted at 250 mM, 450 mM, and 1 M NaCl. The nuclease-free 250 mM fraction shown in Fig. S5*A* was used for the experiment in Fig. 6 and Fig. S5 *C*–*F*. This GFP-MBP-BRCA2 stimulated RAD51-promoted joint molecule formation up to approximately twofold, verifying its activity in vitro (Fig. S5 *C* and *D*).

GST Pull Down Assay. Before the pull down assays, Glutathione Sepharose 4B beads (GE) were equilibrated with binding buffer B: 25 mM Tris acetate, (pH 7.5), 100 μg/mL BSA, 1 mM $MgCl_2$, 2 mM $CaCl_2$, 1 mM DTT, including 100 mM NaCl and 0.01% Igepal CA-630. Each purified GST-BRC peptide (1 μg) was incubated in binding buffer with 0.5–2.0 μg of purified DMC1 for 15 min at 37 °C and then batch bound to 30 μL of glutathione beads for 30 min at 37 °C. The amount of DMC1 pulled down with each GST-BRC peptide in Fig. 1*B* was determined using standard curves generated from known concentrations of DMC1 (Fig. 1*B*, lanes 1–4) and GST-BRC peptides (Fig. 1*B*, lanes 11–14) run in parallel in the same gel. When present, DMC1 retained by nonspecific binding to the beads was subtracted in the quantification. The input concentration of GST-BRC peptide in each pull-down reaction was 0.4 μM and the total input amount for DMC1 ranged from 0.3 to 1.3 μM. As controls for nonspecific binding to the glutathione beads, DMC1 (2.0 μg) was incubated with glutathione beads in the absence of GST-BRC peptide. The complexes were then washed with binding buffer, resuspended in protein sample buffer, heated at 95 °C for 4 min, and loaded onto a 12% SDS-polyacrylamide gel. The gel was run for 1.5 h at 130 V and stained with SYPRO Orange (Invitrogen). The protein bands were quantified by Image Quant software on a Typhoon PhosphorImager (Amersham Biosciences). The binding data of Fig. 1*C* were fit to a hyperbola with a fixed binding stoichiometry of 1:1 by using GraphPad Prism software.

Joint Molecule (D-Loop) Assay. Oligonucleotide oAC203 (90-mer oligonucleotide complementary to pUC19) is 5′- CGGGTGTCGGGGCTGGCTTAACTATGCGGCATCAGAGCAGATTGTACTGAGAGTGCACCATATGCGGTGTGAAATACCGCACAGATGCGT-3′. RAD51 reactions in Fig. S5*C* were carried out at saturating conditions [RAD51 at 75 nM, ssDNA (oAC203) at 225 nM nt], and threefold molar excess of ssDNA relative to pUC19 scDNA. The extent of joint molecule formation was determined using a Typhoon PhosphorImager (Amersham Biosciences). Quantification was performed by using Image Quant software.

DNA Strand Exchange Assay. All oligonucleotide substrates were purified by polyacrylamide gel electrophoresis (PAGE). The following oligonucleotides were used for Fig. 7: TK-167-mer (5′-CTG CTT TAT CAA GAT AAT TTT TCG ACT CAT CAG AAA TAT CCG TTT CCT ATA TTT ATT CCT ATT ATG TTT TAT TCA TTT ACT TAT TCT TTA TGT TCA TTT TTT ATA TCC TTT ACT TTA TTT TCT CTG TTT ATT CAT TTA CTT ATT TTG TAT TA TCC TTA TCT TAT TTA-3′); TK-Oligo1 (5′-TAA TAC AAA ATA AGT AAA TGA ATA AAC AGA GAA AAT AAA G-3′); TK-Oligo2 (5′-CTT TAT TTT CTC TGT TTA TTC ATT TAC TTA TTT TGT ATT A-3′). The dsDNA was generated by first radiolabeling TK-Oligo1 with ^{32}P at the 5′-end and annealing it to TK-Oligo2.

The buffer (B) contained 25 mM Tris acetate (pH 7.5), 1 mM $MgCl_2$, 2 mM $CaCl_2$, 0.1 mg/mL BSA, 2 mM ATP, and 1 mM DTT. All preincubations and reactions were at 37 °C. The DNA and proteins were at the following concentrations: DMC1 (0.22 μM), RAD51 (0.22 μM), RPA (25 nM), 2xMBP-BRCA2 (20, 40, and 80 nM in Fig. 7), ssDNA (4 nM molecules), and dsDNA (4 nM molecules). Where proteins were omitted, storage buffer substituted. The reactions were terminated by adding SDS to 0.25% and proteinase K to 0.5 mg/mL and further incubation for 10 min. The samples were analyzed by PAGE using a 6% gel and 1× TAE buffer, run at 60 V for 60 min at room temperature. The gel was then dried and exposed to PhosphorImager screen. The percentage of DNA strand exchange product was calculated as labeled product divided by total labeled input DNA in each lane using Image Quant software.

ATP Hydrolysis Assay. DMC1 (3 μM) was preincubated with each BRC peptide or BRCA2 for 15 min at 37 °C, followed by addition of the ssDNA 90-mer (oAC203; 9 μM nucleotide, nt) in a

reaction (10 μL) containing 25 mM Tris acetate, (pH 7.5), 0.1 mg/mL BSA, 1 mM $MgCl_2$, 1 mM DTT, 2 mM ATP, and 20 μCi/mL [γ^{32}P] ATP, and further incubated at 37 °C for 1 h. Aliquots (1 μL) were spotted onto a polyethyleneimine (PEI) TLC plate (EMD Chemicals). The spots were air-dried, and the plates were developed in 1 M formic acid and 0.5 M LiCl. The amount of ATP hydrolyzed was determined from dried plates using a Typhoon PhosphorImager (Amersham Biosciences). The amount of $^{32}P_i$ and [γ^{32}P] ATP was quantified by using Image Quant software.

EMSA. In the case of ssDNA binding, DMC1 (25 nM) was preincubated with each BRC peptide at the indicated concentrations for 15 min, followed by addition of ssDNA (90mer, oAC203, labeled with ^{32}P at the 5′ end at 0.2 μM nt) in D-loop reaction buffer. For dsDNA binding, DMC1 (at 0.6 or 0.3 μM in Fig. 5) was preincubated with each BRC peptide at the indicated concentrations for 15 min in a buffer containing 20 mM Tris·HCl (pH 7.5), 10 mM $Mg(OAc)_2$ followed by the addition of dsDNA (^{32}P-labeled at the 5′ end duplex dT_{40}•dA_{40} prepared by annealing to a final concentration of 0.3 μM bp) (Fig. 5). All of the reaction products were resolved by 6% PAGE in TAE. The gels were dried and analyzed on a Typhoon PhosphorImager (Amersham Biosciences) using Image Quant software. The percentage of protein-DNA complexes was quantified as the free radiolabeled DNA remaining in a given lane relative to the protein-free lane. The protein-free lane defined the value of 0% complex.

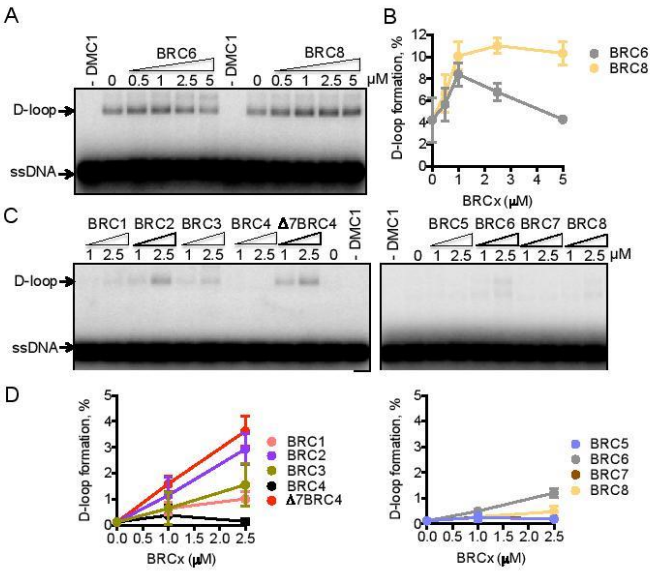

Fig. S1. Effects of BRC6 and BRC8 protein concentration on joint molecule formation by DMC1, and of BRC4, BRC7, and Δ7BRC4 on joint molecule formation at a lower concentration of DMC1. (*A*) Joint molecule reactions were carried out as in Fig. 2*A*, but at higher concentrations of BRC6; BRC8 serves as a control to show that the decrease is specific to BRC6. (*B*) Quantification of *A*. (*C*) Joint molecule formation was carried out as in Fig. 2, but with 25 nM DMC1 and 75 nM (nt) ssDNA [0.8 nM (molecule)] and pUC19 at 0.25 nM molecule. (*D*) Quantification of *C*. Error bars in *B* and *D* represent the SD for three and two independent experiments, respectively.

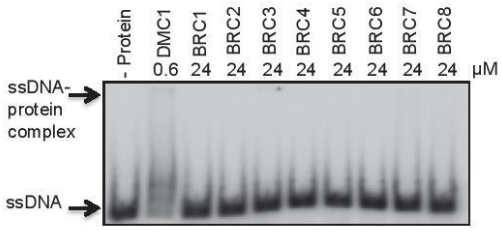

Fig. S2. The BRC repeats do not bind to ssDNA. DNA binding assay (EMSA) where DMC1 (0.6 μM) or the individual BRC repeats (24 μM) were mixed with 5′-end ^{32}P-labeled ssDNA (dT_{40}, 0.3 μM nt) and incubated for 1 h. The complexes were analyzed by PAGE and visualized by autoradiography.

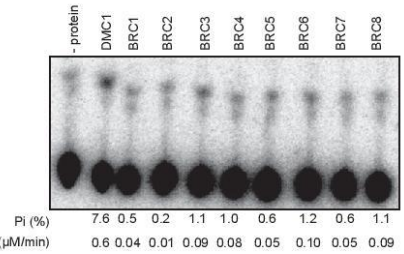

Fig. S3. The BRC repeats do not manifest ATPase activity. Autoradiography of a TLC plate showing an ATPase assay where DMC1 (3 μM) or the GST-BRC peptides (24 μM) were individually mixed with 90-mer ssDNA (9 μM nt) and incubated for 1 h in the presence of 1 mM $MgCl_2$ and 2 mM ATP. The quantification of the percentage of P_i produced, and the calculated rate of ATP hydrolysis is indicated below each lane.

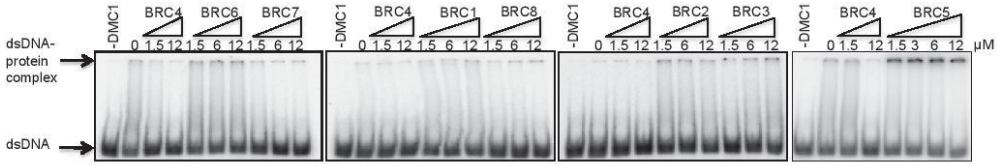

Fig. S4. Binding of DMC1 (0.3 μM) to dsDNA in the presence of the BRC repeats. Shown is the EMSA experiment that is quantified in Fig. 5C.

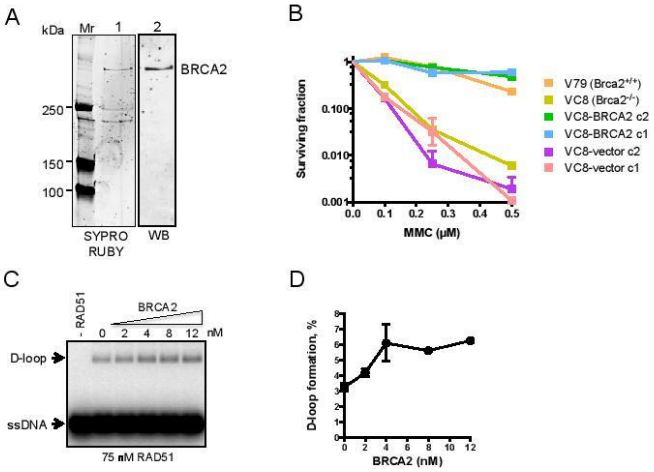

Fig. S5. Purified GFP-MBP-BRCA2 complements *Brca2*-deficient cells and stimulates RAD51-mediated joint molecule formation. (*A*) BRCA2 tagged with GFP-MBP at the N terminus was purified from human HEK293 cells and analyzed by SDS/PAGE. Lane 1: BRCA2 (0.9 μg) was loaded on a precast 7.5% SDS/PAGE gel and stained with SYPRO Ruby. Lane 2: Western blot of purified BRCA2 protein (0.5 μg) using an antibody specific for the carboxy-terminus of BRCA2 (CA1033, EMD). M_r, size markers. (*B*) Mitomycin C survival of stably transfected clones of *Brca2*-deficient hamster cells complemented with human GFP-MBP-tagged BRCA2 (green and blue), the vector containing the GFP-MBP tag (violet and pink), V79 parental cells ($Brca2^{+/+}$) (orange) and VC8 ($Brca2^{-/-}$) (gold). (*C*) RAD51 (75 nM) and the indicated concentrations of BRCA2 were preincubated with a 5′-end ^{32}P-labeled 90-mer ssDNA [2.4 nM (molecule)] for 10 min at 37 °C and scDNA [0.8 nM (molecule)] was added last to start the reaction. The mix was incubated at 37 °C for 30 min, terminated by incubation with Proteinase K, and resolved on a 1% agarose gel. (*D*) Quantification of *C*. Error bars in *D* represent the SD for three independent experiments.

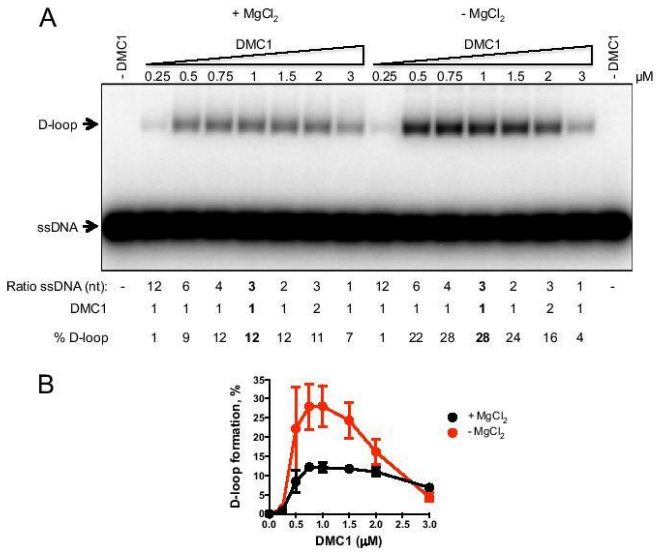

Fig. S6. Comparison of joint molecule formation by DMC1 in Ca^{+2}, in the presence or absence of Mg^{+2}. (*A*) Autoradiograph showing a D-loop assay. DMC1 at the indicated concentrations was preincubated with a 5′-end ^{32}P-labeled 90-mer ssDNA [oAC203, 3 μM (nt), 33 nM (molecule)] for 10 min at 37 °C, and supercoiled DNA (scDNA) [pUC19, 10.3 nM (molecule)] was added last to start the reaction. The mix was incubated at 37 °C for 30 min, and the products were resolved on a 1% agarose gel. (*B*) Quantification of D-loop formation from *A*. Error bars in *B* represent the SD for two independent experiments.

Table S1. Binding affinity of each BRC repeat for DMC1

BRC repeat	K_d, μM
BRC1	28 ± 2
BRC2	37 ± 3
BRC3	30 ± 2
BRC4	172 ± 14
BRC5	136 ± 28
BRC6	8.0 ± 0.8
BRC7	49 ± 2
BRC8	40 ± 4
Δ7BRC4	90 ± 15

The dissociation constants (K_d ± SD) were derived from fitting of the binding curves to a hyperbola using a fixed stoichiometry of 1 BRC repeat per DMC1.

4.3 DISCUSSION & OUTLOOK

Evidence from studies in mice, plants and humans suggested a role of BRCA2 in meiotic recombination. Since BRCA2 and DMC1 were known to interact, it was proposed that BRCA2 has a similar role in mediating DMC1 recombination in meiosis I as for RAD51 in mitosis [92,101,156,180,181,184,187]. The results of our study confirm these assumptions and show that indeed BRCA2 regulates DMC1 activity.

In an earlier study, the interaction of human DMC1 and BRCA2 was mapped to a highly conserved region, a so-called PhePP motif between amino acids 2386 and 2411 by using *in vivo* pull downs, yeast-two-hybrid assays and peptide arrays [92]. Here, DMC1 did not interact with the BRC repeats as it was suggested previously and shown in other organisms [120,184]. Thorslund et al. (2007) argued that the DMC1 interaction site in BRCA2 is different to RAD51 to allow the simultaneous action of the two proteins [92]. In *U. maydis* that lacks a Dmc1 homolog, RAD51 does not only bind to the BRC repeats but also to this PhePP motif of Brh2, which could mean that the site serves as a secondary binding site for DMC1 besides the BRC repeats [245].

In our *in vitro* study we proved the interaction between the BRC repeats and DMC1 and established the binding affinities for each single BRC repeat. The binding affinities were overall lower compared to RAD51 and we could not make out a similar pattern of two classes of binding modules as for RAD51. Nevertheless, we established that the joint molecule formation of DMC1 was enhanced by the BRC repeats, meaning that the mechanism by which BRCA2 mediates recombination is different to the one observed for RAD51. Based on our study we suggest that DMC1 recombination is supported by BRCA2 by facilitating its association with ssDNA and stabilization of the nucleoprotein filaments. In turn, this activity facilitates joint molecule formation and DNA strand exchange.

In contrast to what was shown for RAD51, BRC4 does not have the strongest affinity to DMC1. Instead, it reduces joint molecule formation and ssDNA/dsDNA binding. A mutant peptide of BRC4, Δ7BRC4, is unable to bind RAD51 because it lacks the oligomerization interface for RAD51 interaction. Since Δ7BRC4 readily stimulated DMC1 activity in contrast to BRC4, is possible that this oligomerization interface FxxA is not necessary for the interaction with DMC1. It is hence plausible that a second BRC binding module identified before [146], LFDE, constitutes the primary interaction site for DMC1 in the BRC repeats. To confirm this, further studies using mutant BRC peptides with DMC1 would be needed.

In yeast, Rad51 and Dmc1 localize together to the DSB. Both proteins are required for proper meiotic recombination whereas Rad51 plays only an accessory role [93]. Rad51 is

not needed for its catalytic activity but rather to form a nucleoprotein filament, probably in regulating DMC1 strand exchange activity together with Mei-Sae3. Also, in *A. thaliana,* Rad51 mutants without a catalytic domain could complement *rad51* mutants in meiosis but where defective in mitosis, showing that Dmc1 is the primary recombinase in meiosis but needs the presence of Rad51 [93,246]. The hypothesis that DMC1 is the primary strand-invasion enzyme in meiosis but needs the supportive role of RAD51 also in human, probably by initiating a nucleoprotein filament at the DSB, is in line with our working model. Based on the results from this and my supervisor's earlier work [124] we hypothesize that BRCA2 binds directly free RAD51 monomers via BRC1-5 and DMC1 via BRC6-8 that have a low affinity to free RAD51. The latter pre-forms a nucleoprotein filament on the ssDNA with BRCA2 replacing RPA and blocking RAD51 ATPase and binding to dsDNA [123,124]. DMC1 could then bind to the RAD51 nucleus and start forming filaments that are stabilized by BRCA2 for homology search, strand invasion and exchange (2.2, Figure 8).

This working model requires further investigation, for example, performing joint molecule formation in presence of the two proteins and one or more different BRC repeats. A single molecule approach as shown before for RAD51 and BRC4 [123] but including DMC1 and ssDNA would allow us to address some of these questions. Based on our results in chapters 2 and here, BRCA2 NTD would be positioned at the ssDNA/dsDNA junction where BRC1-5 would load RAD51. DMC1 would bind to the nucleus of RAD51 downstream on the ssDNA.

Given the intrinsic strand exchange activity of RAD51, it is of interest how this activity is inhibited to allow DMC1 to solely promote meiotic recombination. This regulation might depend on accessory factors described for DMC1 and RAD51 such as Hop2-Mnd1 however, the regulation of the two recombinases and how they interplay remains to be investigated [189].

CHAPTER 5

5.1 FUNCTIONAL EVALUATION OF INTERMEDIATE RISK VUS IN BRCA2

The difficulty to assess the clinical relevance of rare missense variants in *BRCA2* found in breast cancer families has been described in detail in Chapter 1.9. In contrast to the mutations that lead to truncated or inactive protein products for which the impact on BRCA2 function can be easily assessed, missense variants are more difficult to evaluate because it is not known whether any of these changes actually alter BRCA2 function sufficiently to predispose carriers of these mutations to cancer [211].

The majority of VUS are rare, they are only found in few families, making the application of multifactorial likelihood models to estimate their cancer risk difficult. Hence, for these variants, it is important to apply *in vitro* and *in vivo* functional assays to complement genetic data and assess breast cancer risk. The majority of *BRCA2* variants (~60 %) remain unclassified (BRCA2share database) [210]. This represents a very important clinical challenge, as the carriers of those variants cannot follow cancer risk assessment [97].

In collaboration with members of the Evidence-based Network Investigating Germline Mutant Alleles (ENIGMA) consortium and the Breast Cancer Association Consortium (BCAC) we contributed to the functional evaluation of 20 BRCA1 and 33 BRCA2 missense variants genotyped on ~40,000 breast cancer cases and 40,000 matched controls using the illumina Collaborative Oncological Gene-Environment Study (iCOGS) custom genotyping array. The goal of the study was to assess the association between these rare VUS and breast cancer risk. Because they confer intermediate phenotype or partial impact on function, the question addressed was whether an intermediate effect in the function corresponds to an intermediate risk. This study shows for the first time that a moderate or intermediate risk can be assigned to VUS using functional as well as case-control approaches.

Here I will present the work conducted in our lab that contributed to the evaluation of these intermediate risk VUS.

5.2 WORK FOR İCOGS STUDY

Previous work from Fergus Couch laboratory found a number of variants from the C-terminal region of BRCA2 that result in an intermediate phenotype in homologous recombination assay. Using a quantitative multifactorial likelihood model, our collaborators in this work estimated for the first time a moderate to high breast cancer risk for variant Y3035S, G2508S and K2729N. In addition, A2717S yielded mildly protective effect. Two class 5 variants (pathogenic variants) were also analyzed but they were not detected in enough cases and controls for estimation of breast cancer risk, D2723H, R3052W [211]. Since the DNA binding activity of BRCA2 is integral to its recombination function, and these variants are located in the C-terminus DNA binding domain, a deleterious phenotype in HR could be due to impaired DNA binding. We contributed to this study by analyzing the DNA binding ability of these variants.

We used a mammalian expression vector coding for EGFP-MBP-BRCA2 (see methods in chapter 2.5) to introduce the missense mutations present in six variants by site-

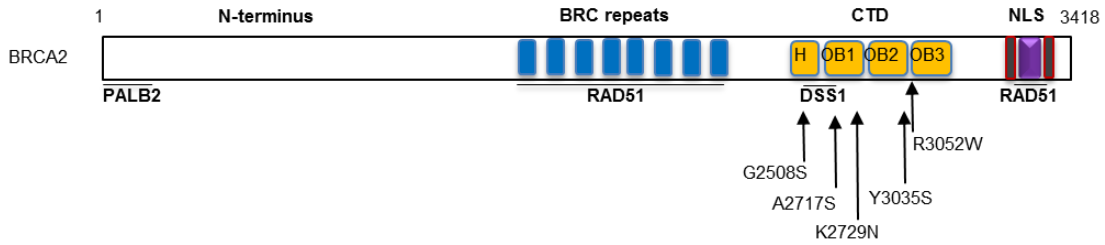

Figure 1: A) Structure of BRCA2 with the VUS indicated in the CTD.

directed mutagenesis. The location of the variants in the context of human BRCA2 scheme is shown in Figure 1A. We then transfected HEK293 cells with the respective construct for overexpression of the protein. The purification, based on a previous publication from my supervisor and colleagues [70] with some modifications, involved two steps:

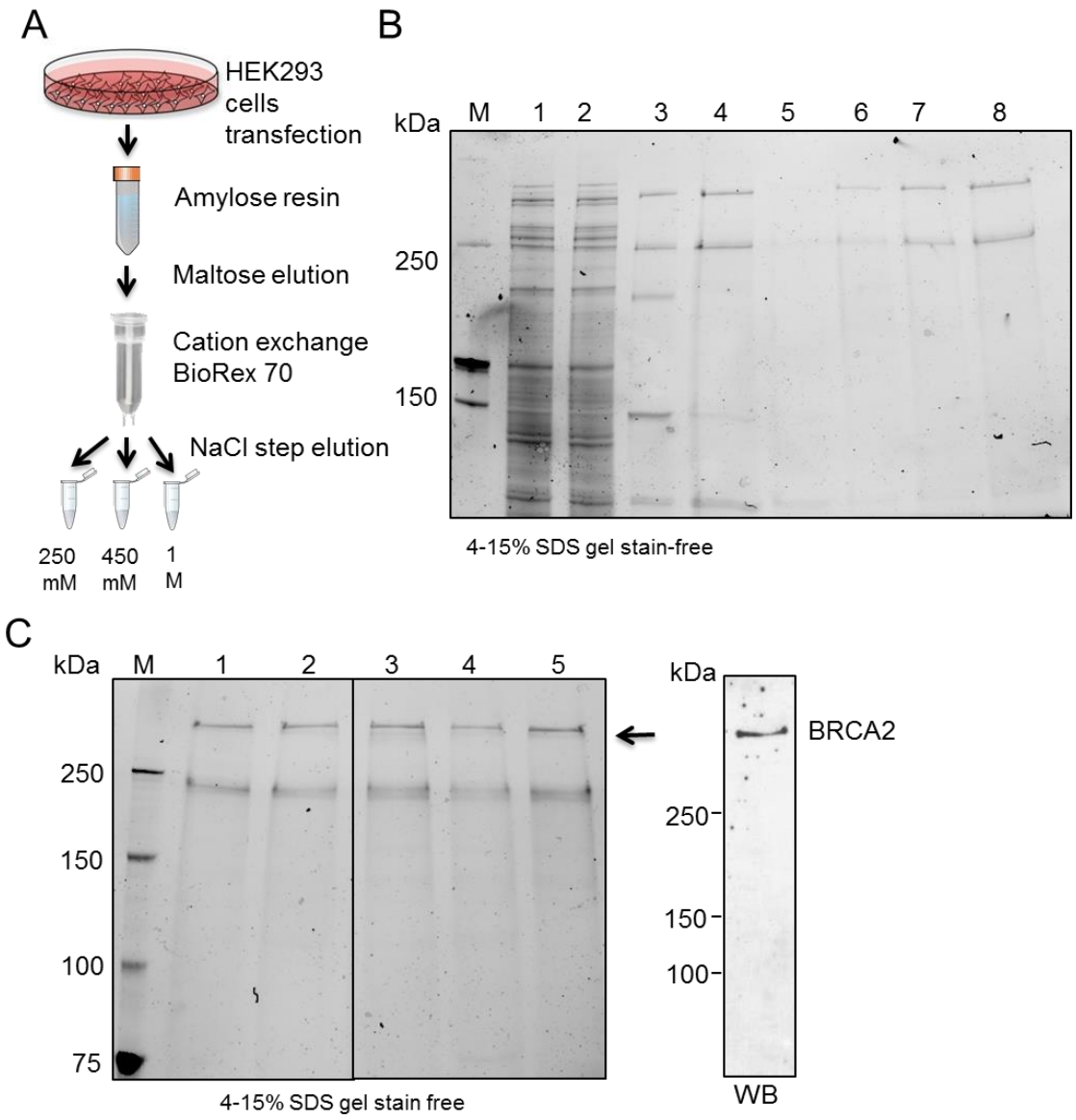

Figure 2: Purification of BRCA2 and variants. **A)** Purification protocol **B)** Representative example of the fractions of a purification (K2729N) shown on a SDS-PAGE: M) molecular weight marker 1) lysate loaded 2) unbound fraction 3) amylose beads 4) maltose elution 5) flow through BioRex70 6) 250 mM NaCl elution 7) 450 mM NaCl elution 8) 1M NaCl elution. **C) Left:** Purified proteins (0.25 µg) on 4-15% SDS-PAGE M) molecular weight marker 1) wild type BRCA2 2) Y3035S 3) K2729N 4) G2508S 5) A2717S. **Right:** Western Blot of BRCA2 detected with anti-BRCA2 antibody OP95.

First, the proteins were isolated from the cell lysate by amylose resin to which the MBP tag binds and the proteins were eluted with maltose. Second, the eluates were further subjected to a weak ion-exchange resin (BioRex 70) and eluted step-wise using NaCl (250 mM, 450 mM, 1M) (Figure 2A, B). We detected the purified proteins on SDS-PAGE gels and verified their identity by western blot using an antibody against the central region of BRCA2 (OP95) (Figure 2C). Even though the yield of the proteins was

small (usually between ~5 and 7 µg) the proteins were stable, free of nucleases and the concentration was enough to test their DNA binding activity.

Using a DNA binding assay (EMSA, see Chapter 2) we then tested the ability of the variants to associate with DNA.

Increasing concentrations of each protein was incubated with 5'-radiolabeled ssDNA

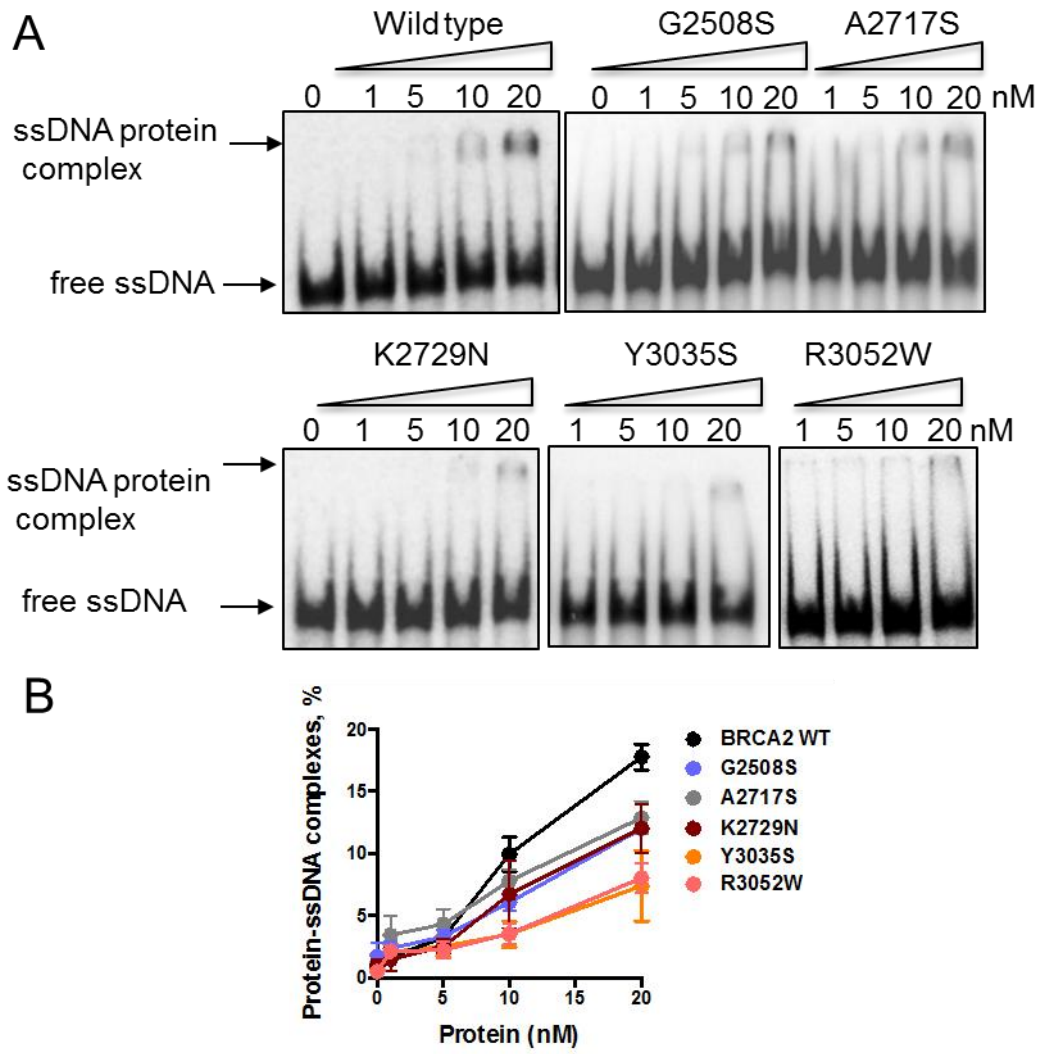

Figure 3: DNA binding assays with wild type and variant BRCA2 proteins. **A)** Autoradiographs from EMSAs with radiolabeled ssDNA (167 nt polymer) and proteins in the indicated concentrations. **B)** Quantification of experiments from (A) (n=3).

(167 nt polymer) at 37°C for 1 hour before loading on a 6% PAGE, dried and exposed overnight. As shown in Figure 3, wild type BRCA2 could form up to 20% of DNA-protein complexes at the maximum attainable concentration (20 nM). The variant protein G2508S, K2729N and A2717S showed a minor reduction of protein-DNA complex formation to 12%. Importantly, Y3035S, associated with moderately increased risk of breast cancer in this study, showed similar impairment of DNA binding as the

pathogenic variant R3052W (~7%). This is consistent with their location close to the DNA binding site in the crystal structure (Figure 4). This phenotype was confirmed by four functional assays including cell-based homologous recombination assay performed by the groups of F. Couch and M. Vreeswijk (see 5.3, Figures 2 & 3).

The combined results from genetic and functional data led us to conclude that hypomorphyic BRCA2 missense variant Y3035S can confer moderate clinically relevant risk of breast cancer.

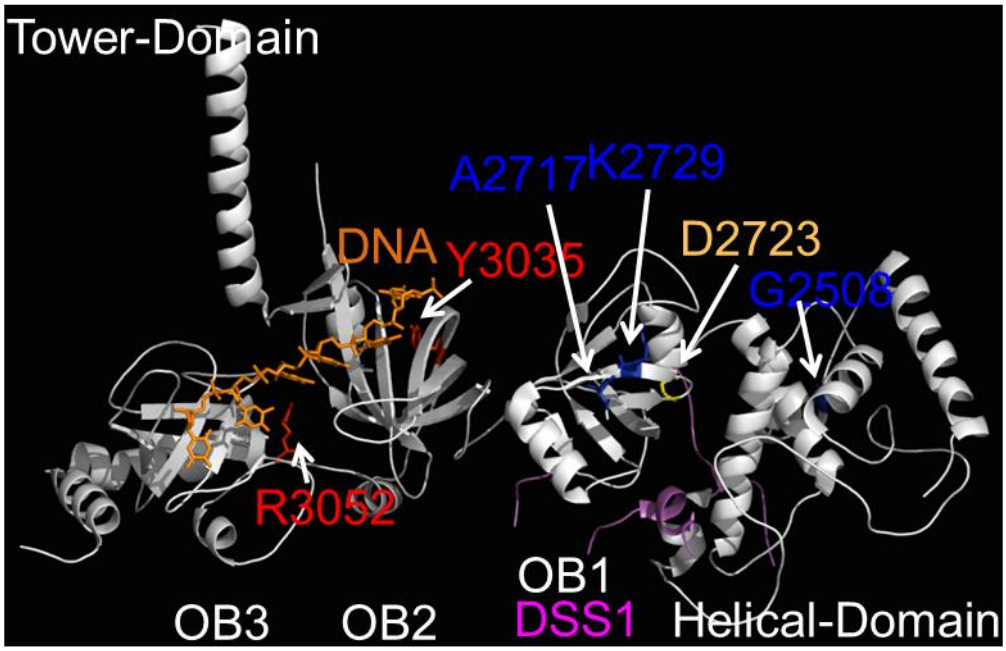

Figure 4: Position of BRCA2 DNA binding domain (DBD) variants on a ribbon diagram of the murine DBD crystal structure [127].
Ribbon diagram of the crystal structure of the mouse BRCA2 DBD-DSS1-ssDNA (PDB ID: 1MJE) generated using MacPyMOL (Molecular Graphics version 1.3.) highlighting the location of the variants analyzed by EMSA. The location of the known deleterious variant p.D2723H is shown in yellow. The human variants displaying a neutral phenotype (G2058, K2729, A2717) are shown in blue. The position of the variant reducing the DNA binding activity (Y3035) is shown in red. The DNA is shown in orange and DSS1 in purple. Courtesy of A. Carreira

5.3 OUTLOOK

In the work presented here, we evaluated the impact of BRCA2 Y3035S and G2508S intermediate risk variants on BRCA2 function using biochemical (DNA binding), cell-based homologous recombination and in vivo embrionic stem cells cell-based assays. We demonstrated for the first time that hypomorphic BRCA2 mutation, like Y3035S, can confer an intermediate risk to develop breast cancer. In contrast, G2508S, that

was also associated with a moderate breast cancer risk, when combined with functional assays, led us to conclude that it might be a neutral variant.

BRCA2 is known to bind DNA via its C-terminal DNA binding domain where many missense mutations are located. A lot of pathogenic mutants have been found in this region probably because they affect the DNA binding and thus the HR proficiency of BRCA2. Until recently, the recombination function was tested using cell-based HDR assays in a *BRCA2*$^{-/-}$ background. Importantly, this is the first time purified full length BRCA2 and variants, and Electrophoretic mobility shift assay, EMSA, is used to evaluate VUS. With the help of the EMSA, we can now get more insight on the mechanism that is defective in the HR assay. This DNA binding assay could be eventually complemented with RAD51-mediated DNA strand exchange assay as described in chapter 2.

In this study we observed that missense mutations with a decreased ssDNA binding activity also displayed a decreased efficiency in the HR assay in two cell-based systems. The DNA binding results fit well with the prediction made on the basis of the crystal structure of the mouse DNA binding domain in complex with DSS1 and DNA [127]. Because of its important functional relevance and, due to the lack of crystal structure available for the human CTD, we set out to do this in collaboration with the group of Xiaodong Zhang (Imperial College London, UK). With the help of the recombinant protein platform of I. Curie, we were able to obtain a soluble and active protein CTD-DSS1 complex in sufficient amounts to use for crystallization (Chapter 2.2, Figure 7). The human CTD-DSS1-ssDNA crystal structure will give more insights into the functionality of this domain and help to predict more accurately the impact on the function of VUS located in this region.

One consideration to keep in mind is that the partial HR and DNA binding proficiency we observe could also stem from the newly identified NTD (Chapter 2). It is plausible that the residual DNA binding activity of the variant Y3035S characterized in this work is due to the NTD, which might also be responsible for the intermediate phenotype in HR. To test this hypothesis we could use a combined mutant Y3035S with C315S and check the effect on DNA binding and HR.

There is a large amount of rare VUS listed in the BRCA databases (ca. 1700 for BRCA2) that remain to be classified. Many of them lie in regions with a defined function such as the BRC repeats or the C-terminus, which helps to apply functional assays for evaluation of variants. Yet, many missense VUS are located in underexplored regions and moreover they are found rarely in families. With the functional characterization of the N-terminus of BRCA2 and the development of functional *in vitro* assays using

purified protein we will further contribute to the classification of VUS found in breast cancer families.

5.4 MANUSCRIPT FOR PUBLICATION

BRCA2 HYPOMORPHIC MUTATIONS ARE ASSOCIATED WITH MODERATE BREAST CANCER RISK

(submitted)

Hermela Shimelis[1]#, Romy L.S. Mesman[2]#, Catharina von Nicolai[3]#, Asa Ehlen[3]#, Lucia Guidugli[4], Charlotte Martin[5], Fabienne M.G.R. Calléja[6], Huong Meeks[7], Emily Hallberg[8], Jamie Hinton[8], Jenna Lilyquist[8], Chunling Hu[1], Kristiina Aittomäki[9], Irene Andrulis[10,11], Hoda Anton- Culver[12], Volker Arndt[13], Matthias W. Beckmann[14], Javier Benitez[15,16], Natalia V. Bogdanova[17,18], Stig E. Bojesen[19,20,21], Manjeet K. Bolla[22], Anne-Lise Borresen-Dale [23,24], Hiltrud Brauch[25,26,27], Paul Brennan[28], Hermann Brenner[13,27,29], Annegien Broeks[30], Barbara Brouwers[31,32], Thomas Brüning[33], Barbara Burwinkel[34,35], Jenny Chang-Claude[36,37], Georgia Chenevix-Trench[38] for kConFab/AOCS Investigators, Ching-Yu Cheng[39], Ji-Yeob Choi[40,41], Margriet Collée[42], Angela Cox[43], Simon S. Cross[44], Kamila Czene[45], Hatef Darabi[45], Joe Dennis[22], Thilo Dörk[18], Isabel dos-Santos-Silva[46], Alison M. Dunning[47], Peter A. Fasching[14,48], Jonine Figueroa[49,50], Henrik Flyger[51], Montserrat García-Closas[50], Graham G. Giles[52,53], Gord Glendon[10], Pascal Guénel[54], Christopher A. Haiman[55], Per Hall[45], Ute Hamann[56], Mikael Hartman[57,58], Frans B. Hogervorst[30], Antoinette Hollestelle[59], John L. Hopper[53], Hidemi Ito[60,61], Anna Jakubowska[62], Daehee Kang[40,41,63], Veli-Matti Kosma [64,65,66], Vessela Kristensen[23,24,67] for NBCS Collaborators, Kah- Nyin Lai[68,69], Diether Lambrechts[70,71], Loic Le Marchand[72], Jingmei Li[45], Annika Lindblom[73], Artitaya Lophatananon[74], Jan Lubinski[62], Eva Machackova[75], Arto Mannermaa[64,65,66], Sara Margolin[76], Frederik Marme[34,77], Keitaro Matsuo[61,78], Hui Miao[57], Kyriaki Michailidou[22,79], Roger
L. Milne[52,53], Kenneth Muir[74,80], Susan L. Neuhausen[81], Heli Nevanlinna[82], Janet E. Olson[8], Curtis Olswold[8], Ana Osorio[15,16], Paolo Peterlongo[83], Julian Peto[46], Paul D.P. Pharoah[22,47], Katri Pylkäs[84,85], Paolo Radice[86], Muhammad Usman Rashid[56,87], Valerie Rhenius[47], Anja Rudolph[36], Suleeporn Sangrajrang[88], Elinor J. Sawyer[89], Marjanka K. Schmidt[30], Minouk J. Schoemaker[90,91], Caroline Seynaeve[59], Mitul Shah[47], Chen-Yang Shen[92,93], Martha Shrubsole[94], Xiao-Ou Shu[94], Susan Slager[8], Melissa C. Southey[95], Daniel O. Stram[55], Anthony Swerdlow[90,91], Soo H. Teo[68,69], Ian Tomlinson[96], Diana Torres[56,97], Thérèse Truong[54], Qin Wang[22], Robert Winqvist[84,85], Anna H. Wu[55], Jyh-Cherng Yu[98], Wei Zheng[94], Ying Zheng[99], Jennifer Leary[100], Logan Walker[101], Lenka Foretova[75], Florentia Fostira[102], Kathleen B.M. Claes[103], Liliana Varesco[104], Setareh Moghadasi [105], Douglas F. Easton[22,47], Amanda B. Spurdle[106], Peter

Devilee[2,107], Harry Vrieling[2], Alvaro N.A. Monteiro[108,109], David E. Goldgar[110]*, Aura Carreira[3]*, Maaike P.G. Vreeswijk[2]*, Fergus J. Couch[1,8]*

#equal contributions

*equal contributions

Corresponding author:
Fergus J. Couch. PhD
Mayo Clinic
Stabile 2-42
200 First Street SW
Rochester,
MN 55905
Phone: 507-284-3623
Fax: 507-538-1937
E-mail: couch.fergus@mayo.edu

The authors disclose no potential conflicts of interest

ABSTRACT

Breast cancer risks conferred by many germline missense variants in the *BRCA1* and *BRCA2* genes, often referred to as variants of uncertain significance (VUS), have not been established. In this study, associations between 19 *BRCA1* and 33 *BRCA2* missense substitution variants and breast cancer risk were investigated through a breast cancer case-control study using genotyping data from 38 studies of predominantly European ancestry (41,890 cases and 41,607 controls) and nine studies of Asian ancestry (6,269 cases and 6,624 controls). The c.9104A>C, p.Tyr3035Ser (OR=2.52, p=0.04) and c.7522G>A, p.Gly2508Ser (OR=2.68, $p=4.0x10^{-3}$) variants in *BRCA2* and c.5096G>A, p.Arg1699Gln (OR=4.29, p=0.009) variant in *BRCA1* wereassociated with moderately increased risks of breast cancer. Detailed functional characterization of BRCA2 p.Tyr3035Ser using five quantitative functional assays showed reduced, intermediate BRCA2 activity. The consistent genetic and functional data establish that hypomorphic BRCA2 missense variants, such as p.Tyr3035Ser, can confer potentially clinically relevant moderately increased risks of breast cancer.

SIGNIFICANCE

The results suggest that calibrated functional assays or genotyping studies can be used to identify clinically relevant *BRCA1* and *BRCA2* missense variants. Because hypomorphic BRCA1 and BRCA2 variants are associated with moderately increased risks of breast cancer, guidelines for risk management of women with these specific variants will be needed.

INTRODUCTION

Mutation screening of the *BRCA1* and *BRCA2* genes has resulted in the discovery of thousands of unique germline *BRCA1* and *BRCA2* variants. Many pathogenic variants of *BRCA1* or *BRCA2* resulting in truncation of these proteins, along with a small number of pathogenic missense variants, have been associated with high risks of breast cancer with cumulative risks of 55% to 85% by age 70 (1). In contrast, the influence on cancer risk of many rare variants of uncertain significance (VUS), accounting for between 2% and 10% of results from genetic testing, is not known (2-4). As a result, carriers of VUS in these predisposition genes cannot benefit from cancer risk management strategies for women with pathogenic mutations.

Clinical classification of *BRCA1* and *BRCA2* VUS has been largely based on probability-based models which incorporate likelihood-ratios associated with family history of cancer, co- segregation of variants with breast and ovarian cancer within families, tumor histopathology, and prior probabilities of pathogenicity associated with cross-species amino acid sequence conservation (5, 6). While over 200 *BRCA1* and *BRCA2* variants have been classified as pathogenic or neutral/non-pathogenic using a multifactorial likelihood model (7-10) , many VUS remain because of limited availability of families segregating the variants. Clinical classification of VUS in *BRCA1* and *BRCA2* has been further complicated by the potential for variants associated with moderate risks (odds ratio (OR) between 2.0 and 5.0) of disease (5, 11, 12), with *BRCA1* c.5096G>A, p.Arg1699Gln (R1699Q) recently associated with a cumulative risk of breast or ovarian cancer by age 70 of 24% and reduced penetrance relative to the pathogenic c.5095C>T, p.Arg1699Trp (R1699W) variant (13). In this study, the influence of 52 missense variants in *BRCA1* and *BRCA2* on breast cancer risk was investigated using the iCOGS breast cancer case-control project (14). In addition, the impact of the *BRCA2* c.9104A>C, p.Tyr3035Ser (Y3035S) and c.7522G>A, p.Gly2508Ser (G2508S) variants on BRCA2 function

were evaluated relative to known pathogenic and neutral variants using biochemical, cell-based homology directed repair (HDR), and *in vivo* embryonic stem (ES) cell-based assays.

METHODS

Participants

Breast cancer cases and controls from 38 studies of predominantly European ancestry (41,890 cases with invasive disease and 41,607 controls) and nine studies of Asian ancestry (6,269 cases and 6,624 controls) from the Breast Cancer Association Consortium (BCAC) were used for genotyping (Supplementary Table S1). All studies were approved by local ethics committees and institutional review boards (Supplementary Table S1).

Variant selection

Missense substitution variants from *BRCA1* (n=19) and *BRCA2* (n=33) were selected by ENIGMA for inclusion on the iCOGS genotyping array based on frequency in the ENIGMA database (15) (Supplementary Tables S2). The *BRCA1* c.4327C>T, p.Arg1443Ter, R1443X variant served as a positive control for known pathogenic alterations. Variants are defined by Human Genome Variant Society (HGVS) nomenclature and are based of Refseq transcripts (BRCA1: NM_007294.3 ; BRCA2: NM_000059.3).

Genotyping

Genotyping was conducted using the custom Illumina Infinium array (iCOGS) (14). DNA samples containing each of the variants were included in iCOGS genotyping as positive controls and were used to inform genotype calling. Genotypes were called with the GenCall algorithm. Descriptions of sample and genotype quality control have been published (14, 16). Cluster plots for rare variants for this study were manually evaluated relative to positive control samples.

Statistical Methods

The association of each variant with breast cancer risk was assessed using unconditional logistic regression, adjusting for study (categorical). Analyses were restricted to either Caucasian or Asian women. Cases selected for iCOGS based on personal or family history of breast cancer were excluded to obtain unbiased OR estimates for the general population. The significance of associations (P-values) was determined by the likelihood ratio test comparing models with and without carrier status as a covariate. Because this study was focused on estimating breast cancer risk associated with each variant analyses were not adjusted for multiple testing. Additional statistical analyses are outlined in Supplementary Methods.

Homology directed repair (HDR) assay

The HDR assay for BRCA2 has been described previously (11). Full-length BRCA2 wild-type and mutant cDNA expression constructs were co-expressed with an I-Sce1 expressing plasmid in BRCA2 deficient V-C8 cells, stably expressing the DR-GFP reporter plasmid. HDR- dependent repair of I-Sce1 induced DNA double strand breaks were quantified by fluorescence- activated cell sorting (FACS) of GFP positive cells after 72 hours. Two independent clones of each variant were evaluated in the HDR assay on three separate occasions. Equivalent expression of wild-type and mutant BRCA2 proteins was confirmed by western blot analysis of anti-Flag-M2 (Sigma F1804) antibody immunoprecipitates from V-C8 cell lysates.

Purification of full-length wild-type and mutated BRCA2 protein

Wild-type and mutant human BRCA2 cDNAs were cloned into the C-terminal MBP-GFP-tagged phCMV1 expression plasmids and purified as described (17). Briefly, 10 x 15-cm plates of HEK293 cells were transiently transfected using TurboFect (Thermo Scientific) following the manufacturer specifications and harvested 30 hours post-transfection. Cell extracts were bound to Amylose resin (NEB), and the protein was eluted with 10 mM maltose. The eluate was further purified by ion exchange using BioRex 70 resin (BIO-RAD) and step eluted at 250mM, 450 mM, and 1M NaCl (17). Each fraction was tested for nuclease contamination. The 1M NaCl fractions were used for the DNA binding assay because they were free of nuclease contamination.

Electrophoretic Mobility Shift Assay (EMSA)

The ssDNA substrate used for DNA binding was obtained from Sigma (Supplementary Methods) and purified by polyacrylamide gel electrophoresis (PAGE). Purified wildtype or mutated BRCA2 at concentrations 0, 1, 5, 10, 20 nM was mixed with the ssDNA oligonucleotide oAC423 167-mer (0.2 µM nt), labeled with ^{32}P at the 5' end, in a buffer containing 25 mM TrisAcO (pH 7.5), 1 mM $MgCl_2$, 2 mM $CaCl_2$, 1mM DTT, 1 mM ATP, 100 µg/ml BSA, and incubated for 60 min at 37□C. Reaction products were resolved by 6% PAGE, imaged on a Typhoon PhosphorImager (Amersham Biosciences), and analyzed with Image J software. The relative amount of product was calculated as labeled complex divided by the total labeled input DNA in each lane. The protein-free lane defined the value of 0% complex.

Embryonic Stem (ES) cell complementation

Selected BRCA2 variants were functionally analyzed based on the ability of human *BRCA2* to complement the lethality of mouse *Brca2* deficiency (18, 19). *BRCA2* exons containing VUS were generated by mutagenesis PCR and engineered into a human BRCA2 (hBRCA2) Bacterial Artificial Chromosome (BAC) by Red/ET BAC recombineering in DH10B *E.coli.* BAC DNA was transfected into mES cells containing a conditional mouse *Brca2* allele and a disrupted *Brca2* allele (*Brca2*$^{-/loxP}$), and the DR-GFP construct integrated at the *pim1* locus. *hBRCA2* containing cells were selected by G418. Per variant, two independent BAC transfections were performed and G418-resistant clones from each BAC transfection were pooled. Cell pools were transfected with Cre-recombinase expression construct to remove the conditional mBrca2 gene. *hBRCA2* RNA and protein expression was confirmed.

ES cell functional assays

After Cre-recombinase transfection, *mBrca2* depleted cells were selected for restoration of the HPRT minigene using hypoxanthine-aminopterin-thymidine (HAT) containing medium.

HAT resistant clones were pooled and evaluated for BRCA2 activity using functional assays. In the mES cell HDR assay, cells were transfected with an I-Sce1 expression vector, pCMV-RED- ISce, and GFP positive cells were quantified by flow cytometry 48 hr after transfection. mES cells were also treated with varying doses of PARP inhibitor (KU-0058948, Astra Zeneca) and viable cells were quantified after 48 hr. Cell survival was calculated as the fraction of treated surviving mES cells relative to the cell count of untreated surviving cells per cell line.

RESULTS

Association of *BRCA1* and *BRCA2* variants with breast cancer risk

A total of 19 *BRCA1* and 33 *BRCA2* variants encoding missense substitution mutations and the pathogenic *BRCA1* c.4327C>T, p.Arg1443Ter (R1443X) mutation on the iCOGS array were genotyped for 48,159 breast cases and 48,231 controls from the Breast Cancer Association Consortium (BCAC) (Supplementary Table S1). Among the *BRCA1* variants, 11 have been classified as Class 1-neutral and one each as Class 3-uncertain and Class 5-pathogenic, using the quantitative multifactorial likelihood model described above (Supplementary Table S2). In addition, *BRCA1* c.5207T>C, p.Val1736Ala (V1736A) (20) and c.5363G>A, p.Gly1788Asp (G1788D) variants have been classified as pathogenic in the ClinVar database. Among the *BRCA2* variants, 18 are located in the DNA binding domain (amino acids 2490-3098), 26 have been classified as Class 1-neutral or Class 2-likely neutral and one has been classified as Class 5-pathogenic using the same multifactorial likelihood model (Supplementary Table S2).

The *BRCA1* R1443X recurrent truncating pathogenic mutation was associated with high risk of breast cancer (odds ratio (OR) = 8.3, p=0.045) in the Caucasian studies in iCOGS

(Table 1), consistent with what has been estimated for pathogenic *BRCA1* mutations. Among the missense variants, c.5096G>A, p.Arg1699Gln (R1699Q) was associated with a moderate risk of breast cancer (OR=4.29, p=0.009) (Table 1). This result was lower than expected for pathogenic *BRCA1* variants, but consistent with the moderate penetrance of this variant estimated from other family-based studies (13). Several *BRCA1* variants including the known pathogenic c.5123C>A, p.Ala1708Glu (A1708E); c.5207T>C, p.Val1736Ala (V1736A); and c.5363G>A, p.Gly1788Asp (G1788D) variants were not observed in sufficient numbers of cases and controls to allow for estimation of breast cancer risks (Supplementary Table S3). Three *BRCA2* variants were statistically significantly associated with breast cancer risk ($p<0.05$) for Caucasian or Asian women. *BRCA2* c.9104A>C, p.Tyr3035Ser (Y3035S) was observed in 18 cases and 7 controls in the Caucasian studies (OR=2.52, p=0.038) (Table 1), c.7522G>A, p.Gly2508Ser (G2508S) was observed in 31 cases and 12 controls in the Asian studies (OR=2.68, p=0.004) but not in any Caucasians, and *BRCA2* c.8187G>T, p.Lys2729Asn (K2729N) was observed in 164 cases and 128 controls in the Asian studies (OR=1.41, p=0.004) (Table 1). In addition, the *BRCA2* c.8149G>T, p.Ala2717Ser (A2717S) (OR=0.77, p=0.02) and c.4258G>T, p.Asp1420Tyr (D1420Y) (OR=0.86, p=0.005) were negatively associated with risk for Caucasian women (Table 1, Supplementary Table S3). None of the remaining *BRCA2* variants, including the Class 5-pathogenic *BRCA2* variants, c.8167G>C, p.Asp2723His (D2723H) and c.9154C>T, p.Arg3052Trp (R3052W), were observed in enough cases and controls for estimation of breast cancer risk (Supplementary Table S3). Thus, for the first time *BRCA2* variants encoding missense alterations (Y3035S, G2508S, and K2729N) have been associated with moderately increased risks of breast cancer.

To assess further the association of the Y3035S moderate risk variant with breast cancer, 19 pedigrees with Y3035S were collected through the ENIGMA consortium (Fig. 1, Supplementary Fig. S1, Supplementary Table S4). Segregation studies of Y3035S, assuming the relative risk was constant with age, indicated an association with breast cancer risk (Risk Ratio (RR)=14.8; 95%CI 2.4-20.0) (Supplementary Table S4). A second analysis, allowing for a similar pattern of age specific effects as for population-based pathogenic *BRCA2* truncating mutations, estimated the optimal cumulative penetrance for Y3035S at 0.75 of known pathogenic truncating *BRCA2* mutations, and yielded a similar risk ratio for breast cancer (Supplementary Table S4). In addition, Y3035S co-occurred with a pathogenic BRCA2 mutation (S1882X) in Pedigree G (Supplementary Fig. S1) and with another VUS in BRCA2 (S1298del) in Pedigree K (Fig. 1), suggesting hypomorphic

effects. Overall, the pedigree analysis suggests that Y3035S is associated with increased breast cancer risk. No segregation studies of G2508S were performed because only one pedigree was collected (not shown).

Cell-based HDR analysis of BRCA2 variants

Inactivation or depletion of BRCA2 has been associated with deficient homology directed repair (HDR) of DNA double strand breaks (21), which can be quantified with a cell-based HDR green fluorescent protein (GFP) reporter assay (22). This assay has shown 100% sensitivity and specificity for known pathogenic missense mutations in the BRCA2 DNA-binding domain and has been used for characterization of BRCA2 VUS (8, 11, 23). In this study, the impact of the G2508S, K2729N, A2717S, and Y3035S missense variants on BRCA2 HDR activity was assessed relative to the D2723H and R3052W known pathogenic and the c.9292T>C p.Tyr3098His (Y3098H) known neutral BRCA2 variants (11)'(24). All wildtype and mutant proteins displayed equal and reproducible levels of expression by western blot for full-length BRCA2 protein (Supplementary Fig. S2). The D2723H and R3052W Class 5 pathogenic variants (11) showed substantial loss of BRCA2 HDR activity (Fig. 2A). In contrast, BRCA2 Y3035S showed intermediate levels (2.3-fold relative to D2723H) (Fig. 2A) of BRCA2 HDR activity that was outside the thresholds for known pathogenic missense variants (HDR fold- change<1.66) and neutral/low clinical significance (HDR fold-change >2.41) variants, which equate to 99% probability of pathogenicity and neutrality/low clinical significance, respectively (11). This intermediate functional effect was consistent with the moderate risk of breast cancer (OR=2.52, p=0.038) observed in the iCOGS case-control study (Table 1) and the estimated 0.75-fold penetrance of pathogenic BRCA2 mutations from segregation studies (Supplementary Table S3), and to our knowledge, is the first evidence that partial loss of BRCA2 function is associated with an intermediate or moderate risk of breast cancer. In contrast, BRCA2 G2508S exhibited 3.2-fold HDR activity relative to D2723H (Fig. 2A). While reduced relative to a wildtype activity of 5.0, this level of HDR activity was associated with >99% probability of neutrality/low clinical significance. Similarly, BRCA2 K2729N showed reduced HDR activity relative to the wildtype protein (Fig. 2A), which was consistent with a mild influence on breast cancer risk (OR=1.41, p=0.004) in the Asian population, and >99% probability of neutrality/low clinical significance (Fig. 2A). Together, these results suggest that the HDR assay is calibrated relative to cancer risk, with minor functional

effects for variants associated with low- or modest risks of breast cancer such as c.9976A>T, p.Lys3326Ter (K3326X) (OR=1.28) (25) and K2729N (OR=1.41), more substantial functional effects for the intermediate risk Y3035S (OR=2.52), and strong effects for known pathogenic variants such as D2723H and R3052W. On this basis, the HDR assay can readily distinguish variants associated with intermediate levels of breast cancer risk from those considered high-risk pathogenic or neutral/low clinical significance.

Single strand DNA (ssDNA) binding activity of BRCA2 variants

BRCA2 directly binds to ssDNA and recruits RAD51 to ssDNA at sites of DNA damage during homologous recombination DNA repair (17, 26). Hence, ssDNA binding is integral to the homologous recombination activity of BRCA2. On this basis, an *in vitro* biochemical assay was used to examine the influence of the BRCA2 variants on BRCA2 ssDNA binding activity. Full- length wildtype and mutant human BRCA2 proteins tagged with (N-terminal) green fluorescence protein (GFP) and maltose binding protein (MBP) (GFP-MBP-BRCA2) were expressed and purified to near homogeneity (Supplementary Fig. S3) as described previously (17). Full-length BRCA2 protein expression was confirmed by western blotting using an antibody against the C- terminus of BRCA2 (Supplementary Fig. S3). The ssDNA binding activity of full-length wildtype and mutant BRCA2 proteins was evaluated using an electrophoretic mobility shift assay (EMSA). The wildtype protein bound to ssDNA with a yield of ~18% at the maximum attainable concentration of BRCA2 protein (Fig. 2B, 2C), consistent with previous results (17). Similar to the R3052W pathogenic variant, the Y3035S variant exhibited 2-fold reduced protein-ssDNA complex formation compared to the wildtype protein (Fig. 2B, 2C). In contrast, G2508S, A2717S, and K2729N showed only partially reduced protein-ssDNA complex formation (Fig. 2C). These results are consistent with predictions from the crystal structure of the BRCA2 DBD, where Y3035S is predicted to impair DNA binding, similarly to R3052W, because of proximity to DNA (Supplementary Fig. S4) (21). Thus, although this is the first time DNA binding has been used for evaluating BRCA2 VUS, the results suggest that the protein-ssDNA binding assay can discriminate between low-risk/neutral variants and high/moderate risk variants when investigating VUS located in the DBD of BRCA2.

Mouse embryonic stem cell-based functional analysis of BRCA2 missense variants

Functional complementation of murine (m) *Brca2*-null ES cell lethality by human (h) BRCA2 variants (18, 19) has been used to characterize BRCA2 VUS. Wildtype human *BRCA2* expression rescues *Brca2* deficient ES cells from lethality, whereas ES cells expressing known pathogenic forms of BRCA2 fail to survive (18). In addition, several variants have shown partial or reduced ES cell survival relative to wildtype BRCA2. Surviving cells expressing these variants have shown moderate defects in HDR assays and sensitivity to cisplatin or a PARP inhibitor (27). In this study three independent pools of BAC clones for each of hBRCA2 W31C, G2508S, A2717S, D2723H, K2729N, Y3035S, and R3052W were tested for complementation of *mBrca2* deficiency, HDR proficiency, and sensitivity to PARP inhibition. Cells expressing hBRCA2p.D2723H or p.R3052W pathogenic variants did not survive after disrupting endogenous mBrca2 expression and were not included in the downstream functional analysis. Instead, we included cells with the W31C variant that complements the lethality but shows a severe defect in HDR activity because of disruption of the BRCA2-PALB2 interaction. BRCA2 G2508S, A2717S, K2729N, and Y3035S BACs partially rescued the lethality of the *mBrca2*-deficient ES cells, suggesting at least partial functional complementation of BRCA2 deficiency. This result for W31C was unexpected, because this variant disrupts the interaction of PALB2 with BRCA2. HDR activity of surviving cells was assessed using the DR-GFP reporter assay. BRCA2 W31C showed only 14% ($p<0.001$) activity, BRCA2 Y3035S, G2508S and K2729N variants displayed 50% (P=0.002), 55% (P=0.007), and 70% (P=0.02) of wildtype HDR activity, respectively, whereas A2717S was not significantly different to wildtype protein (Fig. 3A). The sensitivity of wildtype and mutant BRCA2 expressing ES cells to PARP inhibitor (KU-0058948) was also evaluated by counting viable cells after 48 hours of exposure to different doses of drug. Wildtype BRCA2, G2508S, and A2717S rescued ES cells from sensitivity to PARP inhibitor, whereas W31C expressing cells showed significant sensitivity to PARP inhibitor (Fig. 3B). In contrast, K2729N and Y3035S resulted in partial rescue of ES cell sensitivity (Fig. 3B). Collectively, the results from complementation and HDR assays and to a lesser extent the PARP inhibitor sensitivity assay, in *mBrca2* deficient ES cells show that Y3035S is partially deficient in BRCA2 activity, whereas G2508S and K2729N have a substantially lesser effect, and A2717S has no discernable influence on BRCA2 function.

DISCUSSION

In this study, associations between 52 *BRCA1* and *BRCA2* missense variants and breast cancer risk were evaluated using a large breast cancer case-control study. To our knowledge, this is the largest case-control study conducted to establish the clinical relevance and estimate the risks of individual rare *BRCA1* and *BRCA2* variants encoding missense substitutions. The case-control analysis showed that *BRCA1* c.5096G>A, R1699Q (OR=4.29) and *BRCA2* c.9104A>C, Y3035S (OR=2.52) were associated with moderately increased breast cancer risks for Caucasian women (Table 1), whereas *BRCA2* c.7522G>A, G2508S (OR=2.68) and c.8187G>T, K2729N (OR=1.41, p=0.004) were associated with increased risks for Asian women. This is the first study to estimate low to moderate risks of breast cancer for specific *BRCA1* and *BRCA2* missense variants.

The moderate risk of breast cancer associated with the *BRCA1* R1699Q variant (OR=4.29) is consistent with previous findings from segregation analyses of breast cancer families, which estimated that the penetrance of R1699Q was 0.6-fold that of the corresponding R1699W known pathogenic variant in the same residue. Similarly, R1699Q was estimated to be associated with a cumulative risk of breast or ovarian cancer by age 70 years of 24% relative to the pathogenic R1699W variant and *BRCA1* truncating variants (13). Consistent with these findings, BRCA1 R1699Q mutant protein exhibits only partial protein function in HDR and other *in vitro* experiments (12, 13). While, *in silico* sequence conservation-based prediction models predicted R1699Q as damaging (Supplementary Table S2), quantitative multifactorial likelihood prediction model based on family data and sequence conservation yielded a posterior probability of pathogenicity (cancer risk similar to truncating *BRCA1* mutations) for R1699Q of 0.79 and identified R1699Q as Class 3-uncertain (13). Importantly, the probability model is based on the assumption that all pathogenic variants have the same penetrance as truncating *BRCA1* variants, and is not intended to discriminate between high and moderate risk variants. Thus, the case-control study was effective in confirming that R1699Q is a moderate risk variant in *BRCA1*. Interestingly, previous data suggest that *BRCA1* G1788D and V1736A may also be associated with moderate risks of breast cancer. The G1788D variant is predicted damaging by sequence-based *in silico* models (Supplementary Table S2) and functional studies using a validated transcription activation assay have shown partially reduced activity (9, 28). Similarly,

V1736A is predicted damaging by *in silico* models (Supplementary Table S2), but functional studies have shown only partially reduced transcription activation activity, a mild folding defect, and partially compromised binding specificity (9, 28, 29). The *BRCA1* V1736A variant was also found *in-trans* with a frameshift mutation in the first reported case of a biallelic *BRCA1* pathogenic mutation carrier with Fanconi Anemia like symptoms and ovarian cancer (20). However, risks of breast cancer for these variants have not been defined risks and could not be established in the case-control study because of low numbers of carriers of these variants even among over 40,000 breast cancer cases.

As noted above, *BRCA2* Y3035S was associated with increased risk of disease (OR=2.52) for Caucasian women. While the numbers of cases and controls with the Y3035S variant were small, the moderate risk estimate is supported by family data showing partial co-segregation with breast cancer, and one pedigree in which *BRCA2* Y3035S co-occurred with *BRCA2* c.5645C>A p.Ser1882Ter (S1882X) (Supplementary Fig. S1). Several sequence-based *in silico* prediction models including MetaLR, MetaSVM, Vest3, and A-GVGD (C55 - prior probability of pathogenicity of 0.66) (Supplemental Table S2) predicted Y3035S as deleterious. In addition, the missense substitution is predicted as likely deleterious by a protein likelihood ratio model based on sequence analysis (30). Analyses of splicing defects using Minigene-based assays have shown no influence on RNA splicing (31), suggesting that the increased risks are not due to abnormal splicing. Importantly, functional analysis of Y3035S using multiple independent assays consistently revealed hypomorphic activity. HDR analysis in VC8 cells showed intermediate BRCA2 function outside the range of known pathogenic or neutral variants based on 99% probability of pathogenicity and neutrality. Consistent with this finding, Y3035S failed to restore HR activity and partially rescued sensitivity to PARP inhibition in ES cells (Fig. 3A, 3B). Similarly, Y3035S showed significantly reduced ssDNA complex formation (Fig. 2B, 2C) consistent with the predicted effect on DNA binding based on the location of Y3035 in the crystal structure of the BRCA2 DBD (26), (Supplementary Fig. S4). These results suggest that the reduced HR activity associated with Y3035S is due to defective DNA binding activity. Together these results provide the first evidence that a hypomorphic BRCA2 missense variant confers a moderate risk of breast cancer. However, Y3035S is consistently reported as “likely benign” and “benign” in the ClinVar public database. Since this database is widely used by researchers and clinicians, this under-appreciation of

moderate risks of breast cancer associated with this variant has the potential to impact patient care. Further prospective studies are required to estimate age-dependent risks of cancer and to inform management protocols for carriers of this variant.

The BRCA2 G2508S (OR=2.68, p=0.004) variant was associated with a moderate risk of breast cancer in Asian women, but could not be evaluated in the Caucasian population (Table 1). The variant was predicted neutral by a protein likelihood prediction model (30), but was predicted deleterious by other *in silico* prediction models including MetaLR, MetaSVM, Vest3, and A- GVGD (C55 - prior probability of pathogenicity of 0.66) (Supplementary Table S2). However, the HDR V-C8 cell-based assay showed only mildly reduced activity similar to K2729N (OR=1.41) and p.K3326X (OR=1.28) (25), which are both classified as neutral/non-pathogenic (Fig. 2A). Likewise, the impact of G2508S on ssDNA binding was limited and most similar to K2729N (Fig. 2B, 2C). Although G2508S had a substantial influence on HDR activity in ES cells similar to Y3035S (Fig. 3A), no influence on ES cell sensitivity to PARP inhibitor was observed (Fig. 3B). Thus, the functional results suggest a lower risk of breast cancer for the G2508S variant, consistent with the wide confidence limits (95%CI 1.37-5.23) for the association. As the variant has only been detected in the East Asian population (32, 33), one possibility is that genetic and environmental modifiers in the Asian population account in part for the influence of the variant on breast cancer risk and the discrepancy between the case-control and functional study results. The Asian specific risk association for G2508S was consistent with a recent study of cases and controls from the Shanghai Breast Cancer Study (34), which suggested that G2508S was associated with development of breast cancer, although the effect estimate (OR=16.5, 95%CI:2.2-124.5, $P=2.2\times10^{-4}$) was unstable due to limited numbers of events (16 cases and 1 control). Further studies are needed to resolve this issue, but for now the breast cancer risks associated with this variant must be treated with caution. *BRCA2* K2729N (OR=1.41, p=0.004) is also common in Asians, but rare in Caucasians (33). This variant has previously been classified as neutral/little clinical significance by the multifactorial likelihood classification model (8). Consistent with these findings, functional analysis of K2729N showed only a minor influence on HDR function (8, 11) (Fig. 2A), ssDNA binding (Fig. 2B), and BRCA2 activity in the ES cell- based HR assay (Fig. 3B), and had no impact on ES cell drug sensitivity (Fig. 3A, 3B). The mild defect in HR function

correlated well with the low risk of breast cancer (OR=1.41, P=0.004) associated with the K2729N variant in the Asian case-control study.

To date, 1,167 *BRCA1* and 1,908 *BRCA2* unique missense variants have been reported in the Clinvar database, with 1,006 and 1,779 variants, respectively, classified as VUS. This observation stresses the lack of validated high throughput methods for classification of missense variants in these genes. Current methods of classification rely heavily on family data. However, this study highlights the utility of functional assays for this purpose. In particular, evaluation of missense variants in the BRCA2 DBD is possible with the cell-based HDR assay that has been validated using known pathogenic and non-pathogenic variants in the DBD to have 100% sensitivity (95% confidence interval (CI): 75.3%-100%) and 100% specificity (95% CI: 81.5%-100%) (11). Thresholds of 99.9% probability of pathogenicity and non- pathogenicity/low clinical significance/neutrality have been established for classification of variants (11), with variants showing HDR fold change between these thresholds remaining classified as Class 3 VUS. However, based on variants with moderate levels of risk [K3326X (OR=1.28) (25), K2729N (OR=1.41), Y3035S (OR=2.52)], the HDR assay is now calibrated to differentiate between variants with high, moderate, or low breast cancer risks (Fig. 2A). Thus, the assay can be used to identify other hypomorphic BRCA2 DBD variants associated with moderate breast cancer risk. While not yet validated, ES cell complementation assays have also been effectively used to classify missense variants in the BRCA2 DBD (18, 27, 35, 36). Whether all variants that show reduced HDR activity in V-C8 or ES cells are hypomorphic and associated with moderate risks of breast cancer remains to be determined.

This study also contains the first evidence that a biochemical assay using purified full-length BRCA2 protein can be used to assess missense the DNA binding capacity of variants in the BRCA2 DBD. While purification of wildtype full-length BRCA2 protein to near homogeneity has previously been described (17), in this study the functional integrity of purified mutant BRCA2 proteins was assessed for the first time in a quantitative ssDNA binding assay. Full-length proteins were used to limit potentially inaccurate interpretation of effects from partial protein fragments. As noted in the Results section, defective ssDNA binding activity was observed for the pathogenic R3052W variant and for the moderate risk Y3035S variant, but not for wildtype protein, suggesting that the assay can be used to assess pathogenicity of missense variants in the BRCA2 DBD.

This study highlights the existence of functionally intermediate or hypomorphic missense variants that are associated with moderate risks of breast cancer. Using a combination of large case-control studies and functional assays, a BRCA2 missense variant (Y3035S) was classified as a moderate risk pathogenic variant for breast cancer (OR=2.52, p=0.038) for the first time. In addition, BRCA1 R1699Q was confirmed as a moderate risk (OR=4.29, p=0.009) breast cancer missense variant, consistent with previous penetrance studies. In addition, the consistency of results from the independent cell-based HDR, ssDNA binding, and ES-cell based assays for all of the missense BRCA2 variants in the study, and the close agreement with the results from the iCOGS case-control study, suggests that validated functional assays calibrated to defined levels of risk can be used to classify BRCA2 variants as pathogenic, moderate risk, or neutral.

ACKNOWLEDGEMENTS

This work was supported in part by NIH grants CA116167, CA176785, CA192393, an NIH specialized program of research excellence (SPORE) in breast cancer to the Mayo Clinic (P50 CA116201), the Breast Cancer Research Foundation, the ATIP-AVENIR CNRS/INSERM Young Investigator grant 201201, EC-Marie Curie Career Integration grant CIG293444, Institute National du Cancer INCa-DGOS_8706 to A.C, the Dutch Cancer Society KWF (UL-5649), the Australian National Health and Medical Research Council (ID#1010719), and The Cancer Council Queensland (ID#1086286). HM is supported by the Government of Canada through Genome Canada and the Canadian Institutes of Health Research and the Ministère de l'enseignement supé- rieur, de la recherche, de la science et de la technologie du Québec through Génome Québec as part of the PERSPECTIVE project (CIHR grant GPH-129344). BCAC data management was funded by Cancer Research UK (C1287/A10118 and C1287/A12014) and by the European Community's Seventh Framework Programme under grant agreement 223175 (HEALTH-F2-2009-223175). Funding for the iCOGS infrastructure came from: the European Community's Seventh Framework Programme under grant agreement n° 223175

(HEALTH-F2-2009-223175) (COGS), Cancer Research UK (C1287/A10118, C1287/A 10710, C12292/A11174, C1281/A12014, C5047/A8384, C5047/A15007, C5047/A10692), the National Institutes of Health (CA128978) and Post-Cancer GWAS initiative (1U19 CA148537, 1U19 CA148065 and 1U19 CA148112 - the GAME-ON initiative), the
Canadian Institutes of Health Research (CIHR) for the CIHR Team in Familial Risks of Breast Cancer, Komen Foundation for the Cure, the Breast Cancer Research Foundation.

REFERENCES

1. Antoniou A, Pharoah PD, Narod S, Risch HA, Eyfjord JE, Hopper JL, et al. Average risks of breast and ovarian cancer associated with BRCA1 or BRCA2 mutations detected in case Series unselected for family history: a combined analysis of 22 studies. American journal of human genetics. 2003;72:1117-30.

2. Quiles F, Fernandez-Rodriguez J, Mosca R, Feliubadalo L, Tornero E, Brunet J,et al. Functional and structural analysis of C-terminal BRCA1 missense variants. PLoS One. 2013;8:e61302.

3. Radice P, De Summa S, Caleca L, Tommasi S. Unclassified variants in BRCA genes: guidelines for interpretation. Ann Oncol. 2011;22 Suppl 1:i18-23.

4. Lindor NM, Goldgar DE, Tavtigian SV, Plon SE, Couch FJ. BRCA1/2 sequence variants of uncertain significance: a primer for providers to assist in discussions and in medical management. Oncologist. 2013;18:518-24.

5. Goldgar DE, Easton DF, Deffenbaugh AM, Monteiro AN, Tavtigian SV, Couch FJ. Integrated evaluation of DNA sequence variants of unknown clinical significance: application to BRCA1 and BRCA2. American journal of human genetics. 2004;75:535-44.

6. Vallee MP, Francy TC, Judkins MK, Babikyan D, Lesueur F, Gammon A, et al. Classification of missense substitutions in the BRCA genes: a database dedicated to Ex-UVs. Hum Mutat. 2012;33:22-8.

7. Easton DF, Deffenbaugh AM, Pruss D, Frye C, Wenstrup RJ, Allen-Brady K, et al. A systematic genetic assessment of 1,433 sequence variants of unknown clinical significance in the BRCA1 and BRCA2 breast cancer-predisposition genes. American journal of human genetics. 2007;81:873-83.

8. Farrugia DJ, Agarwal MK, Pankratz VS, Deffenbaugh AM, Pruss D, Frye C, et al.

Functional assays for classification of BRCA2 variants of uncertain significance. Cancer Res. 2008;68:3523-31.

9. Lee MS, Green R, Marsillac SM, Coquelle N, Williams RS, Yeung T, et al. Comprehensive analysis of missense variations in the BRCT domain of BRCA1 by structural and functional assays. Cancer Res. 2010;70:4880-90.

10. Lindor NM, Guidugli L, Wang X, Vallee MP, Monteiro AN, Tavtigian S, et al. A review of a multifactorial probability-based model for classification of BRCA1 and BRCA2 variants of uncertain significance (VUS). Hum Mutat. 2012;33:8-21.

11. Guidugli L, Pankratz VS, Singh N, Thompson J, Erding CA, Engel C, et al. A classification model for BRCA2 DNA binding domain missense variants based on homology- directed repair activity. Cancer Res. 2013;73:265-75.

12. Lovelock PK, Spurdle AB, Mok MT, Farrugia DJ, Lakhani SR, Healey S, et al. Identification of BRCA1 missense substitutions that confer partial functional activity: potential moderate risk variants? Breast Cancer Res. 2007;9:R82.

13. Spurdle AB, Whiley PJ, Thompson B, Feng B, Healey S, Brown MA, et al. BRCA1 R1699Q variant displaying ambiguous functional abrogation confers intermediate breast and ovarian cancer risk. J Med Genet. 2012;49:525-32.

14. Michailidou K, Hall P, Gonzalez-Neira A, Ghoussaini M, Dennis J, Milne RL, et al. Large- scale genotyping identifies 41 new loci associated with breast cancer risk. Nat Genet. 2013;45:353-61, 61e1-2.

15. Spurdle AB, Healey S, Devereau A, Hogervorst FB, Monteiro AN, Nathanson KL, et al. ENIGMA--evidence-based network for the interpretation of germline mutant alleles: an international initiative to evaluate risk and clinical significance associated with sequence variation in BRCA1 and BRCA2 genes. Hum Mutat. 2012;33:2-7.

16. Pharoah PD, Tsai YY, Ramus SJ, Phelan CM, Goode EL, Lawrenson K, et al. GWAS meta-analysis and replication identifies three new susceptibility loci for ovarian cancer. Nat Genet. 2013;45:362-70, 70e1-2.

17. Jensen RB, Carreira A, Kowalczykowski SC. Purified human BRCA2 stimulates RAD51- mediated recombination. Nature. 2010;467:678-83.

18. Kuznetsov SG, Liu P, Sharan SK. Mouse embryonic stem cell-based functional assay to evaluate mutations in BRCA2. Nat Med. 2008;14:875-81.

19. Hendriks G, Morolli B, Calleja FM, Plomp A, Mesman RL, Meijers M, et al. An efficient pipeline for the generation and functional analysis of human BRCA2 variants of uncertain significance. Hum Mutat. 2014;35:1382-91.

20. Domchek SM, Tang J, Stopfer J, Lilli DR, Hamel N, Tischkowitz M, et al. Biallelic deleterious BRCA1 mutations in a woman with early-onset ovarian cancer. Cancer Discov. 2013;3:399-405.

21. Moynahan ME, Chiu JW, Koller BH, Jasin M. Brca1 controls homology-directed DNA repair. Mol Cell. 1999;4:511-8.

22. Wu K, Hinson SR, Ohashi A, Farrugia D, Wendt P, Tavtigian SV, et al. Functional evaluation and cancer risk assessment of BRCA2 unclassified variants. Cancer Res. 2005;65:417-26.

23. Couch FJ, Rasmussen LJ, Hofstra R, Monteiro AN, Greenblatt MS, de Wind N. Assessment of functional effects of unclassified genetic variants. Hum Mutat. 2008;29:1314-26.

24. Lovelock PK, Wong EM, Sprung CN, Marsh A, Hobson K, French JD, et al. Prediction of BRCA1 and BRCA2 mutation status using post-irradiation assays of lymphoblastoid cell lines is compromised by inter-cell-line phenotypic variability. Breast Cancer Res Treat. 2007;104:257- 66.

25. Meeks HD, Song H, Michailidou K, Bolla MK, Dennis J, Wang Q, et al. BRCA2 Polymorphic Stop Codon K3326X and the Risk of Breast, Prostate, and Ovarian Cancers. J Natl Cancer Inst. 2016;108.

26. Yang H, Jeffrey PD, Miller J, Kinnucan E, Sun Y, Thoma NH, et al. BRCA2 function in DNA binding and recombination from a BRCA2-DSS1-ssDNA structure. Science. 2002;297:1837-48.

27. Biswas K, Das R, Eggington JM, Qiao H, North SL, Stauffer S, et al. Functional evaluation of BRCA2 variants mapping to the PALB2-binding and C-terminal DNA-binding domains using a mouse ES cell-based assay. Hum Mol Genet. 2012;21:3993-4006.

28. Carvalho MA, Marsillac SM, Karchin R, Manoukian S, Grist S, Swaby RF, et al. Determination of cancer risk associated with germ line BRCA1 missense variants by functional analysis. Cancer Res. 2007;67:1494-501.

29. Abkevich V, Zharkikh A, Deffenbaugh AM, Frank D, Chen Y, Shattuck D, et al. Analysis of missense variation in human BRCA1 in the context of interspecific sequence variation.

J Med Genet. 2004;41:492-507.

30. Karchin R, Agarwal M, Sali A, Couch F, Beattie MS. Classifying Variants of Undetermined Significance in BRCA2 with protein likelihood ratios. Cancer Inform. 2008;6:203- 16.

31. Thery JC, Krieger S, Gaildrat P, Revillion F, Buisine MP, Killian A, et al. Contribution of bioinformatics predictions and functional splicing assays to the interpretation of unclassified variants of the BRCA genes. Eur J Hum Genet. 2011;19:1052-8.

32. Bodian DL, McCutcheon JN, Kothiyal P, Huddleston KC, Iyer RK, Vockley JG, et al. Germline variation in cancer-susceptibility genes in a healthy, ancestrally diverse cohort: implications for individual genome sequencing. PLoS One. 2014;9:e94554.

33. Lek M, Karczewski K, Minikel E, Samocha K, Banks E, Fennell T, et al. Analysis of protein-coding genetic variation in 60,706 humans. bioRxiv. 2015.

34. Zhang Y, Long J, Lu W, Shu XO, Cai Q, Zheng Y, et al. Rare coding variants and breast cancer risk: evaluation of susceptibility Loci identified in genome-wide association studies. Cancer Epidemiol Biomarkers Prev. 2014;23:622-8.

35. Biswas K, Das R, Alter BP, Kuznetsov SG, Stauffer S, North SL, et al. A comprehensive functional characterization of BRCA2 variants associated with Fanconi anemia using mouse ES cell-based assay. Blood. 2011;118:2430-42.

36. Michailidou K, Hall P, Gonzalez-Neira A, Ghoussaini M, Dennis J, Milne RL, et al. Large-scale genotyping identifies 41 new loci associated with breast cancer risk. Nat Genet.2013;45:353-61.

FIGURE LEGENDS

Figure 1. BRCA2 p.Y3035S segregates with breast cancer in high risk families. Five of the most informative pedigrees are shown. Upper black quadrants reflect breast cancer status. Type of cancer and age at diagnosis are displayed. Variant status is indicated by “Y3035S”. (+), mutation positive; (-), mutation negative reflects results of genetic testing.

Figure 2. (A) HDR and ssDNA binding activity of BRCA2 p.Y3035S is reduced. (A) Activity of BRCA2 missense variants is shown as HDR fold change with standard error (SE) (of three independent measures of duplicates) on a scale of one to five. Solid lines represent

99.9% and 0.1% probability of pathogenicity. (B) Representative Electrophoretic Mobility Shift Assays (EMSA) of DNA-protein complexes formed by mixing increasing concentrations (0, 5, 10, 20 nM) of purified BRCA2 wildtype and mutant proteins with ssDNA. (C) Quantitation of the DNA- protein complex formation shown in Fig. 2B. Error bars represent SE derived from at least three independent experiments. Statistical difference between WT and mutant BRCA2 Protein-DNA complexes formation was determined by two-sample t-test. **P < 0.001; *p < 0.05. WT, wildtype.

Figure 3. HR efficiency and PARP inhibitor sensitivity of mES cells expressing *hBRCA2* variants. (A) GFP expression from the DR-GFP reporter was analyzed as a measure of HR activity. The percentage GFP positive cells for each variant was normalized to wildtype *hBRCA2* expressing cells. Results represent the mean of three independent experiments with two independent pools of BAC clones tested per variant. Error bars represent standard error of three independent experiments. Statistical significance is indicated by " * ". (B) Relative cell survival compared to untreated cells was determined by cell count after 48hr exposure to PARP inhibitor KU-0058948. Data represent the mean of three experiments using three different pools of BAC clones. **P < 0.001; *p < 0.05. WT, wildtype.

Supplementary Figure 1: BRCA2 p.Y3035S pedigrees. Upper black quadrants reflect breast cancer status. Type of cancer and age at diagnosis are displayed. Variant status is indicated by "Y3035S". Genotyping results are indicated by (+), mutation positive; (-), mutation negative. The bilateral breast cancer patient in Pedigree H was a heterozygote for BRCA2 mutations p.R1882X and p.Y3035S.

Supplementary Figure 2: Western blot of ectopically expressed full-length wildtype and mutant hBRCA2 protein in VC8 DR-GFP cells that were subjected to HDR assay.

Supplementary Figure 3. Purification of wildtype and mutant BRCA2 from human cells.

(A) Scheme of the purification protocol of full-length BRCA2 proteins from human cells. (B) SDS-PAGE of purified wildtype and mutant BRCA2 proteins tagged with GFP-MBP at the N terminus. WT, wildtype. (C) Western blot (WB) of purified BRCA2 with an antibody specific for the C-terminal region of BRCA2 (CA1033, EMD).

Supplementary Figure 4. Position of BRCA2 DNA binding domain (DBD) variants on a ribbon diagram of the murine DBD crystal structure.

Ribbon diagram of the crystal structure of the mouse BRCA2 DBD-DSS1-ssDNA (PDB ID: 1MJE) generated using MacPyMOL (Molecular Graphics version 1.3.) highlighting the location of the variants analyzed by EMSA. The location of the known deleterious variant p.D2723H is shown in yellow. The human variants displaying a neutral phenotype (G2058, K2729, A2717) are shown in blue. The position of the variant reducing the DNA binding activity (Y3035) is shown in red. The DNA is shown in orange and DSS1 in purple.

Table 1. Variants in *BRCA1* and *BRCA2* significantly associated with breast cancer risk in a case-control analysis

TABLE 1. VARIANTS IN *BRCA1* AND *BRCA2* SIGNIFICANTLY ASSOCIATED WITH BREAST CANCER RISK IN A CASE-CONTROL ANALYSIS

Sequence Variants[a]				Caucasian					Asian				
Gene	HGVS DNA	HGVS Protein	Protein change	Case n=41,890	Control n=41,607	OR[b]	95% CI	P-value	Case n=6,629	Control n=6,624	OR[c]	95% CI	P-value
BRCA1	c.2521C>T	p.Arg841Trp	R841W	160	207	0.81	0.66-1.00	0.045	1	0	-	-	-
	c.4327C>T	p.Arg1443Ter	R1443X	9	1	8.3	1.05- 5.95	0.045	1	1	1.5	0.09-25.75	0.764
	c.5096G>A	p.Arg1699Gln	R1699Q	16	4	4.3	1.43-12.85	0.009	0	0	ND		-
BRCA2	c.4258G>T	p.Asp1420Tyr	D1420Y	657	749	0.86	0.77 -0.96	0.005	6	8	1.01	-	0.99
	c.7522G>A	p.Gly2508Ser	G2508S	0	0	ND	-	-	31	12	2.7	1.37-5.23	0.004
	c.8149G>T	p.Ala2717Ser	A2717S	137	185	0.8	0.62-0.96	0.02	0	0	ND	-	-
	c.8187G>T	p.Lys2729Asn	K2729N	3	1	2.8	0.29-27.64	0.368	164	128	1.4	1.12-1.78	0.004
	c.9104A>C	p.Tyr3035Ser	Y3035S	18	7	2.5	1.05-6.05	0.038	3	0	ND	-	-
	c.9292T>C	p.Tyr3098His	Y3098H	14	20	0.7	0.35-1.38	0.304	0	0	ND	-	-

[a] Nucleotide numbering in the reference sequences of BRCA1: NM_007294.3 ; BRCA2: NM_000059.3

b. Adjusted for 6 European ancestry principal components

c. Adjusted for 2 Asian ancestry principal components OR : odds ratio

CI: Confidence interval ND: Not determined

Figure 1

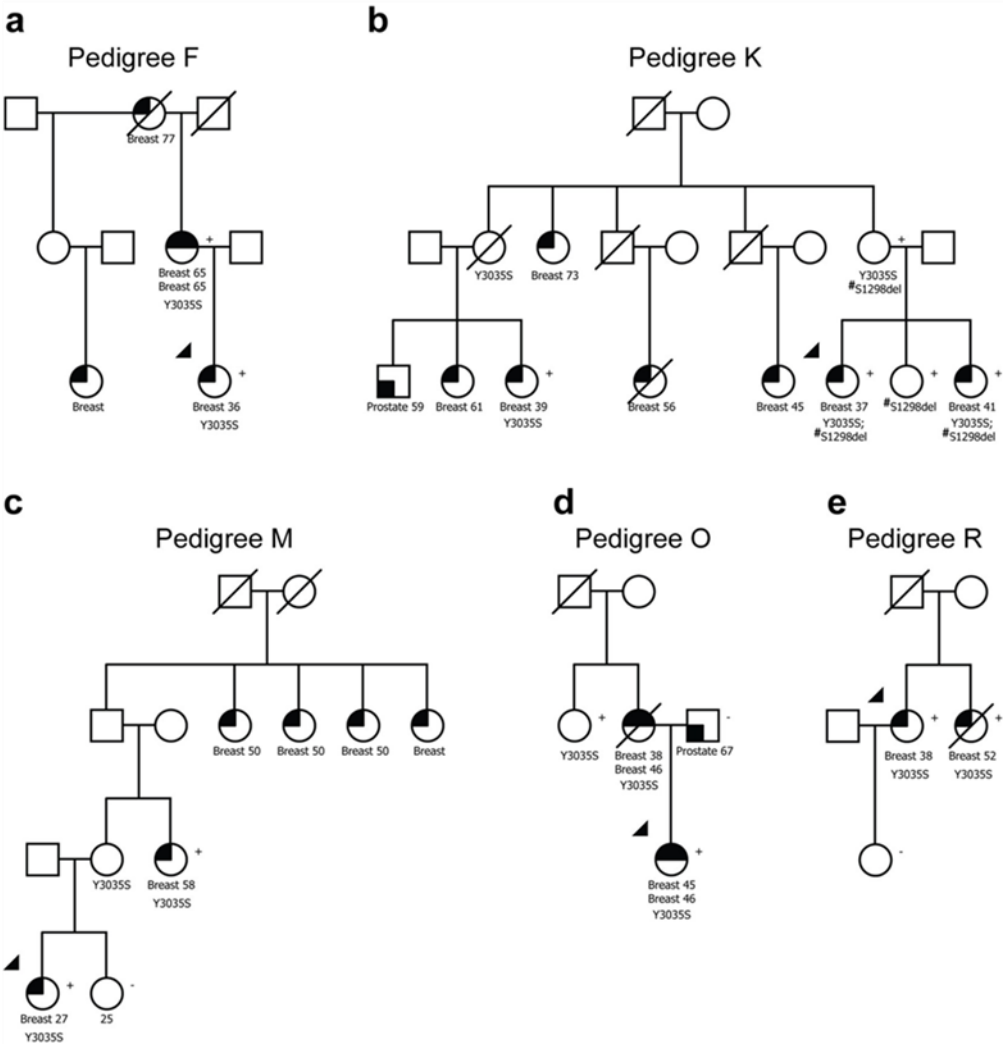
a
Pedigree F
Breast 77
Breast 65
Breast 65
Y3035S
Breast
Breast 36
Y3035S
b
Pedigree K
Y3035S
Breast 73
Y3035S
#S1298del
Prostate 59
Breast 61
Breast 39
Y3035S
Breast 56
Breast 45
Breast 37
Y3035S;
#S1298del
#S1298del
Breast 41
Y3035S;
#S1298del
c
Pedigree M
Breast 50
Breast 50
Breast 50
Breast
Y3035S
Breast 58
Y3035S
Breast 27
Y3035S
25
d
Pedigree O
Y3035S
Breast 38
Breast 46
Y3035S
Prostate 67
Breast 45
Breast 46
Y3035S
e
Pedigree R
Breast 38
Y3035S
Breast 52
Y3035S

Figure 2

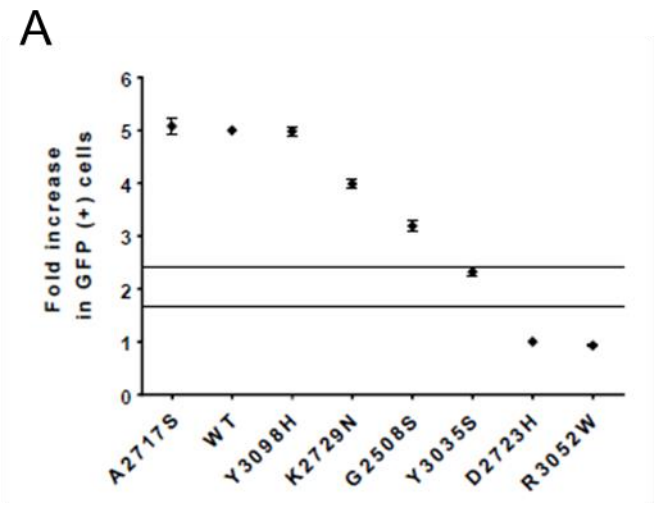
A
Fold increase in GFP (+) cells
0
1
2
3
4
5
6
A2717S
WT
Y3098H
K2729N
G2508S
Y3035S
D2723H
R3052W

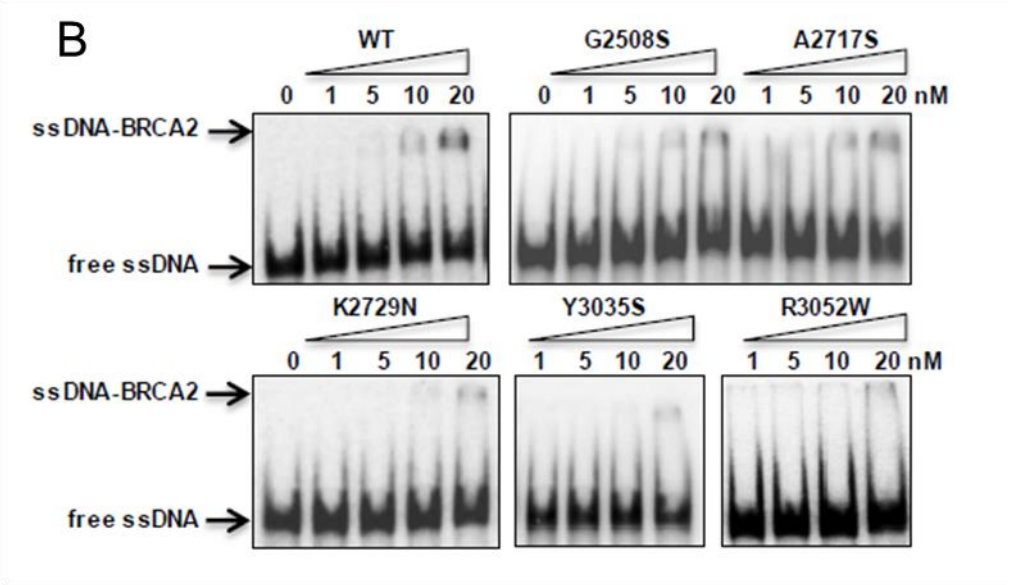
B
WT
G2508S
A2717S
0 1 5 10 20
0 1 5 10 20
1 5 10 20 nM
ssDNA-BRCA2
free ssDNA
K2729N
Y3035S
R3052W
0 1 5 10 20
1 5 10 20
1 5 10 20 nM
ssDNA-BRCA2
free ssDNA

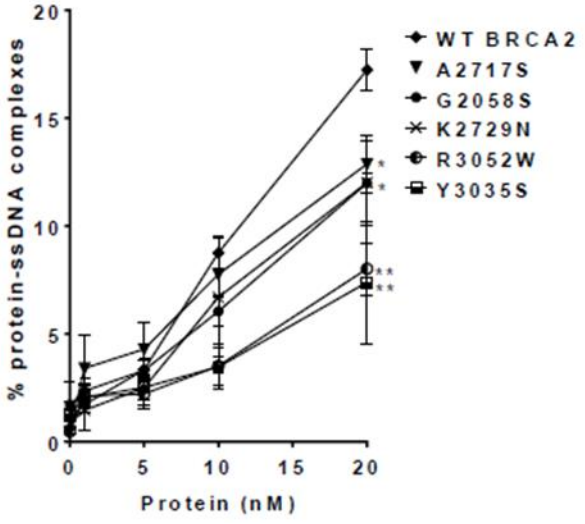
C
% protein-ssDNA complexes
0
5
10
15
20
Protein (nM)
WT BRCA2
A2717S
G2058S
K2729N
R3052W
Y3035S
*
*
**
**

Figure 3

A

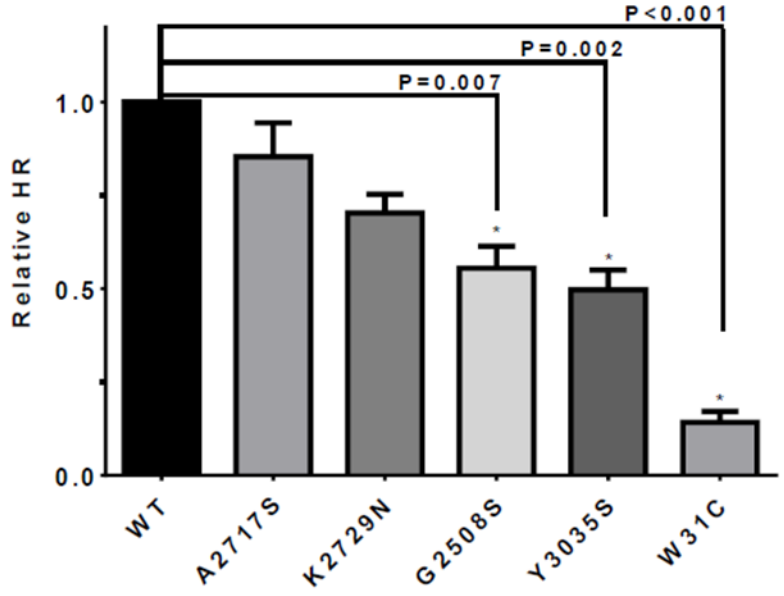
P<0.001
P=0.002
P=0.007
Relative HR
1.0
0.5
0.0
WT
A2717S
K2729N
G2508S
Y3035S
W31C

B

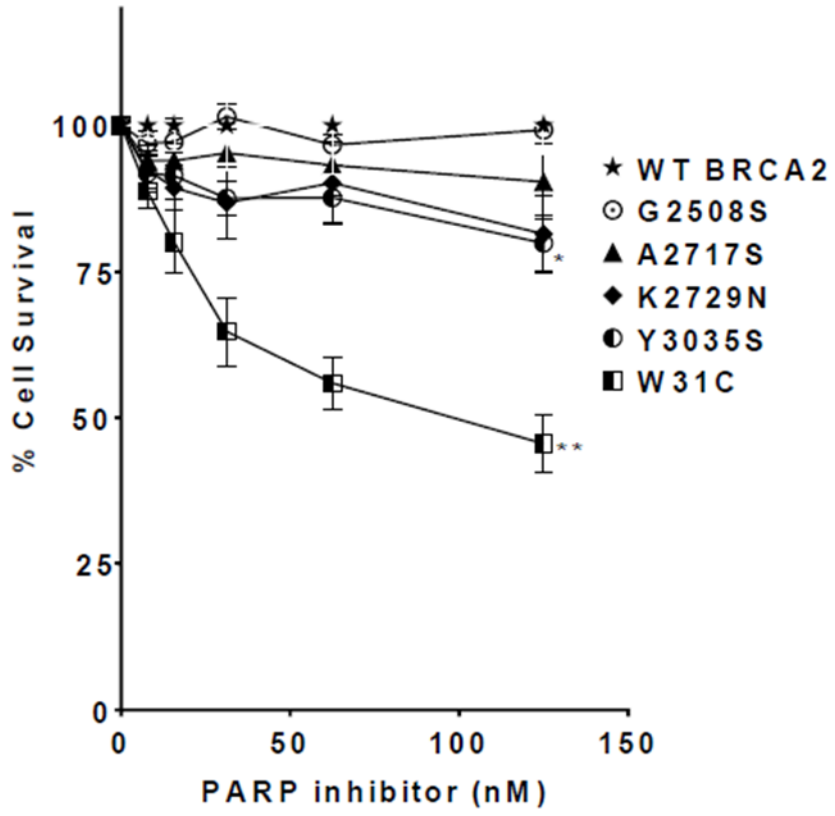
% Cell Survival
100
75
50
25
0
0
50
100
150
PARP inhibitor (nM)
WT BRCA2
G2508S
A2717S
K2729N
Y3035S
W31C

Supplementary Figure 1

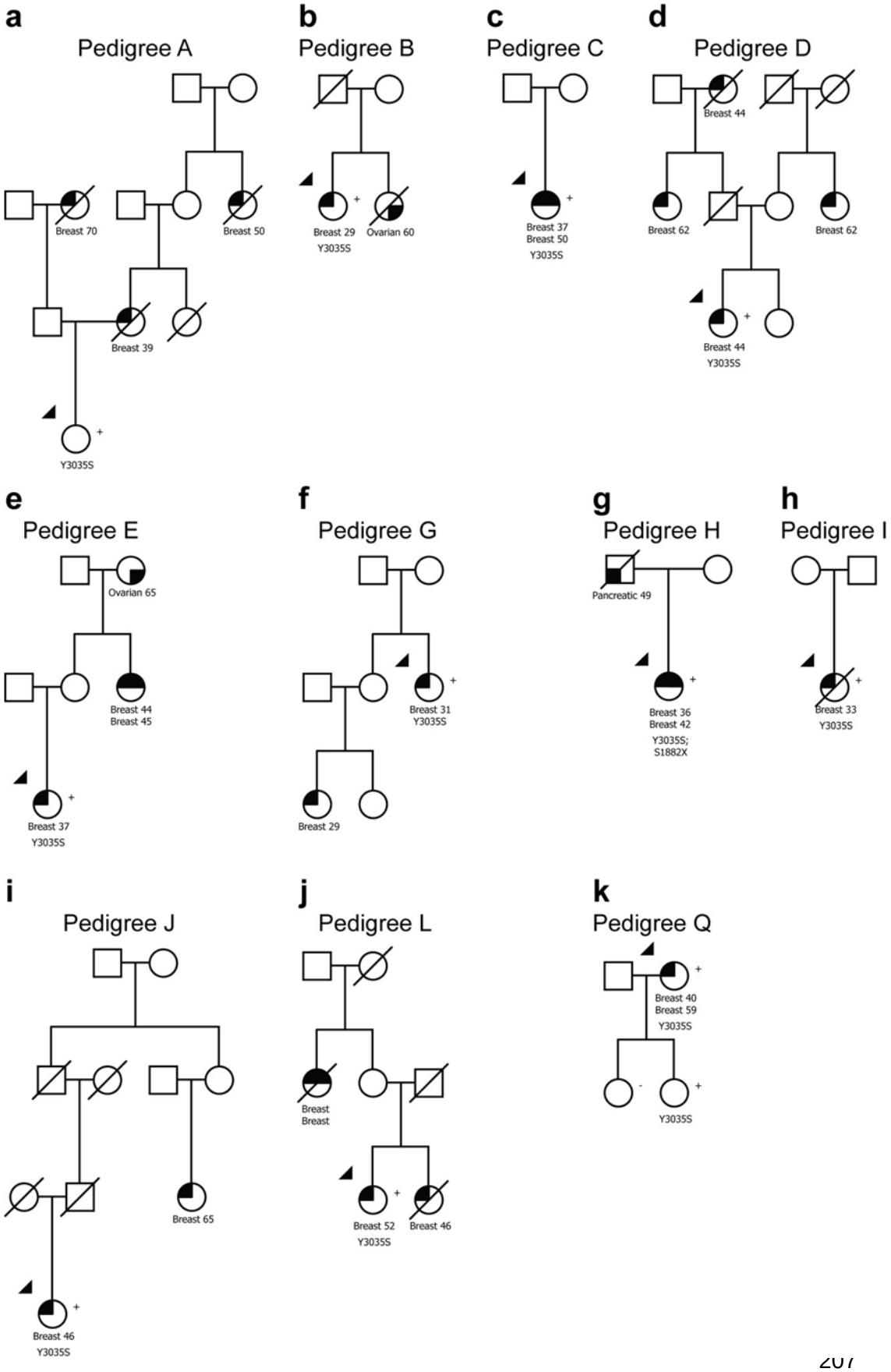

Supplementary Figure 2

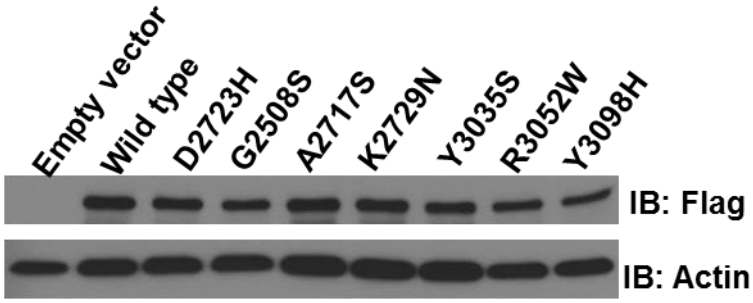

Supplementary Figure 3

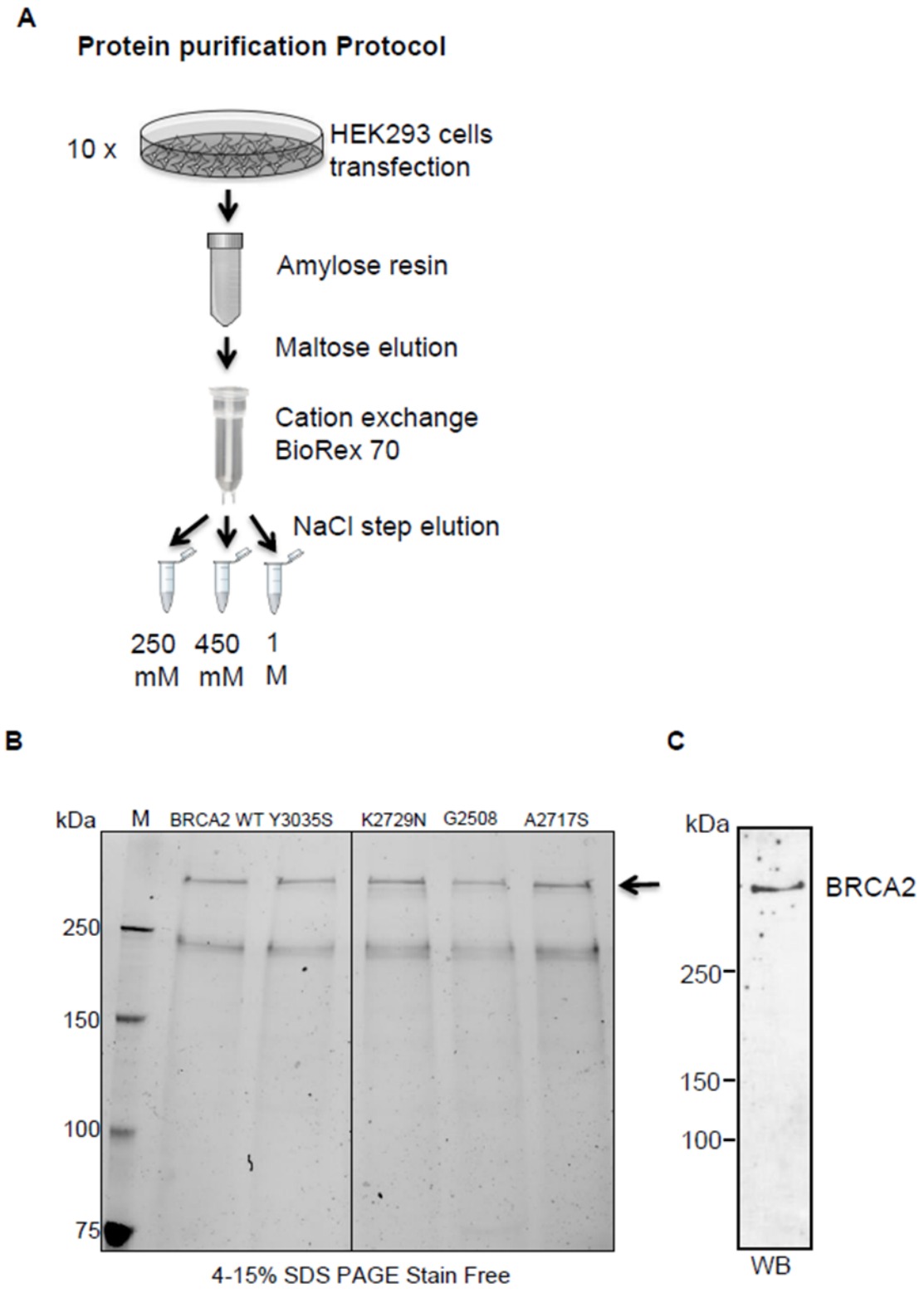

Supplementary Figure 4

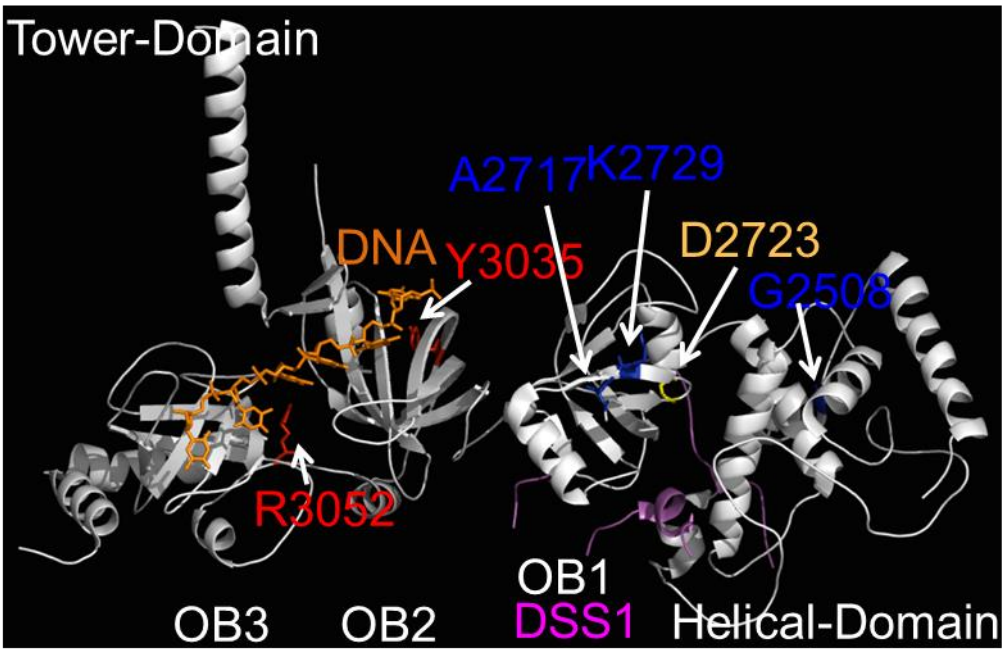

6. FINAL CONCLUSIONS

During my PhD thesis presented here, we were able to uncover new functional aspects of the tumor suppressor protein BRCA2 and evaluate the impact of several variants of unknown clinical significance (VUS) found in breast cancer patients which is illustrated in Figure 1 and 2.

THE N-TERMINUS OF BRCA2 POSSESSES A DNA BINDING DOMAIN

In the study presented in Chapter 2, we identified an N-terminal DNA binding domain (Figure 1 B).

This region, containing a putative zinc finger PARP like domain (zf PARP) unraveled by *in silico* analysis showed DNA binding activity in vitro. As the fragment utilized comprises aa 250-500, it remains to be established whether the DNA binding activity specifically requires the zf PARP domain (267-349), however, the prediction of DNA binding residues coincides with the zf-PARP domain suggesting that this is indeed the case. Moreover the cysteine residues that supposed to be important for the correct assembly of the zinc finger motif showed a reduced DNA binding activity when mutated further supporting this hypothesis.

We observed that NTD and CTD share similar structure specificities but the NTD has a generally higher affinity for DNA. One unexpected result was the ability of the NTD to associate with dsDNA. This revealed a hitherto unknown feature of the DNA binding capacity of BRCA2 that showed only high affinity to ssDNA and tail substrates until this work [70,127]. However, this dsDNA binding activity is most likely responsible for the weak dsDNA binding capacity observed with the full-length BRCA2 protein [70](ref Jensen et al., 2010).

We could show that the NTD can stimulate RAD51 strand exchange activity between RPA-coated ssDNA and homologous dsDNA. We propose that the NTD has a mediator activity by facilitating the loading of RAD51 on substrates with a ssDNA/dsDNA junction due to its high affinity for dsDNA, although it can also stimulate the DNA strand exchange activity of RAD51 on ssDNA.

In the model presented in Chapter 2 (2.3, Figure 18), the NTD and CTD could thus act consecutively at DSBs or daughter strand gaps to facilitate RAD51 loading at the ssDNA/dsDNA junctions. The NTD would be responsible for the binding at the ssDNA/dsDNA junction rendering RPA-coated ssDNA accessible for RAD51 loading by the BRC repeats [124]. The CTD/DSS1 complex could then further promote RAD51 filament

growth by replacing RPA at multiple sites as proposed [69,158]. It remains unclear whether the two DNA binding domains act together on the same substrate in the context of full-length BRCA2 or if they have specialized functions depending on the nature of the DNA damage.

It is also of great interest how the two binding modules coordinate BRCA2 activity *in vivo.* As a part of this study we wanted to investigate if NTD together with a BRC repeat can rescue the phenotype of *BRCA2* deficient cells in response to DNA damage as it was shown for the CTD and proposed for the N-terminus [152,109,157]. So far, despite several attempts, we have not been able to establish an *in cellulo* system with *BRCA2*$^{-/-}$ background to test the $BRCA2_{BRC4\text{-}T2}$ construct. We are currently working on a human FLP-IN system in HEK293 cells in which we can downregulate endogenous *BRCA2* and simultaneously induce the expression of $BRCA2_{T2\text{-}BRC4}$ from a gene locus.

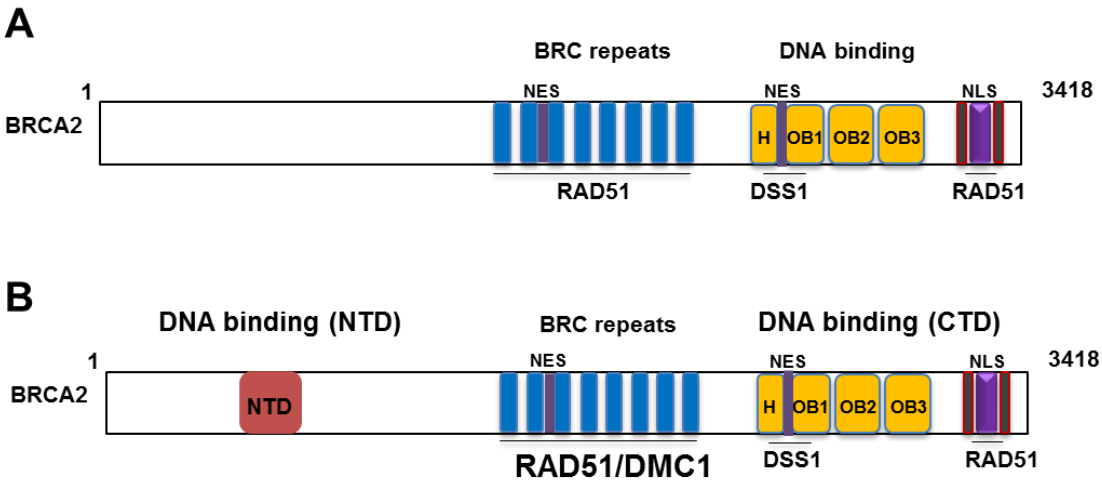

Figure 1: BRCA2 structure with known functional domains and interaction partners. State of the art **A)** before and **B)** after this study showing the identified DNA binding domain in the N-terminus and the DMC1 interaction site at the BRC repeats. Note that not all interaction partners are illustrated.

We will also make use of this system to evaluate the HR capacity of the VUS defective in DNA binding. In this way, we will know if the NTD is sufficient to perform BRCA2 recombination function in cells and at the same time, evaluate the impact of VUS on BRCA2 function which was the focus of my **second objective** (1.14).

VARIANTS OF UNKNOWN CLINICAL SIGNIFICANCE LOCATED IN THE NTD SHOW DEFECTS IN DNA REPAIR AND CYTOKINESIS

We selected VUS located in the DNA binding domain that sufficiently met the criteria for a high probability to exhibit a deleterious phenotype. We subjected these variants to established functional assays [212,118,165,213,164] to evaluate their phenotype in DNA repair and cytokinesis (Figure 2). As described in Chapter 3.2, we found that some missense mutations in the NTD can affect the DNA repair capacity of BRCA2. Moreover, the variants showed cytokinetic delay or failure speaking for defects in the midbody formation and/or abscission as described before [118]. In summary, we observed that one VUS selected in the NTD in Exon 10, G267E, has an impact on BRCA2's functionality cytokinesis (see 3.3, Table 2). The cytokinetic defect observed might be due to a defective localization of BRCA2 to the midbody or interaction with players involved in abscission. By application of more functional assays as described in 3.4, we will be able to further evaluate the phenotype of the VUS in the NTD. Currently, we are testing the purified variants in $BRCA2_{T2}$ in DNA binding assays as described for the cysteine mutants (2.2). Supported by our findings in Chapter 2 it would be interesting to know if C315S also exhibits a phenotype in cytokinesis. So far, we have been able to show that the DNA binding activity of the NTD contributes to the recombination function of BRCA2.
In the future, both the identification of the NTD as well as established functional assays for VUS located in this region will be of advantage for the genetic counseling of VUS carriers.

VUS LOCATED IN THE CTD SHOW AN INTERMEDIATE PHENOTYPE

As described in my second objective, we collaborate with several groups from the ENIGMA network for the evaluation of BRCA2 VUS. In a side project, I contributed to a publication that focused on the evaluation of VUS that had been rated to confer a moderate or increased risk by using likelihood models. *BRCA2* hypomorphic mutations can lead to the expression of proteins that retain partially their functions and thus have an intermediate phenotype. By testing purified variants in DNA binding assays *in vitro*, I could confirm the results observed in *cellulo* assays by our collaborators (Chapter 5.2, Figure 3 and 5.4 Figure 2 & 3). This is the first study that showed the existence of intermediate risk variants and highlights the importance to combine functional assays with case-control studies to optimize the accurate predictions for the impact of VUS on BRCA2 function and on cancer risk.

In Figure 2 I illustrate the variants selected and evaluated in these two studies (Chapter 3 and 5).

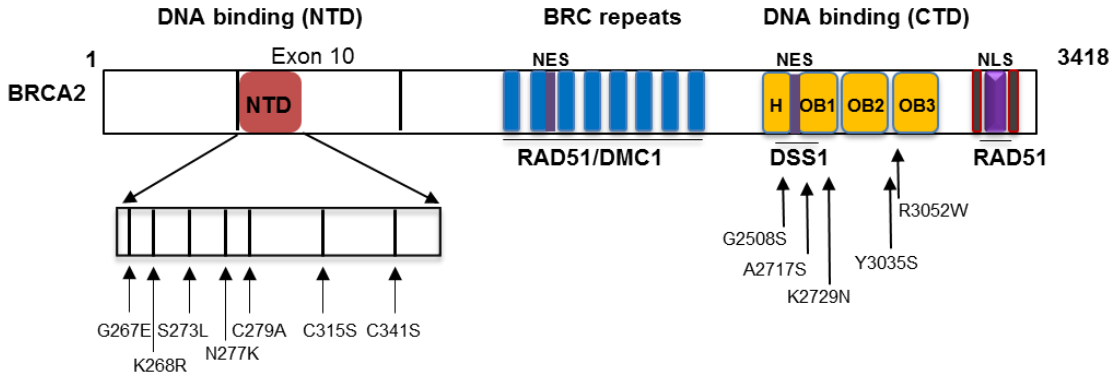

Figure 2: Variants of unknown clinical significance in the NTD and CTD of BRCA2 that were selected and evaluated in this thesis.

BRCA2 REGULATES DMC1 – MEDIATED RECOMBINATION THROUGH THE BRC REPEATS

In the third objective of my PhD I collaborated with JSM from the lab to investigate if BRCA2 mediates DMC1 recombination activity in meiosis as it was shown for RAD51 in mitosis [70]. BRCA2 was shown to be implicated in meiosis and its absence causes infertility and chromosomal aberration [180,181]. In addition, it was shown that BRCA2 and DMC1 interact, however the mechanism and reason for this interaction remained enigmatic [70,92,184].

In our study we revealed that DMC1 interacts with BRCA2 via the BRC repeats (Figure 1B) to stimulate its association with ssDNA and the formation of nucleoprotein filaments (4.2, Figure 8). Moreover, BRCA2 alleviates the kinetic barrier posed by RPA bound to the ssDNA, making it accessible for DMC1 loading. These findings established BRCA2 as a mediator protein of DMC1 recombination in meiosis. Our model is consistent with an accessory role of RAD51 in meiotic recombination as described before in yeast [93,95]. In this model, BRCA2 would bind RAD51 monomers via BRC1-5 to provide a filament that serves as a starting nucleus for DMC1 to allow homofilament assembly on the ssDNA. The DMC1 filament could then grow and start homology search and strand invasion.

In summary, in my PhD I contributed to reveal new functions of BRCA2 in the N-terminus (NTD, cytokinetic defects associated with G267E) but also in the BRC repeats (DMC1 binding) and the C-terminus (residues important for DNA binding, CTD future crystal structure). In addition, we have established new functional assays for the evaluation of BRCA2 variants. In turn, these findings will proof useful for the classification of BRCA2 VUS.

REFERENCES

1. Jackson, S. & Bartek, J. The DNA-damage response in human biology and disease. *Nature* **461,** 1071–1078 (2009).

2. Hoeijmakers, J. H. J. Genome maintenance mechanisms for preventing cancer. *DNA Repair (Amst).* **411,** 366–374 (2001).

3. Khanna, K. K., Lavin, M. F., Jackson, S. P. & Mulhern, T. D. ATM , a central controller of cellular responses to DNA damage. *Cell Death Differ.* 1052–1065 (2001).

4. Zeman, M. K. & Cimprich, K. A. Causes and consequences of replication stress. *Nat. Cell Biol.* **16,** 2–9 (2014).

5. Williams, R. S., Williams, J. S. & Tainer, J. A. Mre11–Rad50–Nbs1 is a keystone complex connecting DNA repair machinery, double-strand break signaling, and the chromatin template. *Biochem. Cell Biol.* **85,** 509–520 (2007).

6. Zhou, B. S. & Elledge, S. J. The DNA damage response: putting checkpoints in perspective. *Nature* **408,** 433–439 (2000).

7. Jeggo, P. A., Pearl, L. H. & Carr, A. M. DNA repair, genome stability and cancer: a historical perspective. *Nat. Rev. Cancer* 1–8 (2015).

8. Ciccia, A. & Elledge, S. J. The DNA Damage Response: Making It Safe to Play with Knives. *Mol. Cell* **40,** 179–204 (2010).

9. Shiloh, Y. ATM and related protein kinases: safeguarding genome integrity. *Nat. Rev. Cancer* **3,** 155–168 (2003).

10. Huen, M. & Chen, J. The DNA damage response pathways: at the crossroad of protein modifications. *Cell Res.* **18,** 8–16 (2008).

11. Harper, J. W. & Elledge, S. J. The DNA damage response: ten years after. *Mol. Cell* **28,** 739–45 (2007).

12. Fu, D., Calvo, J. A. & Samson, L. D. Balancing repair and tolerance of DNA damage caused by alkylating agents. *Nat. Rev. Cancer* **12,** 104–20 (2012).

13. Goldstein, M. & Kastan, M. B. The DNA damage response: implications for tumor responses to radiation and chemotherapy. *Annu. Rev. Med.* **66,** 129–43 (2015).

14. Sharma, R. A. & Dianov, G. L. Targeting base excision repair to improve cancer therapies. *Mol. Aspects Med.* **28,** 345–374 (2007).

15. Robertson, A. B., Klungland, A., Rognes, T. & Leiros, I. Base excision repair: The long and short of it. *Cell. Mol. Life Sci.* **66,** 981–993 (2009).

16. Fromme, B. J. C. & Verdine, G. L. BASE EXCISION REPAIR. *Adv. Protein Chem.* **69,** 1–41 (2004).

17. Sancar, A., Lindsey-Boltz, L. A., Ünsal-Kaçmaz, K. & Linn, S. Molecular Mechanisms of Mammalian DNA Repair and the DNA Damage checkpoints. *Annu.*

Rev. Biochem. **73,** 39–85 (2004).

18. Marteijn, J. a, Lans, H., Vermeulen, W. & Hoeijmakers, J. H. J. Understanding nucleotide excision repair and its roles in cancer and ageing. *Nat. Rev. Mol. Cell Biol.* **15,** 465–81 (2014).

19. Cleaver, J. E., Lam, E. T. & Revet, I. Disorders of nucleotide excision repair: the genetic and molecular basis of heterogeneity. *Nat. Rev. Genet.* **10,** 756–768 (2009).

20. Diderich, K., Alanazi, M. & Hoeijmakers, J. H. J. Premature aging and cancer in nucleotide excision repair-disorders. *DNA Repair (Amst).* **10,** 772–80 (2011).

21. Fukui, K. DNA mismatch repair in eukaryotes and bacteria. *J. Nucleic Acids* **2010,** (2010).

22. Fukui, K., Shimada, A., Iino, H., Masui, R. & Kuramitsu, S. *Biochemical properties of MutL, a DNA mismatch repair endonuclease*. *DNA Repair - On the Pathways to Fixing DNA Damage and Errors* (2011).

23. Li, G.-M. Mechanisms and functions of DNA mismatch repair. *Cell Res.* **18,** 85–98 (2008).

24. Iyer, R. R., Pluciennik, A., Burdett, V. & Modrich, P. L. DNA mismatch repair: functions and mechanisms. *Chem. Rev.* **106,** 302–23 (2006).

25. Gelot, C., Magdalou, I. & Lopez, B. S. Replication stress in mammalian cells and its consequences for mitosis. *Genes (Basel).* **6,** 267–298 (2015).

26. Ghosal, G. & Chen, J. DNA damage tolerance: a double-edged sword guarding the genome. *Transl. Cancer Res.* **2,** 107–129 (2013).

27. Branzei, D. & Foiani, M. Interplay of replication checkpoints and repair proteins at stalled replication forks. *DNA Repair (Amst).* **6,** 994–1003 (2007).

28. Lambert, S. & Carr, A. M. Impediments to replication fork movement: Stabilisation, reactivation and genome instability. *Chromosoma* **122,** 33–45 (2013).

29. Yeeles, J. T. P., Poli, J., Kenneth, J. & Pasero, P. Rescuing Stalled or Damaged Replication Forks. *Perspect. Biol.* 1–16 (2013).

30. Lehmann, A. R. Translesion synthesis in mammalian cells. *Exp. Cell Res.* **312,** 2673–2676 (2006).

31. Costes, A. & Lambert, S. Homologous Recombination as a Replication Fork Escort: Fork-Protection and Recovery. *Biomolecules* **3,** 39–71 (2012).

32. Heyer, W.-D., Ehmsen, K. T. & Liu, J. Regulation of homologous recombination in eukaryotes. *Annu. Rev. Genet.* **44,** 113–39 (2010).

33. Budzowska, M. & Kanaar, R. Mechanisms of dealing with DNA damage-induced replication problems. *Cell Biochem. Biophys.* **53,** 17–31 (2009).

34. Atkinson, J. & McGlynn, P. Replication fork reversal and the maintenance of genome stability. *Nucleic Acids Res.* **37,** 3475–3492 (2009).

35. Schlacher, K. *et al.* Double-Strand Break Repair-Independent Role for BRCA2 in Blocking Stalled Replication Fork Degradation by MRE11. *Cell* **145,** 529–42 (2011).

36. Burrell, R. A. *et al.* Replication stress links structural and numerical cancer chromosomal instability. *Nature* **494,** 492–496 (2013).

37. Aguilera, A. & García-Muse, T. Causes of genome instability. *Annu. Rev. Genet.* **47,** 1–32 (2013).

38. Muniandy, P., Liu, J., Majumdar, A., Liu, S. & Seidman, M. M. *DNA Interstrand Crosslink Repair in Mammalian Cells: Step by Step*. *Critical Reviews in Biochemistry and Molecular Biology* **45,** (2011).

39. Howlett, N. G. *et al.* Biallelic inactivation of BRCA2 in Fanconi anemia. *Science* **297,** 606–609 (2002).

40. Huang, Y. & Li, L. DNA crosslinking damage and cancer - a tale of friend and foe. *Transl. Cancer Res.* **2,** 144–154 (2013).

41. Branzei, D. & Foiani, M. Maintaining genome stability at the replication fork. *Nat. Rev. Mol. Cell Biol.* **11,** 208–19 (2010).

42. Barker, S., Weinfeld, M. & Murray, D. DNA-protein crosslinks: Their induction, repair, and biological consequences. *Mutat. Res.* **589,** 111–135 (2005).

43. Pommier, Y. *et al.* Tyrosyl-DNA-phosphodiesterases (TDP1 and TDP2). *DNA Repair (Amst).* **19,** 114–129 (2014).

44. Stingele, J. & Jentsch, S. DNA–protein crosslink repair. *Nat. Rev. Mol. Cell Biol.* **16,** 455–460 (2015).

45. Caldecott, K. W. DNA single-strand break repair. *Exp. Cell Res.* **329,** 2–8 (2014).

46. Caldecott, K. Single-strand break repair and genetic disease. *Nat. Rev. Genet.* **9,** 341–55 (2008).

47. Fisher, A. E. O., Hochegger, H., Takeda, S. & Caldecott, K. W. Poly (ADP-Ribose) Polymerase 1 Accelerates Single-Strand Break Repair in Concert with Poly (ADP-Ribose) Glycohydrolase. *Mol. Cell. Biol.* **27,** 5597–5605 (2007).

48. Caldecott, K. W. Mammalian single-strand break repair: Mechanisms and links with chromatin. *DNA Repair (Amst).* **6,** 443–453 (2006).

49. Caldecott, K. W. Protein ADP-ribosylation and the cellular response to DNA strand breaks. *DNA Repair (Amst).* **19,** 108–113 (2014).

50. Helleday, T., Lo, J., van Gent, D. C. & Engelward, B. P. DNA double-strand break repair: From mechanistic understanding to cancer treatment. *DNA Repair (Amst).* **6,** 923–935 (2007).

51. Aparicio, T., Baer, R. & Gautier, J. DNA double-strand break repair pathway choice and cancer. *DNA Repair (Amst).* **19,** 169–175 (2014).

52. Karagiannis, T. C. & El-Osta, A. Double-strand breaks: signaling pathways and

repair mechanisms. *Cell. Mol. Life Sci.* **61,** 2137–47 (2004).

53. O'Driscoll, M. & Jeggo, P. a. The role of double-strand break repair - insights from human genetics. *Nat. Rev. Genet.* **7,** 45–54 (2006).

54. Deriano, L. & Roth, D. B. Modernizing the nonhomologous end-joining repertoire: alternative and classical NHEJ share the stage. *Annu. Rev. Genet.* **47,** 433–55 (2013).

55. Ceccaldi, R., Rondinelli, B. & D'Andrea, A. D. Repair Pathway Choices and Consequences at the Double-Strand Break. *Trends Cell Biol.* **26,** 52–64 (2015).

56. Fugger, K. & West, S. C. Keeping homologous recombination in check. *Cell Res.* 1–2 (2016). doi:10.1038/cr.2016.25

57. Chiruvella, K. K., Liang, Z. & Wilson, E. Repair of Double-Strand Breaks by End Joining. *Cold Spring Harb Perspect Biol* **2013,** 1–22 (2013).

58. Orthwein, A. *et al.* A mechanism for the suppression of homologous recombination in G1 cells. *Nature* **528,** 422–426 (2015).

59. Sfeir, A. & Symington, L. S. Microhomology-Mediated End Joining: A Back-up Survival Mechanism or Dedicated Pathway? *Trends Biochem. Sci.* **40,** 701–714 (2015).

60. Symington, L. S. & Gautier, J. Double-Strand Break End Resection and Repair Pathway Choice. *Annu. Rev. Genet.* **45,** 247–271 (2011).

61. Kowalczykowski, S. C. An Overview of the Molecular Mechanisms of Recombinational DNA Repair. *Cold Spring Harb. Perspect. Biol.* **7,** a016410 (2015).

62. Kasparek, T. R. & Humphrey, T. C. DNA double-strand break repair pathways, chromosomal rearrangements and cancer. *Semin. Cell Dev. Biol.* **22,** 886–897 (2011).

63. Moynahan, M. E. & Jasin, M. Mitotic homologous recombination maintains genomic stability and suppresses tumorigenesis. *Nat. Rev. Mol. Cell Biol.* **11,** 196–207 (2010).

64. Sung, P. & Klein, H. Mechanism of homologous recombination : mediators and helicases take on regulatory functions. *Nat. Rev. Mol. Cell Biol.* **7,** 739–750 (2006).

65. Prakash, R., Zhang, Y., Feng, W. & Jasin, M. Homologous recombination and human health: the roles of BRCA1, BRCA2 and associated proteins. *Cold Spring Harb Perspect Biol* **7,** 1–37 (2015).

66. Jasin, M. & Rothstein, R. Repair of strand breaks by homologous recombination. *Cold Spring Harb Perspect Biol* **5,** a012740 (2013).

67. Symington, L. S. End Resection at Double-Strand Breaks : Mechanism and Regulation End Resection at Double-Strand Breaks : Mechanism and Regulation. *Cold Spring Harb Perspect Biol* (2014).

68. Sharan, S. K., Morimatsu, M., Albrecht, U. & Al., E. Embyronic Lethality and

Radiation Hypersensitivity mediated by Rad51 in mice lacking BRCA2. *Nature* **386,** (1997).

69. Zhao, W. *et al.* Promotion of BRCA2-Dependent Homologous Recombination by DSS1 via RPA Targeting and DNA Mimicry. *Mol. Cell* **59,** 176–187 (2015).

70. Jensen, R. B., Carreira, A. & Kowalczykowski, S. C. Purified human BRCA2 stimulates RAD51-mediated recombination. *Nature* **467,** 678–83 (2010).

71. Liu, J., Doty, T., Gibson, B. & Heyer, W.-D. Human BRCA2 protein promotes RAD51 filament formation on RPA-covered single-stranded DNA. *Nat. Struct. Mol. Biol.* **17,** 1260–2 (2010).

72. Thorslund, T. *et al.* The breast cancer tumor suppressor BRCA2 promotes the specific targeting of RAD51 to single-stranded DNA. *Nat. Struct. Mol. Biol.* **17,** 1263–5 (2010).

73. Jensen, R. B., Ozes, A., Kim, T., Estep, A. & Kowalczykowski, S. C. BRCA2 is epistatic to the RAD51 paralogs in response to DNA damage. *DNA Repair (Amst).* **12,** 306–11 (2013).

74. Morrical, S. W. DNA-Pairing and Annealing Processes in Homologous Recombination and Homology-directed repair. *Cold Spring Harb Perspect Biol* 1–22 (2015).

75. Zelensky, A., Kanaar, R. & Wyman, C. Mediators of homologous DNA pairing. *Cold Spring Harb. Perspect. Biol.* **6,** a016451 (2014).

76. Daley, J., Gaines, W., Kwon, Y. & Sung, P. Regulation of DNA strand exchange in homologous recombination. *Perspect. Biol.* **9,** 1264–72 (2014).

77. Heyer, W. D. Regulation of Recombination and Genomic Maintenance. *Cold Spring Harb Perspect Biol* (2015).

78. Heyer, W.-D., Li, X., Rolfsmeier, M. & Zhang, X.-P. Rad54: the Swiss Army knife of homologous recombination? *Nucleic Acids Res.* **34,** 4115–25 (2006).

79. Sebesta, M. *et al.* Role of PCNA and TLS polymerases in D-loop extension during homologous recombination in humans. *DNA Repair (Amst).* **12,** 691–698 (2013).

80. Deans, A. J. & West, S. C. DNA interstrand crosslink repair and cancer. *Nat. Rev. Cancer* **11,** 467–480 (2011).

81. Mehta, A. & Haber, J. E. Sources of DNA double-strand breaks and models of recombinational DNA repair. *Cold Spring Harb. Perspect. Biol.* **6,** (2014).

82. Heyer, W. Biochemistry of eukaryotic homologous recombination. *Curr. Genet.* **17,** (2006).

83. Filippo, J. S., Sung, P. & Klein, H. Mechanism of Eukaryotic Homologous Recombination. *Annu. Rev. Biochem.* 229–260 (2008).

84. Llorente, B., Smith, C. E. & Symington, L. S. Break-induced replication. *Cell Cycle* **7,** 859–864 (2008).

85. Malkova, A. & Grzegorz, I. Break-induced replication: functions and molecular mechanism. *Curr. Opin. Genet dev.* **141,** 520–529 (2013).

86. Khanna, K. K. & Jackson, S. P. DNA double-strand breaks : signaling , repair and the cancer connection. *Cancer Res.* **27,** 247–254 (2001).

87. Gilson, E. & Géli, V. How telomeres are replicated. *Nat. Rev. Mol. Cell Biol.* **8,** 825–38 (2007).

88. Badie, S. *et al.* BRCA2 acts as a RAD51 loader to facilitate telomere replication and capping. *Nat. Struct. Mol. Biol.* **17,** 1461–9 (2010).

89. Min, J. *et al.* The breast cancer susceptibility gene BRCA2 is required for the maintenance of telomere homeostasis. *J. Biol. Chem.* **287,** 5091–5101 (2012).

90. Lam, I. & Keeney, S. Mechanism and control of meiotic recombination initiation. *Cold Spring Harb Perspet Biol* **52,** 1–53 (2015).

91. Neale, M. J. & Keeney, S. Clarifying the mechanics of DNA strand exchange in meiotic recombination. *Nature* **442,** 153–8 (2006).

92. Thorslund, T., Esashi, F. & West, S. C. Interactions between human BRCA2 protein and the meiosis-specific recombinase DMC1. *EMBO J.* **26,** 2915–22 (2007).

93. Cloud, V., Chan, Y., Grubb, J., Budke, B. & Bishop, D. Rad51 is an accessory factor for Dmc1-mediated Joint Molecule formation during meiosis. *Science (80-.).* **337,** 1222–1225 (2012).

94. Martinez, J. S., von Nicolai C., *et al.* BRCA2 regulates DMC1-mediated recombination through the BRC repeats. *PNAS* **33,** 1–6 (2016).

95. Bishop, D. K. Rad51, the lead in mitotic recombinational DNA repair, plays a supporting role in budding yeast meiosis. *Cell Cycle* **11,** 4105–6 (2012).

96. Marston, A. L. & Amon, A. Meiosis: cell-cycle controls shuffle and deal. *Nat. Rev. Mol. Cell Biol.* **5,** 983–997 (2004).

97. Couch, F. J., Nathanson, K. L. & Offit, K. Two decades after BRCA: setting paradigms in personalized cancer care and prevention. *Science* **343,** 1466–70 (2014).

98. Patel, K. J. *et al.* Involvement of Brca2 in DNA repair. *Mol. Cell* **1,** 347–57 (1998).

99. Wong, A. K. C., Pero, R., Ormonde, P. A., Tavtigian, S. V & Bartel, P. L. RAD51 Interacts with the Evolutionarily Conserved BRC Motifs in the Human Breast. *Biochemistry* 1–4 (1997).

100. Lee, H. Cycling with BRCA2 from DNA repair to mitosis. *Exp. Cell Res.* **329,** 78–84 (2014).

101. Lo, T., Pellegrini, L., Venkitaraman, A. R. & Blundell, T. L. Sequence fingerprints in BRCA2 and RAD51: implications for DNA repair and cancer. *DNA Repair (Amst).* **2,** 1015–1028 (2003).

102. Martinez, J. S., Baldeyron, C. & Carreira, A. Molding BRCA2 function through its interacting partners. *Cell Cycle* **14,** 3389–3395 (2015).

103. Prilusky, J. *et al.* FoldIndex(C): a simple tool to predict whether a given protein sequence is intrinsically unfolded. *Bioinformatics* **21,** 3435–3438 (2005).

104. Oldfield, C. J. & Dunker, A. K. Intrinsically Disordered Proteins and Intrinsically Disordered Protein Regions. *Annu. Rev. Biochem.* **83,** 553–584 (2014).

105. Zhang, F. *et al.* Report PALB2 Links BRCA1 and BRCA2 in the DNA-Damage Response. *Curr. Biol.* **19,** 524–529 (2009).

106. Xia, B. *et al.* Control of BRCA2 Cellular and Clinical Functions by a Nuclear Partner , PALB2. 719–729 (2006). doi:10.1016/j.molcel.2006.05.022

107. Oliver, A. W., Swift, S., Lord, C. J., Ashworth, A. & Pearl, L. H. Structural basis for recruitment of BRCA2 by PALB2. *EMBO Rep.* **10,** 990–6 (2009).

108. Buisson, R. *et al.* Cooperation of breast cancer proteins PALB2 and piccolo BRCA2 in stimulating homologous recombination. *Nat. Struct. Mol. Biol.* **17,** 1247–54 (2010).

109. Al Abo, M. *et al.* Compensatory functions and interdependency of the DNABinding domain of BRCA2 with the BRCA1-PALB2-BRCA2 complex. *Cancer Res.* **74,** 797–807 (2014).

110. Milner, J., Ponder, B., Hughes-Davies, L., Seltmann, M. & Kouzarides, T. Transcriptional activation functions of BRCA2. *Nature* **386,** 772–773 (1997).

111. Hughes-Davies, L. *et al.* EMSY Links the BRCA2 Pathway. **115,** 523–535 (2003).

112. Lin, H. R., Ting, N. S. Y., Qin, J. & Lee, W. H. M phase-specific phosphorylation of BRCA2 by polo-like kinase 1 correlates with the dissociation of the BRCA2-P/CAF complex. *J. Biol. Chem.* **278,** 35979–35987 (2003).

113. Lee, M., Daniels, M. J. & Venkitaraman, A. R. Phosphorylation of BRCA2 by the Polo-like kinase Plk1 is regulated by DNA damage and mitotic progression. *Oncogene* **23,** 865–872 (2004).

114. Takaoka, M., Saito, H., Takenaka, K., Miki, Y. & Nakanishi, A. BRCA2 phosphorylated by PLK1 moves to the midbody to regulate cytokinesis mediated by nonmuscle myosin IIC. *Cancer Res.* **74,** 1518–1528 (2014).

115. Yata, K. *et al.* BRCA2 coordinates the activities of cell-cycle kinases to promote genome stability. *Cell Rep.* **7,** 1547–1559 (2014).

116. Fuks, F., Milner, J. & Kouzarides, T. BRCA2 associates with acetyltransferase activity when bound to P/CAF. *Oncogene* **17,** 2531–4 (1998).

117. Choi, E. *et al.* BRCA2 Fine-Tunes the Spindle Assembly Checkpoint through Reinforcement of BubR1 Acetylation. *Dev. Cell* **22,** 295–308 (2012).

118. Mondal, G. *et al.* BRCA2 localization to the midbody by filamin A regulates cep55 signaling and completion of cytokinesis. *Dev. Cell* **23,** 137–52 (2012).

119. Han, X., Saito, H., Miki, Y. & Nakanishi, A. A CRM1-mediated nuclear export signal governs cytoplasmic localization of BRCA2 and is essential for centrosomal localization of BRCA2. *Oncogene* **27,** 2969–2977 (2008).

120. Pellegrini, L. *et al.* Insights into DNA recombination from the structure of a RAD51-BRCA2 complex. *Nature* **420,** 287–93 (2002).

121. Bork, P., Blomberg, N. & Nilges, M. Internal repeats in the BRCA2 sequence. *Nat. Genet.* **13,** 22–23 (1996).

122. Bignell, G., Micklem, G., Stratton, M. R., Ashworth, A. & Wooster, R. The BRC repeats are conserved in mammalian BRCA2 proteins. *Genome* **6,** 53–58 (1997).

123. Carreira, A. *et al.* The BRC repeats of BRCA2 modulate the DNA-binding selectivity of RAD51. *Cell* **136,** 1032–43 (2009).

124. Carreira, A. & Kowalczykowski, S. C. Two classes of BRC repeats in BRCA2 promote RAD51 nucleoprotein filament function by distinct mechanisms. *Proc. Natl. Acad. Sci. U. S. A.* **108,** 10448–53 (2011).

125. Marmorstein, L. Y. *et al.* A human BRCA2 complex containing a structural DNA binding component influences cell cycle progression. *Cell* **104,** 247–257 (2001).

126. Lee, M., Daniels, M. J., Garnett, M. J. & Venkitaraman, A. R. A mitotic function for the high-mobility group protein HMG20b regulated by its interaction with the BRC repeats of the BRCA2 tumor suppressor. *Oncogene* **30,** 3360–3369 (2011).

127. Yang, H. *et al.* BRCA2 function in DNA binding and recombination from a BRCA2-DSS1-ssDNA structure. *Science* **297,** 1837–48 (2002).

128. Filippo, J. S., Chi, P., Sehorn, M. G., Etchin, J. & Krejci, L. Recombination Mediator and Rad51 Targeting Activities of a. *J. Biol. Chem.* **281,** 11649–11657 (2007).

129. Li, J. *et al.* DSS1 is required for the stability of BRCA2. *Oncogene* **25,** 1186–1194 (2006).

130. Kristensen, C. N., Bystol, K. M., Li, B., Serrano, L. & Brenneman, M. A. Depletion of DSS1 protein disables homologous recombinational repair in human cells. *Mutat. Res.* **694,** 60–4 (2010).

131. Jeyasekharan, A. D. *et al.* A cancer-associated BRCA2 mutation reveals masked nuclear export signals controlling localization. *Nat. Struct. Mol. Biol.* **20,** 1191–8 (2013).

132. Rajagopalan, S., Andreeva, A., Rutherford, T. J. & Fersht, A. R. Mapping the physical and functional interactions between the tumor suppressors p53 and BRCA2. *Proc. Natl. Acad. Sci.* **107,** 8587–8592 (2010).

133. Esashi, F. *et al.* CDK-dependent phosphorylation of BRCA2 as a regulatory mechanism for recombinational repair. *Nature* **434,** (2005).

134. Spain, B., Larson, C., Shihabuddin, L., Gage, F. & Verma, I. Truncated BRCA2 is cytoplasmic : Implications for cancer-linked mutations. *PNAS* **96,** 13920–13925 (1999).

135. Katagiri, T. *et al.* Multiple possible sites of BRCA2 interacting with DNA repair protein RAD51. *Genes Chromosom. Cancer* **21,** 217–222 (1998).

136. Yuan, S. F., Lee, S. & Chen, G. BRCA2 Is Required for Ionizing Radiation-induced Assembly of Rad51 Complex in Vivo Advances in Brief Complex in Vivo. *Cancer Res.* 3547–3551 (1999).

137. Yu, V. P. *et al.* Gross chromosomal rearrangements and genetic exchange between nonhomologous chromosomes following BRCA2 inactivation. *Genes Dev.* **14,** 1400–1406 (2000).

138. Tal, A., Arbel-Goren, R. & Stavans, J. Cancer-Associated Mutations in BRC Domains of BRCA2 Affect Homologous Recombination Induced by Rad51. *J. Mol. Biol.* **393,** 1007–1012 (2009).

139. Tutt, A. *et al.* Mutation in Brca2 stimulates error-prone homology-directed repair of DNA double-strand breaks occurring between repeated sequences. *EMBO J.* **20,** (2001).

140. Xia, F. *et al.* Deficiency of human BRCA2 leads to impaired homologous recombination but maintains normal nonhomologous end joining. *Proc. Natl. Acad. Sci. U. S. A.* **98,** 8644–8649 (2001).

141. Davies, A. A. *et al.* Role of BRCA2 in control of the RAD51 recombination and DNA repair protein. *Mol. Cell* **7,** 273–82 (2001).

142. Moynahan, M. E., Pierce, A. J. & Jasin, M. BRCA2 Is Required for Homology-Directed Repair of Chromosomal Breaks. *Mol. Cell* **7,** 263–272 (2001).

143. Stark, J. M., Pierce, A. J., Oh, J., Pastink, A. & Jasin, M. Genetic Steps of Mammalian Homologous Repair with Distinct Mutagenic Consequences. *Mol. Cell. Biol.* **24,** 9305–9316 (2004).

144. Liu, J. & Heyer, W. Who's who in human recombination: BRCA2 and RAD52. **108,** 441–442 (2011).

145. Krejci, L., Altmannova, V., Spirek, M. & Zhao, X. Homologous recombination and its regulation. *Nucleic Acids Res.* **40,** 5795–5818 (2012).

146. Rajendra, E. & Venkitaraman, A. R. Two modules in the BRC repeats of BRCA2 mediate structural and functional interactions with the RAD51 recombinase. *Nucleic Acids Res.* **38,** 82–96 (2010).

147. Shivji, M. K. K. *et al.* The BRC repeats of human BRCA2 differentially regulate RAD51 binding on single- versus double-stranded DNA to stimulate strand exchange. *PNAS* **106,** 13254–13259 (2009).

148. Gudmundsdottir, K., Lord, C. J. & Ashworth, a. The proteasome is involved in determining differential utilization of double-strand break repair pathways. *Oncogene* **26,** 7601–7606 (2007).

149. Esashi, F., Galkin, V. E., Yu, X., Egelman, E. H. & West, S. C. Stabilization of RAD51 nucleoprotein filaments by the C-terminal region of BRCA2. *Nat. Struct. Mol. Biol.* **14,** 468–74 (2007).

150. Davies, O. R. & Pellegrini, L. Interaction with the BRCA2 C terminus protects RAD51-DNA filaments from disassembly by BRC repeats. *Nat. Struct. Mol. Biol.* **14,** 475–83 (2007).

151. Saeki, H. *et al.* Suppression of the DNA repair defects of BRCA2-deficient cells with heterologous protein fusions. *Proc. Natl. Acad. Sci. U. S. A.* **103,** 8768–73 (2006).

152. San Filippo, J. *et al.* Recombination mediator and Rad51 targeting activities of a human BRCA2 polypeptide. *J. Biol. Chem.* **281,** 11649–11657 (2006).

153. Venkitaraman, A. R. Linking the Cellular Functions of *BRCA* Genes to Cancer Pathogenesis and Treatment. *Annu. Rev. Pathol. Mech. Dis.* **4,** 461–487 (2009).

154. Kojic, M., Zhou, Q., Lisby, M., William, K. & Holloman, W. K. Brh2-Dss1 Interplay Enables Properly Controlled Recombination in Ustilago maydis. *Mol. Cell. Biol.* **25,** 2547–2557 (2005).

155. Zhou, Q., Kojic, M. & Holloman, W. K. Dss1 release activates DNA binding potential in Brh2. *Biochemistry* **51,** 9137–9146 (2012).

156. Siaud, N. *et al.* Plasticity of BRCA2 function in homologous recombination: genetic interactions of the PALB2 and DNA binding domains. *PLoS Genet.* **7,** e1002409 (2011).

157. Edwards, S. L. *et al.* Resistance to therapy caused by intragenic deletion in BRCA2. *Nature* **451,** 1111–5 (2008).

158. Shahid, T. *et al.* Structure and mechanism of action of the BRCA2 breast cancer tumor suppressor. *Nat. Struct. Mol. Biol.* (2014).

159. Zhou, Q., Kojic, M. & Holloman, W. K. DNA-binding Domain within the Brh2 N Terminus Is the Primary Interaction Site for Association with DNA. *J. Biol. Chem.* **284,** 8265–73 (2009).

160. Wali, N. *et al.* Centrosomal BRCA2 is a target protein of membrane type-1 matrix metalloproteinase (MT1-MMP). *Biochem. Biophys. Res. Commun.* 1–5 (2013).

161. Venkitaraman, A. R. Cancer suppression by the chromosome custodians, BRCA1 and BRCA2. *Science* **343,** 1470–5 (2014).

162. Conduit, P. T., Wainman, A. & Raff, J. W. Centrosome function and assembly in animal cells. *Nat. Rev. Mol. Cell Biol.* **16,** 611–624 (2015).

163. Nakanishi, A. *et al.* Interference with BRCA2, which localizes to the centrosome during S and early M phase, leads to abnormal nuclear division. *Biochem. Biophys. Res. Commun.* **355,** 34–40 (2007).

164. Kraakman-van der Zwet, M. *et al.* Brca2 (XRCC11) Deficiency Results in Radioresistant DNA Synthesis and a Higher Frequency of Spontaneous Deletions. *Mol. Cell. Biol.* **22,** 669–679 (2002).

165. Wu, K. *et al.* Functional Evaluation and Cancer Risk Assessment of BRCA2 Unclassified Variants. *Cancer Res.* **65 (2),** 417–426 (2005).

166. Kastan, M. B. & Bartek, J. Cell-cycle checkpoints and cancer. *Nature* **432,** 316–323 (2004).

167. Chen, C., Chen, P., Zhong, Q., Sharp, Z. D. & Lee, W. Expression of BRC Repeats in Breast Cancer Cells Disrupts the BRCA2-Rad51 Complex and Leads to Radiation Hypersensitivity and Loss of G 2 / M Checkpoint Control *. *Biochemistry* **274,** 32931–32935 (1999).

168. Ayoub, N. *et al.* The carboxyl terminus of Brca2 links the disassembly of Rad51 complexes to mitotic entry. *Curr. Biol.* **19,** 1075–85 (2009).

169. Menzel, T. *et al.* A genetic screen identifies BRCA2 and PALB2 as key regulators of G2 checkpoint maintenance. *EMBO Rep.* **12,** 705–12 (2011).

170. Tutt, A. *et al.* Absence of Brca2 causes genome instability by chromosome breakage and loss associated with centrosome amplification. 1107–1111 (1999).

171. Park, I. *et al.* Loss of BubR1 acetylation causes defects in spindle assembly checkpoint signaling and promotes tumor formation. *J. Cell Biol.* **202,** 295–309 (2013).

172. Lin, H., Ting, N. S. Y., Qin, J. & Lee, W. M Phase-specific Phosphorylation of BRCA2 by Polo-like Kinase 1 Correlates with the Dissociation of the BRCA2-P / CAF Complex *. *J. Biol. Chem.* **278,** 35979–35987 (2003).

173. Daniels, M. J., Yunmei, W., Lee, M. & Venkitaraman, A. R. Abnormal Cytokinesis in Cells Deficient in the Breast Cancer Susceptibility Protein BRCA2. *Science (80-.).* **306,** 876–879 (2004).

174. Steigemann, P. & Gerlich, D. W. Cytokinetic abscission: cellular dynamics at the midbody. *Trends Cell Biol.* **19,** 606–616 (2009).

175. Mueller, M., Adell, M. A. Y. & Teis, D. Membrane abscission: First glimpse at dynamic ESCRTs. *Curr. Biol.* **22,** 603–605 (2012).

176. Zhao, W., Seki, A. & Fang, G. Cep55, a Microtubule-bundling Protein, Associates with Centralsplindin to control the midbody integrity and cell abscission during cytokinesis. *Mol. Biol. Cell* **18,** 986–994 (2006).

177. Jeffery, J., Sinha, D., Srihari, S., Kalimutho, M. & Khanna, K. K. Beyond cytokinesis: the emerging roles of CEP55 in tumorigenesis. *Oncogene* **35,** 1–8 (2015).

178. Jonsdottir, A. B. *et al.* BRCA2 heterozygosity delays cytokinesis in primary human fibroblasts. *Cell. Oncol.* **31,** 191–201 (2009).

179. Lekomtsev, S., Guizetti, J., Pozniakovsky, A., Gerlich, D. W. & Petronczki, M. Evidence that the tumor-suppressor protein BRCA2 does not regulate cytokinesis in human cells. *J. Cell Sci.* **123,** 1395–1400 (2010).

180. Sharan, S. K. *et al.* BRCA2 deficiency in mice leads to meiotic impairment and infertility. *Development* **131,** 131–142 (2004).

181. Seeliger, K., Dukowic-Schulze, S., Wurz-Wildersinn, R., Pacher, M. & Puchta, H. BRCA2 is a mediator of RAD51- and DMC1-facilitated homologous recombination in

Arabidopsis thaliana. *New Phytol.* **193,** 364–75 (2012).

182. Kojic, M., Kostrub, C. F., Buchman, A. R. & Holloman, W. K. BRCA2 homolog required for proficiency in DNA repair, recombination, and genome stability in Ustilago maydis. *Mol. Cell* **10,** 683–691 (2002).

183. Siaud, N. *et al.* Brca2 is involved in meiosis in Arabidopsis thaliana as suggested by its interaction with Dmc1. *EMBO J.* **23,** 1392–1401 (2004).

184. Dray, E., Siaud, N., Dubois, E. & Doutriaux, M. Interaction between Arabidopsis Brca2 and Its Partners Rad51, Dmc1 and Dss1. *Plant Physiol.* **140,** 1059–1069 (2006).

185. Sheridan, S. D. *et al.* A comparative analysis of Dmc1 and Rad51 nucleoprotein filaments. *Nucleic Acids Res.* **36,** 4057–66 (2008).

186. Brown, M. S. & Bishop, D. K. DNA Strand Exchange and RecA Homologs. *Cold Spring Harb. Perspect. Biol.* 1–30 (2014).

187. Biswas, K. *et al.* Functional evaluation of BRCA2 variants mapping to the PALB2-binding and C-terminal DNA-binding domains using a mouse es cell-based assay. *Hum. Mol. Genet.* **21,** 3993–4006 (2012).

188. Bugreev, D. V, Pezza, R. J. & Mazin, A. V. The resistance of DMC1 D-loops to dissociation. *Nat. Struct. Mol. Biol.* **18,** 56–60 (2011).

189. Zhao, W. *et al.* Mechanistic insights into the role of Hop2-Mnd1 in meiotic homologous DNA pairing. *Nucleic Acids Res.* **42,** 906–917 (2014).

190. Bugreev, D. V., Golub, E. I., Stasiak, A. Z., Stasiak, A. & Mazin, A. V. Activation of human meiosis-specific recombinase Dmc1 by Ca2+. *J. Biol. Chem.* **280,** 26886–26895 (2005).

191. Abbott, D. W., Freeman, M. L. & Holt, J. T. Double-Strand Break Repair Deficiency and Radiation Sensitivity in BRCA2 Mutant Cancer Cells. *J. Natl. Cancer Inst.* **90,** 978–985 (1998).

192. Wooster et al. Identification of the breast cancer susceptibility gene BRCA2. *Lett. to Nat.* (1995).

193. King, M.-C., Marks, J. H., Mandell, J. B. & New York Breast Cancer Study, G. Breast and ovarian cancer risks due to inherited mutations in BRCA1 and BRCA2. *Science* **302,** 643–646 (2003).

194. Chen, S. & Parmigiani, G. Meta-Analysis of BRCA1 and BRCA2 Penetrance. *J Clin Oncol* **25,** 1329–1333 (2007).

195. Ford, D. *et al.* Genetic Heterogeneity and Penetrance Analysis of the BRCA1 and BRCA2 Genes in Breast Cancer Families. *Am. J. Hum. Genet.* **62,** 676–689 (1998).

196. Alves, A. M. *et al.* Localization of a Breast Cancer Susceptibility Gene , BRCA2 , to Chromosome 13q1 2-13. 15–17 (1993).

197. Nathanson, K. L., Wooster, R., Weber, B. L. & Nathanson, K. N. Breast cancer

genetics: what we know and what we need. *Nat. Med.* **7,** 552–6 (2001).

198. Welcsh, P. L. & King, M. C. BRCA1 and BRCA2 and the genetics of breast and ovarian cancer. *Hum. Mol. Genet.* **10,** 705–13 (2001).

199. Kinzler, K. W. & Vogelstein, B. Cancer-susceptibility genes. Gatekeepers and caretakers. *Nature* **386,** 761, 763 (1997).

200. Lord, C. J. & Ashworth, A. BRCAness revisited. *Nat. Rev. Cancer* 1–11 (2016).

201. Lomonosov, M., Anand, S., Sangrithi, M., Davies, R. & Venkitaraman, A. R. Stabilization of stalled DNA replication forks by the BRCA2 breast cancer susceptibility protein. *Genes Dev.* **17,** 3017–22 (2003).

202. Ganem, N. J., Godinho, S. A. & Pellman, D. A mechanism linking extra centrosomes to chromosomal instability. *Nature* **460,** 278–282 (2009).

203. Tutt, A. *et al.* Absence of Brca2 causes genome instability by chromosome breakage and loss associated with centrosome amplification. *Curr. Biol.* **9,** 1107–10 (1999).

204. Plon, S. E. *et al.* Sequence variant classification and reporting: recommendations for improving the interpretation of cancer susceptibility genetic test results. *Hum. Mutat.* **29,** 1282–1291 (2008).

205. Spurdle, A. B., Healey, S., Devereau, A., Hogervorst, F. B. L. & Na, A. ENIGMA network. **33,** 2–7 (2012).

206. Frank, B. T. S. *et al.* Clinical Characteristics of Individuals With Germline Scope of Analysis. *J. Clin. Oncol.* **20,** 1480–1490 (2002).

207. Goldgar, D. E. *et al.* Integrated evaluation of DNA sequence variants of unknown clinical significance: application to BRCA1 and BRCA2. *Am. J. Hum. Genet.* **75,** 535–44 (2004).

208. Lindor, N. M. *et al.* A review of a multifactorial probability-based model for classification of BRCA1 and BRCA2 variants of uncertain significance (VUS). *Hum. Mutat.* **33,** 8–21 (2012).

209. Szabo, C., Masiello, A., Ryan, J. F. & Brody, L. C. The Breast Cancer Information Core: Database design, structure, and scope. *Hum. Mutat.* **16,** 123–131 (2000).

210. Caputo, S. *et al.* Description and analysis of genetic variants in French hereditary breast and ovarian cancer families recorded in the UMD-BRCA1/BRCA2 databases. *Nucleic Acids Res.* **40,** D992–D1002 (2011).

211. Guidugli, L. *et al.* A classification model for BRCA2 DNA binding domain missense variants based on homology-directed repair activity. *Cancer Res.* **73,** 265–75 (2013).

212. Guidugli, L. *et al.* Functional assays for analysis of VUS in BRCA2. *Hum. Mutat.* **18,** 1199–1216 (2014).

213. Farrugia, D. J. *et al.* Functional assays for classification of BRCA2 variants of

uncertain significance. *Cancer Res.* **68,** 3523–31 (2008).

214. Farmer, H. *et al.* Targeting the DNA repair defect in BRCA mutant cells as a therapeutic strategy. *Nature* **434,** 917–21 (2005).

215. Bryant, H. E. *et al.* Specific killing of BRCA2-deficient tumours with inhibitors of poly(ADP-ribose) polymerase. *Nature* **434,** 913–917 (2005).

216. Smith, K. L. & Isaacs, C. BRCA Mutation Testing in Determining Breast Cancer Therapy. *Cancer J.* **17,** 492–499 (2011).

217. Tutt, A. *et al.* Exploiting the DNA repair defect in BRCA mutant cells in the design of new therapeutic strategies for cancer. *Cold Spring Harb. Symp. Quant. Biol.* **70,** 139–148 (2005).

218. Lord, C. J. & Ashworth, A. The DNA damage response and cancer therapy. *DNA Repair (Amst).* **481,** 287–294 (2012).

219. Connor, M. J. O. Targeting the DNA damage response in cancer. *Mol. Cell* **109,** 2929–2950 (2015).

220. Lord, C. J. & Ashworth, A. Targeted therapy for cancer using PARP inhibitors. *Curr. Opin. Pharmacol.* **8,** 363–369 (2008).

221. Sakai, W. *et al.* Secondary mutations as a mechanism of cisplatin resistance in BRCA2-mutated cancers. **451,** 1116–1120 (2008).

222. Walsh, T. *et al.* Mutations in 12 genes for inherited ovarian, fallopian tube, and peritoneal carcinoma identified by massively parallel sequencing. *Proc. Natl. Acad. Sci. U. S. A.* **108,** 18032–7 (2011).

223. Letunic, I., Doerks, T. & Bork, P. SMART: recent updates, new developments and status in 2015. *Nucleic Acids Res.* **43,** D257–D260 (2015).

224. Callebaut, I. *et al.* Deciphering protein sequence information through hydrophobic cluster analysis (HCA): current status and perspectives. *Cell. Mol. Life Sci.* **53,** 621–45 (1997).

225. Wang, L. & Brown, S. J. BindN: A web-based tool for efficient prediction of DNA and RNA binding sites in amino acid sequences. *Nucleic Acids Res.* **34,** 243–248 (2006).

226. Sehorn, M. G., Sigurdsson, S., Bussen, W., Unger, V. M. & Sung, P. Human meiotic recombinase Dmc1 promotes ATP-dependent homologous DNA strand exchange. *Lett. to Nat.* **429,** 433–437 (2004).

227. Mitchell, A. *et al.* The InterPro protein families database: The classification resource after 15 years. *Nucleic Acids Res.* **43,** D213–D221 (2015).

228. Sievers, F. *et al.* Fast, scalable generation of high-quality protein multiple sequence alignments using Clustal Omega. *Mol. Syst. Biol.* **7,** 539–539 (2014).

229. Petrucco, S. Sensing DNA damage by PARP-like fingers. *Nucleic Acids Res.* **31,** 6689–6699 (2003).

230. Laity, J. H., Lee, B. M. & Wright, P. E. Zinc finger proteins: New insights into structural and functional diversity. *Curr. Opin. Struct. Biol.* **11,** 39–46 (2001).

231. Petrucco, S. & Percudani, R. Structural recognition of DNA by poly(ADP-ribose)polymerase-like zinc finger families. *FEBS J.* **275,** 883–93 (2008).

232. Iuchi, S. C H Zinc Fingers As DNA Binding Domains. *Landes Biosci.* (2005).

233. Buisson, R. & Masson, J. Y. PALB2 self-interaction controls homologous recombination. *Nucleic Acids Res.* **40,** 10312–10323 (2012).

234. Oldfield, C. J. & Dunker, A. K. Intrinsically Disordered Proteins and Intrinsically Disordered Protein Regions. *Annu. Rev. Biochem.* **83,** 553–584 (2014).

235. Peng, Z. & Kurgan, L. High-throughput prediction of RNA, DNA and protein binding regions mediated by intrinsic disorder. *Nucleic Acids Res.* 1–10 (2015).

236. Morimatsu, K. & Kowalczykowski, S. C. RecFOR proteins load RecA protein onto gapped DNA to accelerate DNA strand exchange: a universal step of recombinational repair. *Mol. Cell* **11,** 1337–47 (2003).

237. Zhou, Q. & Holloman, W. K. Dual DNA-binding domains shape the interaction of Brh2 with DNA. *DNA Repair (Amst).* **22,** 104–11 (2014).

238. Grantham, R. Amino acid difference formula to help explain protein evolution. *Science* **185,** 862–864 (1974).

239. Chen, J., Villanueva, N., Rould, M. a & Morrical, S. W. Insights into the mechanism of Rad51 recombinase from the structure and properties of a filament interface mutant. *Nucleic Acids Res.* **38,** 4889–906 (2010).

240. Morita, E. *et al.* Human ESCRT and ALIX proteins interact with proteins of the midbody and function in cytokinesis. *EMBO J.* **26,** 4215–27 (2007).

241. Houdayer, C. *et al.* Guidelines for splicing analysis in molecular diagnosis derived from a set of 327 combined in silico/in vitro studies on BRCA1 and BRCA2 variants. *Hum. Mutat.* **33,** 1228–38 (2012).

242. Fabbro, M. *et al.* Cdk1/Erk2- and Plk1-dependent phosphorylation of a centrosome protein, Cep55, is required for its recruitment to midbody and cytokinesis. *Dev. Cell* **9,** 477–88 (2005).

243. Tavtigian, S. V, Samollow, P. B., de Silva, D. & Thomas, A. An analysis of unclassified missense substitutions in human BRCA1. *Fam. Cancer* **5,** 77–88 (2006).

244. Yata, K. *et al.* Plk1 and CK2 Act in Concert to Regulate Rad51 during DNA Double Strand Break Repair. *Mol. Cell* **45,** 371–383 (2012).

245. Kojic, M., Zhou, Q., Fan, J. & Holloman, W. K. Mutational analysis of Brh2 reveals requirements for compensating mediator functions. *Mol. Microbiol.* **79,** 180–91 (2011).

246. Da Ines, O. *et al.* Meiotic Recombination in Arabidopsis Is Catalysed by DMC1, with

RAD51 Playing a Supporting Role. *PLoS Genet.* **9,** (2013).

247. Sulli, G., Di Micco, R. & di Fagagna, F. d'Adda. Crosstalk between chromatin state and DNA damage response in cellular senescence and cancer. *Nat. Rev. Cancer* **12,** 709–720 (2012).

248. Roos, W. P., Thomas, A. D. & Kaina, B. DNA damage and the balance between survival and death in cancer biology. *Nat. Rev. Cancer* **16,** 20–33 (2015).

APPENDIX

MATERIALS

PLASMIDS

Name	Insert	Cloning Strategy	Purpose
pAC012	2x MBP BRCA2	Gift from S.C. Kowalczykowski	Expression and purification of 2xMBP BRCA2
pAC013	2x MBP BRCA2 NT (1-1000 aa)	BbvCI/XhoI from pAC012	Expression and purification of 2xMBP BRCA2 NT
pAC022	GST-BRC4	BamH/XhoI	Expression of BRC4
pAC037	GFP-MBP-BRCA2 siRNA res	MBP-tag of a phCMV1 2x MBP-BRCA2 substituted by eGFP and cloned by KpnI digest (gift S.Kowalczykowski)	Expression of GFP MBP BRCA2 for purification and for in vivo assays
pAC039	GFP-MBP-BRCA2 siRNA res K268R	Mutagenesis	Expression of GFP MBP BRCA2 K268R mutant for purification and for in vivo assays
pAC040	2x MBP 2 NLS BRCA	Insertion of 2 NLS in pAC013 with NotI/BbvCI	Expression and purification of 2xMBP BRCA2 NT
pAC044	GFP-1MBP*	Cut out BRCA2	Negative control for BRCA2 assays
pAC045	2x MBP 2 NLS BRCA2 si resistant	siRNA-resistance SDM	cloning

pAC048	GFP-MBP-BRCA2 siRNA res S273L	Mutagenesis	Expression of GFP MBP BRCA2 S273L mutant for purification and for in vivo assays
pAC055	GFP-MBP-BRCA2 siRNA res G267E	Mutagenesis	Expression of GFP MBP BRCA2 G267E mutant for purification and for in vivo assays
pAC086	pEGFP-MBP-BRCA2-D2723H	Mutagenesis	Expression of GFP MBP BRCA2 G267E mutant for purification
pAC097	2x MBP BRCA2-NT T1 (1-250 aa of BRCA2)	Cloning with Xho/NotI in pAC045	Expression and purification of 2xMBP BRCA2 1-250 aa
pAC098	2x MBP BRCA2-NT T2 (250-500 aa of BRCA2)	Cloning with Xho/NotI in pAC045	Expression and purification of 2xMBP BRCA2 250-500 aa
pAC101	2x MBP BRCA2-NT LT2 (1-500 aa of BRCA2)	Cloning with BbvCI/XhoI in pAC045	Expression and purification of 2xMBP BRCA2 1-500 aa
pAC102	2x MBP BRCA2-NT LT3 (1-750 aa of BRCA2)	Cloning with BbvCI/XhoI in pAC045	Expression and purification of 2xMBP BRCA2 1-500 aa
pAC122	pEGFP-MBP-BRCA2-N277K	Mutagenesis	Expression of GFP MBP BRCA2 N277K for purification and in vivo assays
pAC138	GFP MBP 2NLS BRC4	Gibson Assembly with pAC022	For further cloning
pAC150	pGEX-BRC1	Gift from S.C. Kowalczykowski	Expression and purification GST-

			BRC1
pAC151	pGEX-BRC2	Gift from S.C. Kowalczykowski	Expression and purification GST-BRC2
pAC152	pGEX-BRC3	Gift from S.C. Kowalczykowski	Expression and purification GST-BRC3
pAC153	pGEX-BRC5	Gift from S.C. Kowalczykowski	Expression and purification GST-BRC5
pAC154	pGEX-BRC6	Gift from S.C. Kowalczykowski	Expression and purification GST-BRC6
pAC155	pGEX-BRC7	Gift from S.C. Kowalczykowski	Expression and purification GST-BRC7
pAC156	pGEX-BRC8	Gift from S.C. Kowalczykowski	Expression and purification GST-BRC8
pAC162	Trex flag eGFP BRCA2	Gift from Fumiko Esashi	FLP-in system - to insert FLAG eGFP BRCA2 at FRT site
pAC164	6His SUMO pET28	P. Duchambon	Cloning
pAC165	6His SUMO pET28 BRCA2 2474-3190 (CTD)	Cloning of BRCA2 2474-3190 (CTD) into 6His SUMO pET28	Expression and purification of CTD
pAC173	2x MBP 2 NLS T2 C279A	Mutagenesis	Expression and purification T2 C279A
pAC174	2x MBP 2 NLS T2 C341	Mutagenesis	Expression and purification T2 C341S
pAC177	GFP-MBP-BRCA2	Gift from F. Couch	Expression and

	siRNA res Y3035S		purification
pAC178	GFP-MBP-BRCA2 siRNA res R3052Q	Gift from F. Couch	Expression and purification
pAC179	GFP-MBP-BRCA2 siRNA res K2729N	Gift from F. Couch	Expression and purification
pAC180	GFP-MBP-BRCA2 siRNA res G2508S	Gift from F. Couch	Expression and purification
pAC181	GFP-MBP-BRCA2 siRNA res A2717S	Gift from F. Couch	Expression and purification
pAC189	2xMBP-T2-C315S	Mutagenesis	Expression and purification T2 C315S
pAC192	pCDF DSS1	pCDF (A.el Marjou) Gibson Assembly with DSS1	Coexpression DSS1 with CTD for purification
pAC194	2xMBP-T2-C279A C341S	Mutagenesis	Expression and purification T2 C279A C341S
pAC197	2xMBP-T2-C315S C341S	Mutagenesis	Expression and purification T2 C315S C341S
pAC201	2xMBP-T2-C279A C315S	Mutagenesis	Expression and purification T2 C279A C315S
pAC232	2x MBP BRC4 T2	Gibson Assembly	Expression and Purification
pAC249	GFP-MBP-2NLS -T2 C315S -BRC4	Mutagenesis	in vivo assays
pET28 6His SUMO vector.	-	Gift A. el Marjou	Expression and Purification
pFASTBAC	DSS1	Gift R.Jensen	Expression and

Dual-DSS1			Purification
pUC19		Gift from S. Kowalzcykowksi	Joint molecule assay
pCDF 6his SUMO	RAD51		

PRIMER

Name	**Purpose**	**Sequence**
oAC014	RT PCR N-ter	ATGACTGGTACCATGGTGAGCAAGGGCGAGGAGC
oAC033	RT PCR N-ter	CCTGTTATAGCCTTTATCGCCG
oAC041	RT PCR C-ter	AGGAGTTGTGGCACCAAATACGAAACACCC
oAC188	RT PCR C-ter	CGGCCGCAATTGTTAGATATATTTTTTAGTTG
oAC203	Joint molecule assay ATP assay EMSAs	CGGGTGTCGGGGCTGGCTTAACTATGCGGCATCAGAGCAGATTGTACTGAGAGTGCACCATATGCGGTGTGAAATACCGCACAGATGCGT
oAC361	Mutagenesis BRCA2 N277K	CAGGGAATTCATTTAAAGTAAAGAGCTGCAAAGACC
oAC362	Mutagenesis BRCA2 N277K	TATTTTGGTACCCCCGAGGTTGTTGTTATTGTTATT
oAC403	Oligo for DNA binding 42-mer 5' to anneal to 167-mer (oAC423)	CGGATATTTCTGATGAGTCGAAAAATTATCTTGATAAAGCAG
oAC379	dT40 for EMSA	TTTTTTTTTTTTTTTTTTTTTTTTTTTTTTTTTTT
oAC405	40mer for EMSA, anneal with oAC406	TAATACAAAATAAGTAAATGAATAAACAGAGAAAATAAAG
oAC406	40mer for EMSA, anneal with oAC405	CTTTATTTTCTCTGTTTATTCATTTACTTATTTTGTATTA

oAC423	167mer for EMSA	CTGCTTTATCAAGATAATTTTTCGACTCATCAGA AATATCCGTTTCCTATATTTATTCCTATTATGTTT TATTCATTTACTTATTCTTTATGTTCATTTTTTAT ATCCTTTACTTTATTTTCTCTGTTTATTCATTTAC TTATTTTGTATTATCCTTATCTTATTTA
oAC490	42mer for 3'tail substrate with 167mer (oAC423)	TAAATAAGATAAGGATAATACAAAATAAGTAAAT GAATAAAC
oAC491	Mutagenesis C279A in T2 BRCA2	AAG TAA ATA GCG CCA AAG ACC ACA TTG GAA AGT CAA TGC CAA ATG
oAC492	Mutagenesis C279A in T2 BRCA2	AAG TAA ATA GCG CCA AAG ACC ACA TTG GAA AGT CAA TGC CAA ATG
oAC493	Mutagenesis C341S in T2 BRCA2	CTTGGTTTTTAGATTTTTCACTTTCATCAGCGTT TGCTTCATGG
oAC494	Mutagenesis C341S in T2 BRCA2	CCATGAAGCAAACGCTGATGAAAGTGAAAAAT CTAAAAACCAAG
oAC520	Mutagenesis C315S in T2 BRCA2	GTTTTTCATTATGTTTTTCTAAAAGTAGAACAAA AAATCTACAAAAAG
oAC596	PCR for Gibson Assembly on pAC138 to make NotI 2NLS BRC4	TTCCAGGGGCCCGGCGGCCGCGATCCAAAAA AGAAGAGAAAGG
oAC597	PCR for Gibson Assembly on pAC138 to make NotI 2NLS BRC4	GTGTTTTCACTTTGCTCTTTTTCATCAAAAAGG
oAC598	PCR gibson assembly on pAC098 for overlap T2 BRC4	AAAGAGCAAAGTGAAAACACAAATCAAAGAG
oAC599	PCR gibson assembly on pAC098 for T2 stop	GCTGATTATGATCTAGACTCGAGTTAACCCTGA AATGAAGAAGC

PRIMARY AND SECONDARY ANTIBODIES

Name	**Antigen**	**Vendor**
BRCA2 OP95	BRC repeats BRCA2	EMD Millipore (OP95-100UG)
BRCA2 E36	BRCA2 NT (188-563)	Genetex (GTX70121)
BRCA2 CA 1033	BRCA2 (C-ter)	EMD Millipore (CA1033)
Centrin-2(N-17)	Centrin-2 N-terminus	Santa Cruz Biotechnology (sc-27793-R)
DSS1 (FL-70)	DSS1 full length	Santa Cruz Biotechnology (sc-28848)
GFP	GFP	Life Technologies (A11122)
GFP	GFP	SIGMA (Roche) (11814460)
His (6x)	6-His peptide	Eurogentec (PEP-156P)
Histone H3	H3	Abcam (ab1791)
HRP goat anti-mouse	2ndary AB anti-mouse antigen	Santa Cruz Biotechnology (sc-2055)
HRP goat anti-rabbit	2ndary AB anti-rabbit antigen	Santa Cruz Biotechnology (sc-2055)
MBP	Maltose binding protein	Invitrogen (33-5100)
RAD51 (H-92)	N-ter 1-92 of RAD51	Santa Cruz Biotechnology (sc-8349)
Tubulin (alpha)	Alpha-tubulin	Genetex (GTX102078)
AlexaFluor555 goat anti-mouse IgG	Gamma Immunoglobins heavy and light chains	Invitrogen A-31570
AlexaFluor555 donkey anti-rabbit IgG	Gamma Immunoglobins Heavy and Light chains	Invitrogen A-21428

CELL LINES

Name	**Origin**	**Grow in**
HEK293	Human embryonic kidney cells	DMEM medium, FCS serum

VC8	*BRCA2*$^{-/-}$ cell line from V79 chinese hamster lung fibroblast	HAM's medium, FCS serum
VC8 stable cell lines	VC8, complemented with GFP-MBP BRCA2 WT or mutant DNA	HAM's medium, FCS serum G418 selection 10 ug/ml

BACTERIAL STRAINS

Designation	**Supplier**
E. coli BL21 DE3 pISO Dscb	Gift from A. el Marjou
DH5 alpha electrocompetent cells	Gift from C.Janke
XL-10 gold supercompetent cells	Agilent (XL kit)
BL21(DE3)pLysS chemo-competent cells	Made by the lab
E. Coli BL21 BRL	Recombinant platform I. Curie

EQUIPMENT, KITS, INVENTORY

Designation	**Supplier**
1kb DNA Ladder	Invitrogen
3D deconvolution microscope	Nikon
4-5 D video microscope deconvolution	Nikon
AKTA prime plus chromatograph	GE Life Sciences
Amersham ECL Prime Western Blotting Detection Reagent	VWR
Amylose Magnetic Beads	NEB
Amylose resin	NEB
ATP [γ-32P]- 3000Ci/mmol 10mCi/ml EasyTide	Perkin Elmer
BioRexin resin	BioRAD
Cell culture material	TPP

Cell culture media (HAM's, DMEM)	Eurobio
Centrifuge Refrigerated Model 5810 R	Eppendorf
ChemiDoc camera	Bio-Rad
Coomassie Brilliant Blue	Bio-Rad
Disintegrator CellD	Constant System
Disposable columns	Pierce
Dynabeads MyOne Streptavidin	Thermo Scientific
FACSCalibur	BD Biosciences
FCS	Sigma
UV Transilluminator	Vilber
Gel casting system Hoefer	Dutscher
Gibson Assembly Cloning kit HiFi	NEB
Glutathione sepharose 4B beads	Dutscher
Graph Pad Prism	Software
HiSpeed Plasmid Maxi kit	QIAGEN
HiTrap Heparin HP column 5 ml	GE Healthcare
Hoefer Protein vertical electrophoresis system Mighty Small II SE 250	Dutscher
Hybond ECL Membrane	VWR
illustra MicroSpin G-25 columns	GE Healthcare
Illustra Minispin Kit	GE healthcare
Image Quant (GE)	Software
Image Quant Software	GE Healthcare
Microcentrifuge 5424	Eppendorf
Mini Transblot Cell	Bio-Rad
Mini-PROTAN Tetra cell	Bio-Rad
Mini-PROTEAN TGX SDS gels (4-15%, 7.5%, 10%, 12%)	Bio-Rad
Mini-PROTEAN TGX stain-free SDS gels (4-15%, 7.5%, 10%, 12%)	Bio-Rad
Nanodrop 2000	Thermo Scientific
NanoOrange Protein Quantitation Kit	Thermo Fisher
NucleoBond Xtra Midi kit	Macherey Nagel

Plate reader Victor 3	perkin elmer
Polyethyleneimine (PEI) thin layer chromatography (TLC) plate	EMD chemicals
Precision plus SDS-PAGE Standards dual colors	Bio-Rad
Precision plus SDS-PAGE Unstained	Bio-Rad
ProLong® Gold antifade reagent with DAPI	Thermo Fisher
PROTEIN CONCENTRATORS, 9K MWCO	Thermo Scientific
Protein-Assay	Bio-Rad
Protino® Ni-NTA agarose	Macherey Nagel
PVDF Hybond Membrane	Dutscher
QuikChange II site-directed mutagenesis kit	Agilent
QuikChange XL site-directed mutagenesis kit	Agilent
Refrigerated Microcentrifuge 5424 R	Eppendorf
SPECTRA/POR Dialysis Tubing	Thermo Scientific
Storage phosphor screen	GE healthcare
SYPRO Orange staining solution	Sigma-Aldrich
T100 Thermal Cycler	Bio-Rad
TITANIUM One-Step RT-PCR kit	Clontech
TurboFect Transfection Reagent	Thermo Scientific
Typhoon PhosphorImager FLA7000	Amersham Biosciences
Watman paper	GE Healthcare
Wizard SV Gel and PCR clean-up system	Promega

ENZYMES

Designation	**Suppplier**
Proteinase K recombinant	Roche
Restriction Enzymes	NEB
SUMO Protease	Thermo Scientific
T4 DNA ligase and Ligase Buffer 10x	NEB
T4 Polynucleotide Kinase and Buffer 10x	NEB
Taq DNA Polymerase and ThermoPol Buffer	NEB

10x	

CHEMICALS

Designation	**Supplier**
100 mM dNTP set	Invitrogen
1x PBS	Laverie Curie
20% SDS	Euromedex
ABT-888 Veliparib	Selleck Chemicals
Acetic acid,ReagentPlus(R)	Sigma-Aldrich
Adenosine 5’ triphosphate (ATP)	Sigma-Aldrich
Agarose 100%	Euromedex
Ammoniumpersulfate (APS)	Bio-Rad
Ampicillin sodium salt	Sigma-Aldrich
Bromophenol blue	Bio-Rad
BSA	Sigma-Aldrich
Calcium Chloride	Sigma-Aldrich
Crystal Violet	Bio-Rad
DMSO - Dimethyl Sulfoxide	Sigma-Aldrich
DNase I recombinant RNAse free	Roche
DTT	Sigma-Aldrich
EDTA	Magasin Curie
EDTA-free Protease Inhibitor Cocktail	Roche
EGTA	Sigma-Aldrich
Ethanol absolute 99.9 %	Magasin Curie
Ethidium Bromide	Sigma-Aldrich
Formic Acid	Sigma-Aldrich
G418 Disulfate salt	Sigma-Aldrich
Glutaraldehyde	Sigma-Aldrich
Glutaraldehyde	Sigma Aldrich
Glycerol 99%	Laverie Curie
Glycine	Magasin Curie
HEPES	Euromedex

HEPES	Euromedex
Imidazole	Sigma-Aldrich
IPTG - Isopropyl beta-D-1-thiogalactopyranoside	Sigma-Aldrich
Kanamycin monosulfate	Sigma-Aldrich
L-(+)-Arabinose	Sigma-Aldrich
LB plates & media for bacterial growth	Laverie Curie
L-Glutamin	Eurobio
Lithium Chloride	VWR
Lysozyme	Sigma-Aldrich
Magnesium Chloride	Sigma-Aldrich
Maltose	Magasin Curie
Methanol 99.9 %	Magasin Curie
Mitomycin C	Sigma-Aldrich
MTT - Thiazolyl Blue Tetrazolium Bromide	Sigma-Aldrich
Nonidet P40	Magasin Curie
Paraformaldehyde 16%	Euromedex
PIPES	Euromedex
PMSF	Sigma-Aldrich
Potassium Chloride	Sigma-Aldrich
Potassium phosphate monobasic	Sigma-Aldrich
Sodium Chloride (NaCl)	Magasin Curie
Sodium hydrogen carbonate	Sigma-Aldrich
Sucrose	Sigma-Aldrich
TEMED	Bio-Rad
TRIS acetate salt	Sigma-Aldrich
Triton X-100	Euromedex
Trizma(R) base,	Sigma Aldrich
TRIzol Reagent	life technologies
Trypsine/EDTA	Gibco
Zinc Chloride	Sigma-Aldrich
B-Mercaptoethanol	Bio-Rad

BUFFERS

Designation	**Composition**
6x DNA loading buffer	0.25% xylene cyanol solution (1%), 0.25% bromophenol blue 1% solution (0.25%), 30% glycerol
6x Laemmli Buffer for SDS PAGE	6% SDS, 0.003% Bromophenol blue, 48% glycerol, 375 mM Tris pH6.8, 9% β-Mercaptoethanol
Agarose gel electrophoresis buffer	1x Tris-Acetate EDTA
SDS PAGE running buffer	1x TrisGlycine, 0.1% SDS
Transfer buffer	1x TrisGlycine, 10% Methanol, 0.025% SDS

RESUMÉE EN FRANÇAIS

université PARIS-SACLAY | ÉCOLE DOCTORALE Cancérologie, biologie, médecine, santé (CBMS)

Titre : Caractérisation d'un nouveau domaine de fixation à l'ADN dans le N-terminus de BRCA2 et évaluation des variantes *BRCA2* non-classifiées identifiées dans les patients de cancer du sein dans la même région

Mots clés : Réparation d'ADN, Recombinaison Homologue (RH), BRCA2, cancer du sein

Résumée

Les mutations héréditaires dans le gène *BRCA2* sont associées à une forte susceptibilité au développement du cancer du sein et de l'ovaire. La protéine suppresseur de tumeur BRCA2 est essentielle pour préserver l'intégrité des chromosomes après endommagement de l'ADN. BRCA2 est impliquée dans la recombinaison homologue (RH), une voie fiable de réparation des cassures de l'ADN. BRCA2 exerce aussi un rôle pendant la mitose afin d'assurer un point de contrôle et une division cellulaire correcte. Bien que le rôle de BRCA2 dans la RH soit bien établi, la littérature décrive une restauration partielle de la fonction de RH dans des cellules ne possédant pas le site de liaison à l'ADN en C-terminal (CT-DBD), ce que nous a encouragé à voir s'il existait un domaine secondaire de liaison à l'ADN. L'analyse *in silico* a révélé un domaine zf-PARP putatif dans la région N-terminale. Normalement, ce type de domaine s'associe à l'ADN, ce que nous a porté à l'examiner. En utilisant des fragments purifiés de la partie N-terminale comprenant le site putatif dans des analyses de ***changements de mobilité électrophorétique,*** nous avons montré une activité de liaison à l'ADN. En comparaison avec le CT-DBD canonique, le site de liaison à l'ADN en N-terminal (NT-DBD) manifeste une affinité plus forte pour divers substrats et contrairement du CT-DBD il est capable de s'associer à l'ADN à double brin. En utilisant des tests d'échange de brin, nous avons également montré que le NT-DBD peut stimuler la fonction de recombinaison de RAD51. De plus, des variantes faux-sens dans le NT-DBD trouvé chez

les patients atteints de cancer du sein ont montré une activité réduite d'association à l'ADN et une stimulation diminuée de l'activité de RAD51 ce qui implique que ces amino-acides sont importants pour les deux fonctions. Ce travail révèle un nouveau site de liaison à l'ADN, ce qui contrairement au CT-DBD est capable de s'associer à l'ADN double-bras(db) et stimuler l'activité de recombinaison de RAD51. Nous proposons que le NT-DBD positionne RAD51 à la jonction entre ADNdb et ADNsb, ce qui facilite le chargement de RAD51 sur l'ADN recouvert de RPA. Cette activité pourrait promouvoir la RH pendant la réparation des cassures de l'ADN (von Nicolai, C et al., 2016, under revision).

Afin de définir la prévalence des mutations de NT-DBD pour la prédisposition au cancer, nous avons sélectionné des variants faux-sens non-classifiés (variants of unknown clinical significance), identifiés dans des familles à risque élevé de développer un cancer du sein. Nous avons effectué des tests afin d'étudier l'impact de ces variants sur la fonction de BRCA2 dans la RH et la mitose. Certains de ces variants ont conduit à une hypersensibilité aux agents endommageant l'ADN et aux inhibiteurs de PARP, caractéristique d'une RH défectueuse alors qu'un de ces variants était compétent pour la réparation. Tous les variants ont induit une duplication normale des centrosomes, mais la cytokinèse était défectueuse. Ce phénotype suggère un défaut dans la formation du midbody et de l'abscission. Cette étude aidera à classifier les VUS dans le NT-DBD et facilitera la consultation génétique pour des individus. BRCA2 est un médiateur de la RH dépendante de RAD51. Son homologue méiotique, DMC1, partage structure et fonction similaire et s'associe à BRCA2. Néanmoins, la pertinence fonctionnelle de cette interaction reste élusive. Nous avons montré que BRCA2 interagit avec DMC1 au travers des répétitions BRC et promeut la formation de molécules d'adhérence. Cet effet stimulant est dû au renforcement de la liaison de DMC1 à l'ADN. BRCA2 complet et fonctionnel était surtout capable de stimuler l'activité d'échange de brin de DMC1, ce qui confirme les résultats obtenus avec les répétitions BRC. Nos résultats identifient BRCA2 comme une protéine de médiation de la recombinaison méiotique et renforcent le rôle des répetitions BRC dans cette fonction (Martinez, von Nicolai, *et al.*, PNAS, 2016).

ABSTRACT

Title : Characterization of a novel DNA binding domain in the N-terminus of BRCA2 and evaluation of *BRCA2* variants identified in breast cancer patients in the same region

Keywords : DNA repair, Homologous Recombination (HR), BRCA2, breast cancer

Abstract :

Germline mutations in the *BRCA2* gene lead to high susceptibility to the development of breast and ovarian cancer. The tumor suppressor protein BRCA2 is essential for preserving chromosome integrity after DNA damage emerging from endogenous or exogenous sources. BRCA2 functions in Homologous Recombination (HR), the most reliable pathway to repair DNA double strand breaks. BRCA2 exerts its tumor suppressor role also at several stages during mitosis where it ensures checkpoint control and proper cell division.

Although the function of BRCA2 in HR is well established, evidence from the literature describing a partial restoration of HR function in cells lacking the C-terminal DNA binding domain (CT-DBD) brought us to test the hypothesis of a secondary DNA binding domain in BRCA2.

In silico analysis of the protein revealed a putative zinc finger-PARP domain in exon 10 of the N-terminal region. This type of domain usually binds DNA which prompted us to examine this activity *in vitro.* Using purified N-terminal fragments comprising the putative DNA binding domain in electrophoresis mobility shift assay we demonstrated the DNA binding activity of the N-terminus of BRCA2. When compared to the canonical CT-DBD, the N-terminal DNA binding domain (NT-DBD) exhibits stronger affinity for various DNA substrates and unlike the CT-DBD, it can also associate with dsDNA. Using a DNA strand exchange assay we also showed that the NT-DBD stimulates the recombination function of RAD51. In addition, BRCA2 missense variants in the NT-DBD found in breast cancer patients showed reduced dsDNA binding and decreased stimulation of RAD51 recombination activity on dsDNA/ssDNA containing substrates, implying that these residues are important for both functions. This work revealed a novel DNA binding domain in the N-terminus of BRCA2 that, in contrast to the CT-DBD, can

associate with dsDNA and promote RAD51 recombination activity. We propose that the NT-DBD positions RAD51 at the ssDNA/dsDNA junction facilitating RAD51 loading onto the RPA-coated ssDNA. This activity may promote HR in DSB repair and in daughter strand gap repair (von Nicolai, C et al., 2016, under revision).

To define the relevance of NT DBD on cancer predisposition, we selected several missense variants of unknown clinical significance (VUS) found in families at high risk to develop breast cancer located in this region. We used *in vitro* and *in vivo* functional assays to study the impact of the mutations on BRCA2 function in HR and mitosis. Some of the variants exhibited hypersensitivity to DNA damaging agents and PARP inhibitors, a hallmark of defective HR while one variant was proficient in repair. All variants showed normal centrosome duplication, but exhibited delayed or failed cytokinesis. This phenotype suggests a defect of the variants in midbody formation and abscission as a consequence of impaired BRCA2 function. It remains to be established if the defects in HR and cytokinesis are related. In the future, this study will help to classify VUS in the NT-DBD and facilitate genetic counselling of individuals carrying these mutations.

BRCA2 is a mediator protein in RAD51-dependent HR. Its meiotic counterpart, DMC1, shares similar structure and function and binds BRCA2. However, the functional relevance of this interaction remained elusive. In this work, we showed that through the BRC repeats, BRCA2 interacts with DMC1 and promotes joint molecule formation. This stimulatory effect is due to the enhancement of DMC1 assembly on ssDNA. Importantly, full-length BRCA2 also stimulated the DNA strand exchange activity of DMC1, confirming the results with the isolated BRC repeats. Our results identify BRCA2 as a mediator of meiotic recombination and underline the role of the BRC repeats on this function (Martinez, von Nicolai, *et al*., 2016, PNAS).

ANNEXE

SYNTHESE DU MANUSCRIPT EN FRANCAIS

HYPOTHESES ET OBJECTIFS DE CE TRAVAIL

Les mutations héréditaires dans le gène *BRCA2* sont associées à une forte susceptibilité au développement du cancer du sein et de l'ovaire. La protéine suppresseur de tumeur BRCA2 est essentielle pour préserver l'intégrité des chromosomes après endommagement de l'ADN. BRCA2 est impliquée dans la recombinaison homologue (RH), une voie fiable de réparation des cassures de l'ADN. Ici, BRCA2 servit pour le recrutement de la recombinase RAD51 à l'ADN et favorise sa fonction dans la RH afin de réparer les cassures d'ADN. Ainsi, le mauvais fonctionnement de BRCA2 peut conduire à l'instabilité génomique, une marque de la formation des tumeurs. L'absence de BRCA2 peut également conduire à l'amplification du centrosome et l'échec dans les derniers pas dans la cytokinèse, suggérant une fonction de BRCA2 dans ce processus, ce qui pourrait expliquer l'aneuploïdie dans les cancers qui sont liés à l'absence de BRCA2. Plusieurs domaines fonctionnels de BRCA2 ont été décrits, néanmoins, le rôle d'autres domaines comme le domaine N-terminale restent énigmatiques. Les fonctions, modifications et partenaire d'interaction de BRCA2 sont sous l'examen minutieux.

OBJECTIF 1: INVESTIGATION ET CARACTERISATION D'UN DOMAINE DE FIXATION A L'ADN PUTATIVE DANS LE N-TERMINUS DE BRCA2

Les premiers 40 acides aminés de BRCA2 sont bien conservés et contiennent un domaine d'interaction avec PALB2. Cependant, on sait peu des choses sur la région N-terminale laquelle constitue un tiers de la protéine. Des études avec des cellules humaines résistantes aux inhibiteurs de PARP ainsi qu'avec l'orthologue de BRCA2, Brh2 dans *U. maydis* ont été montré que des mutants manquant du domaine de fixation à l'ADN C--terminale ont été capables de restaurer la compétence la recombinaison en réponse aux dommages d'ADN. Ces indications nous ont conduits à émettre l'hypothèse que la compétence en RH et la résistance aux dommages d'ADN observés dans les cellules exprimant une version tronqué de BRCA2 ce qui manquent le domaine de fixation à l'ADN

C—terminale, proviennent d'un deuxième domaine de fixation à l'ADN dans le N-terminus. En utilisant la séquence primaire de BRCA2 avec l'outil in silico SMART, nous avons révélé un domaine zf-PARP putatif dans la région N-terminale. Normalement, ce type de domaine s'associe à l'ADN, ce que nous a porté à l'examiner.

Mon premier objectif de ce travail était donc l'investigation de ce domaine de fixation à l'ADN putatif dans le N-terminus de BRCA2 humaine (NTD)

OBJECTIF 2: CARACTERISATION DES VARIANTS FAUX-SENS NON-CLASSIFIES (VARIANTS OF UNKNOWN CLINICAL SIGNIFICANCE) DANS LE DOMAINE DE FIXATION A L'ADN N-TERMINALE DE BRCA2 (NTD)

Afin de caractériser la pertinence fonctionnelle du N-terminus et le domaine de fixation de l'ADN en particulier, nous avons décidé d'étudier des variants faux-sens identifiés (VUS) dans des familles à risque élevé de développer un cancer du sein situés dans cette région. Nous avons voulu étudier la pertinence du nouveau domaine en examinant l'impact de ces variants dans leur fonction et au même temps ça nous permettra d'évaluer des variants faux-sens non-classifiés qui sont très rares et leur causalité pour le développement du cancer du sein est difficile à évaluer.
Nous avons sélectionné des VUS situés dans le NTD qui sont probablement nuisibles pour les individus portant la mutation. Tous les VUS sont bien conservés dans les mammifères et prévues de se lier à l'ADN. Dans ce travail, j'ai effectué des tests afin d'étudier l'impact de ces variants sur la fonction de BRCA2 dans la RH et la mitose.

OBJECTIF 3: ETUDE DU ROLE DE BRCA2 DANS LA RECOMBINAISON MEIOTIQUE

Dans les cellules somatiques BRCA2 catalyse le rôle du médiateur de RAD51 dans le RH. Son homologue méiotique, DMC1, partage structure et fonction similaire et s'associe à BRCA2 afin de stimuler l'activité d'échange de brin de DMC1. Une interaction physique a été établie pour BRCA2 pleine longueur et DMC1. Dans les plantes, cette interaction était trouvé d'être réalisée via les répétitions BRC alors que chez les humains, un motif conservé PhePP était suggéré d'être responsable pour la liaison avec DMC1. Cependant,

le domaine PhePP parait négligeable dans les souris ce qu'il indique qu'il existe probablement un autre site pour l'interaction de DMC1 dans BRCA2. De plus, l'alignement des séquences avec les paralogues de RAD51 a montré que le motif pour interagir avec les répétitions BRC est très bien conservé dans DMC1. Nous avons donc examiné si les répétitions BRC pourraient également se lier à DMC1 et la pertinence fonctionnelle de cette interaction.

RESULTATS

Objectif 1: Investigation et caractérisation d'un domaine de fixation à l'ADN putative dans le N-terminus de BRCA2

Afin d'effectuer des analyses biochimiques du N-terminus de BRCA2, nous avons construit la région N-terminale comprenant les premiers 750 acides aminés de BRCA2 humaines. Nous avons purifié le fragment des cellules humaines HEK293s et nous avons réussi en obtenant la protéine pure et non-dégradée (Figure 1).

Après avoir obtenu la protéine, nous l'avons utilisé dans des analyses de *changements de mobilité électrophorétique (EMSA).* Nous avons incubé la protéine avec une ADN à simple brin radio marqué avec $^{32}\gamma$ ATP (ssDNA*). La séparation des complexes protéine-ADN et l'ADN seule a été effectuer sur un gel natif de polyacrylamide (Figure 2A). Comme indiqué dans la figure 2B, $BRCA2_{LT3}$ s'est lié à l'ADN et a formé des complexes protéine-ADN, contrairement au contrôle négatif, le tag de 2xMBP seul.

A

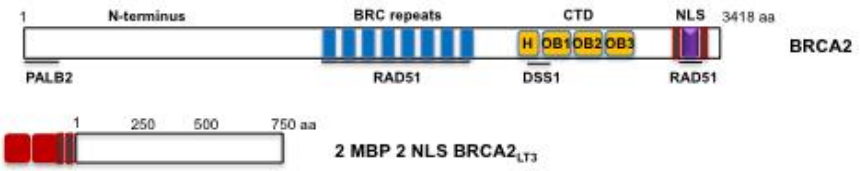

B

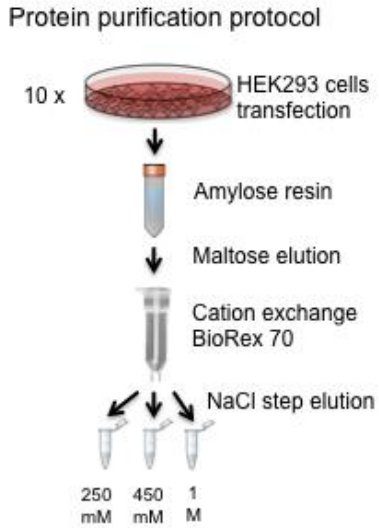

C

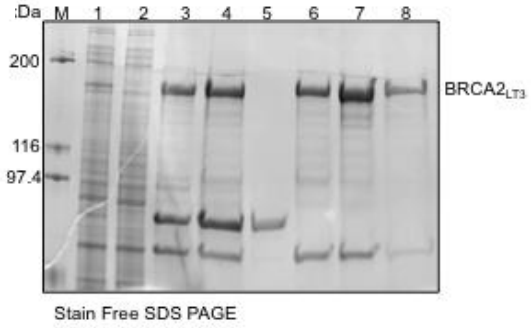

Figure 1: Purification du domaine N-terminale de BRCA2. A) structure de BRCA2 et le fragment $BRCA2_{LT3}$ utilisé pour la transfection des cellules et purification B) protocole pour la purification C) SDS PAGE montrant la procédure de la purification et la protéine obtenue dans la voie 8.

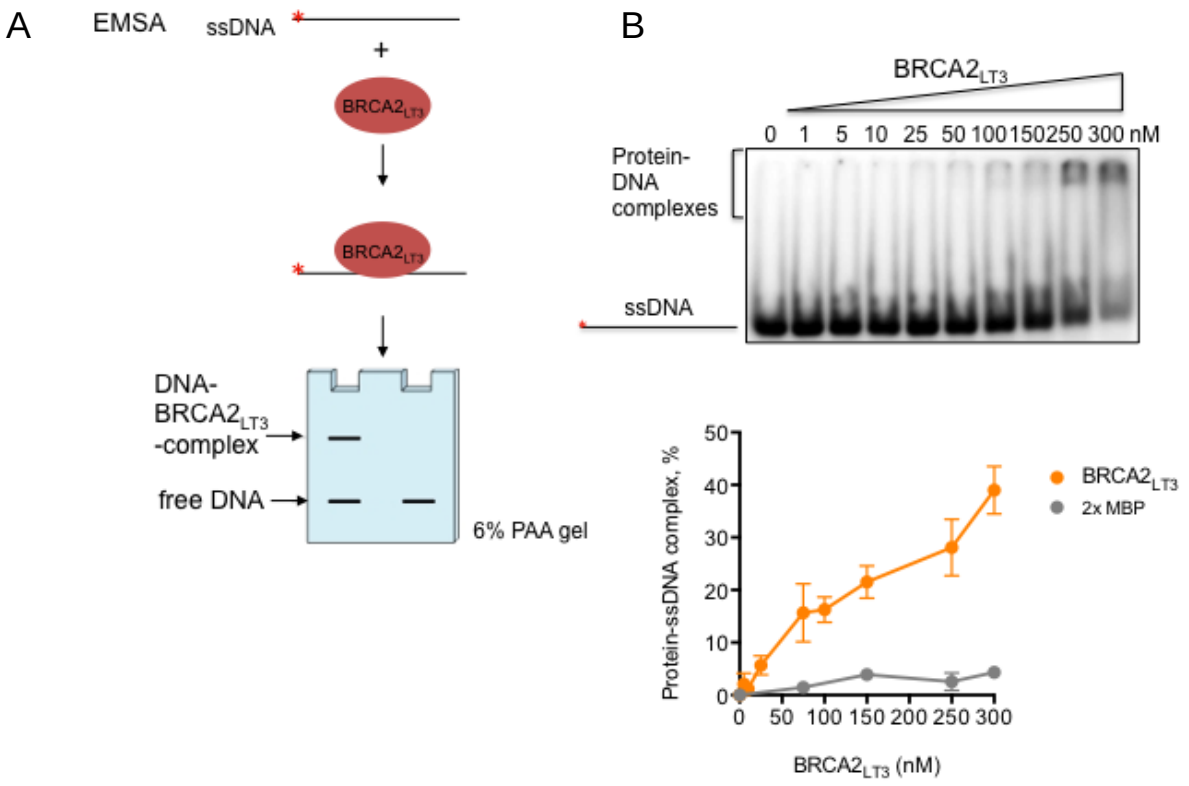

Figure 2: EMSA avec $BRCA2_{LT3}$ et une ADN à simple brin radio marqué avec $^{32}\gamma$ ATP ssDNA * (A) mécanisme d'EMSA B) résultat d'EMSA en montrant des complexes de la protéine et l'ADN et la quantification.

Pour trouver le domaine spécifique qui se lie à l'ADN, on a construit des fragments de $BRCA2_{LT3}$ plus petits : $BRCA2_{T1}$ (1-250 aa), $BRCA2_{T2}$ (250-500 aa) et $BRCA2_{LT2}$ (100-500 aa) (Figure 3A). Nous avons purifiés les fragments comme démontré pour $BRCA2_{LT3}$ et les utilisé pour EMSA. Comme indiqué dans 3B, $BRCA_{T1}$ n'a pas été capable de se lier avec l'ADN, contrairement au $BRCA2_{T2}$ et $BRCA2_{LT2}$ qui s'est liés avec l'ADN, indiquant que le domaine de fixation à l'ADN du N-terminus se trouve dans $BRCA2_{T2}$ (250-500 aa) comme prévu dans les analyses in silico.

A

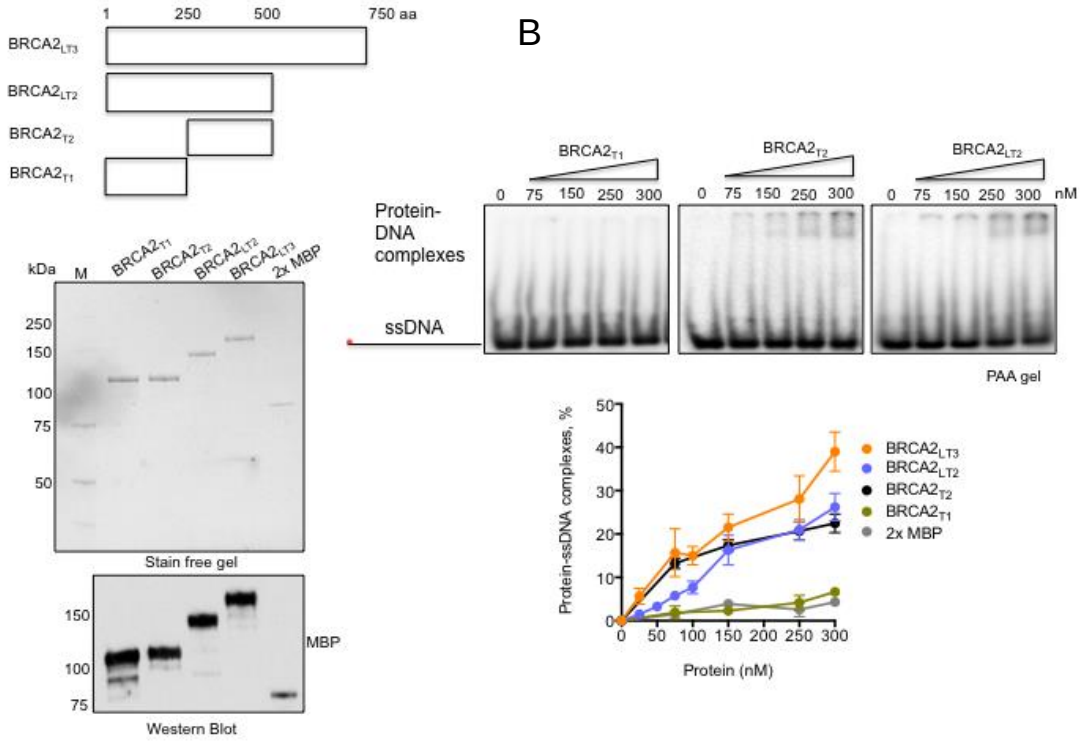

Figure 3 A) fragments pour la purification et SDS PAGE montrant les fragments purifiés et confirmé avec Western Blot B) EMSA avec les fragments et ssDNA* et sa quantification.

Après avoir montré la localisation du domaine de fixation à l'ADN dans le NTD, nous avons conçu de comparer l'activité NTD avec le domaine C-terminale canonique (CTD). Pour cela, nous avons construit un fragment du CTD en complexes avec DSS1 et nous les avons exprimés dans les cellules *E.coli* (Fig 4A). Nous avons purifié le complexe en utilisant Ni NTA resin et puis une colonne d'héparine. Le complexe était purifié sans dégradation en complexe avec DSS1 (Fig 4B).

Ensuite, nous avons utilisé les deux protéines (NTD et CTD) afin de les comparer en utilisant EMSA. J'ai préparé des substrats d'ADN radio marqué avec $^{32}\gamma$ ATP imitant la jonction entre ADNdb et ADNsb après les cassures double-bras d'ADN : ssDNA, dsDNA, 3'tails, 5'tails et gapped substrats. J'ai pu montrer que le NTD ainsi le CTD est capable de se lier avec tous les substrats ssDNA, 3'tails, 5'tails et gapped substrats. Contrairement au CTD, le NTD a montré une association forte avec le dsDNA, indiquant que cette fonction est particulière pour le NTD. De plus, j'ai observé que l'affinité pour l'ADN en général est plus forte pour le NTD car j'ai vu la formation de complexes avec l'ADN déjà en faibles concentrations contrairement au CTD (Figure 5).

A

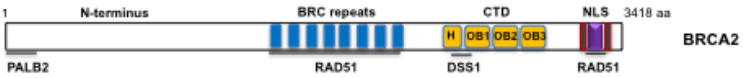

B

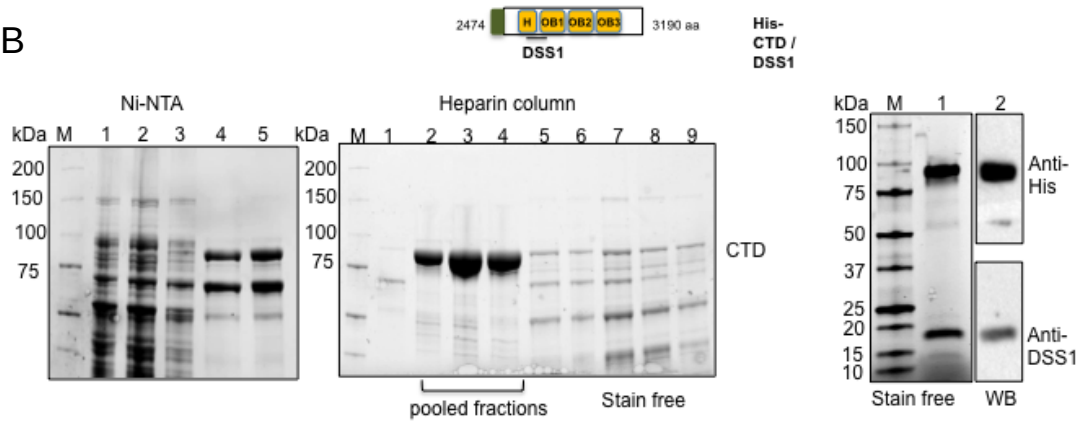

Figure 4: Purification du CTD. A) construction du CTD en complexe avec DSS1 pour la purification B) Purification du CTD avec Ni-NTA resin et colonne d'heparine (gauche). Droite : SDS PAGE et Western Blot de la protéine purifié en complexe avec DSS1.

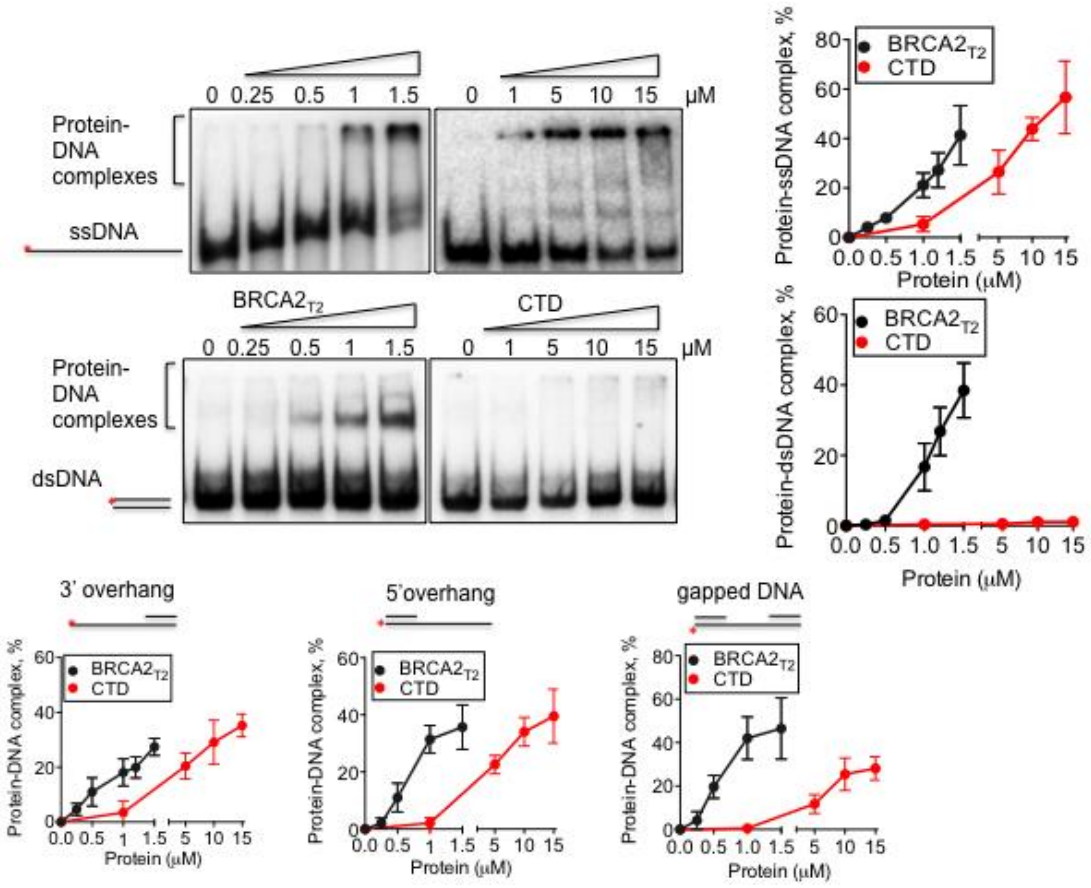

Figure 5: EMSAs et quantifications pour la comparaison du NTD et CTD en utilisant des substrats différents d'ADN. Explications dans le texte.

Comme le domaine de fixation à l'ADN était décrit comme zinc-finger PARP-like domaine, nous étions intéressés si de résidus de Cystéines et Histidine, normalement responsables pour la fixation à l'ADN dans des zinc-fingers, jouent un rôle important pour le NTD. J'ai effectué une mutagenèse de cystéines différentes dans $BRCA2_{T2}$ et également des combinaisons des mutations. Comme indiqué dans Figure 6, j'ai purifié les fragments (variants) pour des EMSAs en utilisant ssDNA et dsDNA.

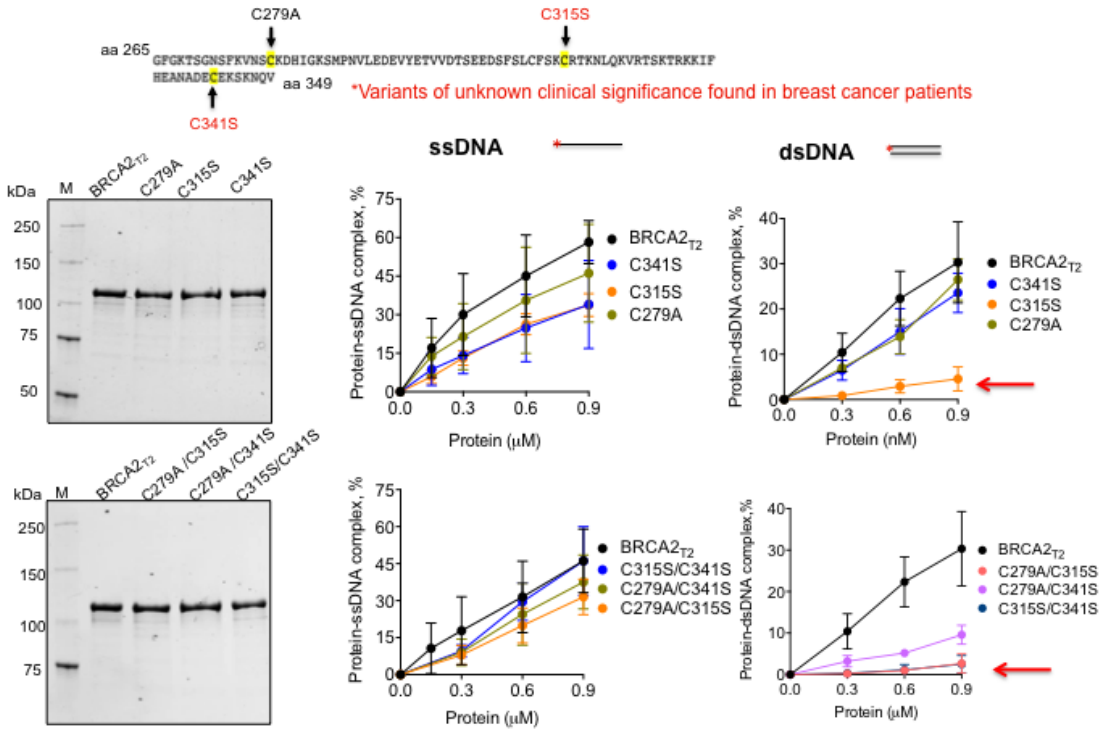

Figure 6: Cystéines sélectionnés pour la mutagenèse dans $BRCA2_{T2}$. En bas, le SDS PAGE des variants purifiés est montré. À gauche, la quantification des EMSAs avec ssDNA et dsDNA.

Pour les réactions avec ssDNA, je n'ai pas pu observer un impact négatif des mutations sur la capacité de $BRCA2_{T2}$ de former des complexes avec l'ADN. Au contraire, en utilisant dsDNA, j'ai remarqué une réduction de formation des complexes protéine-dsDNA pour la mutante C315S et les double-mutants portant la même mutation. Ça pourrait indiquer que ce résidu est important pour le fonctionnement du NTD dans la réparation d'ADN par RH.

BRCA2 joue un rôle principal comme médiator de la recombinaison de RAD51 en RH. Ici, son fonction est d'interagir avec RAD51 via les répétitions BRC afin de la localiser au site du dommage d'ADN et de l'aider à se lier avec ssDNA. BRCA2 est capable d'enlever la barrière cinétique de RPA pour que RAD51 puisse former des filaments nucléoprotéiques et accomplir son rôle en RH. Il a été prouvé ultérieurement que le domaine de fixation d'ADN CTD de BRCA2 et une seule répétition BRC sont suffisants de stimuler l'activité d'échange de brin de RAD51. Nous avons demandé si l'activité du NTD avec une répétition BRC étaient aussi assez pour assumer cette fonction. J'ai donc construit un fragment se composant de BRC4 et $BRCA2_{T2}$, puis j'ai exprimé et purifié $BRCA2_{BRC4T2}$ comme décrit avant. On utilise des tests in vitro pour mesurer l'activité d'échange de brin de RAD51. Ici, quand on incube un substrat 3'tail d'ADN avec RPA, RAD51 n'est pas

capable de se lier avec l'ADN. BRCA2 ou un fragment composé d'une répétition BRC et un domaine de fixation à l'ADN peuvent atténuer l'inhibition de RPA est RAD51 forme des produits d'échange de brin comme indiqué dans la Figure 7. Quand nous testaient le fragment $BRCA2_{BRC4T2}$ dans cette manipulation, on a pu observer que la protéine était capable d'enlever RPA et aider à RAD51 d'échanger les brins. Curieusement, en utilisant $BRCA2_{T2}$ seul dans les mêmes conditions, il était aussi capable de stimuler RAD51 et la quantification montre que les deux fragments avec ou sans BRC4, ont eu un effet dans les mêmes proportions. Par contre, le CTD n'a pas eu le même effet que $BRCA_{T2}$ seul, ce qui nous a conduit à spéculer que l'effet est dû à la capacité du NTD de se lier avec dsDNA. De cette façon, le NTD pourrait s'attacher particulièrement à la jonction ssDNA/dsDNA en remplaçant RPA et permettant l'assemblement de RAD51 au ssDNA.

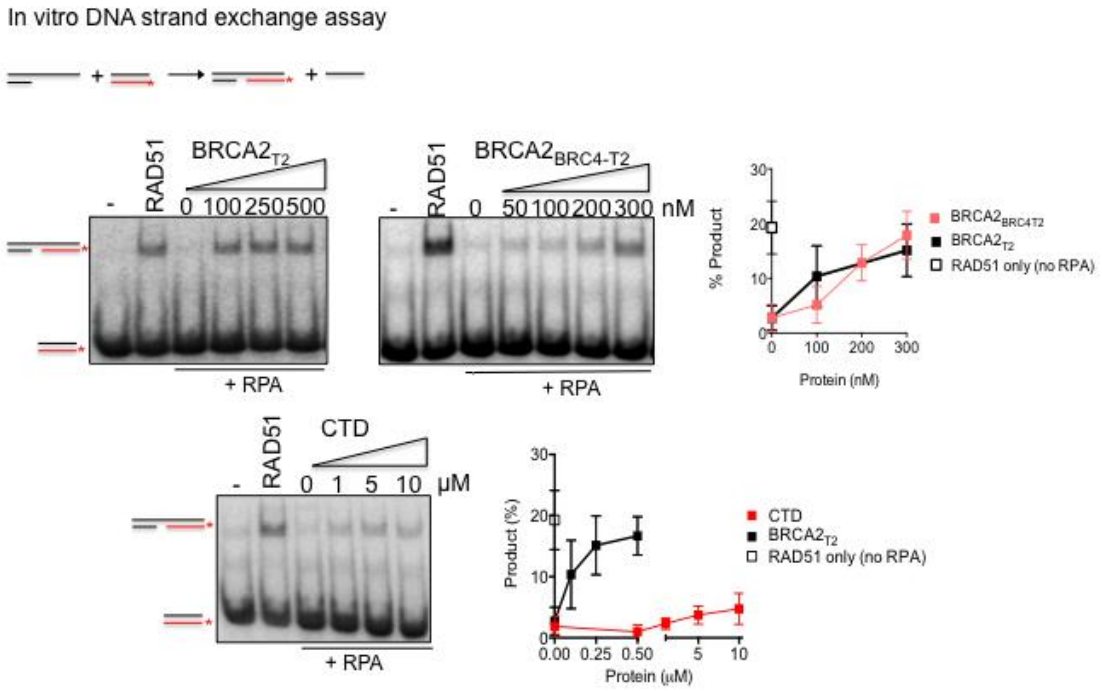

Figure 7: DNA strand exchange assays avec $BRCA2_{T2,}$ $BRCA2_{BRC4T2}$ et CTD et ses quantifications. Explications dans le texte.

Afin de tester cette hypothèse, nous avons effectué les mêmes tests en utilisant la mutante C315S montrant un défaut de se lier à dsDNA (Figure 8). En effet, C315S a montré d'être moins capable de stimuler l'activité de RAD51. En plus, le double mutant C279A/C315S a eu une réduction plus forte que C315S. Comme contrôle négative, nous avons effectué le même test avec un substrat ssDNA au lieu du 3'tail et nous avons

observé que l'activité était rétablie, indiquant que le mutant peut se lier avec ssDNA pour stimuler l'activité de RAD51.

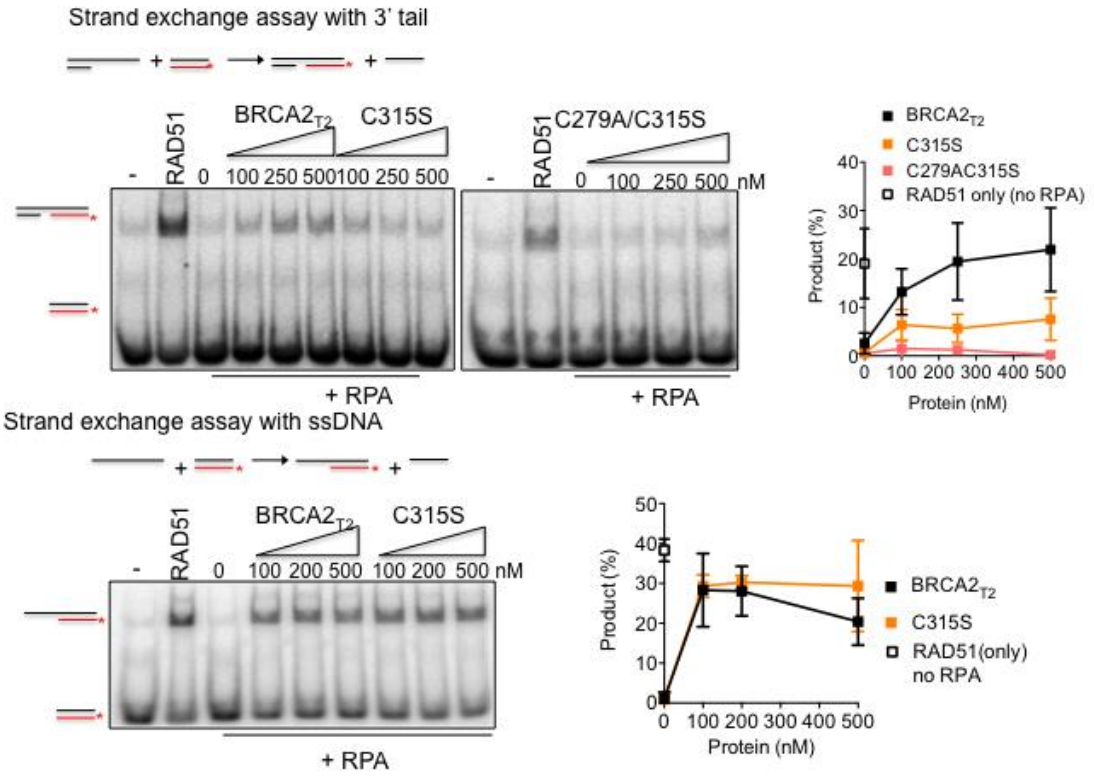

Figure 8: Strand exchange assays et quantifications avec $BRCA2_{T2}$ et les mutants C315S ainsi que C279AC315S avec 3'tail substrat (panneau supérieur) ou ssDNA (panneau inférieur).

Dans notre modèle (Fig 9), on propose que soit aux cassures d'ADN double-bras soit aux fourches de réplication bloquées, le NTD de BRCA2 est capable de s'associer aux jonctions ssDNA/dsDNA comme premier contact avec l'ADN en replaçant RPA. Ici, les répétitions BRC délivrent des monomères de RAD51 au site, et permettent RAD51 de s'associer à ssDNA en bloquant l'association avec dsDNA. Le domaine C-terminale (CTD) est ensuite capable d'enlever RPA par interaction avec DSS1 et RAD51 peut former les filaments nucléoprotéiques pour réaliser son rôle d'échange des brins d'ADN avec le modèle homologue pour la réparation du dommage. Ce modèle expliquerait pourquoi les fragments de BRCA2 en manque du CTD sont encore capables de servir comme médiateur dans le RH et permettent aux cellules de survivre des dommages d'ADN.

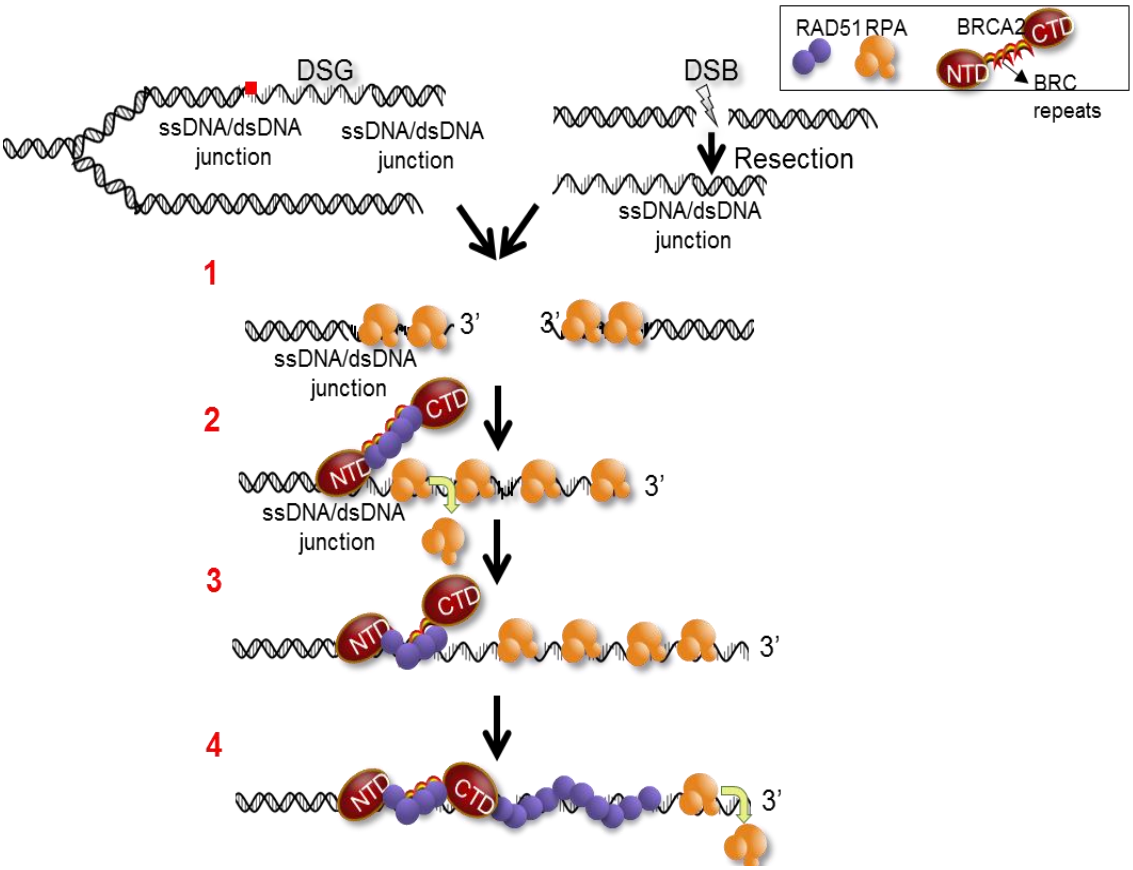

Figure 9: Modèle pour l'interaction du NTD et CTD pour la réparation d'ADN.

OBJECTIF 2: CARACTERISATION DES VARIANTS FAUX-SENS NON-CLASSIFIES (VARIANTS OF UNKNOWN CLINICAL SIGNIFICANCE) DANS LE DOMAINE DE FIXATION A L'ADN N-TERMINALE DE BRCA2 (NTD)

Pour mon deuxième objectif, j'ai sélectionné des variants faux-sens non-classifiés (variants of unknown clinical significance VUS) dans le domaine de fixation à l'ADN (NTD) que nous avons identifié. Ces mutations faux-sens étaient identifiées dans des patients du cancer du sein mais leur impact sur le fonctionnement de la protéine et donc le risque de développer un cancer pour les individus avec un de ces mutations restent inconnu. Les VUS sont enregistrés dans les bases des données BRCAshare et BIC et sont aussi prévus d'être délétères (Fig 1).

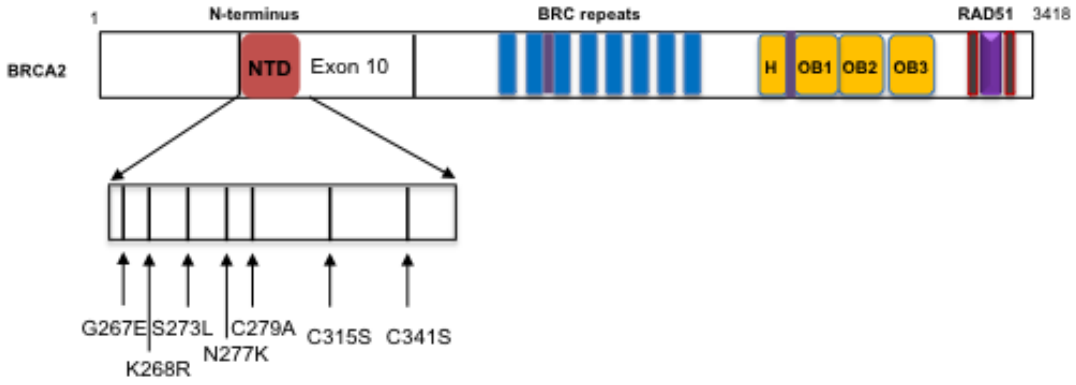

Figure 1: variants faux-sens (VUS) situé dans la NTD de BRCA2 sélectionnés pour cette étude.

RESULTATS ET CONCLUSIONS

Nous avons appliqué plusieurs tests fonctionnels sur ces variants qui sont résumés dans le tableau récapitulatif 1. Afin d'étudier les VUS in vivo, nous avons complémentés des cellules *BRCA2*$^{-/-}$ *(VC8)* avec cDNA du wild type ou variant et établi des lignées cellulaires stables. De plus, nous avons introduit les mutations dans le fragment BRCA2$_{T2}$ pour la purification des mutants pour tester leur capacité de s'associer avec l'ADN. Les cellules du VUS G267E n'ont pas été sensitives aux dommages ADN (MMC et inhibiteurs de PARP) ce qu'exclus un défaut du RH. Toutefois nous avons observé un défait du cytokinèse car les cellules, même en absence des agents nuisibles, ont montré une croissance diminuée. En utilisant time-lapse microscopy on a pu observer que l'abscission des cellules dans la

cytokinèse est retardé ou même absent ce que corresponde à un niveau élevé des cellules multinuclées. Les deux phénomènes indiquent un défait probable dans les dernières étapes de la cytokinèse, mais ils ne sont ni dus à une interaction interrompu avec les protéines du midbody testés ni à l'amplification du centrosome.

Les autres variants testé ont eu un phénotype délétère dans les tests du RH. Comme nous n'avons pas pu détecter leur expression en qualité égal comme pour BRCA2 et G267E, nous ne pouvons pas conclure que l'effet provient d'un fonctionnement perturbé ou de l'absence d'expression des protéines variants. Jusqu'à présent, nous pouvons seulement être certains que les variants localisent jusqu'au nucleus et interagissent avec les protéines du midbody testés quand on les surexprime dans les cellules HEK293.
Le variant K268R est une mutation artificielle non-enregistrée dans les bases données pour les VUS de BRCA2. Dans les survival assays avec MMC et après le traitement avec les inhibiteurs de PARP, les cellules ont eu un phénotype qui est sensitif aux dommages d'ADN. Elles ont aussi montrés un défait en cytokinèse mais nous n'avons pas encore pu analyser leur statut en multinucleation et amplification des centrosomes. La protéine a été capable d'interagir avec les components du midbody. Nous allons tester si le défait en RH est connecté avec le défait de croissance observé.
Nous avons observé le même phénotype pour le VUS S273L qui est enregistré deux fois dans les bases données. Les analyses fonctionnelles identiques seront donc appliquer à S273L.
Nous avons sélectionné le mutant N277K car il a été déjà analysé dans les tests fonctionnels qui ont relevé un phénotype défectueux pour la formation du midbody et dans l'abscission. Nous avons été intéressés à son comportement dans les tests pour analyser la RH. Les traitements avec MMC et les inhibiteurs de PARP ont relevé un défait dans la réparation d'ADN. Maintenant nous sommes curieux de savoir s'il y a une connexion entre les défaits en RH et la mitose car BRCA2 est également impliquée sur des postes de contrôle dans le cycle cellulaire.
Car les VUS sont localisés dans le NTD, nous sommes intéressés si les mutants montrent des défaits dans la liaison avec l'ADN comme nous avons montré pour C315S dans l'objectif 1. En utilisant EMSAs, nous pouvons tester l'association des VUS avec ssDNA ou dsDNA. Les quatres variants ont pu se lier à ssDNA par contre C273L a montré une capacité baisse de se lier à dsDNA ce qu'il pourrait expliquer un phénotype délétère en RH.

D’autre part, nous sommes en train de caractériser les VUS que nous avons testé dans l’objectif 1 pour leur capacité de l’association à l’ADN (C279A, C315S et C341) en

Variant	**MMC/ PARPi sensitive**	**Cyto-kinetic defect**	**Multi-nucleation**	**Centrosome amplification**	**Interaction with midbody proteins**	**DNA binding proficient**
G267E	No	yes	yes	no	Yes	yes
K268R	Yes	yes	TBT	TBT	Yes	yes
S273L	Yes	yes	TBT	TBT	Yes	Yes
N277K	Yes	yes	TBT	TBT	Yes	yes

appliquant clonogenic survival assay et tests pour la compétence de RH.

À l’avenir, nous avons planifié d’établir ces lignes cellulaires humaines *BRCA2*$^{-/-}$ qui expriment les VUS d’un locus endogène (HEK293 FLP in system ou DLD1 cells) afin de reproduire les résultats obtenu avec les VC8 et tester les phénotypes d’autres variant pas encore testé en cytokinèse comme pour G267E. De plus nous allons mettre en place un test de RH (GFP reporter assay et RAD51 foci). Pour mieux comprendre le défait du mutant G267E dans la formation du midbody et l’abscission nous avons planifié de tester l’interaction avec autres component du midbody, la localisation et le profil du cycle cellulaire.

OBJECTIF 3: ETUDE DU ROLE DE BRCA2 DANS LA RECOMBINAISON MEIOTIQUE

DMC1 est la contrepartie méiotique de RAD51 car elle forme des filaments nucléoprotéique pour la recherche d'homologie et l'invasion du brin homologue (D-loop formation) dans la méiose I de manière similaire. Comme décrit, l'interaction physique entre DMC1 et BRCA2 a été démontré déjà avant, néanmoins, la signifiance fonctionnelle de cette interaction est restée incertain. Dans les humaines, un motif conservé a été rapporté d'être responsable pour l'association. Dans les souris, une mutation prévue de perturber le motif conservé n'a eu aucun impact sur la recombinaison méiotique. Ici, nous avons étudié si les répétions BRC peuvent interagir avec DMC1 et si, BRCA2 ou non agit comme une protéine médiateur pour la recombinaison méiotique, dans la même manière comme dans la recombinaison mitotique. Les résultats de cette étude ainsi la discussion sont présentés ci-après dans la publication qui se retrouve dans le chapitre 4.2.

CONCLUSIONS FINALES

Dans cette étude de thèse, nous avons réussi à découvrir des nouveaux aspectes du suppresseur de tumeur BRCA2 et évaluer l'impact des VUS identifiés dans les patients du cancer du sein comme illustré dans Figure 1.

LE DOMAINE N-TERMINALE DE BRCA2 POSSEDE UN DOMAINE DE FIXATION A L'ADN

Nous avons identifié un domaine de fixation à l'ADN dans la région N-terminale de BRCA2 (Figure 1 A).

Cette région contenant un zinc finger PARP like domaine (zf PARP) putatif a montré in vitro une activité de liaison à l'ADN dans la région de $BRCA2_{T2.}$ Il reste à établir si vraiment le domaine zf PARP est requis pour cette activité. De plus, quelques résidus de cystéine mutés qui sont censés d'être importants pour assembler le motif du zinc finger ont montré une activité réduits de se lier à l'ADN.

Nous avons observé que le NTD et le CTD partagent des affinités ressemblants pour des substrats d'ADN mais le NTD possède une affinité plus élevée pour l'ADN que l CTD. Un résultat inattendu a été la capacité du NTD de se lier à dsDNA. Nous assumons que cette activité avec dsDNA est probablement responsable pour l'activité de se lier à dsDNA montré dans la BRCA2 full-length.

Nous avons pu montrer que le NTD stimule l'activité d'échange des brins de RAD51 dans la présence de RPA. On propose que le NTD possède une activité de médiateur en facilitant l'association de RAD51 à l'ADN en remplaçant RPA grâce à son affinité élevé pour les jonctions de dsDNA/ssDNA. Nous proposons que le NTD et le CTD puissent agir consécutivement aux DSB ou daughter strand gaps pour faciliter l'association de RAD51. Le NTD représenterait le site primaire pour l'interaction avec l'ADN en rendant l'ADN plus accessible pour RAD51 qui est délivré par les répétitions BRC. Le complexe entre CTD/DSS1 pourrait ainsi promouvoir la formation des filaments de RAD51 en remplaçant RPA comme proposé avant. C'est un grand intérêt d'examiner comment BRCA2 coordonne les deux modules in vivo. Nous allons investir si le NTD avec BRC4 pourrait sauver le phénotype en surexprimant le construct dans les cellules *BRCA2*$^{-/-}$ comme décrit dans l'objectif 2.

A

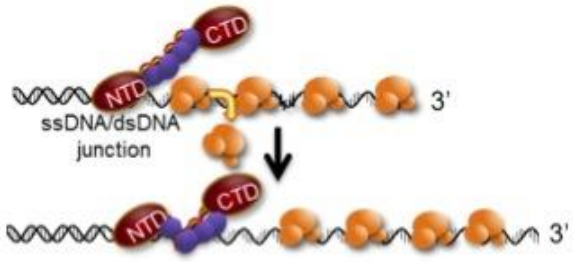

von Nicolai C *et al.*, 2016: A novel DNA binding site in human BRCA2 promotes homologous recombination. (under revision)

C

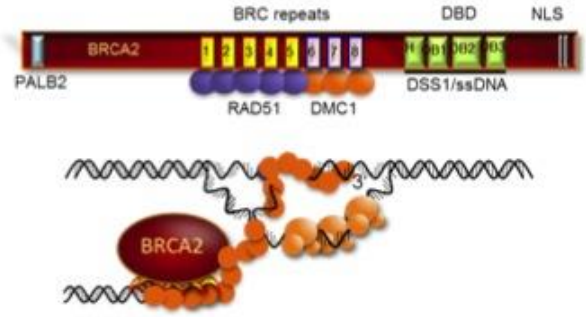

Martinez* JS, von Nicolai* C *et al.*, 2016: BRCA2 regulates DMC1-mediated recombination through the BRC repeats, *PNAS*. * *equal contribution*

B

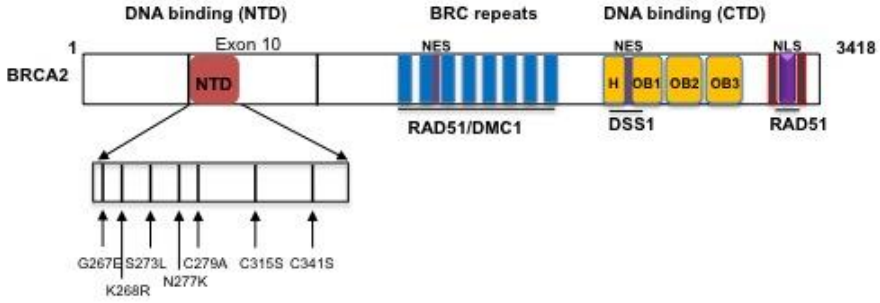

Figure 1: Résumé des résultats de ces travaux.

VARIANTS FAUX-SENS NON-CLASSIFIES (VARIANTS OF UNKNOWN CLINICAL SIGNIFICANCE) DANS LE DOMAINE DE FIXATION A L'ADN N-TERMINALE DE BRCA2 MONTRENT DES DEFAITS EN RH ET CYTOKINESE

Nous avons selectionné des VUS dans le NTD et appliqué des tests fonctionnels in vivo et in vitro pour l'évaluation de leur phénotype dans la réparation d'ADN et la cytokinèse (Figure 1 B) Comme décrit dans le chapitre 3.2, nous avons trouvé des mutants faux-sens dans le NTD qui peuvent affecter la capacité de la fixation à l'ADN de BRCA2. De plus, des variants ont montré des délais ou bien l'échec dans la cytokinèse ce qui parle pour des défauts dans la formation du midbody et/ou abscission comme décrit avant. En résumé, nous avons observé que un VUS sélectionné dans le NTD, G267E a un impacte

sur la fonctionnalité de BRCA2 en cytokinèse. Ce défaut pourrait être lié à une localisation défectueuse de BRCA2 vers le midbody ou l'interaction abrogé avec les protéines requises pour l'abscission.

Les VUS ne montrent pas une diminution évidente dans leur capacité de se lier à ssDNA en comparaison avec $BRCA2_{T2}$, par contre le variant S273L n'est pas capable d'interagir avec dsDNA ce qu'il pourrait expliquer le phénotype délétère en RH.

En appliquant des tests fonctionnels supplémentaires, nous serons capables d'évaluer plus profondément le phénotype des VUS dans la RH ainsi dans la mitose.

Dans l'avenir, l'identification du NTD ainsi que les tests fonctionnels établi pour l'évaluation de VUS dans ce région seront très avantageux pour le service de conseil des porteurs de VUS dans BRCA2.

BRCA2 EST LE MEDIATEUR DE LA RECOMBINASE DMC1 DANS LA MEIOSE

Pour mon troisième objectif j'ai collaboré avec JSM du laboratoire pour enquêter si BRCA2 fait la médiation de l'activité de recombinaison de DMC1 dans la méiose comme montré pour RAD51 dans la mitose. BRCA2 a été montré d'être impliqué dans méiose et son absence cause infertilité et des aberrations chromosomiques. De plus, il est connu que BRCA2 et DMC1 interagissent, bien que le mécanisme et la raison pour cette interaction restent énigmatiques. Dans notre étude, nous avons relevé que DMC1 interagit avec BRCA2 via les répétitions BRC pour stimuler son association avec ssDNA et la formation des filaments nucléoprotéiques. BRCA2 soulage la barrière cinétique posée par RPA lié à ssDNA, ce qui le rend accessible pour DMC1. Ces découvertes établissent BRCA2 comme protéine médiateur pour la recombinaison méiotique de DMC1. Notre modèle est cohérent avec un rôle accessoire de RAD51 dans la recombinaison dans la méiose comme décrit dans la levure. Dans ce modèle, BRCA2 se lierait aux monomères de RAD51 via BRC1-5 pour assurer un filament qui sert comme une base de nucléation pour DMC1 permettant l'assemblement des homofilaments. Le filament de DMC1 pourrait ainsi grandit et commence la recherche d'homologie (Figure 1C)

En résumé, pendant cette thèse, j'ai contribué de relever des nouvelles fonctions du N-terminus de BRCA2 (NTD, défauts cytokinétique) mais aussi l'association des répétitions BRC avec DMC1. De plus, nous avons établi des tests fonctionnels pour l'évaluation des VUS de BRCA2.